Title
TRANSPORT OF A PARTIALLY IONIZED PLASMA. ACROSS A MAGNETIC FIELD

Author
Warren, Laird.

Publication Date
1968-09-30

TRANSPORT OF A PARTIALLY IONIZED PLASMA ACROSS A MAGNETIC FIELD

Laird Warren

(Ph. D. Thesis)

September 30, 1968

LAWRENCE RADIATION LABORATORY
UNIVERSITY of CALIFORNIA BERKELEY

DISCLAIMER

UCRL-17601

UNIVERSITY OF CALIFORNIA

Lawrence Radiation Laboratory
Berkeley, California

AEC Contract No. W-7405-eng-48

TRANSPORT OF A PARTIALLY IONIZED PLASMA ACROSS A MAGNETIC FIELD

Laird Warren

(Ph. D. Thesis)

September 30, 1968

TRANSPORT OF A PARTIALLY IONIZED PLASMA ACROSS A MAGNETIC FIELD

Contents

TRANSPORT OF A PARTIALLY IONIZED PLASMA ACROSS A MAGNETIC FIELD

Laird Warren

Lawrence Radiation Laboratory
University of California
Berkeley, California

September 30, 1968

ABSTRACT

The transport of a plasma across a magnetic field is one of the fundamental problems of plasma physics. In the absence of temperature gradients the transport of a partially ionized plasma is describable in terms of diffusion in the presence of density gradients, and mobility and convection in the presence of electric fields. Many experiments have been done to study the nature of this transport in a partially ionized plasma, and it is often concluded that some "anomalous" diffusion mechanism is operative. However, the interpretation of experiments depends critically on assumptions made concerning the effects of electric fields and boundary conditions and on the values of various plasma parameters. It would seem that in many cases there is insufficient experimental knowledge of the plasma being studied to determine if the theoretical models were correctly applied.

We have undertaken a series of experiments on the partially ionized secondary plasma of a magnetically collimated hollow-cathode arc discharge. Experiments were done in He, H_2, Ar, and N_2 for neutral pressures of 1.5 to 7 mTorr with a magnetic field of 300 to 1680 G

in a diffusion chamber 58.2 cm long and 20 cm in diameter. The plasma produced falls off radially from a density of 10^{13} to 10^{14} cm^{-3} with $kT_e \approx 8$ eV in the center of the discharge to 10^{10} to 10^{11} cm^{-3} with $kT_e < 0.5$ eV near the wall. Detailed measurements on the plasma density, potential, and electron temperature as a function of spatial position have been made with Langmuir probes for a variety of experimental conditions. From these measurements the values of the diffusion coefficients and electric fields are estimated, and the particle transport rates and particle accumulation rates due to various processes are deduced and compared.

The transport of this partially ionized plasma across a magnetic field is determined by diffusion, mobility, and convection. Radial diffusion due to charged-particle collisions for the ions is the same order of magnitude as diffusion by collisions with neutrals, and for the electrons is much larger than neutral collisional diffusion. When the concentric ring end electrodes of the system are electrically grounded, there is a radial ion transport due to mobility in the presence of a radial electric field which is much larger than the transport due to diffusion. In addition, convection due to azimuthal electric field and density fluctuations gives a radial ion transport comparable to the other radial transport processes. When the end electrodes are electrically isolated the radial electric field becomes negligible. However, small transverse electric fields are established which cause the plasma to drift in a preferred direction, producing an azimuthally asymmetric plasma distribution which is sensitive to small

changes in magnetic field alignment. A change in any externally applied transverse magnetic field of the order of $0.0004\ B_z$ will cause the asymmetry to change markedly.

The axial ion transport is limited by the rate at which ions can diffuse to the ends. Most electrons are axially trapped by reflecting end sheaths. The electron temperature in the secondary plasma is found to be significantly above the neutral gas temperature, and superelastic collisions with neutrals excited by resonance radiation from the primary arc column are thought to be the dominant electron heating mechanism.

I. INTRODUCTION

One of the central problems in plasma physics has been to understand the nature of transport of a plasma across a magnetic field. A plasma confined by a magnetic field with density or temperature gradients is not in thermal equilibrium. It exhibits a tendency toward equilibrium by collisional processes. Because of the free energy available to the system the plasma can also develop macroscopic electric fields, fluctuations, and perhaps turbulence, which will help to bring the system toward equilibrium by transporting the plasma across the magnetic field.

If the plasma varies slowly compared with the period of ion gyration, and if the particles experience many collisions before they are lost from the system, the transport of the plasma can be described in terms of diffusion in the presence of density gradients, and mobility and convection in the presence of electric fields. If the gradients of the ion or electron temperature are significant, there also may be transport due to thermal effects.

Diffusion occurs whenever the interaction of particles in the plasma with other particles or fields gives rise to a random walk of particles. In the presence of a density gradient, the particle transport obeys Fick's Law, where the flux is proportional to the density gradient with the proportionality being given by the diffusion tensor. Collisions between the ions or the electrons and the neutral gas atoms give rise to neutral collisional diffusion. Collisions between the ions and electrons give rise to "fully ionized diffusion," that is,

diffusion in a fully ionized plasma. The presence of a magnetic field reduces the rate at which charged particles diffuse perpendicular to the magnetic field. In addition to diffusion due to collisional processes there may also be enhanced diffusion of the plasma across the magnetic field due to statistically fluctuating electric fields in the plasma. Bohm, Burhop, and Massey[1] were the first to point out the possibility of enhanced diffusion, and it has long been thought that in many experiments enhanced diffusion due to instabilities may play a significant role in the transport of plasma across a magnetic field.

In the presence of a macroscopic electric field in the plasma, collisions between the ions or electrons and the neutral atoms will also give rise to a mobility $\mu_{jk}^{\alpha n}$ and to the transport of particles parallel to the electric field. The mobility coefficient $\mu_{jk}^{\alpha n}$ and the neutral collisional diffusion coefficient $D_{jk}^{\alpha n}$ arise from the same collisional process and are related by the Einstein relationship $\mu_{jk}^{\alpha n} = q_\alpha D_{jk}^{\alpha n}/kT_\alpha$. This is discussed in the review article by Allis.[2] Convection of the plasma across the magnetic field occurs because of the well known E x B drift motion of the plasma if there are electric-field components of the plasma perpendicular to the magnetic field. This motion is described in the off-diagonal terms of the mobility tensor. When one considers the transport due to both static and fluctuating electric fields, and due to density fluctuations, one finds for a particular experiment that there may be convection of the plasma across the magnetic field.

Many experiments have been done under steady-state or pulsed

conditions, or on the decaying afterflow plasmas, to understand the nature of plasma transport. The plasmas have been produced by means of arc discharges with hollow or thermionic cathodes, reflex arc discharges, positive columns, radio-frequency and microwave discharges, and pulsed electrodeless discharges as well as by contact ionization. Although the basic transport mechanisms are the same, each experiment is distinct in the method of production of the plasma, the extent to which production is important in the diffusion region, and the specific boundary conditions applicable.

Various authors have investigated the dependence of the spatial plasma distribution on discharge parameters such as neutral pressure, magnetic field strength, and system length, and sometimes found reasonably good quantitative agreement with one or another of the theories.[3,4] Other times[1,5] the experiments have implied diffusion as much as two orders of magnitude larger than expected from collisional considerations.

The deduction of transport rates from experimental measurements is an indirect process in which one fits the observed plasma distribution with that predicted by a model. Assumptions concerning azimuthal symmetry, the shape of the axial plasma distribution, the axial, radial steady-state, and fluctuating electric fields, the ion and electron currents to the ends of the system, and the boundary conditions critically affect the outcome of the analysis. It would seem that in many previous experiments there was insufficient experimental knowledge of the plasma being studied to determine if the theoretical models were correctly applied or not.

To do a thorough investigation of the transport of a plasma in a magnetic field we have chosen to study in detail the partially ionized secondary plasma surrounding a magnetically collimated hollow-cathode arc discharge. The arc runs from a tungsten cathode into a differentially pumped diffusion chamber and produces a plasma with a charged particle density of 10^{13} to 10^{14} cm^{-3} in the central arc column. The plasma density falls off radially to 10^{10} to 10^{11} cm^{-3} at the walls of the system. The diffusion chamber is 20 cm in diameter and has a length of 58.2 cm, which is much larger than the ion-transport mean free path λ_{in}, which is typically 1.2 cm. The ends of the diffusion chamber terminate on end plates consisting of five concentric ring electrodes which give some control over the axial boundary conditions. There is a uniform axial magnetic field of 560 to 1680 G. Most of the measurements were made in a helium discharge with a neutral pressure of 1.5 to 7 mTorr. Observations were also made in argon, hydrogen, and nitrogen discharges.

Detailed measurements of the plasma density, potential, and electron temperature in the secondary plasma outside the central arc column were made as a function of spatial position with Langmuir probes. From these measurements the values of the transport coefficients, ion temperature, density gradients, and electric fields are estimated. The initial experiments showed that the radial density profile as a function of magnetic field behaved as one would expect for collisional diffusion. However, measurements as a function of neutral pressure gave results which could not be interpreted as simple diffusion. Many

processes were found to be significant, and it was not possible to solve a set of simultaneous equations for the spatial dependence of the plasma density and potential. Rather it was necessary to estimate the transport rates for a specific set of experimental conditions and to show that this provides a consistent explanation of the observations.

The radial ion motion is found to be determined by diffusion, mobility, and convection. The effect of temperature gradients on the transport is found to be negligible. The axial ion motion is governed by neutral collisional diffusion with the estimated ion flux to the end electrodes, being in agreement with the observed electrode current in the secondary plasma. The electron motion is dominated by the requirement of charge neutrality, and rough agreement in the electron balance is obtained. The end sheaths adjust themselves to balance the electron losses and maintain charge neutrality. For grounded end electrodes there is a radial electric field produced which is some cases can significantly affect the radial ion transport. For floating end electrodes the radial electric field becomes negligible, but the plasma tends to be azimuthally asymmetric due to small transverse electric fields, which cause the plasma to drift in a preferred direction. The electric fields in an axially bounded system may significantly affect the plasma by introducing radial convection, mobility currents, azimuthal asymmetry, or fluctuations.

In Section II we discuss the deduction of transport rates from experimental measurements. In Section III we consider previous experimental and theoretical attempts to understand transport measurements

in arc discharges. After describing the experiments and the results in Section IV, we discuss in Section V the effects of various processes on transport and consider in detail the particle transport rates and particle accumulation rates for a specific set of measurements in helium. In addition we discuss possible mechanisms for producing plasma fluctuations and electron heating. In Section VI we conclude that electric fields, both static and fluctuating do contribute significantly to the transport of the plasma across a magnetic field, and can supplement the effects of diffusive transport in determining the plasma distribution.

II. DEDUCTION OF TRANSPORT RATES FROM EXPERIMENTAL MEASUREMENTS

In the absence of local production and recombination the plasma density is determined by the rate at which the plasma is transported along and across the magnetic field. We can measure the spatial dependence of the plasma density, electron temperature, and to a certain extent the electric fields in the plasma. From these measurements, and a knowledge of the plasma density, neutral background gas density, and momentum-transfer cross sections, one can calculate the ion temperature and the diffusion coefficients. The transport flux within the plasma can be inferred only by assuming a model of the plasma transport.

A. The Transport Equations

For the moment we assume that our plasma is cylindrically symmetric with the source of plasma on the axis. We also assume that the density gradients and static electric fields are only in the radial and axial directions. However, fluctuating azimuthal electric fields may also contribute to transport. Both static and fluctuating electric fields are derivable from a scalar potential. As noted in Appendix C, the effects of fluctuating magnetic fields are negligible in our experiment. Our plasma is partially ionized, i.e., we must consider the effects of both collisions between charged particles and neutral particles (charge-neutral collisions) as with a weakly ionized plasma, and the effects of charged-particle collisions as with a fully ionized plasma.

We assume that the transport can be adequately described in terms

of partially ionized collisional transport theory (a) with temperature gradient effects neglected, Eq. (C.15); (b) with additional transport due to convection, Eq. (C.26); and (c) enhanced diffusion, Eq. (C.28), as is discussed in Appendix C. Under these assumptions we can write the radial particle flux for the ions as

$$nv_r^i = -(D_\perp^{in} + D^{ie}) \frac{\partial n}{\partial r} + \mu_\perp^{in} n E_r - D_{enh}^i \frac{\partial n}{\partial r} + \langle nv_r \rangle_{conv}^i, \quad (2.1)$$

and for the electrons as

$$nv_r^e = - (D_\perp^{en} + D^{ei}) \frac{\partial n}{\partial r} + \mu_\perp^{en} n E_r - D_{enh}^e \frac{\partial n}{\partial r} + \langle nv_r \rangle_{conv}^e. \quad (2.2)$$

For the conditions of our experiment the transport mean free path for neutral collisions λ_{in} is much shorter than the system length L, so that the axial transport is given by the collisional transport as indicated in Appendix C, Eq. (C.15). For the ions,

$$nv_z^i = - D_\parallel^{in} \frac{\partial n}{\partial z} + \mu_\parallel^{in} n E_z, \quad (2.3)$$

and for the electrons,

$$nv_z^e = - D_\parallel^{en} \frac{\partial n}{\partial z} + \mu_\parallel^{en} n E_z. \quad (2.4)$$

The electron mean free path λ_{en} is of the order of the system length L. Because of the large potential drop at the end sheath in the secondary plasma most of the electrons are reflected at the end sheaths and are in more or less Maxwell-Boltzmann equilibrium,[6,7]

$n(z) = n_0 \exp[e(\phi - \phi_0)/kT_e]$. This then gives rise to an axial electric field $E_z = -(kT_e/e)(1/n)(\partial n/\partial z)$, so that the axial electron flux to lowest order is zero. The ion flux is then given by

$$nv_z^i = -D_{\parallel}^{in}(1 + kT_e/kT_i)\frac{\partial n}{\partial z} . \tag{2.5}$$

In addition to transport radially and axially, there will also be particle transport perpendicular to both the density gradient and the magnetic field in the Hall directions. This is given by the off-diagonal components of Eq. (C.15),

$$nv_\theta^\alpha = -\frac{q_\alpha ckT_\alpha}{e^2B}\left(\frac{\Omega_\alpha^2\tau_{\alpha n}^2}{1 + \Omega_\alpha^2\tau_{\alpha n}^2}\right)\frac{\partial n}{\partial r} - \frac{cnE_r}{B}\left(\frac{\Omega_\alpha^2\tau_{\alpha n}^2}{1 + \Omega_\alpha^2\tau_{\alpha n}^2}\right). \tag{2.6}$$

These currents, in the cylindrical case, give rise to a rotation of the plasma as a whole. As we have assumed for the time being azimuthal symmetry, there will be no net particle accumulation because of drifts in the Hall direction.

The rate at which ions and electrons accumulate in a region of a plasma is given by the continuity equation for each species,

$$\frac{\partial n_\alpha}{\partial t} + \vec{\nabla}\cdot n\vec{v}_\alpha = -\alpha_R n^2 + \beta_I n, \tag{2.7}$$

where α_R is the volume recombination coefficient and β_I the volume production rate due to ionization. Recombination and volume production in the secondary plasma are found experimentally to be small. We estimate the rate at which particles accumulate, using our transport

equations. Using Eqs. (2.1) and (2.5) in the continuity equation, we have, for the ions,

$$\frac{\partial n_i}{\partial t} = +\frac{1}{r}\frac{\partial}{\partial r}\left[r(D_\perp^{in} + D^{ie})\frac{\partial n_i}{\partial r}\right] - \frac{1}{r}\frac{\partial}{\partial r}\left[r\mu_\perp^{in} n_i E_r\right] + \frac{1}{r}\frac{\partial}{\partial r}\left[rD_{enh}^{i}\frac{\partial n_i}{\partial r}\right]$$
$$- \frac{1}{r}\frac{\partial}{\partial r}\left[r\langle nv_r\rangle_{conv}^{i}\right] + \frac{\partial}{\partial z}\left[D_\parallel^{in}\left(1 + \frac{T_e}{T_i}\right)\frac{\partial n_i}{\partial z}\right]. \qquad (2.8)$$

For the electrons the axial loss rate to lowest order is zero. So, following Simon,[8,9] we approximate the loss per unit volume by dividing twice the rate at which they are being lost out one end of the system by the length $(\partial/\partial z)(nv_z^e) = 2\langle nv_z\rangle_{wall}^{e}/L$. When Eq. (2.2) for the radial electron transport is used, the electron accumulation equation becomes

$$\frac{\partial n_e}{\partial t} = \frac{1}{r}\frac{\partial}{\partial r}\left[r(D_\perp^{en} + D^{ei})\frac{\partial n_e}{\partial r}\right] - \frac{1}{r}\frac{\partial}{\partial r}\left[r\mu_\perp^{en} n_e E_r\right] + \frac{1}{r}\frac{\partial}{\partial r}\left[rD_{enh}^{e}\frac{\partial n_e}{\partial r}\right]$$
$$- \frac{1}{r}\frac{\partial}{\partial r}\left[r\langle nv_r\rangle_{conv}^{e}\right] - \frac{2\langle nv_z\rangle_{wall}^{e}}{L}. \qquad (2.9)$$

By requiring quasi-neutrality, $n_i = n_e$, and by assuming steady state, $\partial n/\partial t$, we have two equations that relate the spatial distribution of the plasma density $n(r,z)$ to (a) the radial electric fields, (b) radial convection, and (c) the diffusion coefficients for neutral collisional, fully ionized, and enhanced transport across the magnetic field.

B. Simple Diffusion Theory

Early attempts to understand the nature of transport of the secondary plasma in arc discharges assumed that the transport could be adequately approximated by considering diffusion processes alone. Neglecting radial convection and the radial electric field, and assuming that the effect of fully ionized transport is negligible in the secondary plasma, and that the system is azimuthally symmetric, we find that the continuity equation for the ions can be written

$$\frac{\partial n_i}{\partial t} = \frac{1}{r}\frac{\partial}{\partial r}\left[rD^i_{\perp eff}\frac{\partial n_i}{\partial r}\right] + \frac{\partial}{\partial z}\left[D^{in}_{\parallel}\left(1 + \frac{T_e}{T_i}\right)\frac{\partial n_i}{\partial z}\right] = 0, \qquad (2.10)$$

where $D^i_{\perp eff} = D^{in}_{\perp} + D^i_{enh}$. The boundary condition on the density states that $n(z = \pm L_{eff}/2) = 0$ at each end of the system, and that $n(z = 0)$ is a maximum. Assuming that the diffusion coefficients are independent of postion, and that $n(r,z) = n(r)\cos(\pi z/L_{eff})$, one gets

$$D^i_{\perp eff}\frac{1}{r}\frac{\partial}{\partial r}\left[r\frac{\partial n(r)}{\partial r}\right] - \frac{\pi^2}{L^2_{eff}}D^{in}_{\parallel}\left(1 + \frac{T_e}{T_i}\right)n(r) = 0. \qquad (2.11)$$

This equation has the solutions

$$K_0(r/q) \sim (\pi q/2r)^{1/2}e^{-r/q}$$

and

$$I_0(r/q) \sim (q/2\pi r)^{1/2}e^{r/q}$$

for $r \gg q$; K_0 and I_0 are the Bessel functions of imaginary arguments. The radial scale length is

$$q = \frac{L_{eff}}{\pi} \sqrt{\frac{D_{\perp eff}}{D_{\parallel}^{in}(1 + T_e/T_i)}} \quad . \tag{2.12}$$

The radial solution is then

$$n(r) = AK_0(r/q) + BI_0(r/q), \tag{2.13}$$

where A and B are determined by the radial boundary conditions that $n(R) = 0$ at the chamber wall, and that $n(r_1) = N_1$ at some radius r_1 in the secondary plasma. If $q \ll R$, the solution except near $r = R$ will be of the form $n(r) \approx (q/r)^{1/2} e^{-r/q}$ which, except for the slowly varying factor $(q/r)^{1/2}$, gives a prediction of exponential radial variation of the plasma density. The radial density scale length q is a function of the effective radial and axial diffusion coefficients and the effective length of the system.

Many experiments have been undertaken which measure the radial density profile of arc discharges and find approximate exponential behavior over some region of the plasma.[3-5,8,10-13] However, in some experiments the slope of the radial density profile is observed to change with radius, falling off more slowly over some regions than over others.[12,13] From observations of the radial density scale length, attempts are often made to infer the effective radial diffusion coefficient through arguments similar to Eq. (2.12), and to determine if collisional diffusion or some enhanced diffusion mechanism is operating. Schwirzke, for instance, has correlated a region of the secondary plasma where the density falls off slowly with a

large-amplitude fluctuation, and suggests that perhaps in this region there might be significant enhanced diffusion.[13]

A model which considers only diffusion processes is an over-simplification. We find in our experiments that electric fields play a significant role in plasma transport. The electric fields are established not only by deviations from charge neutrality and the need to balance ion and electron loss from the system, but also by the effects of boundary conditions.

C. Boundary Conditions

At the ends of the system along the magnetic field lines there is a sheath over which the density of the plasma rapidly drops to zero and over which the potential changes from the plasma potential $\phi(z = L/2)$ to the wall potential ϕ_{wall}. This sheath has a thickness of the order of the Debye length. The Debye length in the secondary plasma is typically of the order of 10^{-4} cm. This potential difference is related to the electron and ion temperatures and to the ratio of ion current $\langle nv_z \rangle^i_{wall}$ to electron current $\langle nv_z \rangle^e_{wall}$ being collected at the end wall. The potential just inside the sheath is given by[14]

$$\phi\left(z = \pm \frac{L}{2}\right) = \phi_{wall} + \frac{kT_e}{2} \ln \frac{kT_e}{m_e} \frac{m_i}{kT_i} + kT_e \ln \frac{\langle nv_z \rangle^e_{wall}}{\langle nv_z \rangle^i_{wall}} . \qquad (2.14)$$

There will also be a potential drop from the inside of the sheath to the midplane of the system because of the axial electric field; however, it is generally quite small compared with the potential drop at the sheath. The ion current to the end wall is limited to the rate

at which ions can diffuse to the wall,

$$(nv_z)^i_{wall} = D^{in}_{\parallel}(1 + T_e/T_i)(\partial n/\partial z),$$

evaluated at $z = L/2$. The electrons have a long mean free path along the magnetic field; however, because of the axial electric field their net current is about zero. Slight adjustments in the electron flux to the end walls cause the sheath potential drop to change. One thus cannot impose a physical constraint on the plasma potential because of sheath effects.

There is also a boundary condition on the plasma density, namely the density is zero at the end walls. For a long system, where the system length L is much larger than the ion neutral collisional mean free path λ_{in}, the ion losses to the ends are diffusion-limited. The apparent length of the system as seen by the plasma is of the order of $2/3\ \lambda^{in}_{eff}$ longer at each end of the chamber, where λ^{in}_{eff} is the effective-length theory of neutron transport theory.[15] As the axial electric field increases the ion transport, we shall assume that the ion neutral mean free path is increased by the same factor $\lambda^{in}_{eff} = \lambda_{in}(1 + T_e/T_i)$. The effective length of the diffusion chamber is

$$L_{eff} = L + 4/3\lambda_{in}(1 + T_e/T_i). \qquad (2.15)$$

For the neutral pressures of the experiment the correction is of the order of 6.5 cm out of an overall length L = 58.2 cm. For a long system such as ours it is a small correction. For a short system, in which the system length is the order of the ion collisional mean free path, the axial ion loss is estimated, following Bohm, Burhop, Massey and Williams[16] and Simon,[9] from the mean rate of streaming of the ions to the ends, due to thermal motion.

III. PREVIOUS ATTEMPTS TO UNDERSTAND TRANSPORT MEASUREMENTS IN ARC DISCHARGES

Many experiments have been done to study the transport of the secondary plasma surrounding a magnetically collimated arc discharge in order to better understand the nature of transport of a plasma across a magnetic field. One of the earliest studies is the work of Bohm, Burhop, Massey, and Williams.[10] They considered the results of experiments conducted on a small rectangular arc in the pressure range of 0.6 to 2 mTorr in argon. They argued that to preserve charge neutrality a radial ambipolar electric field would be established that would reduce the radial ion diffusion to the same rate as the radial electron diffusion. Their measurements, however, showed a diffusion rate to be two orders of magnitude larger. To explain their observations they concluded that there was an enhanced "drain diffusion" mechanism acting, and proposed what has come to be known as "Bohm" diffusion, where the diffusion coefficient is $D_{Bohm} = (1/16)(ckT_e/eB)$.

Simon and Neidigh[4,17] reconsidered the work of Bohm et al. and concluded that there was no need to introduce enhanced transport to explain those observations. The transport was due to collisional diffusion with a short-circuit effect due to the presence of conducting ends. The electric fields of the plasma, they argued, are effectively shorted out by the presence of conducting ends of the system along the field lines. The ions diffuse across the magnetic field at a rate given by the neutral collisional diffusion coefficient $D_{\perp}^{in}$ unhindered by the electron motion. The ion diffusion along the magnetic field is given by the ambipolar

value determined by equal ion and electron flow along the field lines. Assuming a sinusoidal axial density dependence in a system with an effective length L, we find that the radial density scale length as given by Eq. (2.12) is

$$q = \frac{L}{\pi} \sqrt{\frac{D_{\perp}^{in}}{D_{\parallel}^{in}(1 + T_e/T_i)}} \,. \tag{3.1}$$

In further experiments Neidigh[11] showed that the radial variation of the saturated ion current to a probe (which for constant electron temperature is proportional to the plasma density) was approximately exponential from about r = 1.3 cm to r = 3.4 cm out of a total radius of r = 5 cm. In the pressure range of 1 to 4 mTorr in nitrogen the radial scale length q was, in agreement with theory, proportional to P for a long system $\lambda_{in} \ll L$, and was proportional to $P^{1/2}$ for a shorter system $\lambda_{in} \approx L$, where λ_{in} is the ion mean free path along magnetic field lines. The experimentally determined radial diffusion coefficient is a factor of four larger than the theoretically predicted value if an ion temperature $kT_i = 2$ eV is assumed. However, the ion and electron temperatures and other plasma parameters were not measured, and there is no experimental evidence to determine the accuracy of their estimation. Later experiments and calculations by this and other authors[3,18] indicate that the ion temperature in the secondary plasma is probably an order of magnitude lower. The ion-neutral collisional diffusion coefficient across a magnetic field is proportional to $kT_i^{3/2}$. Using this lower ion temperature increases the discrepancy between the experimental

and theoretical estimates of the radial diffusion coefficient.

Zharinov,[6] from measurements of the currents at the end plates of his arc with a movable probe, postulated that perhaps the electrons were trapped in a potential well produced by the end-plate sheaths and were in Maxwell-Boltzmann equilibrium. He also said that to a first approximation we can consider the ion and electron motion decoupled, with the ions diffusing with their usual collisional rates along and across the field. In this case

$$q = \frac{L}{\pi}\sqrt{\frac{D_{\perp}^{in}}{D_{\parallel}^{in}}} \,. \tag{3.2}$$

Tonks[7] undertook a more general analysis of the problem of plasma transport in two dimensions. He assumed the plasma had constant but unequal ion and electron temperatures, that the plasma was neutral-collision-dominated, that to first approximation the electrons were in Maxwell-Boltzmann equilibrium along field lines, and that the electron flux at the boundary wall of the plasma could be represented as a fixed fraction of the ion current to the wall,

$$\langle nv_z \rangle_{wall}^{e} = \beta \langle nv_z \rangle_{wall}^{i} \,. \tag{3.3}$$

His result reduced to Zharinov's for $\beta = 0$, i.e., electron trapping. For $\beta = 1$, which would correspond to a system with insulating end plates, he obtained

$$q = \sqrt{\frac{\mu_{\parallel}^{in}}{\mu_{\parallel}^{en}}} \frac{L}{\pi} \sqrt{\frac{D_{\perp}^{in}}{D_{\parallel}^{in}}} . \qquad (3.4)$$

The above results are also discussed in review articles by Hoh[19] and Boeschoten.[20]

Yoshikawa and Rose[21] studied the behavior of a hollow-cathode arc in which the field lines are terminated on glass walls outside the region of plasma. They used argon with a neutral gas pressure of the order of 3 mTorr. They measured the current to an annular electrode $I_{\perp}$ as a function of its voltage $V_{\perp}$ for various magnetic fields. The voltage would induce a radial electric field which, because of ion mobility, would cause a radial current to flow. They hoped to see whether the transverse current scaled as n_0/B, as it would in enhanced diffusion, or as n_0^2/B^2, as it would in collisional diffusion (n_0 is the neutral density and B is the magnetic field strength). Their results lay somewhat between the two cases. They did not investigate whether the potential drop between their electrodes was evenly distributed or whether it was confined to the sheath region.

Rothleder[22] conducted a series of experiments on a hollow-cathode arc discharge running into a diffusion chamber 10 cm in diameter and 16 cm long. He made measurements of the radial and axial plasma density profile in the presence of an axial magnetic field of 300 to 1150 gauss. By introducing a probe through a rotating seal and using a cathetometer to position the probe, he made measurements of the axial variation of the plasma density over 4 cm to either side of the midplane. The measurements indicated that the density was uniform to within 10% for

insulating end electrodes and to within 15% for conducting ends. He indicates, however, that the measurements were made at a radius of 2 cm, where the radial density gradient is steep, and that uncertainties in the cathetometer measurements could affect this result. The neutral gas pressure was of the order of 0.5 mTorr Ar, and the electron temperature was measured and found to be 2 to 3 eV, indicating that the dominant radial transport mechanism was fully ionized diffusion.

By using the energy balance equations he was able to fit the form of the observed radial plasma profile for the case with insulating ends. For conducting ends, using a set of concentric ring segmented electrodes, he found that the innermost ring drew a net electron current, while the outer rings drew a net ion current. He was not so successful in fitting the radial profile when conducting ends were used. His experiments were some of the first to measure axial as well as radial dependence of the plasma parameters and to attempt to investigate the effect of the axial boundary conditions on the plasma transport.

Boeschoten and Schwirzke,[12] in an experiment with a duoplasmatron arc running into a diffusion chamber 140 cm long and 20 cm in diameter, showed that indeed the radial density profile was exponential over at least part of the radius and that the radial density scale length $q \approx 1/B$. Because of the finite ion gyro-radius they argue the plasma density can never fall off faster than on the order of the ion gyro-radius. It is possible to distinguish a diffusion-determined distribution only if the system length along the magnetic field is much longer than the ion neutral mean free path $L \geq 20\, \lambda_{in}$.

In further experiments in H_2, He, and N_2 Schwirzke[5,13] finds that $q \approx LP/B$ for a pressure P greater than some critical pressure P_c up to some maximum pressure at which the radial density scale length q reaches a maximum. $P_c \approx 0.8 \times 10^{-3}$ Torr He at B = 1.5 kG. Boeschoten comments that the value of the radial density scale length q is two orders of magnitude larger than the results expected from Simon's short-circuit theory. Moreover, he remarks that the axial dependence of the density is not cosinusoidal, as assumed by the theory, and the reproducibility of the measurements is questionable.[23]

Berkner et al.[3] measured the spatial dependence of the secondary plasma from a hollow cathode arc discharge. They found the axial distribution of their 30-cm-long plasma to be roughly cosinusoidal. Measurements in a Sr-seeded Ar plasma at a pressure of 2×10^{-3} Torr yielded good order-of-magnitude agreement with the Zharinov-Tonks model. The ends of the plasma were terminated with conducting end plates. In the same experiment the Sr ion temperature was measured to be less than 1 eV from the emission spectra in the central arc column and to be 0.1 ± 0.1 eV from absorption measurements at r = 5 cm. This work grew out of extending these measurements to a longer system L = 58.2 cm, where the radial plasma profile should be even more strongly dependent on collisional diffusion.

When this experimental work was begun there had been a variety of other experiments, some that agreed with one theory or another, and some that did not. The agreement or lack of agreement depended on the choice of model, and on the choice of plasma parameters used in analyzing the

experiment. The measurements that had been made were often not sufficiently detailed to determine if the theoretical models had been correctly applied or not. We set out to make a thorough investigation of the transport of a plasma across a magnetic field. By obtaining a lot of information on the behavior of the plasma for several different experimental conditions, the various assumptions of the model for plasma transport could be checked.

IV. THE EXPERIMENTS

A. The Apparatus

The plasma chosen for experimental study is the partially ionized secondary plasma of a magnetically collimated hollow-cathode arc as shown in Fig. 1. The plasma is produced on the axis of the cylindrical diffusion chamber, and drifts and diffuses along and across the magnetic field to form the partially ionized secondary plasma on which the measurements are made.

1. The Arc

An arc discharge is a low-voltage self-sustaining high-current electrical discharge. The arc runs by ionizing a neutral gas--H_2, D_2, He, Ar, or N_2--which is fed through the hollow cathode C_I to the hot 2700-^{o}K tip, where ionization and electron emission take place. The cathode is a hollow tungsten tube 0.476 cm in diameter by 0.076 cm in wall thickness. The arc is struck by running a small high-voltage discharge using a Tesla coil from a probe to the cathode. Once started, the ion bombardment through the cathode sheath maintains the cathode at emission temperatures and the arc is self-sustaining.[24] The arc runs with a gas feed of 3 to 30 cm^3 per minute STP with a total current of 5 to 40 A. The cathode voltage with respect to the anode potential is about -30 to -60 V in Ar and -60 to -100 V in He. The arc is usually run with a current of 10 to 20 A, giving a nominal power dissipation of 1 to 2 kW. The arc runs from the hot tungsten cathode to various electrodes, A_I, E_I, E_{II}, and A_{II}, as shown in Fig. 1, which serve as anodes. There is an axial magnetic field of 300 to 1680 G provided by six

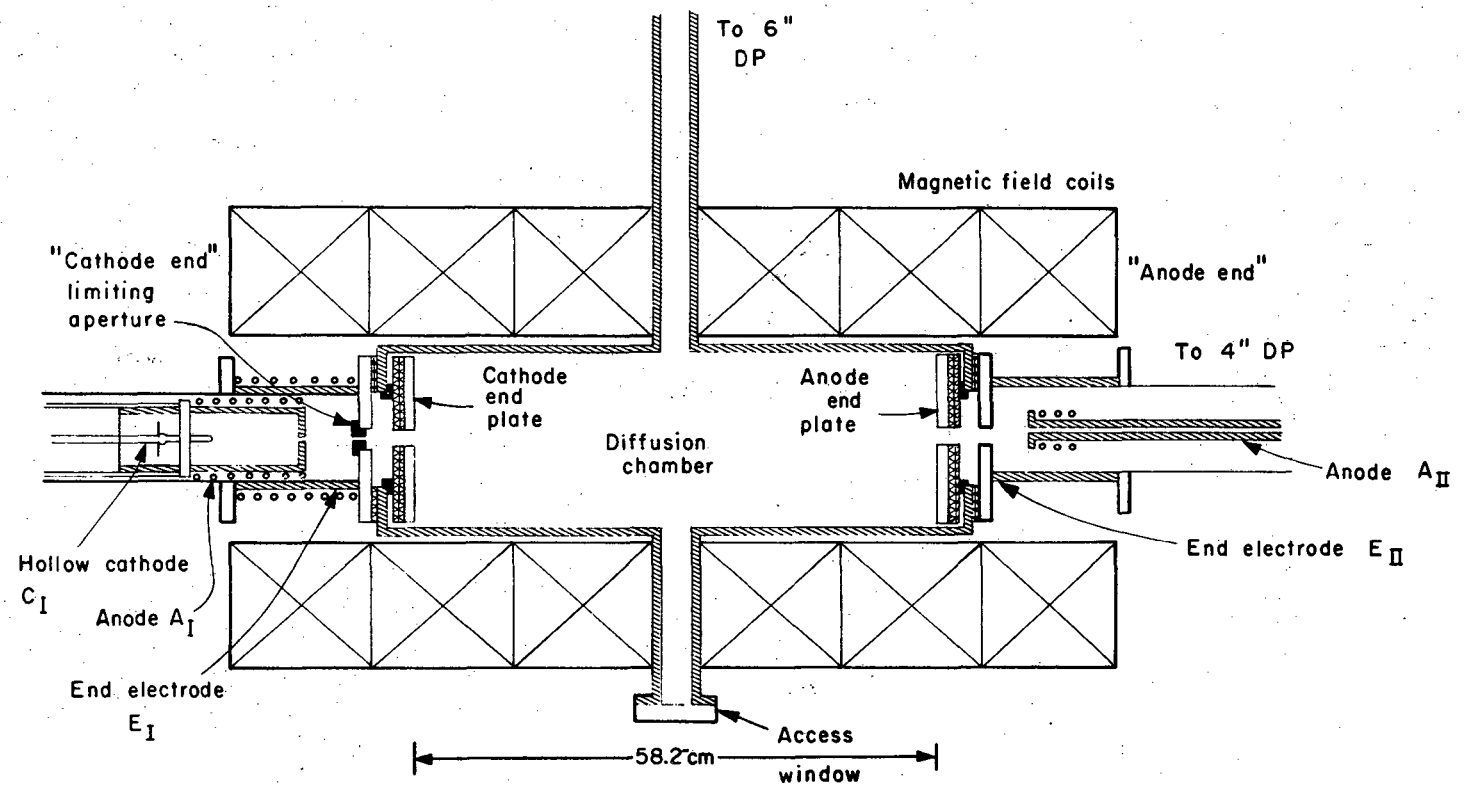

Fig. 1. Hollow-cathode arc discharge facility.

XBL676-3255

modular coils, which serves to collimate the primary discharge of the diffusion chamber.

2. Electrode Configurations

Various electrode configurations were used at different stages of the experimental work. In the first experiments the arc was run from a bare tungsten cathode C_I with the 1.9-cm aperture of the first end electrode E_I serving as primary anode. A large fraction of the total current ran to the first end-plate rings A_1 and C_1 at each end of the diffusion chamber, and to the second end electrode, E_{II}, and anode, A_{II}, at the far end of the system. In this configuration the pressure in the diffusion chamber affected the arc operation, limiting in particular the lowest pressure at which the arc could be made to run to about 1 mTorr in He. The plasma density in the central arc column was quite large, and it was difficult to separate effects and instabilities associated with the cathode region from those associated with the diffusion region.

In later experiments the arc was run with a double cathode. An identical bare cathode assembly was placed at the "anode end." The primary anodes were the end electrodes, E_I and E_{II}, and the first ring at each end plate. It has been observed, when a single cathode was used, that the axial plasma distribution in the diffusion region was shifted toward the "cathode end." The double cathode approach was a brute-force technique to make the axial distribution symmetric.

In final experiments the arc was run with a single cathode with an additional anode A_I with 0.64-cm limiting aperture. A_I is water-cooled and typically receives 50% of the total arc current. The reminaing current follows through the 0.64-cm exit hole in A_I and on to E_I, which

typically receives 30 to 40% of the current. Most of the remaining current is collected on the first end-plate rings. Only of the order of 200 mA of the total current of 20 A is collected at E_{II} and A_{II}. The nominal aperture in the end electrode E_I is 1.90 cm; however, this can be reduced by the insertion of a limiting aperture, 0.16, 0.32, or 0.64 cm in diameter. This reduces the plasma density on the diffusion chamber axis and helps to electrically isolate the diffusion chamber from disturbances in the cathode region. The presence of A_I improves differential pumping, allowing a higher pressure in the vicinity of the cathode while reducing the total throughput of gas and lowering the lowest diffusion chamber pressure at which the arc will continue to run to 0.5 mTorr. The relative positions of the cathode C_I and anode A_I, and the limiting aperture in E_I can be changed while the arc is running.

3. The Diffusion Chamber

The plasma and hot electrons from the arc stream along the magnetic field lines through the apertures in the end electrodes into the diffusion chamber. This produces a highly ionized primary plasma with a particle density of 10^{13} to 10^{14} cm^{-3} on the axis of the diffusion chamber. The electron temperature on the axis is of the order of 5 to 8 eV, as estimated by probe measurements. This is in agreement with the measurements by Lidsky et al.[24] and Hudis et al.[18] The ion temperature on the axis has been estimated to be less than 1 eV from measurements of emission line broadening,[3] which is also in agreement with measurements by Hudis et al. of 0.8 eV.[18]

The diffusion chamber itself is a stainless steel cylinder 64.7

cm long and 20 cm in diameter. At the midplane between the magnetic field coils is a rectangular access port 3.6 by 22 cm. At the front of the port is a Lucite window through which a variety of probes can be inserted and through which visual and spectroscopic observation of the plasma can be made. At each end of the diffusion chamber along the magnetic field lines are five concentric ring electrodes mounted on a ceramic end plate, as shown in Fig. 2. Each of the rings is (ideally) electrically isolated from its neighbor. An electrical connection is brought out of the vacuum through a special seal to a monitor panel where the current and voltage of each ring can be measured. The rings can be floated, grounded, or electrically biased independently in order to affect the axial boundary conditions of the plasma. With the end plates in place the over-all length of the diffusion chamber is 58.2 cm, as is shown on Fig. 1.

The "anode end" and the "cathode end" of the system are each pumped by a 200-liter/sec liquid-nitrogen-trapped mercury diffusion pump. The diffusion chamber itself is pumped from the rear access port by a 1400-liter/sec oil diffusion pump. The base pressure for the system at the "anode" and "cathode" ends of the system is 1 to 2 x 10^{-6} Torr. In the diffusion chamber the higher base pressure of 7 x 10^{-6} Torr is probably due to the use of two epoxy seals for the end plate connection seals and to the numerous sliding vacuum seals. During measurements of the diffusion chamber pressure is maintained at 1 to 10 mTorr by introducing additional neutral gas, controlled by a needle valve, through the access window.

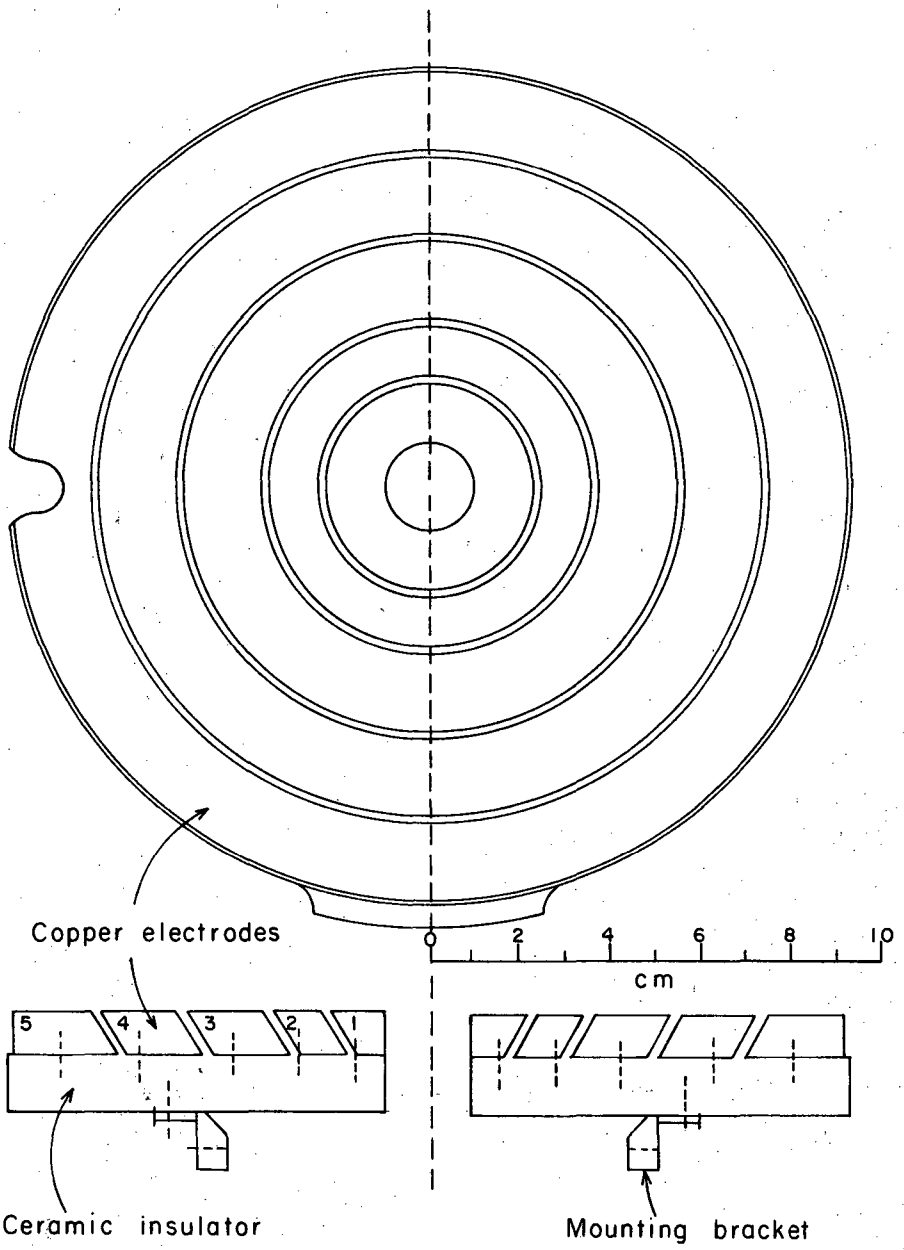

Fig. 2. Concentric ring electrode end plate

4. Magnetic Field

The axial magnetic field is produced by six modular magnetic field coils, 22.9 cm i.d. by 50.8 cm o.d. and 15.6 cm long. The coils have 120 turns each of 1.11-cm square copper conductor with a 0.64-cm-bore water cooling channel. Because of the spacing of the coils, it is necessary to adjust the current through each coil to provide a uniform magnetic field. The next to the last coils at each end are in parallel, with all the other coils in series with them. In addition, a water-cooled shunt resistance is placed across the middle pair of coils to drop the current in these coils by 20%. The result is a field that is uniform within 5% over the 60-cm length of the diffusion chamber. Measurements with a Rawson rotating coil gaussmeter indicate that the field on the center axis at the midplane is 5.60 G/A. Changing the magnetic field configuration by increasing the midplane field by 20% by removing the shunt from the middle pair of coils had no noticeable qualitative effect on the behavior of the discharge or the secondary plasma.

5. Alignment

Great care was taken in the mechanical alignment of the system. A precision alignment telescope was mounted on a solid instrument stand at the anode end of the system. The telescope was set on the center axis defined by the mechanical centers of the anode and cathode end plates, which are positioned by a bracket in the ends of the diffusion chamber. The cathode and anode end electrodes E_I and E_{II} were then installed to this center axis so that everying was in line to within less than 0.05 cm.

Next the system was closed off and the pressure reduced to about 1 Torr. With the magnetic field on, a small glow discharge was struck from the top radial probe, which was placed on the center axis. The position at which this discharge when through the end apertures was observed and the position of each of the magnetic field coils was shifted so that the discharge ran as nearly as possible on the mechanical axis of our system. It is estimated that with this procedure the alignment of the mechanical and magnetic axes of the system is good to within 0.05 cm over the 60 cm length of the diffusion chamber. The alignment telescope was then replaces with a cathetometer telescope with which the cathode and the first and second anodes could be aligned with respect to the end electrode apertures.

B. Langmuir Probe Measurements

Measurements of the plasma have been made by use of Langmuir probes. The probe tips are 0.051-cm tungsten wire extending to 0.2 cm beyond the 0.3-cm quartz sleeve. The tungsten wire runs through a vacuum seal to a coaxial cable running to the measurement circuity. The shank of the probe, a 0.6-cm Pyrex tubing, leaves the vacuum through a 0.64-cm Wilson sliding seal. The electron temperature, as well as the average value and fluctuations of the saturated ion current and probe floating potential, are measured as a function of position, axially, horizontally, and vertically, for a variety of discharge parameters. Probes are introduced into the diffusion chamber from the top and along the magnetic axis at the rear through permanent 0.64-cm Wilson seals, and through a variety of arrangements on the front access port. Figure 3 shows one such arrangement.

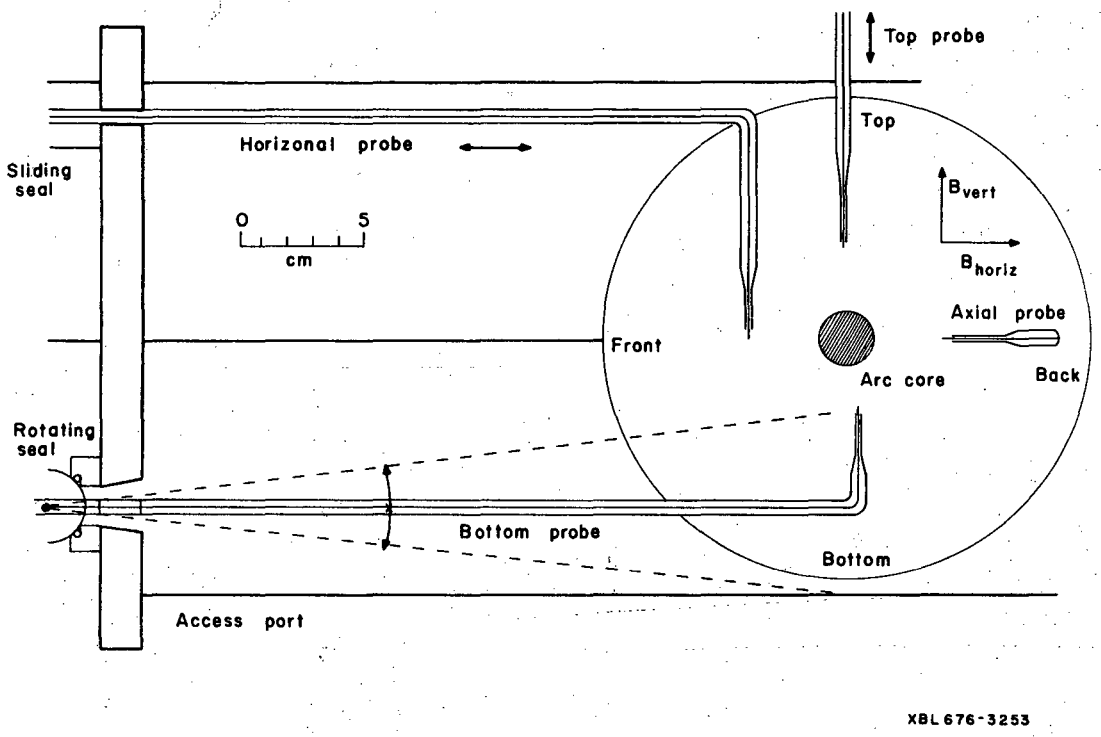

Fig. 3. Probe arrangement at the midplane of the diffusion chamber looking toward the "cathode end" showing probes used to measure azimuthal asymmetry (probes are not drawn to scale).

The probe is driven by a Langmuir probe sweeper chassis, shown in Fig. 4, which provides a low-impedance voltage ramp for the probe. The probe voltage is measured through a 100-megohm resistor to the megohm input impedance of the oscilloscope, giving a 100:1 voltage reduction at the oscilloscope. The current is measured by the voltage drop through a 100-ohm or 1000-ohm resistor R_I to ground potential defined by the anode potential. The complete Langmuir probe curve--probe current as a function of probe voltage, $I(\phi_{probe})$--is displayed on a Tektronix 502A oscilloscope, where it can be photographed. The current drawn by the probe depends upon the local plasma density, the electron temperature, the area and geometry of the probe tip, and the difference in potential between the plasma and the probe $V = (\phi_{probe} - \phi_{plasma})$, as discussed in Appendix B. From the photograph one can read the saturated ion current I_{si}, and by plotting log $[I(V) - I_{se}]$ one can obtain the electron temperature kT_e. The probe floating potential ϕ_f is obtained by connecting the probe directly to a high-impedance voltmeter.

From the values of the saturated ion current and the electron temperature, together with a knowledge of the ion species and the probe collection area, one can deduce the plasma density as given by Eq. (B.3) in Appendix B,

$$n_i = (1.13 \times 10^{12}) \frac{I_{si}}{A_{probe}} \sqrt{\frac{M}{kT_e}} \ \text{cm}^{-3},$$

where I_{si} is in mA, A_{probe} is in mm^2, kT_e is in eV, and M, the ion mass, is in amu.

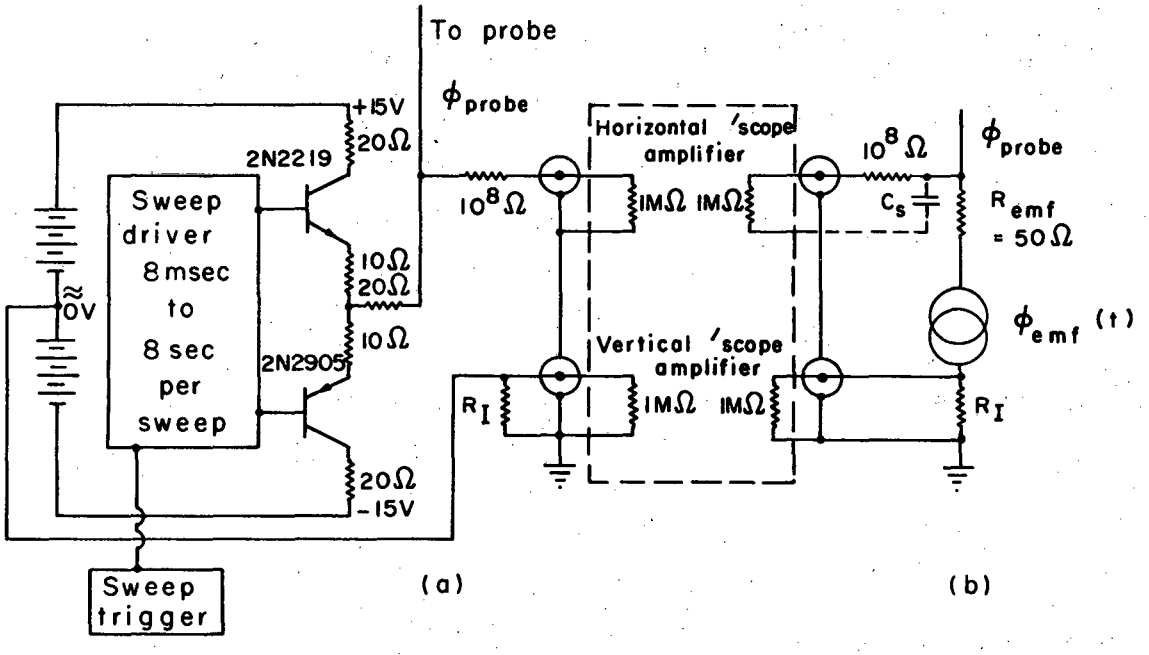

XBL688-3654

Fig. 4. Langmuir probe sweep chassis. (a) Schematic. (b) Equivalent circuit.

For some cases a knowledge of the spatial behavior of the saturated ion current alone is sufficient. In these cases the probe is connected directly to a battery to bias the probe at a fixed voltage, -22.5 V, -45 V, or -67.5 V, well onto the saturated part of the ion current curve. The current path is to ground through a 1000-Ohm resistor. By measuring the voltage drop across the resistor one has a measure of the probe saturated ion current. In the secondary plasma r = 2 to 10 cm, the electron temperature is fairly constant, and the saturated ion current as a function of position provides a reliable estimate of the density profile.

Fluctuations in the plasma density and potential modulate the probe curves as shown in Fig. 37 of Appendix B. Because the potential and density fluctuations are correlated, there is some distortion of the curves. Measurement of the electron temperature from the minimum and maximum of the envelope of the time-varying curve differs by as much as 30%, introducing some uncertainty into the electron temperature measurement. Time-resolved electron temperature measurements obtained by gating the oscilloscope beam show that the actual electron temperature lies between the "minimum" and "maximum" values. This is discussed in Appendix B. The fluctuations in the probe floating potential and saturated ion current at constant voltage are also measured. Time-resolved measurements are made by observing the signals on an oscilloscope. Root-mean-square (rms) average measurements are made with a high-impedance rms voltmeter.

The validity of Langmuir probe measurements in the presence of a magnetic field is also discussed in Appendix B. Although the magnetic

field greatly affects the saturated electron current collected by a probe, in our experiment the ion gyroradius is typically larger than the probe radius, so that the probe ion collection is not greatly affected by the magnetic field.

C. Results

1. Initial Experiments

In our initial experiments we set out to investigate the dependence of the plasma density profile on diffusion chamber parameters such as neutral gas pressure, magnetic field strength, and end-plate boundary conditions. From these observations we had hoped to deduce whether the radial transport of the plasma was determined by collisional diffusion or enhanced diffusion, and to get some measure of the transport rate. Early measurements in argon and helium indicated that the radial density scale length q varies proportionally to 1/B, as would be expected from collisional diffusion.[25]

Measurements of the axial plasma density profile at several radii were found to be similar, indicating that the axial and radial distributions of the plasma are separable.[25] However, the axial profile was found to be asymmetric toward the cathode end. In order to determine if this was a real effect or due to measurement technique, the radial position of the axial probe was checked and found to be at the same radius, to within 0.25 cm, along the 58.2 cm between end plates. No significant variation of the saturated ion current is observed when the external probe support is moved, indicating that the probe is solidly held by the sliding seals. When the arc was run with the cathode and

anode positions interchanged, the asymmetry pattern reversed, again being asymmetric toward the cathode side. The axial asymmetry of the plasma was more pronounced in argon than in helium. When the arc was run with two cathodes, one at each end, the axial profile became symmetric and approximately cosinusoidal. For some of the results presented below the arc was run with two cathodes to insure that the axial profile would be symmetric about the midplane.

While the magnetic field dependence of the radial plasma density profile was indicative of collisional diffusion, the neutral pressure dependence was inconclusive. Both in argon and in helium for some arc conditions the slope of the radial plasma density profile appeared to be more or less independent of neutral gas pressure. This effect was found to coincide with the presence of a radial electric field which was largest at low pressures, where the transport due to diffusion was smallest. It was found that the reproducibility of measurements depended particularly on the cathode alignment.[26] In addition, in argon there was a local region from $r = 4$ to 7 cm where the density profile flattened out, indicating a possible enhanced transport. Schwirzke[13] has observed a similar effect in hydrogen and nitrogen plasmas. This effect was not prominent in helium, which was one of the motivations for our choice of helium in later experiments. Further, we would occasionally observe the slope of the radial density profile to reverse sign at $r = 6$ or 7 cm, indicating that at large radii the density was radially increasing instead of decreasing. This was certainly a peculiar result.

Finally, in our early experiments we had hoped to gain some understanding of the transport processes by controlling the axial boundary conditions by means of our segmented end plates. We observed the radial density profile as we changed the electrode potentials from grounded to electrically floating to strongly negatively biased. No systematic effect was observed, except that when the ends were negatively biased the electron temperature and density in the secondary plasma were higher.[26]

It soon became apparent that electric fields were important in the transport of the plasma, and that before we could understand the dependence of the plasma profile on parameters such as neutral pressure, magnetic field strength, and boundary conditions we would have to understand the transport in detail for a specific set of circumstances. Detailed measurements of the spatial dependence of the plasma density, potential, and electron temperature were made. In each case the arc conditions were optimized by adjusting the gas feed rates, diffusion chamber pressure, and cathode alignment, so that the arc would run stably over the measurement period, and so that the fluctuation amplitude would be as small as possible. Generally the fluctuations were smallest at higher neutral pressure and lower magnetic field values.

2. Detailed Measurements

We present six sets of detailed measurements made under different conditions, which are summarized in Table 4.1.

In Data Set 1 we consider a case in which there is a moderate radial electric field and where the arc is run from a single cathode.

Table 4.1. Data presented, showing discharge conditions for detailed measurments.

Data Set	B (G)	P_T (mTorr)	End conditions	E_r (V/cm)	q (cm)	Cathode	Comments
1	560	4.0	grounded	0.2 ± 0.15	2.3 ± 0.17	single	Moderate radial electric field
2	560	4.0	grounded	0.7 ± 0.15	3.0	double	Azimuthal symmetry
3	560	2.6 1.5	grounded	≈0.25 ≈0.6	2.3	double	Moderate radial electric field
4	1680	2.9 3.9	grounded	1.5 ± 0.3 1.0 ± 0.2	1.25 1.6	double	Large radial electric field
5	560	3.0	floating	0 ± 0.1	1.6	double	No radial electric field
6	560	4.6	floating	~0	1.95 2.2 2.85	single	Azimuthal asymmetry

The end plates are electrically grounded and the neutral gas pressure is 4.0 mTorr He. The axial magnetic field is 560 G. Radial measurements along one azimuth and axial measurements at a radius line were made. In addition to time-averaged measurements of the probe-saturated ion current and potential and the electron temperature, the time-resolved fluctuation measurements in the probe-saturated ion current and potential, and azimuthal electric fields are made. The axial plasma distribution is more or less cosinusoidal, but shifted slightly toward the "cathode end." We shall use these measurements to estimate the over-all particle transport for the ions and electrons.

In Data Set 2 we find that the azimuthal plasma distribution in the grounded-end case is symmetric. Because of the method of making the probe measurements (the probe comes in perpendicular to the radius) and because of the rotation of the plasma due to the radial electric field, there is a shadow effect. Measurements of the plasma density and potential and of electron temperature are made with a neutral pressure of 4.0 mTorr He. The plasma distribution is azimuthally symmetric under these conditions. The fluctuations in the azimuthal electric field are also measured. The axial distribution is assumed to be cosinusoidal. The conditions are quite similar to Data Set 1 except that two cathodes are used, and the radial electric field and density scale length are slightly larger.

In Data Set 3 we consider a case in which there is a moderate radial electric field, and in which the arc is run from two cathodes. The ends of the system are electrically grounded, and measurements of

the average saturated ion current and floating potential are made for two pressures, 1.5 and 2.6 mTorr He. The observed radial electric field is somewhat larger than in Data Set 1.

In Data Set 4 we consider a case in which there is a larger radial electric field owing to the much larger magnetic field, B = 1680 G. Measurements are made for two values of neutral gas pressure, 2.9 and 3.9 mTorr He. The arc is run with two cathodes. A large radial electric field is observed which dominates the radial ion transport.

In Data Set 5 we consider conditions similar to Data Sets 2 and 3. The end electrodes of the system, however, are electrically floating, in which case the radial electric field becomes negligible. The arc is run with two cathodes, with a neutral pressure of 3.0 mTorr He in the diffusion region and with a magnetic field of 560 G. The axial plasma distribution is cosinusoidal, centered at the midplane.

In Data Set 6 we consider the effect of the magnetic and mechanical alignment of the system on the azimuthal symmetry of the plasma in floating-end electrodes. The arc is run from a single cathode with an additional anode A_I and a 0.64-cm limiting aperture in electrode E_I. The neutral pressure is 4.6 mTorr He and the magnetic field is 560 G. Using three probes, we measure the radial variation of the probe saturated ion current (plasma density) and potential along four azimuths. The results show that the plasma in the case of floating-end electrodes is azimuthally asymmetric, with the degree of asymmetry depending critically on the physical and magnetic alignment of the system.

Data Set 1. Moderate Radial Electric Field. Single Cathode.

Time-Averaged Measurements

The arc was run from a single cathode through the 1.9-cm electrode with the end plates grounded and with a magnetic field strength of 560 G in helium. The neutral gas pressure was 4 mTorr. Figures 5 through 8 show the results under these conditions.

The mean plasma density, Fig. 5, shows typical exponential behavior beyond r = 2 cm with an e-folding length q = 2.3 cm. The mean probe floating potential, Fig. 6, is very negative near the central arc column, but becomes positive by r = 2 cm and reaches a maximum at r = 3 to 4 cm. It then falls off slowly to the outside wall. The electron temperature is quite high, kT_e = 7 eV at r = 1 cm, but falls off very rapidly, due to collisions with neutrals, to 0.28 eV at r = 4 cm and is considerably larger than the neutral gas temperature, kT_n = 0.03 eV. When one takes into account the difference between the probe floating potential and the plasma potential due to the finite temperature, Eq. (B.5) of Appendix B, one can estimate the actual plasma potential, which is also shown on Fig. 6. From this we estimate an average radial electric field $E_r = 0.2 \pm 0.15$ V/cm. The large uncertainty in the radial electric field measurement is estimated in the discussion in Appendix D.

In Fig. 7 we see that the axial density profile measured at r = 4.2 cm with a probe at the back of the diffusion chamber can be approximated by $n(z) = n_0 \cos(\pi z/L_{eff})$, where $L_{eff} = L + (4/3)\lambda_{eff} = 64.5$ cm. The entire distribution is shifted slightly toward the cathode end. The

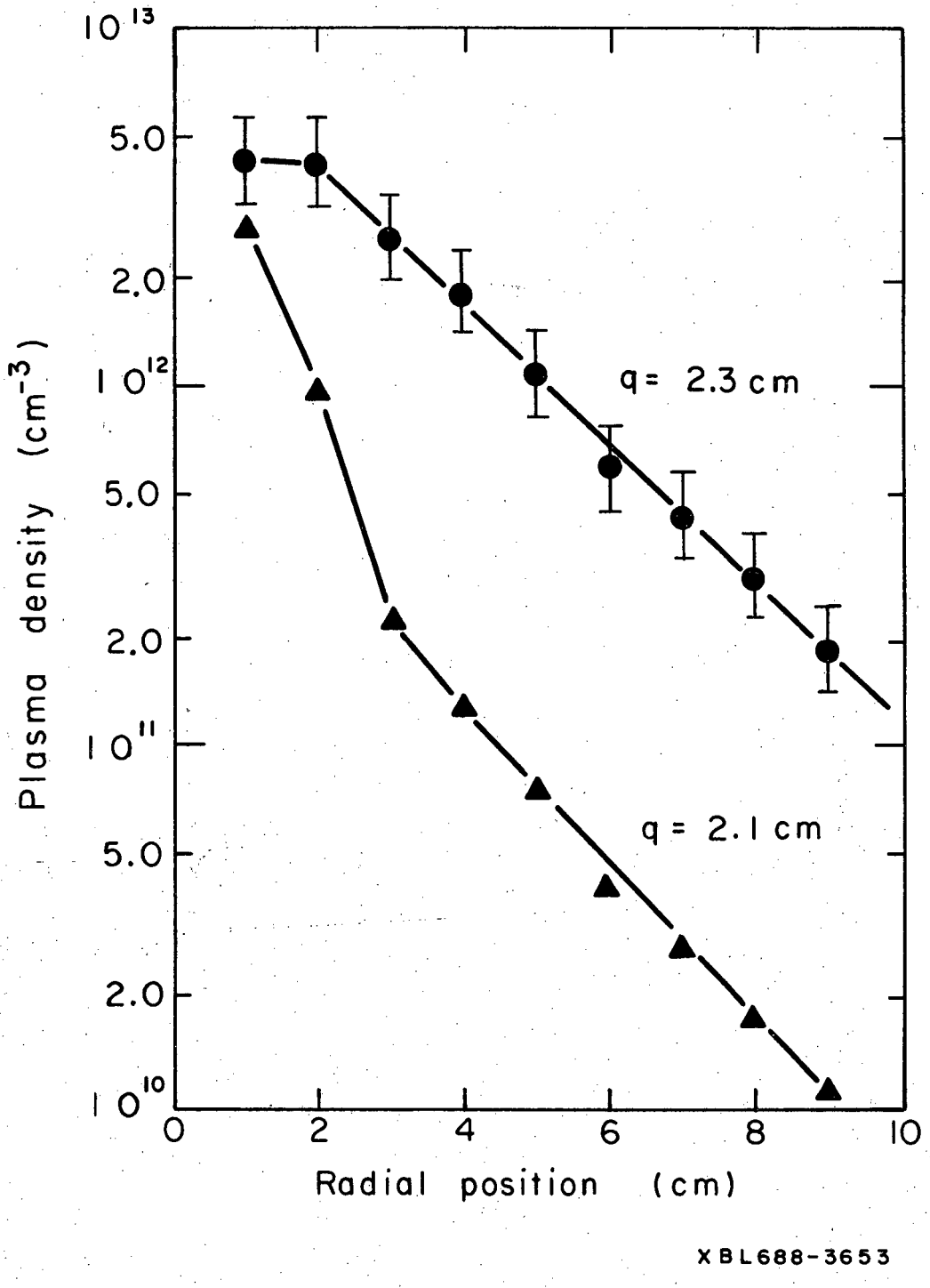

Fig. 5. Data Set 1. Plasma density as a function of radial position showing exponential density variation. ●, Time average density; ▲, rms density fluctuation. B = 560 G. P_T = 4.0 mTorr He. Ends grounded. Single cathode.

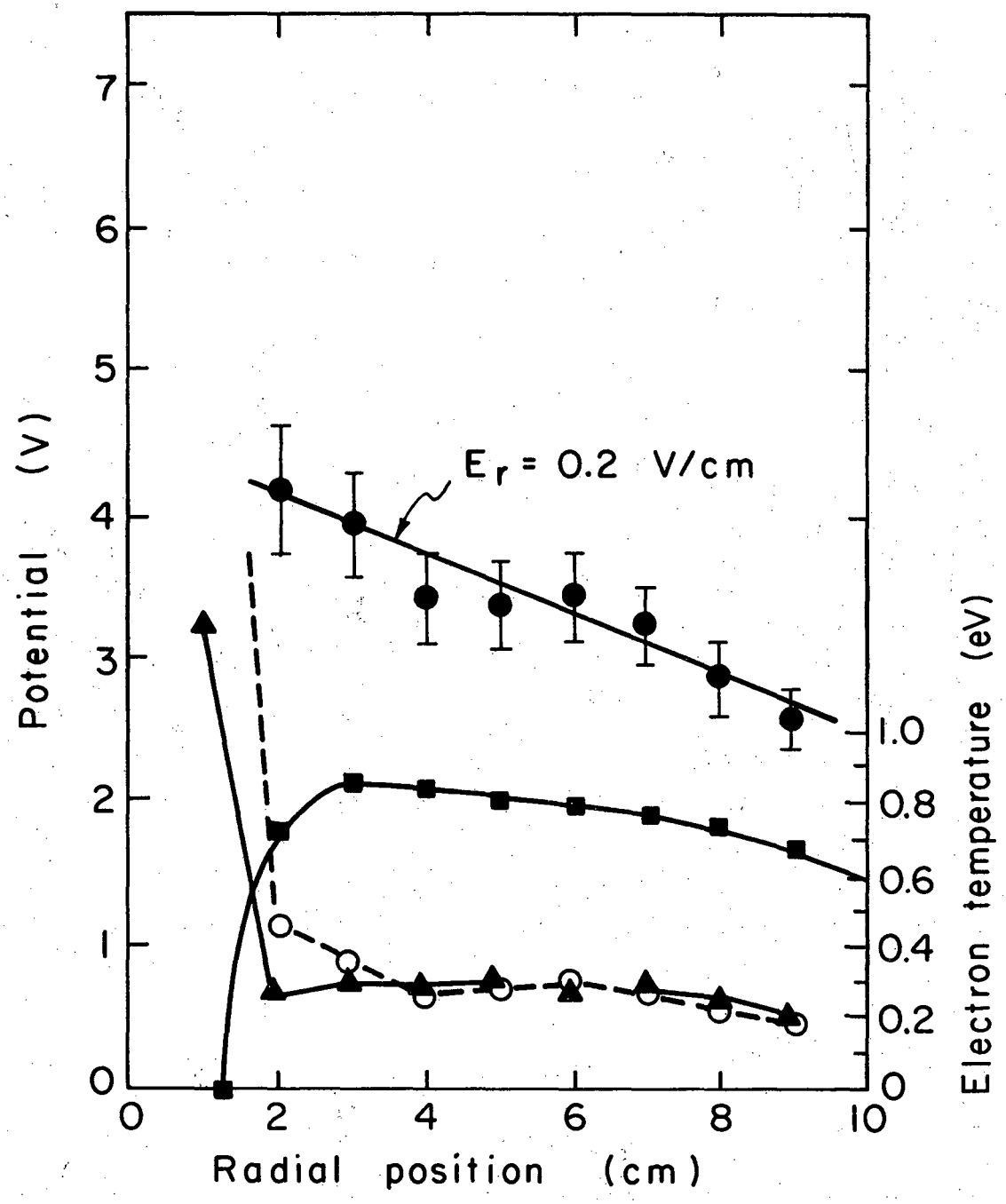

XBL688-3652

Fig. 6. Data Set 1. Plasma potential, probe floating potential and electron temperature as a function of radial position. ●, average plasma potential; ■, average probe floating potential; ▲, rms potential fluctuation; and o, electron temperature. B = 560 G. P_T = 4.0 mTorr He. Ends grounded. Single cathode.

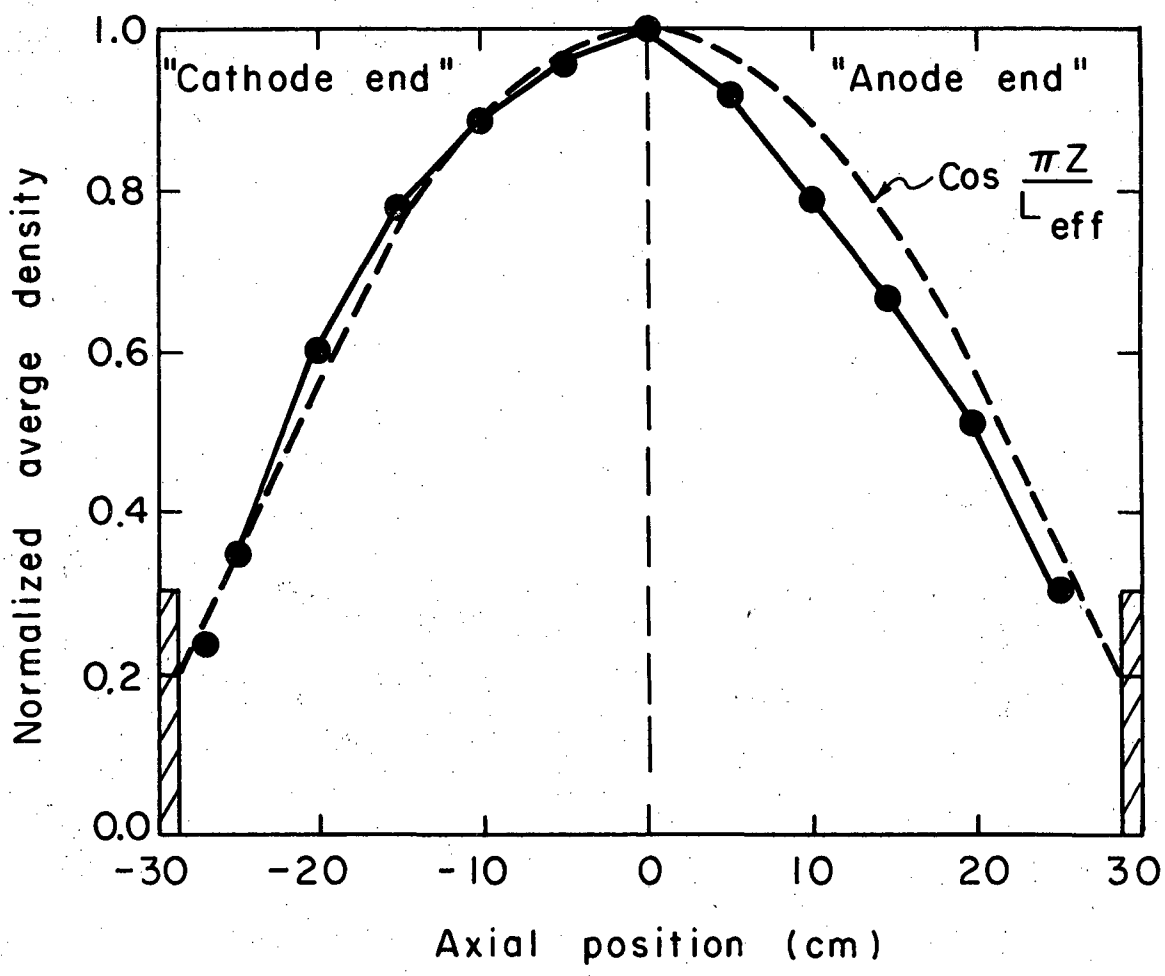

XBL688-3651

Fig. 7. Data Set 1. Relative plasma density as a function of axial position at a radius of 4.2 cm at the rear of the diffusion chamber. L_{eff} = 64.5 cm. B = 560 G. P_T = 4.0 mTorr He. Ends grounded. Single cathode.

electron temperature, Fig. 8, is independent of z within our ability to measure it, and the probe floating potential ϕ_f varies only slightly with z.

The currents and voltages to the various electrodes and end-plate rings were measured before and after the experimental period of 2.5 hours. There is typically some redistribution of the currents during the operation; however, the qualitative distribution of currents did not change significantly. The values of the discharge parameters and boundary conditions are shown in Table 4.2.

The concentric ring end-plate electrodes are all grounded, i.e., tied to the anode potential ϕ = 0 V, and quite typically the first end electrodes C_1 and A_1 will draw a net electron current. Depending on diffusion chamber conditions, neutral pressure, and magnetic field strength, the second end electrode at one or both ends of the system C_2 and A_2 may also draw a net electron current.

Beyond the outside radius of the second end electrode, which is at r = 3.5 cm, the grounded end electrodes consistently collect a net positive ion current. It has been demonstrated that the current collected by the end electrodes is close to the "saturated ion current," i.e., that almost all the electrons are reflected at the end sheath and are not collected at the ends. In Fig. 9 we see the current to ring electrode C_4 at the cathode end, I_{C4}, as a function of ring voltage V_{C4} for a neutral pressure slightly lower than for the above data. All the other end electrodes are grounded. When the electrode is allowed to electrically float it assumes a potential of 3.3 V, which is typical

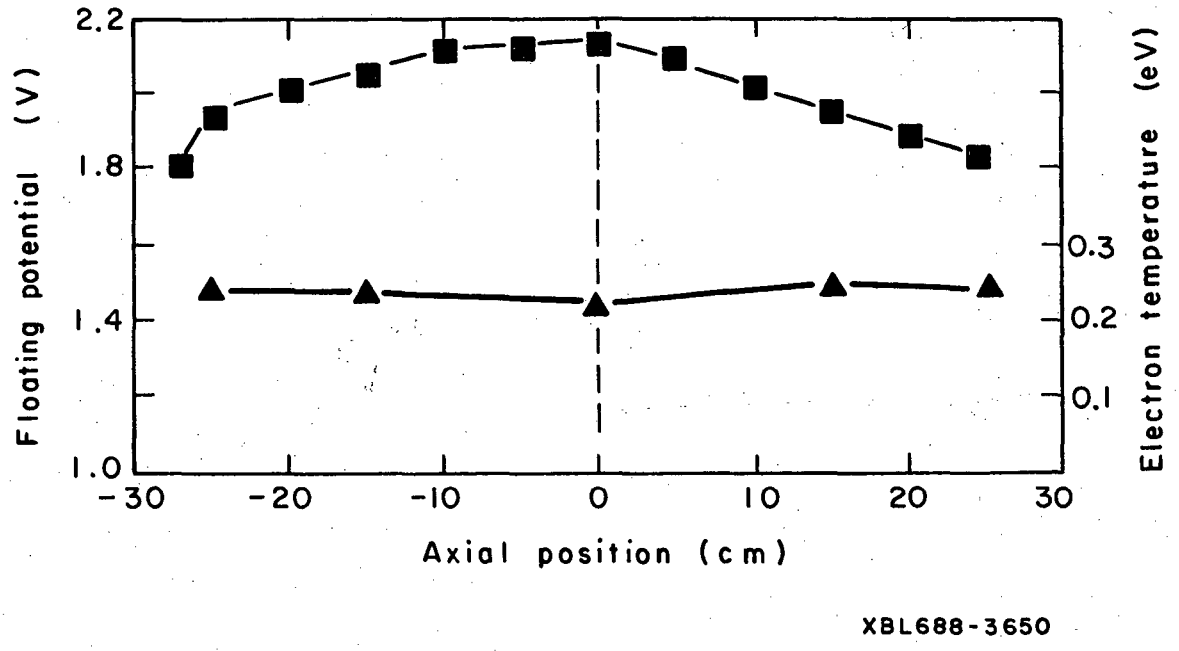

Fig. 8. Data Set 1. ■, Average probe floating potential; and ▲, electron temperature as a function of axial position.

Table 4.2. Data Set 1. Discharge parameters before and after the 2.5-hour experimental period in which the typical data shown in Figs. 6 through 8 and 10 through 14 were taken.

A. Discharge Parameters		Before	After
Magnet current	I_B	100 A	102 A
Discharge current	I_{CI}	19.5 A	19.5 A
Discharge voltage	V_{CI}	87 V	90 V
Chamber pressure	P_T	3.9	4.0×10^{-3} Torr He
Anode end pressure	P_A	3.8	3.8×10^{-3} Torr He
Cathode end pressure	P_C	2.9	2.6×10^{-3} Torr He

B. Boundary Currents		"Cathode end" Before	"Cathode end" After		"Anode end" Before	"Anode end" After
Ring 1	I_{C1}	-2.4 A	-1.4 A	I_{A1}	-3.5 A	-3.0 A
Ring 2	I_{C2}	-0.30	-1.0	I_{A2}	0.20	0.20
Ring 3	I_{C3}	0.30	0.34	I_{A3}	0.13	0.27
Ring 4	I_{C4}	0.085	0.15	I_{A4}	0.03	0.13
Ring 5	I_{C5}	0.03	0.05	I_{A5}	0.03	0.05
Anode electrode	I_{AI}	-4.4	-4.0	I_{AII}	-6.5	-7.8
End electrode	I_{EI}	-2.1	-1.9	I_{EII}	-0.9	-1.6
Chamber wall current	I_T	0.015	0.03			

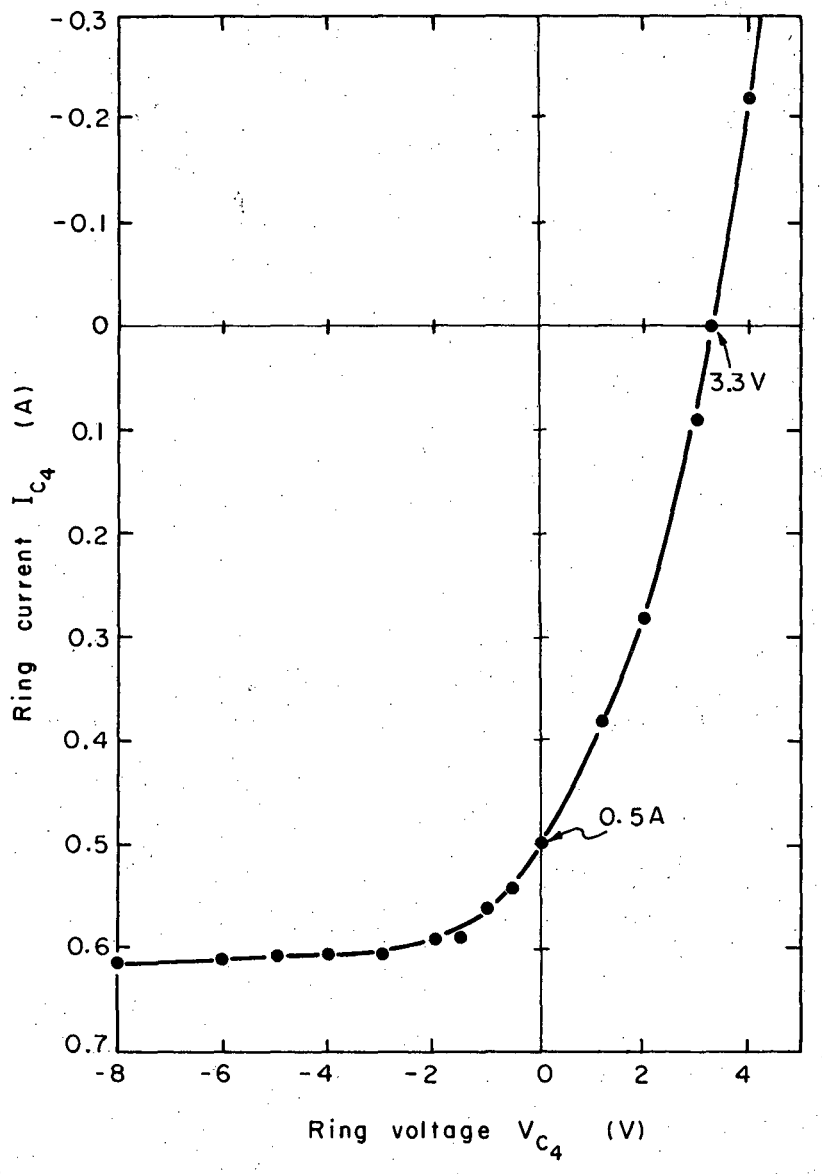

XBL688-3649

Fig. 9. Current to cathode end-ring electrode C_4 as a function of electrode voltage V_{C4} with all other end electrodes grounded. P_T = 1.9 mTorr He, B = 560 G. The curve shows that most of the electrons of the plasma are reflected. kT_e = 0.08 eV, from the shape of the curve. The ring electrode C_4 extends from r = 5.4 to r = 7.3 cm.

of the probe floating potential under these conditions. At zero volts the ring draws 0.5 A. As the ring is made more negative the ring draws the saturated ion current of 0.6 A. The indicated electron temperature is of the order of 0.8 eV, which is somewhat larger than we would expect under these conditions. The ratio of electron current to ion current collected at the end wall at zero voltage is of the order of $\beta = 0.2$. This is about an order of magnitude larger than we would expect from considering the reflection of electrons by the measured sheath potential drop, as discussed in Section V.D below. We have no detailed information on the effect of varying the ring voltage V_{C4} on the plasma distribution as a whole. Some of the increase in current with the application of a negative voltage may well be due to increased radial transport of the plasma.

There is further evidence for the presence of an electron reflecting sheath. In Fig. 8 we see that the floating potential of a probe at z = 27 cm is about 1.8 V. The end wall is at z = 29.1 cm and is at zero potential. The potential drop across this remaining distance is sufficient to effectively reflect almost all the electrons, whose mean energy is only 0.24 eV, and effectively trap them in the volume of the plasma.

As we are primarily interested in the transport of the plasma in the volume of the plasma, the axial measurements over the 50 cm about the midplane of the system are sufficient to determine the shape of the axial distribution. Measurements made near the walls show that the plasma density continues to fall off to zero as one approaches the

end wall, although the slope becomes noticeably steeper with the last ion-neutral mean free path from the wall. Measurements made to within 0.5 cm of the end wall, where the plasma density has fallen to 22% of its midplane value, show that the probe floating potential has not yet fallen off appreciably, indicating that most of the potential drop occurs at the sheath.

If the electrons are trapped axially long enough to experience several collisions, they establish an approximate Maxwell-Boltzmann equilibrium along the magnetic field lines in agreement with the model of Zharinov[6] and Tonks.[7] One should then expect the axial plasma distribution to have the form

$$n(z) = n_0 \exp\left\{ e[\phi(z) - \phi_0]/kT_e \right\} ,$$

and indeed we find in Fig. 10 that there is this type of relationship. The electron temperature estimated from the observed slope of the density as a function of floating potential is consistent with the measured value of $kT_e = 0.28$ eV. For such a distribution there is an axial electric field which limits the electron current along the magnetic field lines to a quite small value. The axial electric field will be of the order of

$$E_z = -\frac{kT_e}{e}\frac{1}{n}\frac{\partial n}{\partial z} = \frac{\pi kT_e}{Le} = 0.013 \text{ V/cm.}$$

Similar results have been obtained under other experimental conditions.

In Table 4.2 one also notes that the ring electrode currents to

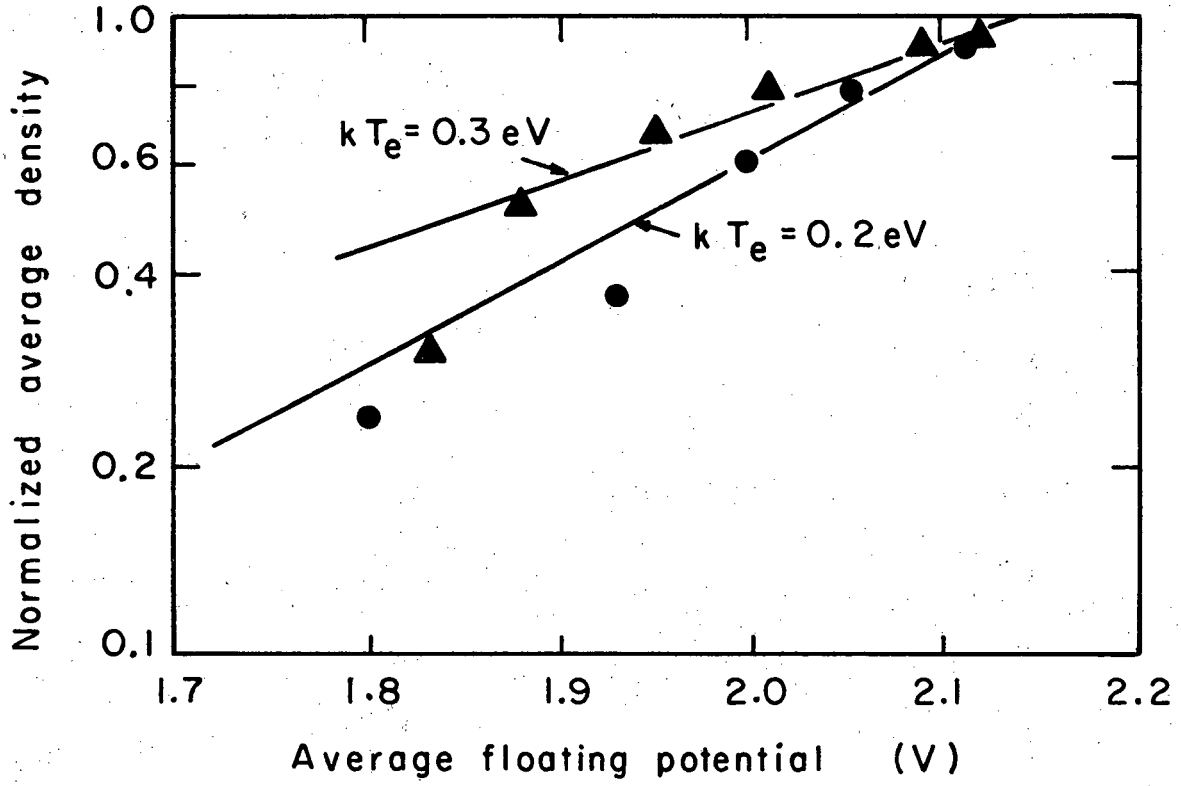

XBL688-3648

Fig. 10. Data Set 1. Relative plasma density as a function of probe floating potential for the axial measurements: ▲, at the "cathode end," ●, at the "anode end." The electron temperatures estimated from the slopes of the lines are 0.2 and 0.3 eV. The measured electron temperature is kT_e = 0.28 eV. ϕ_0 = 2.13 V.

the "cathode" and "anode" ends of the diffusion chamber are not identical. For a single cathode discharge the ion currents tend to be slightly larger to the "cathode" end and the electron currents are larger to the "anode" end. This is probably due to the fact that, since the plasma source is at the "cathode" end,and the mean free path for ion-neutral collisions along the field lines is short, $\lambda_{in} \approx 1.15$ cm (see Appendix A, Table A.1), there is a tendency for the plasma distribution to be skewed toward the source end, as indicated in Fig. 7. Unless the radial transport is slow, the distribution does not have sufficient time to fill out to a perfectly axially symmetric distribution. At lower pressures the axial distribution is noticeably flatter; however, the asymmetry remains.

Fluctuation Measurements

Measurements of the fluctuations in the plasma density, probe floating potential, and electric fields have been made. Before starting the experiment the conditions of the arc, cathode alignment, gas flow rates, and neutral gas pressure were adjusted to minimize the fluctuation levels. The radial behavior of the root-mean-square value of the fluctuations of the density and potential fluctuations are indicated on Figs. 5 and 6 respectively. The fluctuations are typically large near the core of the arc, with the amplitude falling off rapidly as one goes out in radius. It is necessary to measure the fluctuations in order to determine their effect on transport. In early experiments a survey of the fluctuation spectrum was made by using a Panoramic Ultrasonic 0- to 300-kHz Analyzer. It was found for most arc conditions

that oscillations were confined to a few discrete frequencies. Because the phase relationship between the density and potential fluctuations were found to be important, it was decided to make time-resolved measurements.

In Fig. 11 we see the time behavior of the fluctuations for various radial positions. The top trace of each photograph (also on subsequent Figs. 12 and 13) is the potential of a reference probe ϕ_{ref} placed at approximately r = 4 cm at the bottom of the diffusion chamber at the midplane. The middle trace is the fluctuation of the saturated ion current to one tip of a double probe, and the bottom trace is the potential fluctuation of the saturated ion current to the other tip. The dotted appearance of the bottom two traces is due to chopping between the two signals in the oscilloscope preamplifier. Only the fluctuating part of the signal has been recorded.

There is a fluctuation in both the Langmuir probe potential and the saturated ion current at about 48 kHz. At r = 1 cm it is very large; the ion current fluctuation is about 10.5 mA rms out of an average current of 16.2 mA; and the potential fluctuations have an amplitude of 3.2 V rms. Although the fluctuations at 48 kHz are apparent all the way out to r = 9 cm, the amplitude drops off very quickly with radius, so that at r = 3 cm the rms density fluctuation is less than 10% of the mean density, and the potential fluctuation is less than 1 V rms. The potential and density fluctuations in the central arc column are of large amplitude, and clearly an m = 1 azimuthal perturbation. The phases of the potential and density fluctuations

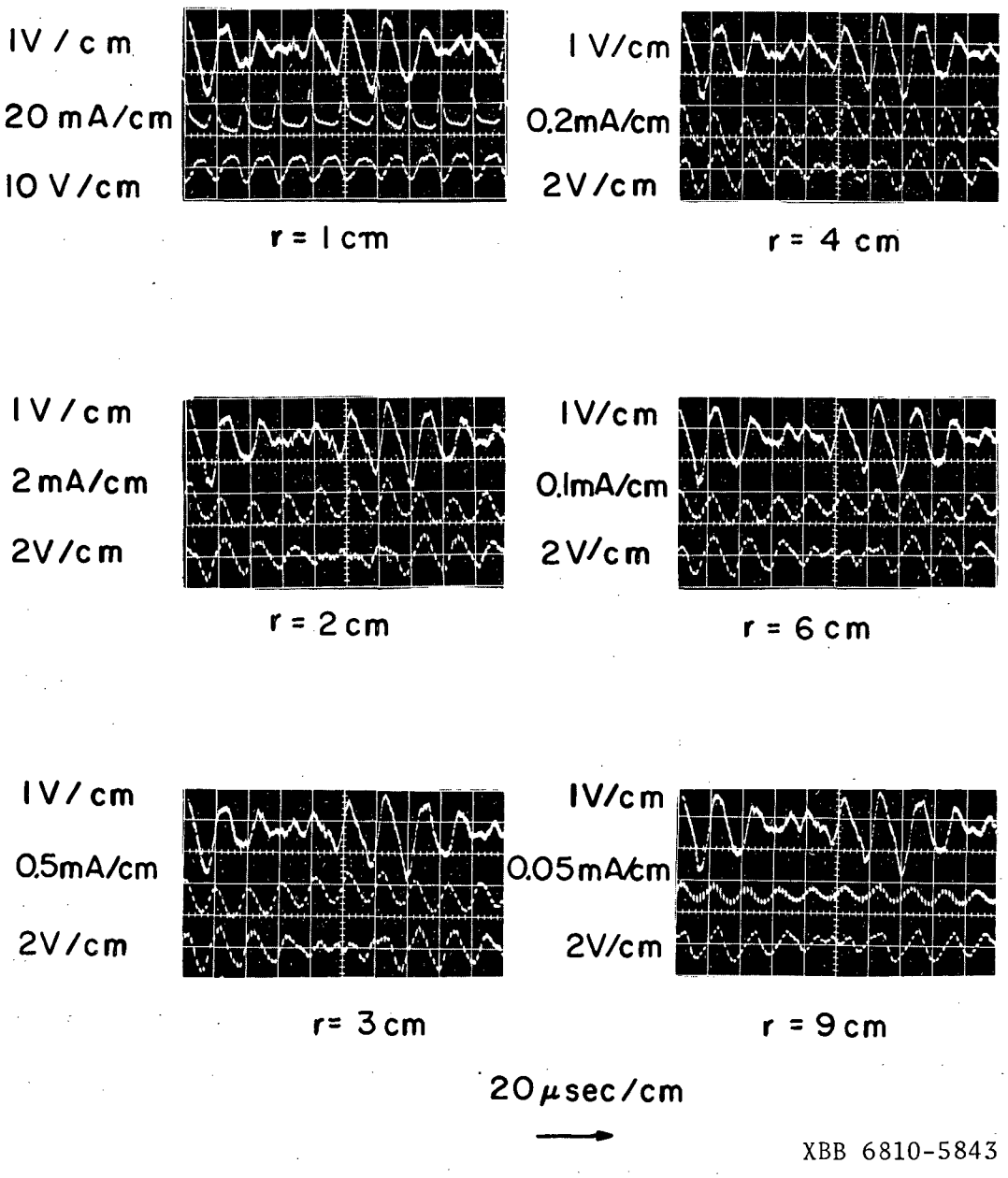

Fig. 11. Data Set 1. Time resolved measurements of the fluctuating part of the Langmuir probe saturated ion current and probe floating potential as a function of radial position measured with a double probe introduced radially through the front access window. In each photograph the upper trace is ϕ_{ref}, reference probe floating potential, from a probe at about r = 4 cm at the bottom of the diffusion chamber. The middle trace is the saturated ion current fluctuation and the bottom trace is the probe potential fluctuation.

with respect to the signal from a reference probe in the secondary plasma change with radius near the core, but are independent of radial position beyond a radius of 2 cm. In the secondary plasma the phase relationship between the potential and saturated ion current fluctuations is clearly defined when the potential fluctuation is of large amplitude. The maximum of the density perturbation in the secondary plasma is about 1/8 of a cycle or 45 deg earlier in time than the maximum of the potential fluctuation.

The Langmuir probe saturated ion current was indicated by the voltage signal across a low-inductance metal-film precision resistor. The measurement signals from the probes were run to the oscilloscope on idential cables. When potential signals from the double probe aligned along the magnetic field lines were displayed, the signals were in phase within our ability to measure them, which is within about 15 deg. The error in phase measurements introduced because of phase shift in the electronics is smaller than our ability to measure the phase. There is also a low-frequency amplitude modulation of the 48-kHz potential fluctuation, which propagates azimuthally in the secondary plasma with a frequency of 3.1 kHz. In Fig. 11 at r = 4 cm the minimum amplitude of the potential fluctuation on the reference probe is 30 μsec earler in time than the minimum amplitude of the potential fluctuation on the radial probe at the front at the same radius. A mass rotation of the plasma at this frequency due to $E_r \times B_z$ drift motion would require a radial electric field of only $E_r = -0.014$ V/cm. The observed radial field is $E_r = 0.2 \pm 0.15$ v/cm

and is in the wrong sense, so that mass rotation is probably not the origin of this effect.

The 3.1-kHz modulation is observed to be in phase along a radius at the same azimuth in the secondary plasma, as shown in Fig. 11, and repeats itself with remarkable consistency. The effect was also observed on more than one day. When the amplitude of the potential fluctuation is large there is a clear phase relationship between the fluctuation in the saturated ion current (plasma density) and the potential fluctuation to a probe at the same position in the secondary plasma. However, when the amplitude of the potential fluctuation is small, the phase between the ion current and potential fluctuations becomes uncertain, as can be seen in Fig. 11.

Other observations indicate that the amplitude modulation originates in the central arc column. The 48-kHz density and potential perturbation of the central column is not a simple m = 1 rotation, but changes in amplitude with azimuth. The position of the maximum amplitude of the perturbation in the central arc column rotates azimuthally with the 3.1-kHz frequency, which is also observed in the secondary plasma. The oscillation of the central arc column, from our discussion in Sec. V.F, is most likely a drift instability driven by a density or temperature gradient, and the amplitude to which it grows depends sensitively on the detailed behavior of the plasma. Modulation of the amplitude of the oscillation for such a complex system is not unlikely.

The potential density fluctuations are well correlated along the magnetic field lines. Figure 12 shows the probe potential fluctuations

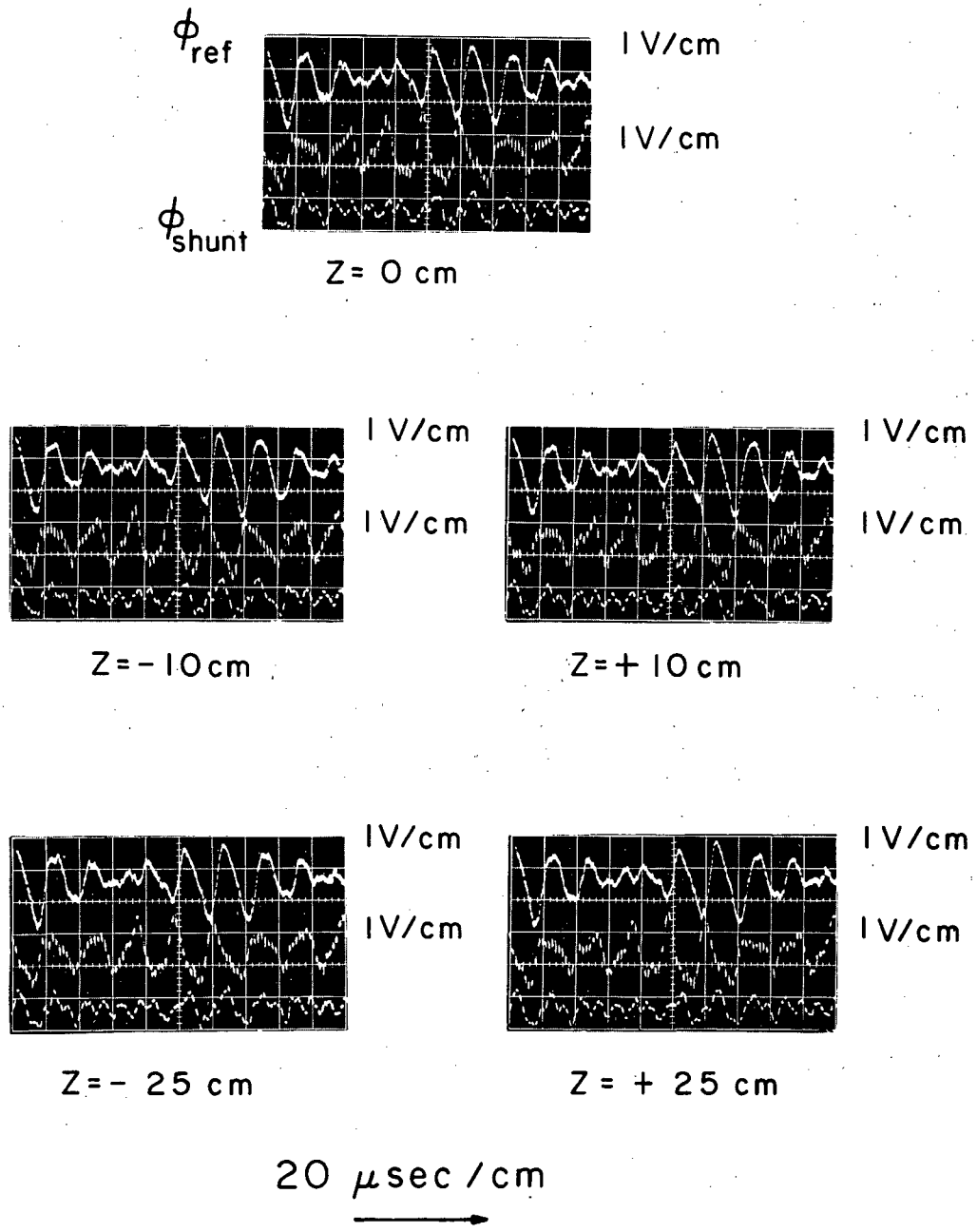

Fig. 12. Data Set 1. Time resolved measurement of the fluctuating part of the probe floating potential as a function of axial position showing that the potential fluctuations are independent of axial position. Upper trace in each photograph shows the reference probe floating potential fluctuation, ϕ_{ref}, and the middle trace shows the potential fluctuation on the axial probe at r = 4.2 cm. The lower trace shows the potential drop across the current shunt to electrode A_{II} used as a phase reference, ϕ_{shunt}.

(the middle trace on each photograph) for various axial positions. The top trace is the reference potential, ϕ_{ref}, the same as in Fig. 11, and the bottom trace is the voltage signal appearing across the first anode current shunt; they are used as phase references. The phase and amplitude of the potential fluctuation is essentially unchanged as one moves the probe from z = -25 cm to z = +25 cm. In Fig. 13 the middle trace is the saturated ion current fluctuation as a function of axial position. Although the amplitude is slightly smaller near the ends, the phase of the fluctuations is constant along the magnetic field lines. The axial wavelength $1/k_z$ is much greater than the length of our system L. By comparison of Figs. 12 and 13 we see that the maximum of the density perturbation at 48 kHz again appears to be about 45 deg ahead of the maximum of the potential fluctuation, an agreement with the radial measurements in Fig. 11.

Because the phase of the potential fluctuation varies with azimuth, there is an azimuthal fluctuating electric field. We observe this electric field E_θ by measuring the potential difference between the tips of a double probe spaced a distance d = 0.7 cm apart. In Fig. 14 the lower trace of each oscillograph shows the time variation of the floating potential on one-half of the double probe compared with the upper trace, which is the difference in potential between the two tips. The measurements are made for various radial positions. When the two probes are aligned transverse to the magnetic field, this difference gives us a measure of the transverse electric field E_θ x d. The frequency of the azimuthal electric field is 48 kHz. Although the

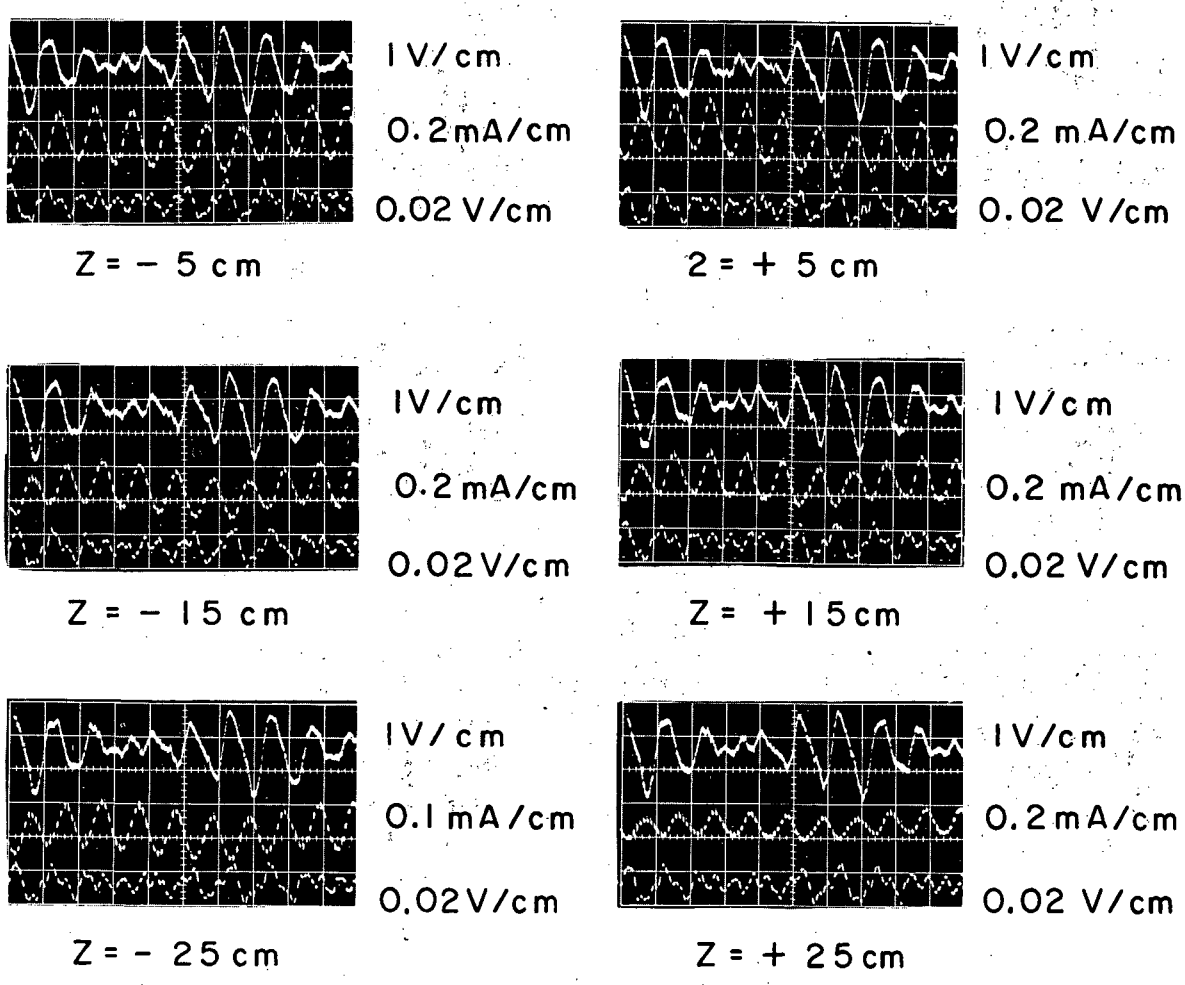

Fig. 13. Data Set 1. Time resolved measurement of the fluctuating part of the saturated ion current showing that the phases of the fluctuations are independent of axial position. The upper trace in each photograph is the reference probe potential fluctuation ϕ_{ref}. The middle trace shows the saturated ion current to the axial probe at a radius of 4.2 cm. The lower trace is the electrode A_{II} shunt potential drop ϕ_{shunt}.

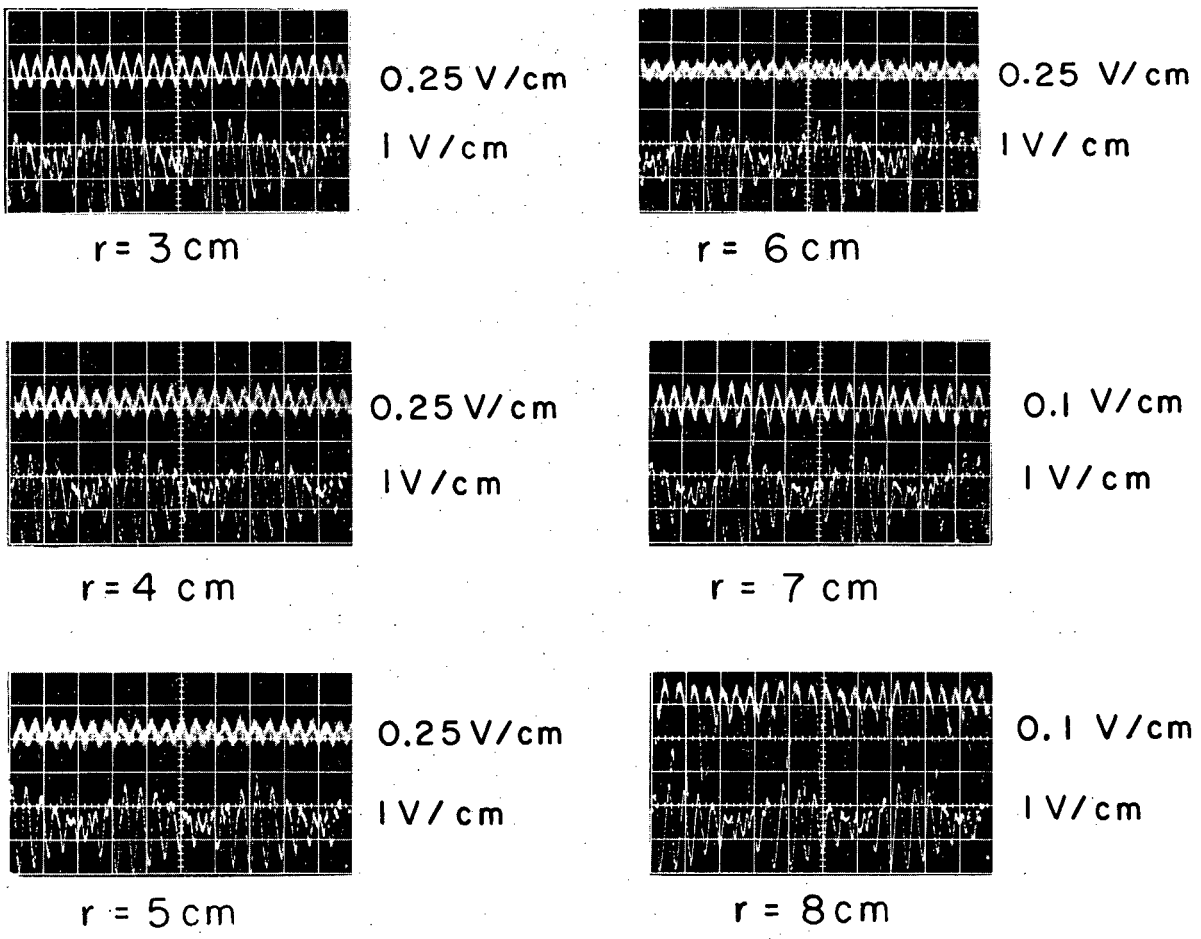

Fig. 14. Data Set 1. Time-resolved azimuthal electric field as a function of radial position. The upper trace is the potential difference, $\phi_A - \phi_B = E_\theta \times d$, between two probes a distance d = 0.7 cm apart perpendicular to the magnetic field, introduced radially through the front access port. The lower trace is the potential on one of the probes ϕ_A.

amplitude of the potential fluctuation is modulated at 3.1 kHz there is no observed amplitude modulation of the azimuthal electric field.

At a radius of r = 4 cm the potential difference is 0.25 V peak to peak, as indicated in Fig. 14. This gives us an azimuthal fluctuating electric field of 0.36 V/cm peak to peak or E_θ = 0.12 V/cm rms. From the rms potential measurement at r = 4 cm shown in Fig. 6 we find that $\delta\phi$ = 0.72 V rms, which for an m = 1 instability would give rise to E_θ = 0.18 V/cm rms. However, because the potential fluctuation in this experiment is modulated at 3.1 kHz and the measured azimuthal electric field is not modulated, it is not certain the rms azimuthal electric field is simply related to the rms potential fluctuation. It does, however, give an estimate which is the right order of magnitude. We shall assume that the direct measurement of the azimuthal electric field is more reliable, and estimate that the uncertainty in the electric field measurement is of the order of 30%. As there is no observed azimuthal electric field associated with the 3.1-kHz amplitude modulation, this modulation does not produce convective transport of the plasma, and should not significantly affect the macroscopic plasma transport.

The maximum of the electric field, i.e., the maximum of the potential difference, appears to be 90 deg earlier in time than the maximum of the potential fluctuation. Figure 15 shows the measurement of the fluctuations in the axial and azimuthal electric fields compared with the potential fluctuation at the same position at a radius of 4 cm for experimental conditions similar to the preceding data but in the absence of the low-frequency amplitude modulation. When the double

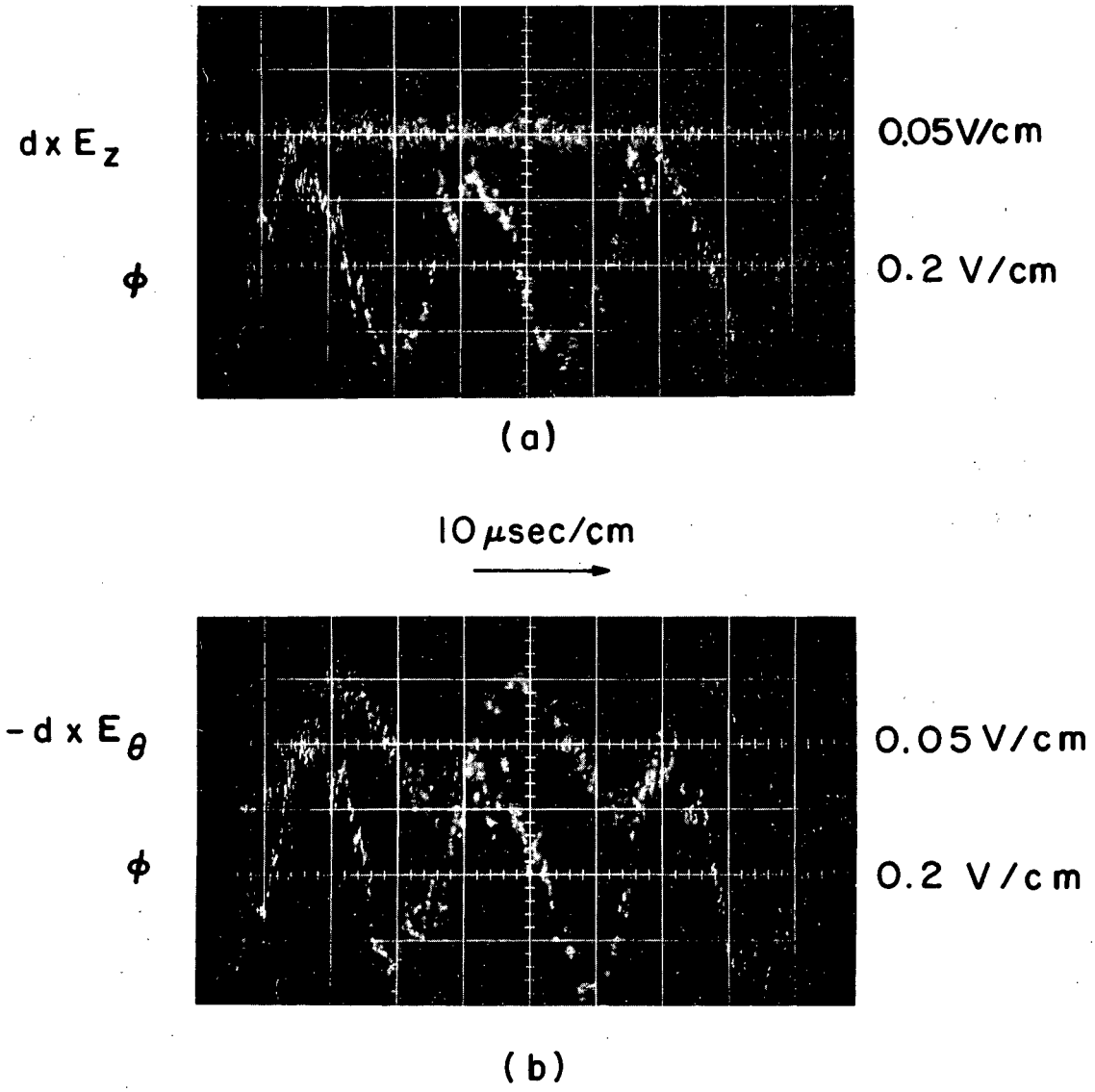

Fig. 15. Data Set 1. Time-resolved electric field measurements. (a) The upper trace shows the potential difference between the two probes aligned along the magnetic field lines, E_z x d. (b) The upper trace shows the potential difference between the two probes perpendicular to the magnetic field $-E_\theta$ x d. The maximum of the azimuthal electric field is 90 deg earlier in time than the maximum of the potential fluctuation, which is shown in the lower trace.

probe was aligned along the magnetic field there was no perceptible fluctuation in the 50-kHz range, as shown in photograph a. This indicates that there is no axial electric field fluctuating at the principal frequency. When the double probe is aligned transverse to the magnetic field, we see a definite azimuthal electric field, as shown in photograph b. The maximum of the electric field is 90 deg earlier in time than the maximum of the potential fluctuation. The measured azimuthal electric field is E_θ = 0.2 V peak to peak, which agrees with the electric field estimated from a m = 1 potential fluctuation with an amplitude of 0.8 V peak to peak at a radius of r = 4 cm.

In addition to the fluctuations in the 50-kHz range, there is also a small-amplitude high-frequency noise at frequencies greater than 1 MHz. This is particularly evident in Fig. 15. The presence of high-frequency fluctuations is discussed further in Sec. IV.C.4 below. It is typically an order of magnitude smaller than the lower-frequency fluctuations. Although it may contribute slightly to electron heating, because it does not seem to be correlated with density fluctuations and because enhanced diffusion is largest for low frequencies, as is shown by Eq. (C.32) in Appendix C, the effect of these high frequencies on transport should be negligible.

In summary, in the results of the Data Set 1 we find that the radial density profile falls off with a scale length q = 2.3 ± 0.17 cm. [The Zharinov-Tonks model, Eq. (3.2) for these conditions predicts q = 2.7 cm, and the Simon model, Eq. (3.1) predicts q = 5.5 cm.] The electron temperature in the secondary plasma is of the order of

kT_e = 0.28 eV and is uniform along magnetic field lines. There is a radial electric field E_r = 0.2 ± 0.15 V/cm. The axial density distribution is approximately cosinusoidal, with an effective length L_{eff} = 64.5 cm. In the secondary plasma there are electron-reflecting sheaths at the ends which tend to trap the electrons so that they are more or less in Maxwell-Boltzmann equilibrium along field lines.

There is a fluctuation of the plasma potential and density at 48 kHz driven from the central arc column. The potential fluctuation is of the order of 0.7 V/cm rms, and the density fluctuation is of the order of 7% in the secondary plasma. There is a fluctuating 48-kHz azimuthal electric field, E_θ = 0.12 V/cm ± 0.04 V/cm rms at r = 4 cm, whose phase is 90 deg earlier in time than the potential fluctuation, and which is 45 deg out of phase with the density perturbation. The fluctuations are well correlated along magnetic field lines.

Data Set 2. Azimuthal Symmetry. Two Cathodes. Grounded Ends.

To determine if the plasma distribution is azimuthally symmetric in the case of grounded end electrodes, where there is a moderate radial electric field, a set of measurements of the Langmuir probe saturated ion current as a function of radial position was taken at four azimuths, by using the probe configuration shown in Fig. 3. The results are shown in Fig. 16. The horizontal profile taken for a magnetic field of 560 G indicates that the density at the front is about 20% lower than at the back. The tip of the horizontal probe is perpendicular to the chamber radius. Because of the presence of an outward radial electric field when the end electrodes are grounded, the plasma

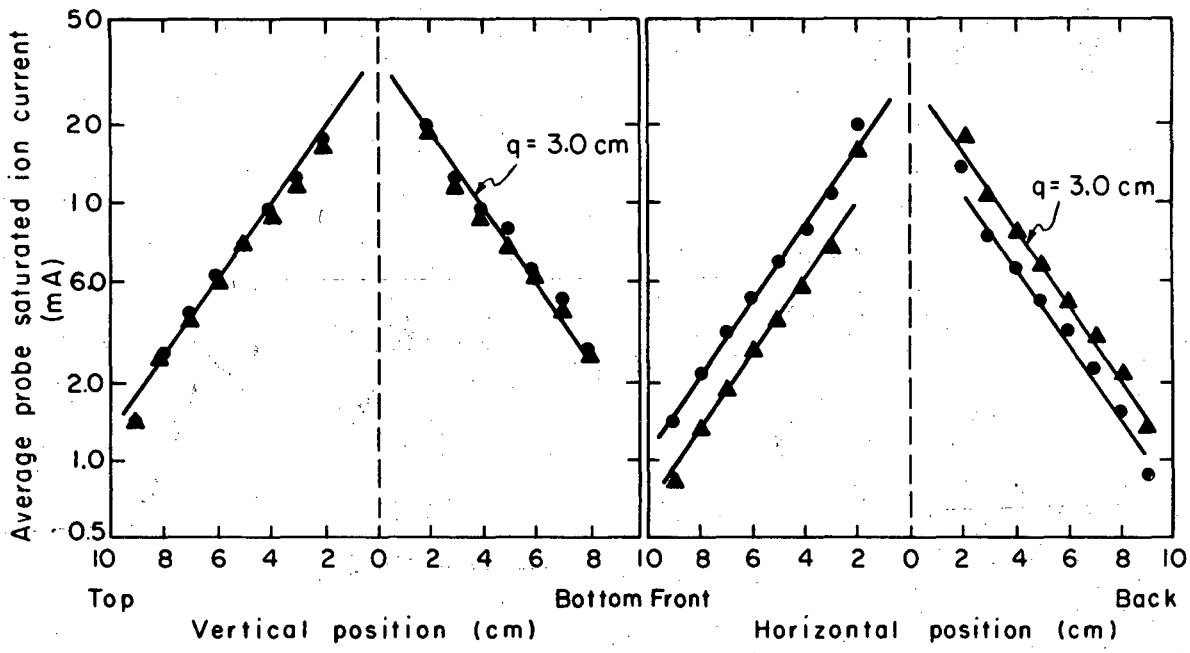

Fig. 16. Data Set 2. Saturated ion current as a function of vertical and horizontal position for two directions of the magnetic field, showing the effect of plasma rotation on probe measurements. P_T = 4.0 mTorr He. Two cathode ends grounded. ▲, B = 560 G; ●, B = -560 G.

as a whole tends to rotate in the counterclockwise direction as seen looking toward the "cathode end." The quartz sleeve on the probe tends to shield the tip of the probe somewhat from the plasma and reduce the ion collection by the probe.

If one reverses the direction of the axial magnetic field, one should expect the rotation to reverse, and if there is really a shielding effect then the apparent plasma density should be lower at the back. This is shown on the horizontal profile of Fig. 16. The vertical profile shows that measurements made at the top and bottom where the probe extends along a radius are unaffected, and the data repeat quite nicely.

In addition, measurements of the Langmuir probe curves and the plasma probe floating potential were taken as a function of horizontal position for neutral pressure of 4 mTorr He and with a magnetic field of 560 G. From these measurements the plasma density, potential, and electron temperature were deduced. The plasma density is shown in Fig. 17. The double points indicate the minimum and maximum densities as calculated from the fluctuating Langmuir probe curves. The density in the front of the chamber is again slightly lower than that to the rear, indicating the shadow effect. The radial density scale length is identical, i.e., q = 3 cm, indicating that the plasma is symmetric.

As is discussed earlier in Sec. IV.B, there is some uncertainty in the electron temperature measurement due to rapid fluctuations in the plasma density and plasma potential in time. In Fig. 18 we see the horizontal profile of the electron temperature T_{min} as calculated

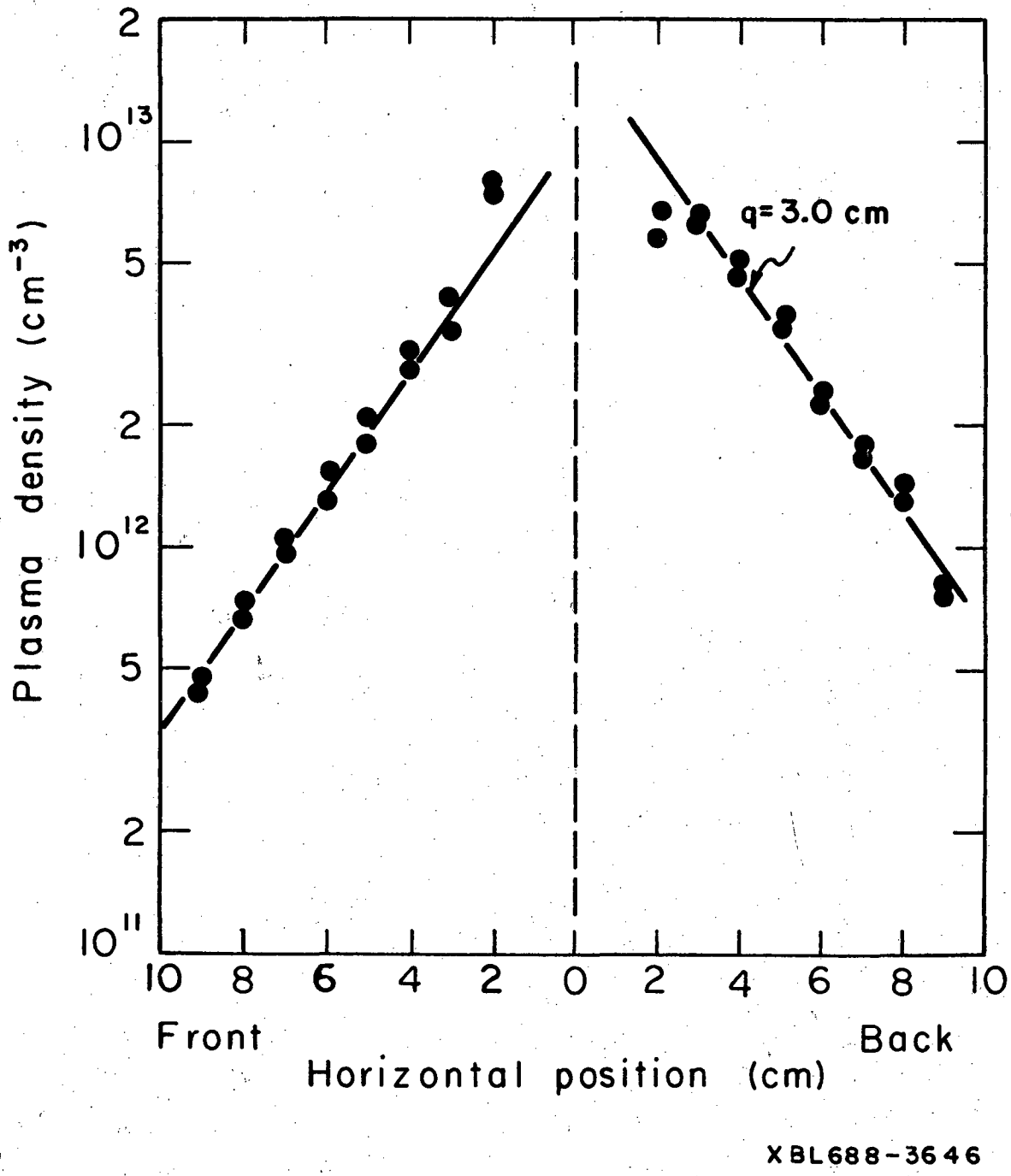

Fig. 17. Data Set 2. Plasma density as a function of horizontal position. The lines indicate a density scale length of q = 3 cm. P_T = 4.0 mTorr He. Two cathodes. Ends grounded. B = 560 G.

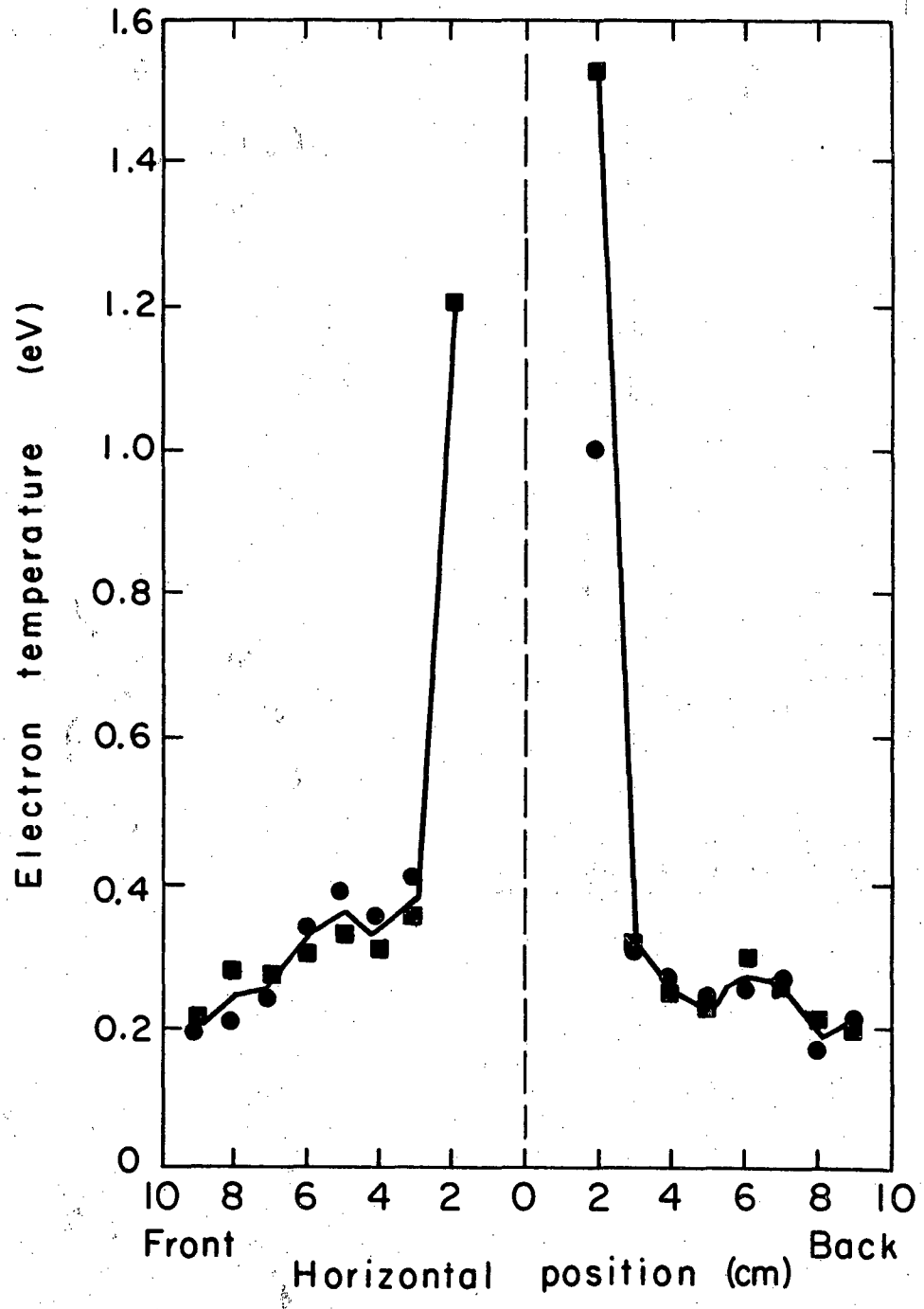

XBL688-3645

Fig. 18. Data Set 2. Electron temperature as a function of horizontal position. ■, T_{min} calculated from the minimum of the Langmuir probe curve; and ●, T_{max} calculated from the maximum, showing uncertainty in the electron temperature measurement.

from the minimum ion current for a given voltage of the Langmuir probe curve. The circles show the electron temperature T_{max} as calculated from the maximum ion current collected. From our discussion in Appendix B we find that the electron temperature at a given point in time lies between these two values. For purposes of our calculations we assume that the average electron temperature is the average of the two extreme values. At a radius of 2 cm, where the electron temperature is typically of the order of 1 eV, there is a large-amplitude fluctuation of the probe curve and it is difficult to estimate a reliable electron temperature.

In Fig. 19 we see the time-averaged probe floating potential, and the plasma as calculated from the two temperatures from Fig. 18. The figure shows a radial electric field of $E_r = 0.7 \pm 0.15$ V/cm from r = 3 to 8 cm to the back of the chamber and from r = 3 to 7 cm to the front of the chamber. There is more scatter in the data measured at the front; however, this is where there is some change in probe collection due to plasma rotation and probe orientation, as was discussed previously.

Measurements were also made of the fluctuating component of the probe floating potential, and of the fluctuating azimuthal and axial electric fields. In Fig. 20 we see the electric field measurements for four different orientations of a double probe. The upper trace in each photograph is the difference between the potential of probe A and probe B. The lower trace is the potential on probe A. From these measurements we find that at r = 5 cm there is an azimuthally fluctua-

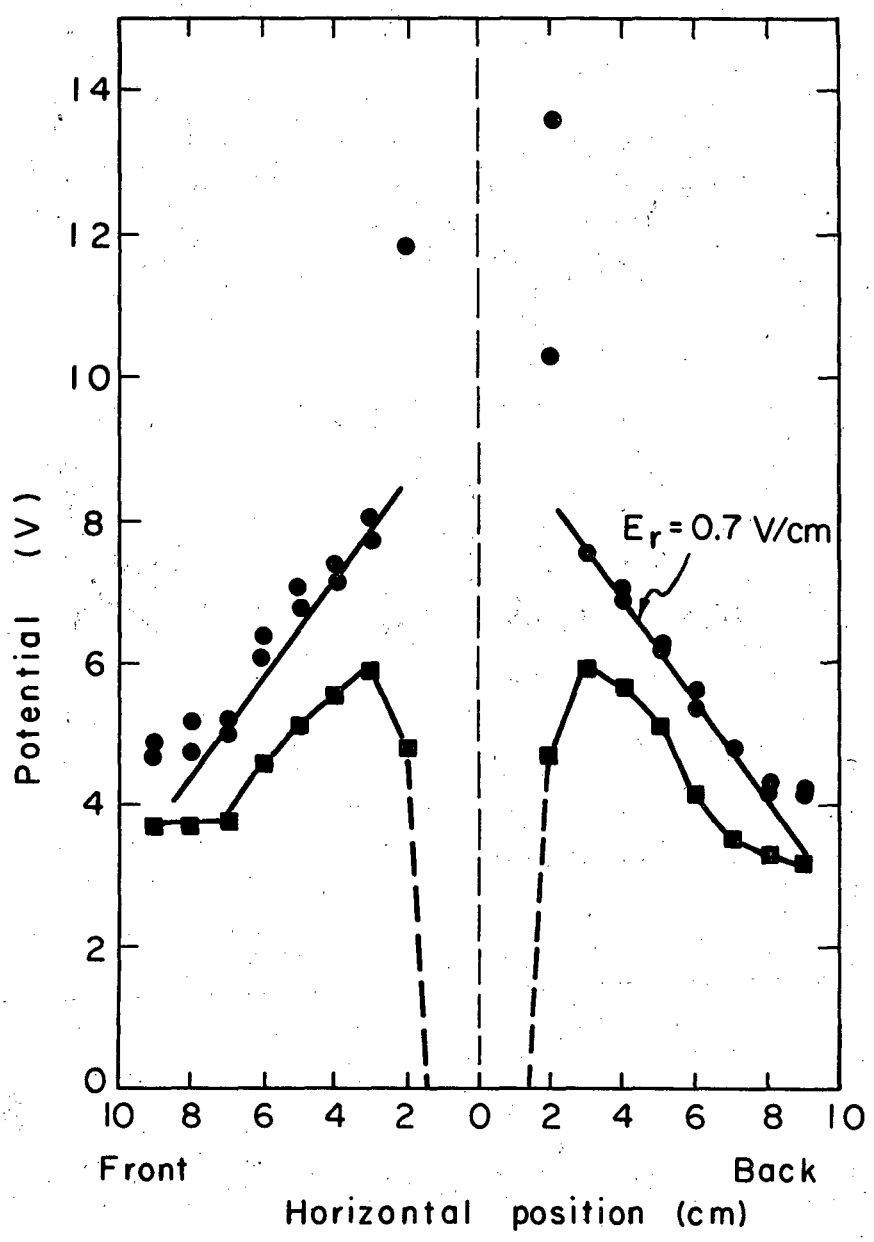

Fig. 19. Data Set 2. Time averaged probe floating and plasma potential as a function of horizontal position. ■, Measured average probe floating potential; ●, plasma potential (calculated using temperatures from Fig. 18) showing a radial electric field of $E_r \approx 0.7$ V/cm.

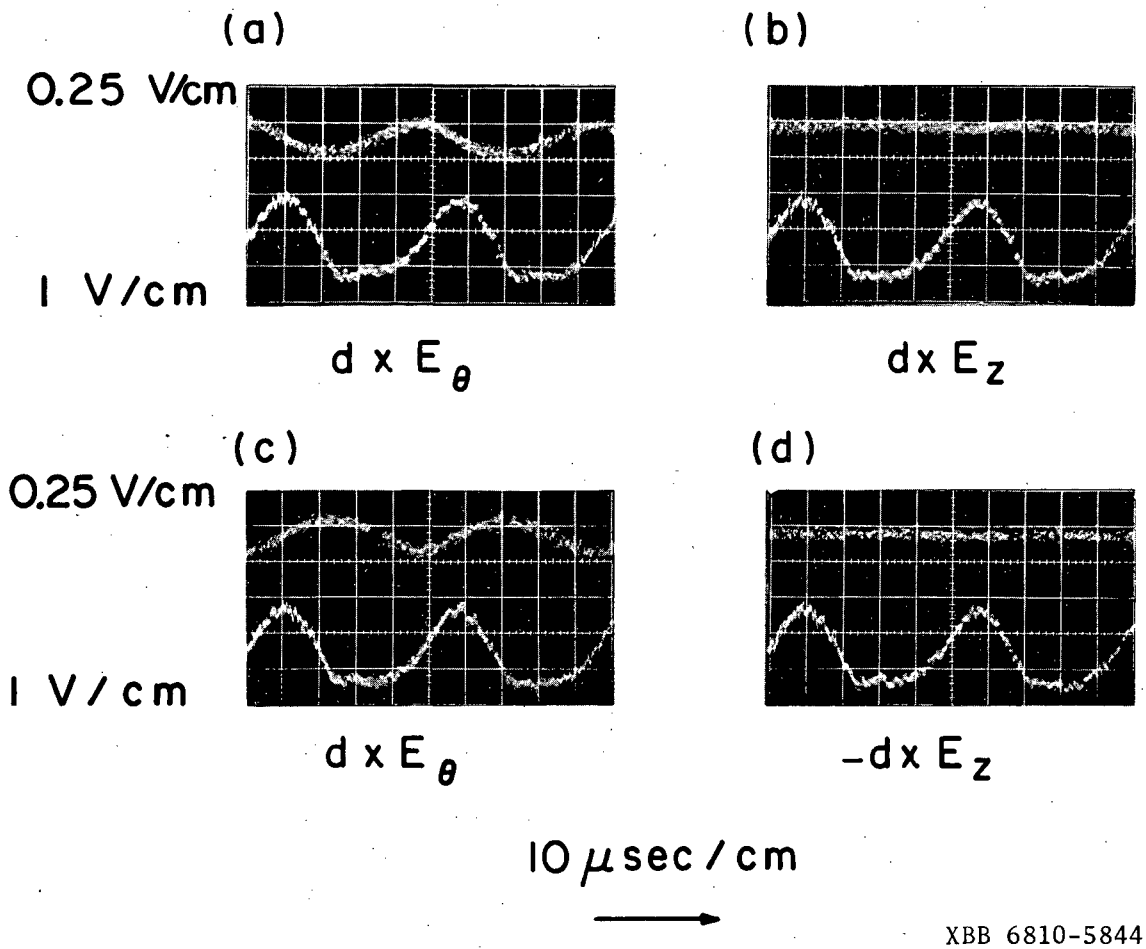

Fig. 20. Data Set 2. Fluctuating azimuthal and axial electric field measurement using a double probe spaced 0.7 cm apart, inserted radially from the fron access window. B = 560 G pointing toward the "cathode end." Upper trace in each photograph shows the potential difference $\phi_A - \phi_B$ for four different orientations of the probe. (a) B above A, d x E_θ; (b) B to left of A, d x E_z; (c) B below A, d x $-E_\theta$; and (d) B to right of A, d x $-E_z$. The lower trace shows the potential on probe A, ϕ_A. The peak to peak potential difference is about 0.25 V, and the maximum of the electric field fluctuation is 90 deg earlier in time than the maximum of the fluctuation in potential.

ting electric field of about E_θ = 0.36 V/cm peak to peak or 0.13 V/cm rms. The maximum of the electric field fluctuations is 90 deg earlier in time than the maximum of the potential fluctuation at the same point, in agreement with the observations in Data Set 1. The fluctuating electric field E_z is zero. The fluctuation is driven from the central arc column and has a period of 38 μsec, or a frequency of 21 kHz. In the central arc column it is a m = 1 rotation of the plasma in the electron diamagnetic drift direction and propagates with the same direction of rotation in the secondary plasma. This is in the opposite direction to the drift motion caused by the outward radial electric field.

Data Set 3. Moderate Radial Electric Field. Two Cathodes.

Because the axial distribution tended to be shifted toward the "cathode end" of the diffusion chamber, another experiment was done. As a brute-force attempt to make the axial distribution more symmetric, a second cathode was installed at the "anode end." Measurement were made for conditions similar to Set 1 in the pressure range from 1.4 to 5.4 mTorr He with a magnetic field strength of 560 G and with the end electrodes grounded. Figure 21 shows the approximate plasma density as a function of radial position obtained from saturated ion-current measurements for two values of neutral pressure, 1.5 and 2.6 mTorr He. The electron temperature beyond r = 2 cm decreases monotonically with radius and is found to be about kT_e = 0.6 eV in Case A, where P_T = 2.6 mTorr He, and 1.0 eV in Case B, where P_T = 1.5 mTorr He. This is larger than the electron temperature in the secondary plasma in Data

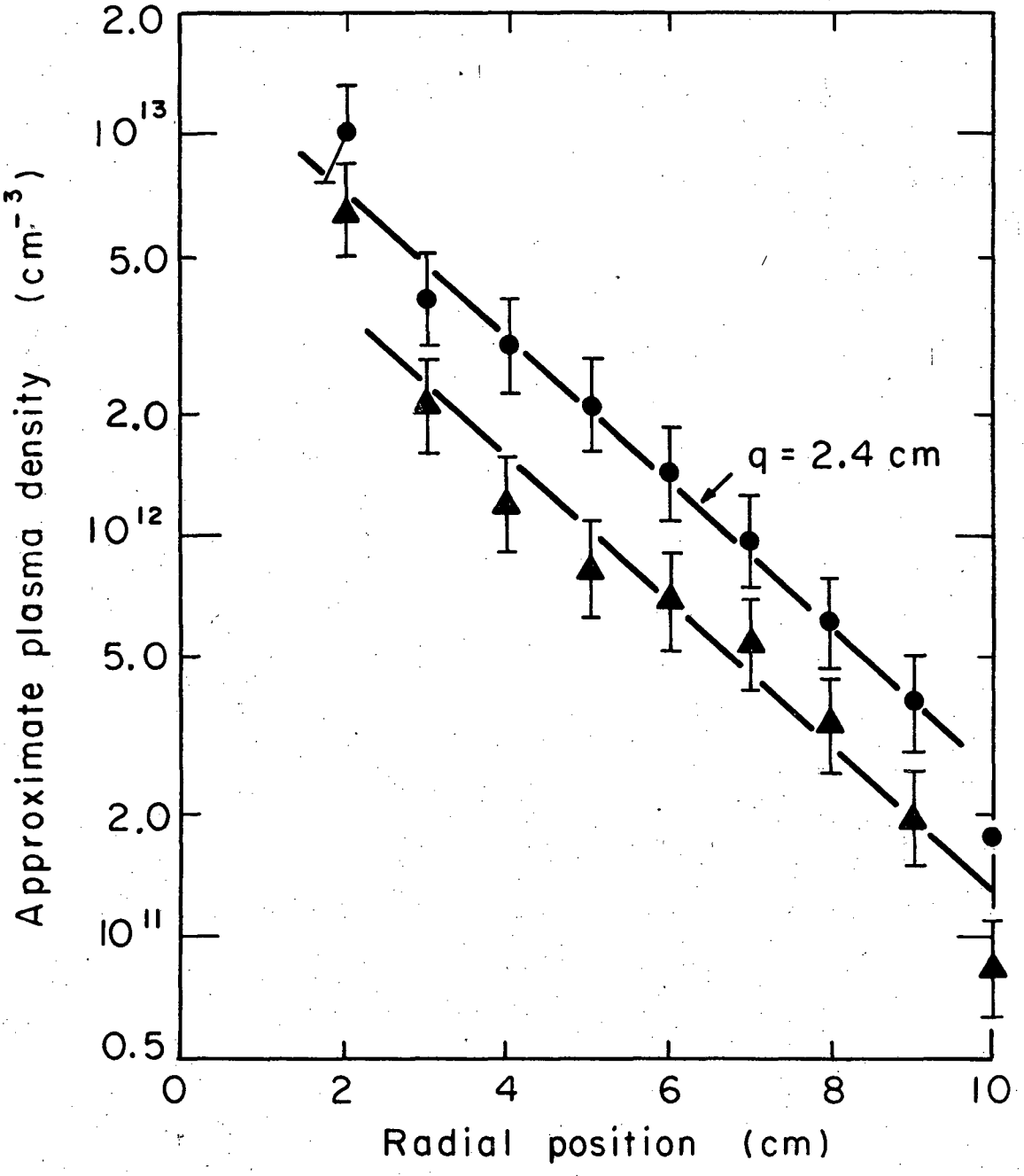

XBL689-6837

Fig. 21. Data Set 3. Approximate plasma density estimated from saturated ion current measurements as a function of radial position. Case A, ●, P_T = 2.6 mTorr He. Case B, ▲, P_T = 1.5 mTorr He.

Set 1.. The density scale length q = 2.4 cm in Case A, similar to the measurements in Data Set 1, is found to be more or less independent of neutral pressure over the whole range from 1.4 to 5.4 mTorr He. In Case B, Fig. 21, the over-all density is somewhat lower, but the density scale length is similar.

In Fig. 22 we see the probe floating potential as a function of radial position. The electron temperature profile is not known with sufficient accuracy to estimate the plasma potential. However, on the basis of floating potential measurements we estimate that the radial electric field is at least 0.25 V/cm in Case A and 0.6 V/cm in Case B. The correction to the plasma potential due to the monotonically decreasing electron temperature would tend to make this outward radial electric field somewhat larger. These and other measurements have shown that at lower pressure the radial electric field is larger, and this larger field explains why the density scale length is observed to be more or less independent of neutral pressure under some conditions. This is discussed further in Sec. V.D below.

Data Set 4. Large Radial Electric Field. Two Cathodes

Generally the radial electric field present in the secondary plasma with grounded end electrodes is larger at larger magnetic field values, and at lower pressures. The pressure effect can already be seen in Data Set 3, Fig. 22. In Data Set 4 measurements were made at an axial magnetic field strength of 1680 G for two neutral pressures--Case A, P_T = 2.9 mTorr He and Case B, P_T = 3.9 mTorr He--with use of the two-cathode discharge. The radial density scale length increased

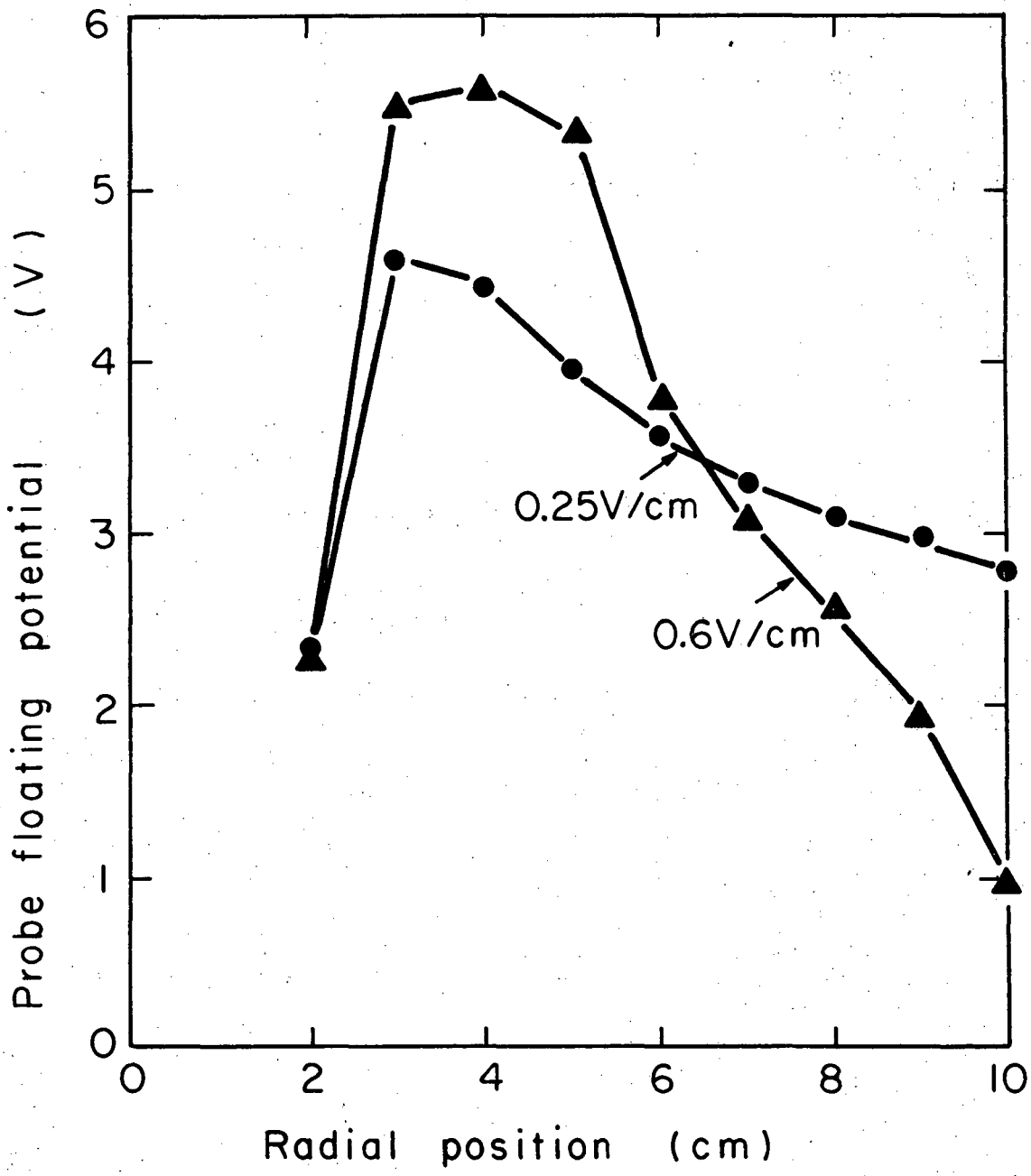

XBL688-3643

Fig. 22. Data Set 3. Probe floating potential as a function of radial position. The estimated radial electric field is indicated. Case A, ●, P_T = 2.6 mTorr He. Case B, ▲, P_T = 1.5 mTorr He.

from 1.25 to 1.5 cm with the neutral pressure, as shown in Fig. 23. The radial electric field, as shown in Fig. 24, decreased from $E_r = 1.5 \pm 0.3$ V/cm to $E_r = 1.0 \pm 0.2$ V/cm with the increase in pressure. The axial distribution, Fig. 25, is quite symmetric, similar to the results of Data Set 3.

Data Set 5. No Radial Electric Field. Two Cathodes

Another experiment was done for conditions similar to Data Set 3; however, the end electrodes of the system were allowed to electrically float, in which case the radial electric field goes to zero. The neutral pressure was 3.0 mTorr He and B was 560 G. Figure 26 shows the exponential radial density falloff with a scale length of $q = 1.6$ cm, which is much less than the scale length of $q = 2.4$ cm of Data Set 3. As in Data Set 1 the rms density fluctuation falls off more rapidly than the mean value of the density. Figure 27 shows the probe floating potential, electron temperature, and deduced plasma potential for this case. The radial electric field has gone to 0 ± 0.1 V/cm between $r = 3$ and $r = 7$ cm within our ability to measure it. The axial distribution is cosinusoidal, with effective length $L_{eff} = 64.5$ cm, as shown in Fig. 28.

Data Set 6. Azimuthal Asymmetry. Single Cathode. Floating Ends.

One of the rarely questioned assumptions which one makes when considering diffusion experiments in cylindrical geometry is that of azimuthal symmetry. Our measurements with grounded end electrodes confirms the time-averaged azimuthal symmetry of the plasma; however, very early in the experiments with floating end electrodes there was

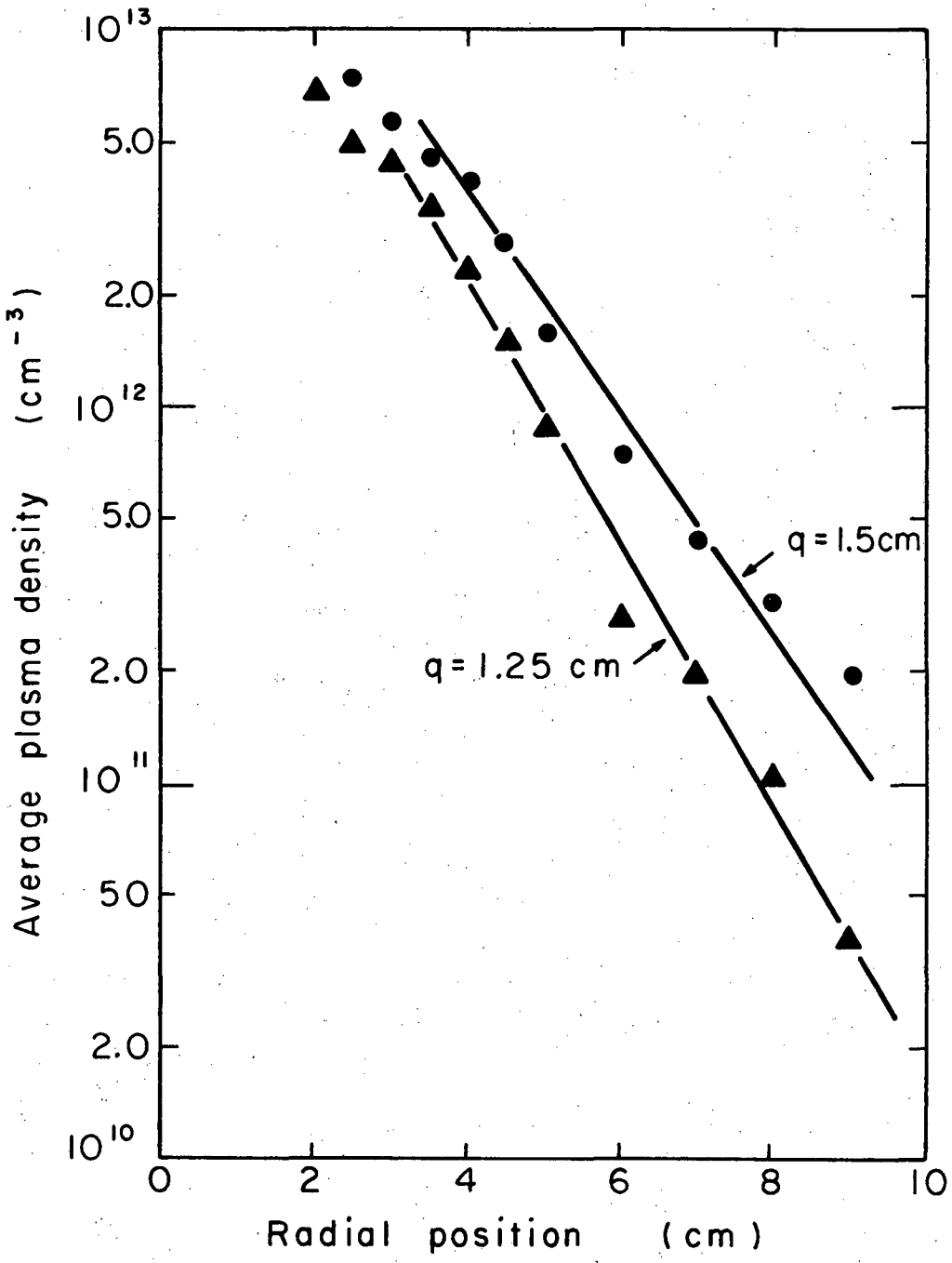

Fig. 23. Data Set 4. Plasma density as a function or radial position. B = 1680 G. Ends grounded. Two cathodes. Case A: ▲, P_T = 2.9 mTorr He. Case B: ●, P_T = 3.9 mTorr He.

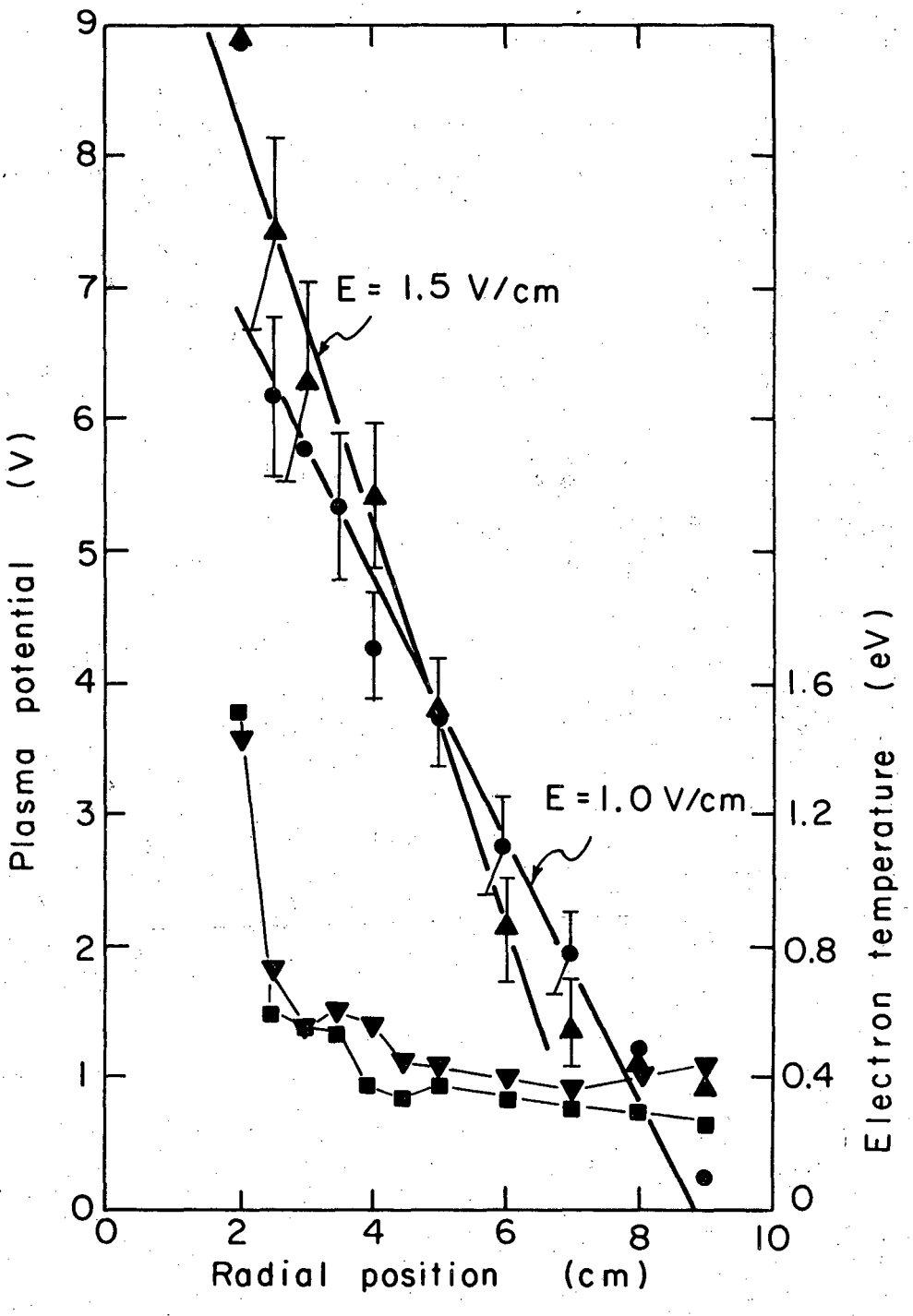

XBL688-3641

Fig. 24. Data Set 4. Plasma potential and electron temperature as a function of radial position. B = 1680 G. Ends grounded. Two cathodes. Case A: P_T = 2.9 mTorr He; ▲, plasma potential; ▼, electron temperature. Case B: P_T = 3.9 mTorr He; ●, plasma potential; ■, electron temperature.

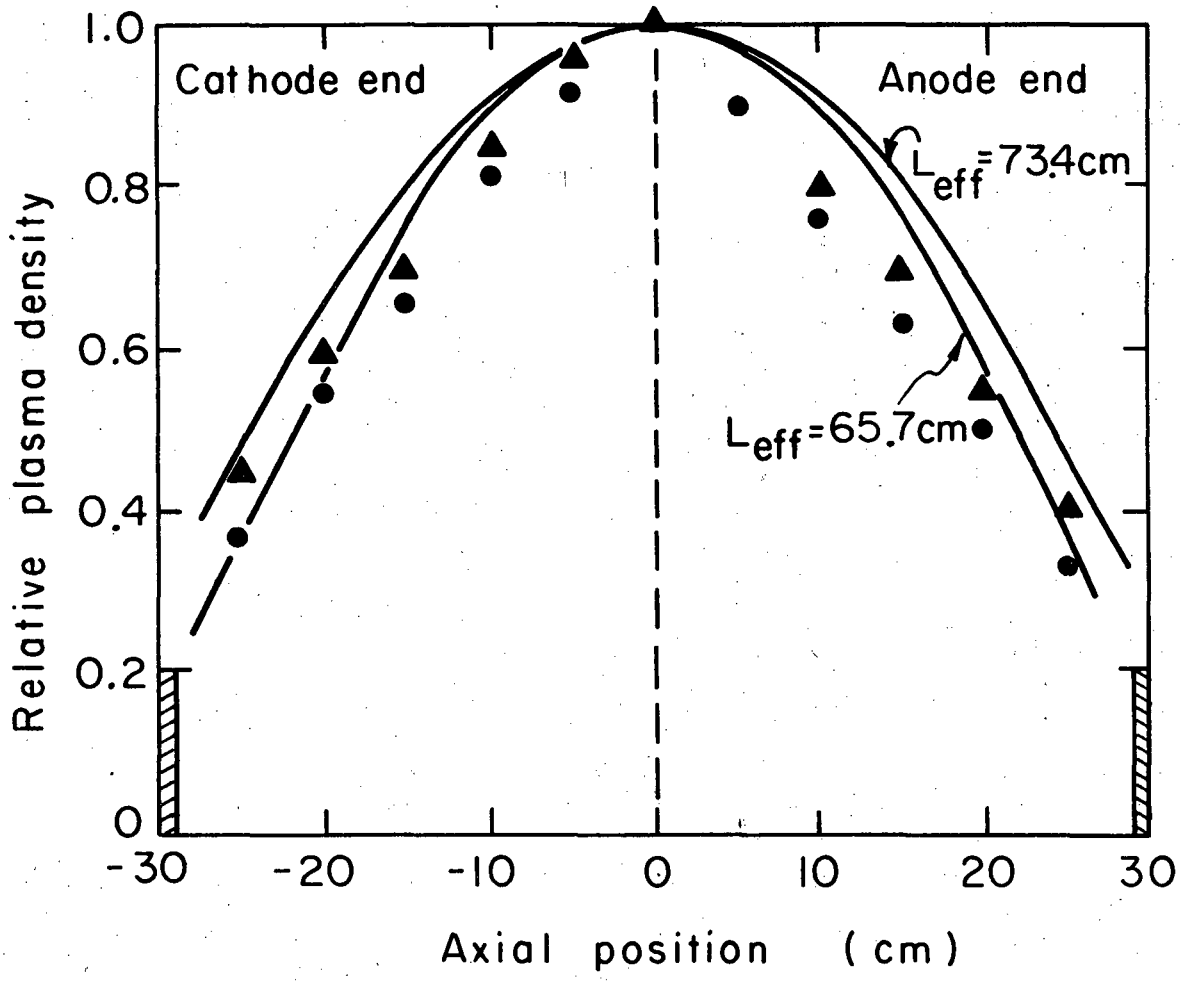

XBL 688-3640

Fig. 25. Data Set 4. Relative plasma density as a function of axial position. B = 1680 G. Ends grounded. Two cathodes. Case A: ▲, P_T = 2.9 mTorr He; L_{eff} = 73.4 cm. Case B: ●, P_T = 3.9 mTorr He; L_{eff} = 65.7 cm.

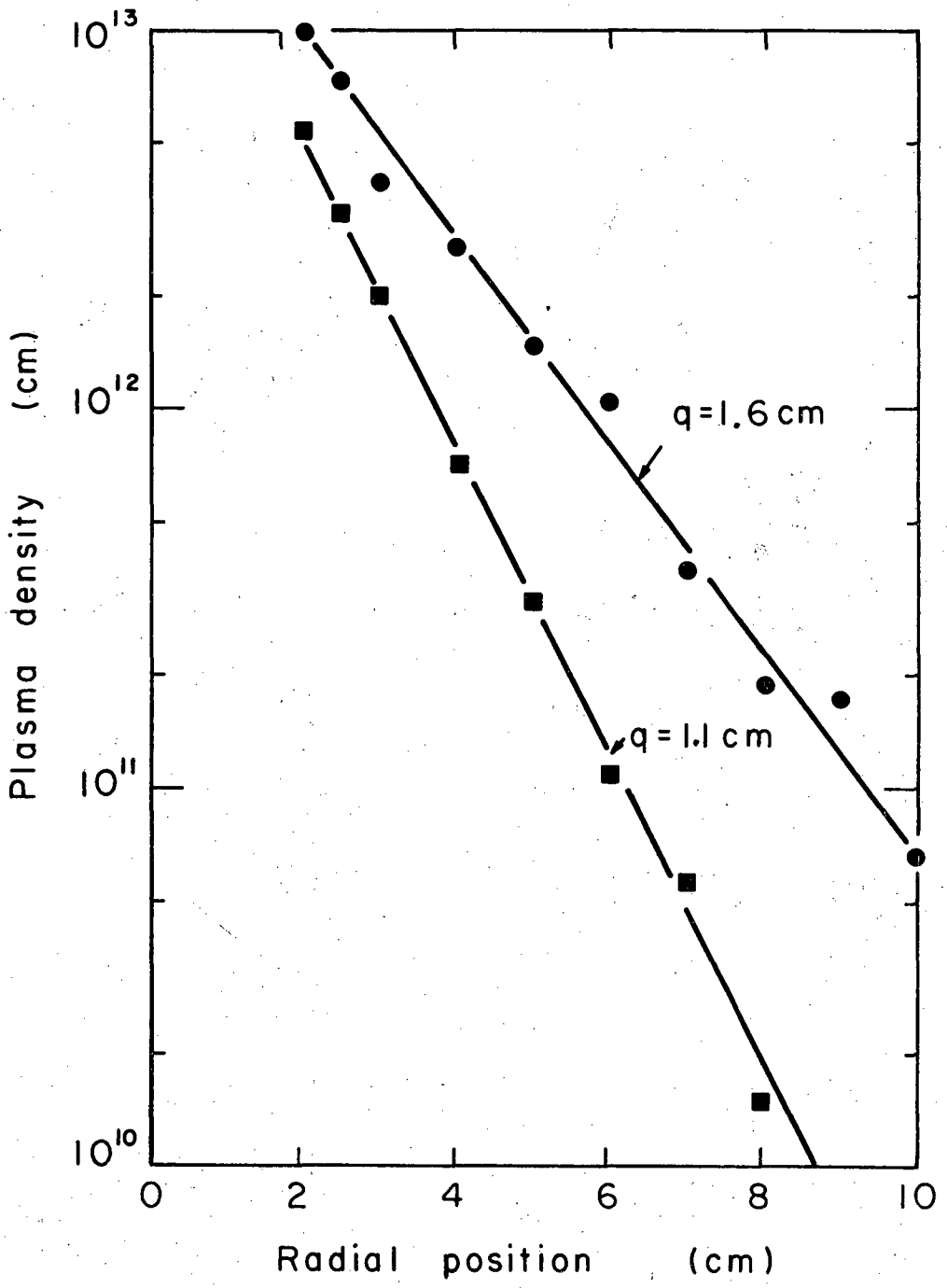

XBL688-3639

Fig. 26. Data Set 5. Plasma density as a function of radial position. ●, Time averaged density; ■, rms density fluctuation. B = 560 G. P_T = 3.0 mTorr He. Ends floating. Two cathodes.

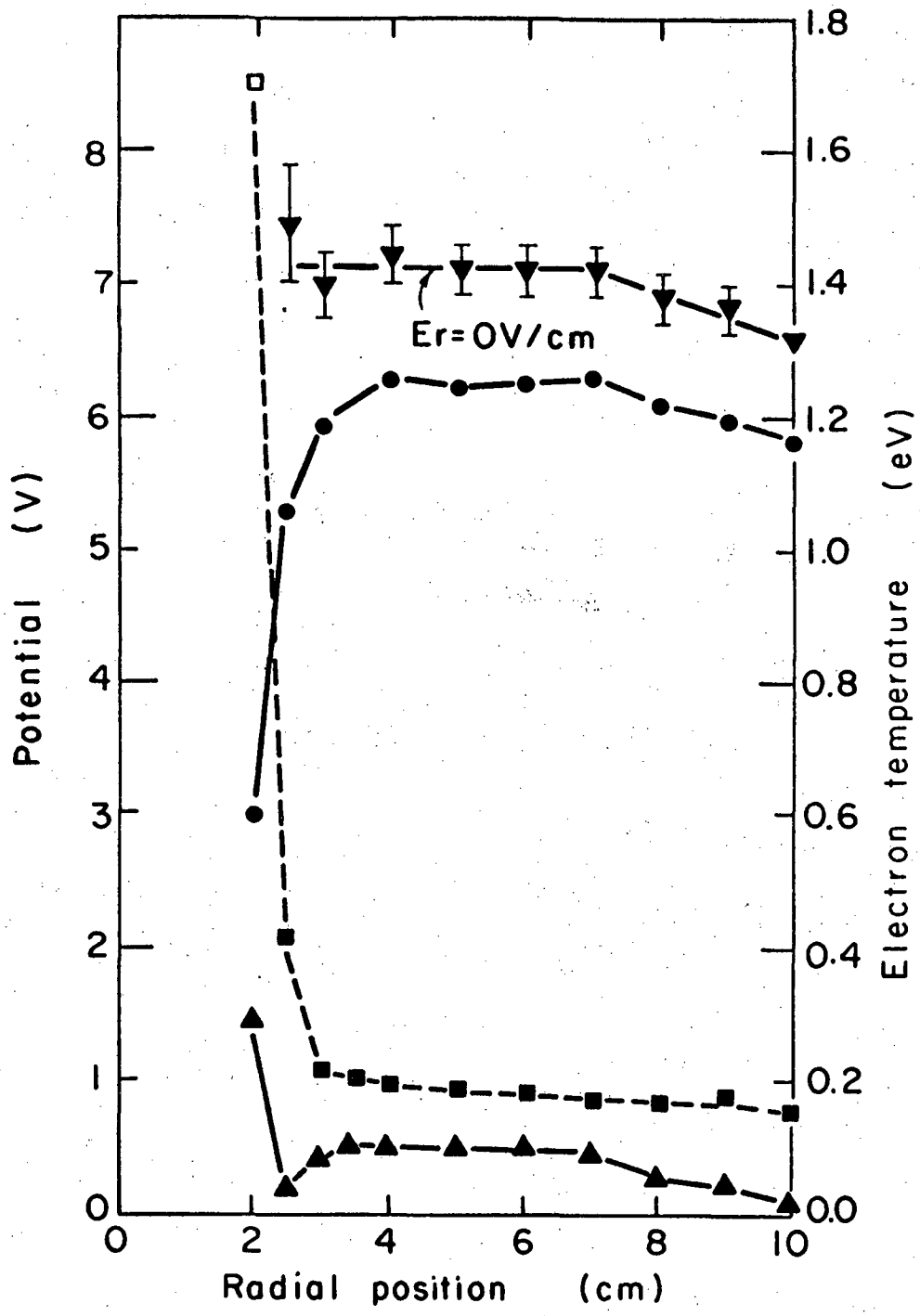

XBL688-3638

Fig. 27. Data Set 5. ▼, average plasma potential; ●, average probe floating potential; ▲, rms probe floating potential; and ■, electron temperature as a function of radial position. B = 560 G. P_T = 3.0 mTorr He. Ends floating. Two cathodes.

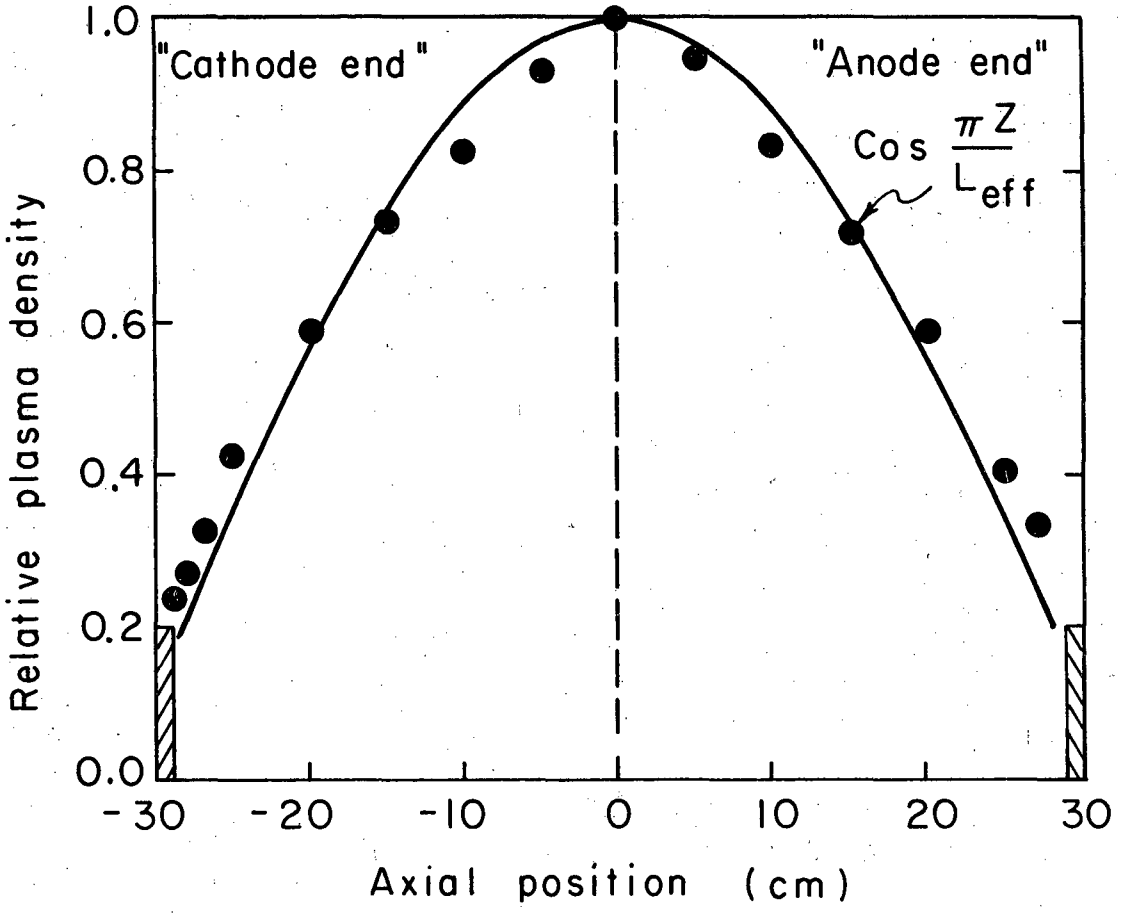

Fig. 28. Data Set 5. Relative plasma density as a function of axial position at a radius of 6.5 cm at the rear of the diffusion chamber. L_{eff} = 64.5 cm. B = 560 G. P_T = 3.0 mTorr He. Ends floating. Two cathodes.

concern over lack of quantitative agreement between measurements of the saturated ion current and the potential taken radially at the front of the chamber and those taken axially at the rear of the chamber. Furthermore, occasionally the radial density profile would fall to almost zero at about r = 6 cm and then reverse its slope, becoming larger again. A small change in cathode alignment would change this effect markedly. These observations remained vague mysteries until it was noticed that the bright bluish halo of the secondary plasma in helium was visibly asymmetric.

To study the plasma further, measurements of the probe floating potential and saturated ion currents were made along four azimuths--top, bottom, front, and back--at the midplane of the diffusion chamber, by using the probe arrangement shown in Fig. 3. The arc was run as shown in Fig. 1. A water-cooled anode A_I with a 0.64-cm exit aperture and a 0.64-cm limiting aperture in E_I were used to reduce the total plasma density and fluctuation level, and to improve differential pumping between the cathode region and the diffusion chamber. The end rings of the diffusion chamber were electrically floated, eliminating the radial electric field and rotation of the plasma as a whole.

Figure 29 shows the saturated ion current for four different azimuths. Beyond r = 2 cm this should be a good relative measurement of the plasma density. The approximate plasma density, assuming an electron temperature of 0.5 eV, is indicated. We see that on three azimuths, the plasma density shows good exponential behavior over an order of magnitude, but the radial density scale length is quite

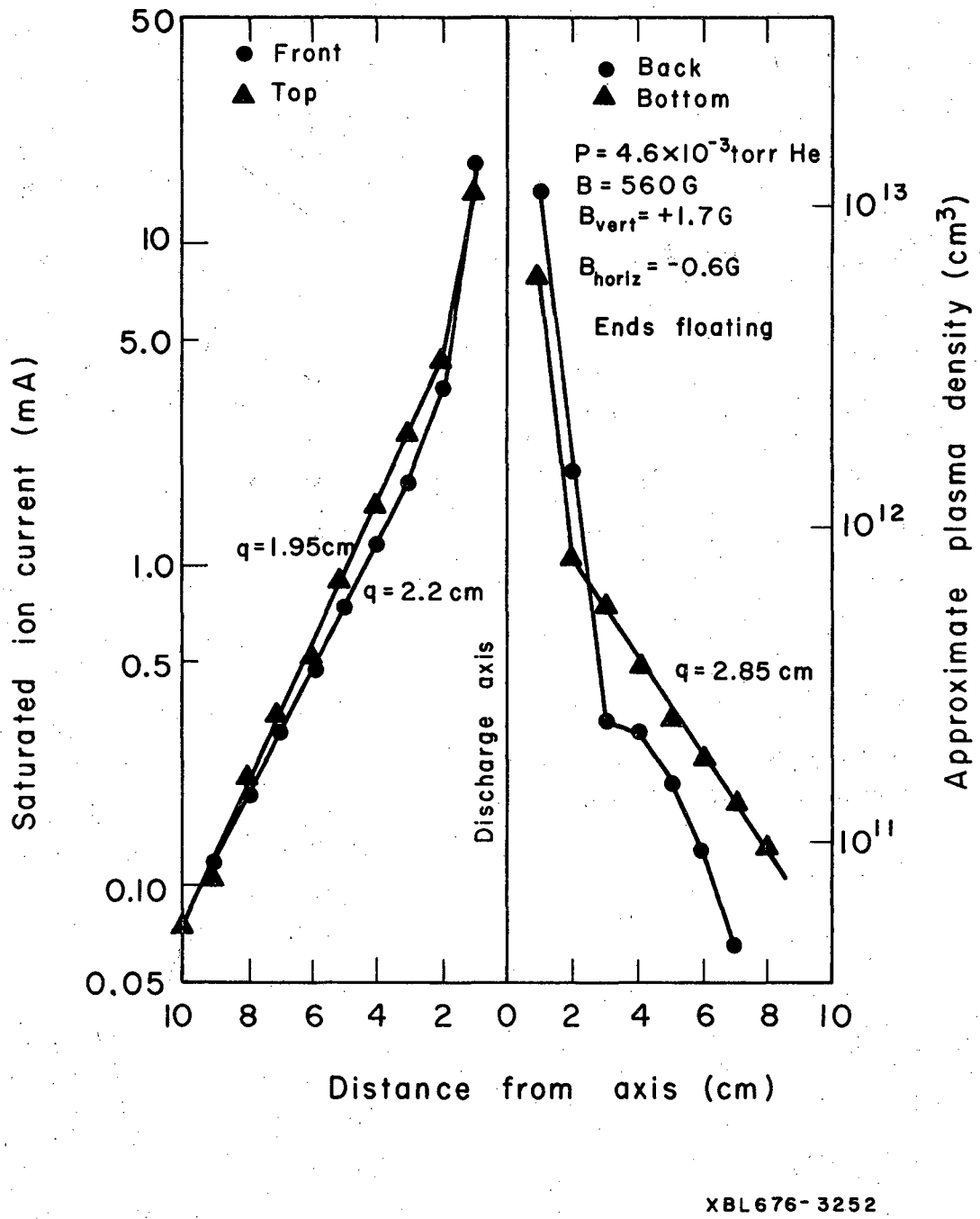

Fig. 29. Data Set 6. Time-averaged saturated ion current to a probe as a function of radial position along four azimuths, showing azimuthal asymmetry.

different on different azimuths, varying from q = 1.95 cm at the top to q = 2.85 cm at the bottom of the diffusion chamber. The plasma distribution appears to be pushed toward the front and top of the system. By moving the cathode or anodes A_I or A_{II}, the distribution could be made more asymmetric. It was not possible, however, to get rid of the asymmetry. When the cathode and anode A_I were carefully aligned in the center of the aperture in electrode E_I (as is indicated in Fig. 1) the plasma distribution was still asymmetric.

In Data Set 2, where the end electrodes are electrically grounded, and there the time-averaged plasma distribution is observed to be azimuthally symmetric, there is a radial electric field which produces rotation of the plasma as a whole. The density scale length measured at the four azimuths was found to be identical, q = 3.0 cm. Even though the time-averaged plasma distribution is symmetric, the time-resolved measurements of the plasma density indicate that under some conditions there is actually a somewhat asymmetric dis tribution, which rotates about the axis of the diffusion chamber in time. A stationary probe then samples the plasma from all azimuths, as the plasma rotates. Such asymmetric rotation is shown in Fig. 35, photograph b, and in Fig. 36, photograph a, and generally takes the character of large-amplitude low-frequency density perturbation on the plasma. Under conditions of cathode misalignment the plasma distribution can become stationary and visibly asymmetric, sometimes even in the case of grounded electrodes. For the experimental measurements presented in Data Sets 1 through 6, the discharge alignment and other arc conditions

were adjusted so as to eliminate the low-frequency asymmetric azimuthal rotation of the plasma distribution.

Figure 30 shows the time-averaged probe floating potential for the same conditions as Fig. 29. The error bars indicate the uncertainty in the measurements due to drift of the floating potential during the time of the measurements. There was no drift during the top measurement. The floating potential at r = 4 cm at the front was checked for each azimuth as an estimate of the potential drift. Because the concentric ring end plates are allowed to float electrically, the plasma potential reference is established only over small areas at E_I, E_{II}, and the tank wall. Minute changes in pumping speed, gas flow, etc., can change sheath conditions so as to change the over-all potential level. Saturated ion-current profiles, however, did not show a measurable drift during the data-taking period. Figure 30 clearly shows that the floating potential and most likely the plasma potential are also asymmetric. Unfortunately, the electron temperatures were not measured, so that no reliable estimate of electric fields can be made. From the appearance of the plasma density profile we can conclude that the secondary plasma is not rotating. For these conditions the radial ion diffusion velocity $v_r = (D_\perp^{in} + D^{ie})(\nabla n/n)$ is of the order of 1200 cm/sec. To produce an asymmetric transverse drift of the plasma in a preferred direction which is of the same order of magnitude as the radial transport due to diffusion would require a static transverse electric field only of the order of 7×10^{-3} V/cm.

An additional disturbing feature of the asymmetry was its refusal

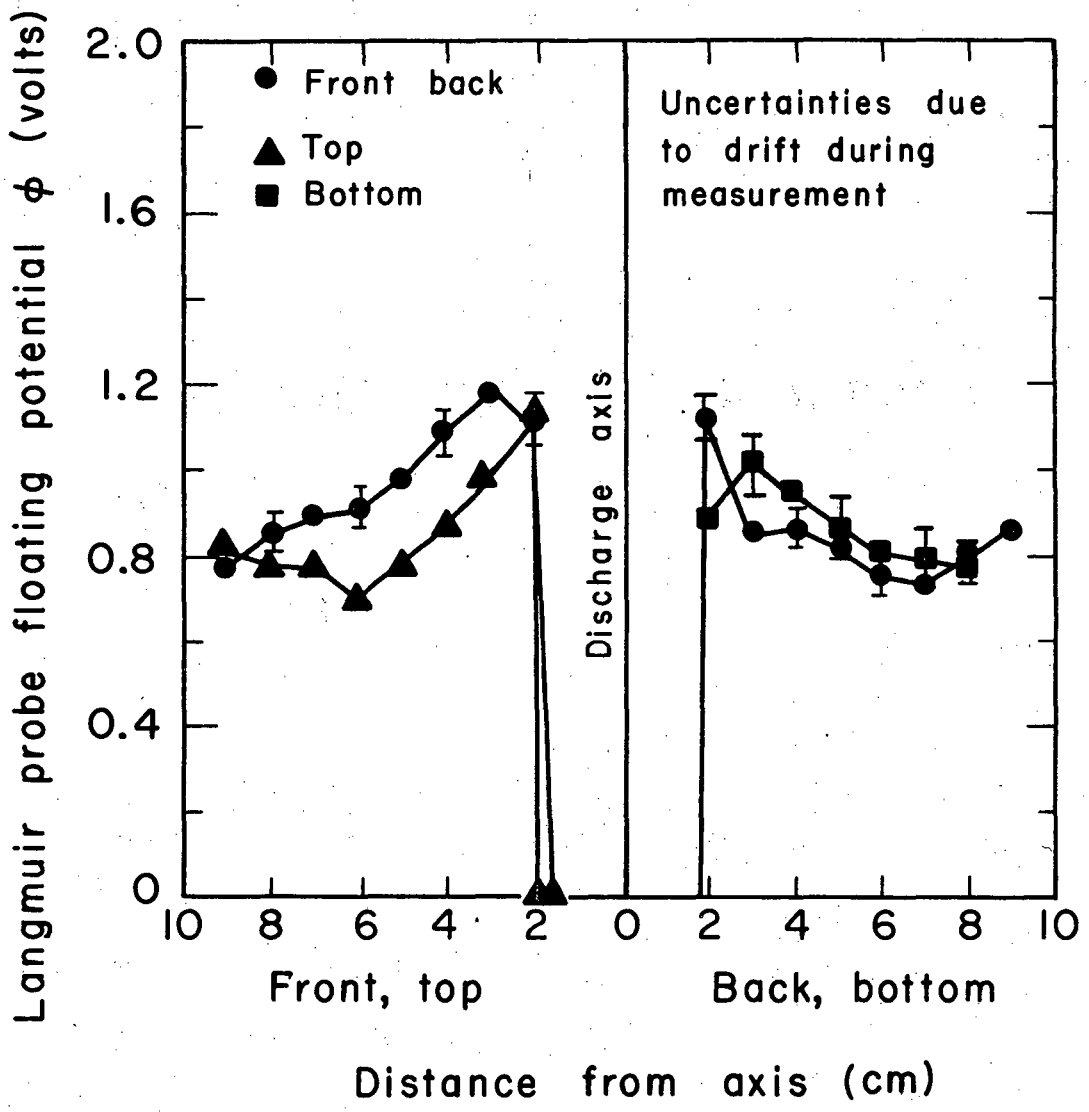

Fig. 30. Data Set 6. Time-averaged probe floating potential as a function of radial position along four azimuths. P_T = 4.6 mTorr He. B = 560 G. B_{vert} = 1.7 G. B_{horiz} = -0.6 G. Ends floating.

to repeat itself from day to day. The suggestion was made that perhaps the earth's magnetic field or some other stray transverse magnetic field might have some effect on the asymmetry. As a check of this, two pairs of rectangular five-turn coils approximately 40 by 115 cm, capable of carrying about 30 A, were placed around the main magnet coils. These coils would produce a small transverse magnetic field of 0.115 G/A in the horizontal and vertical plane with positive B_{horiz} pointing toward the rear and B_{vert} pointing upward, as indicated in Fig. 3. When these coils were activated there was a definite change in the asymmetry.

To measure the transverse field components a small search coil was inserted on the axis of the chamber. By rotating the coil and integrating the output voltage one could measure B_{horiz} and B_{vert} in the absence of an applied transverse field. The stray field on the axis at the midplane was very small, of the order of 0.2 G. However, in the vicinity of each end plate stray fields of the order of 2 G were observed. Furthermore, the stray field would change magnitude and direction as the magnetic field was turned on and off, being very nonreproducible. Apparently there is sufficient magnetic material near the end of the diffusion chamber to cause magnetic polarization.

The asymmetric plasma distribution is very sensitive to changes in the transverse field. Figure 31 shows the horizontal and vertical profile of the saturated ion current for two different values of B_{vert}. B_{horiz} was kept constant, as were all other discharge parameters. The applied B_{vert} was changed from 1.4 to 1.7 G. The density at a point on

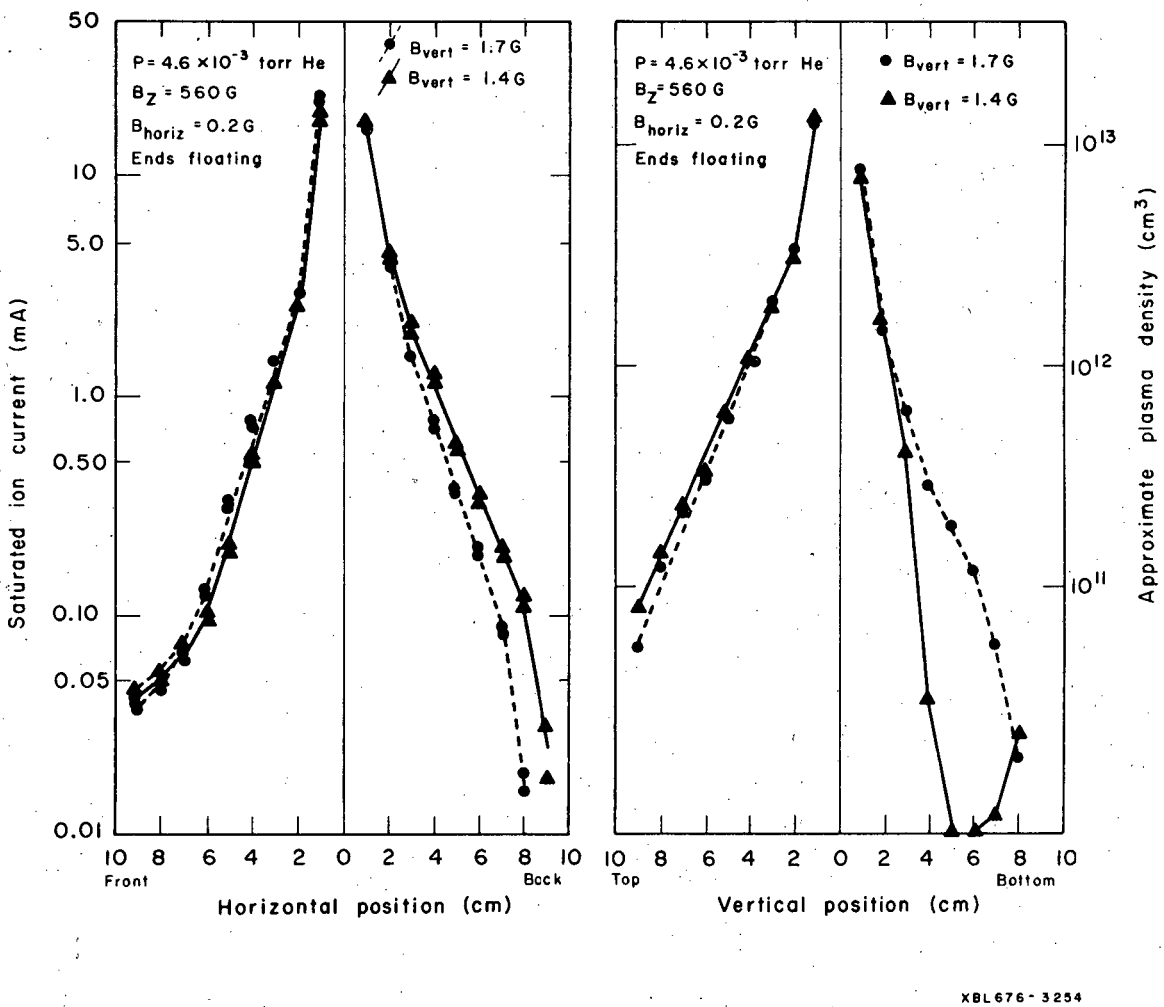

Fig. 31. Data Set 6. Time averaged saturated ion current to a probe as a function of radial position along four azimuths, for two values of transverse magnetic field, B_{vert}, showing sensitivity of plasma distribution to axial alignment.

the profile changes typically by up to 100% when the magnetic field is changed by 0.3 G in 560 G, which is a remarkably small change of only 0.05%. The double points on the horizontal profile indicate repeated measurements over the 20-minute data-taking period to ensure that the observed large effect is real.

One wonders how the plasma can be so sensitive to small changes in the magnetic field. Using a 1/16-in. limiting aperture in E_I to give us a fine electron beam traversing the length of our system, one can see that the application of a 2-G transverse magnetic field will cause this beam to deflect on the order of 0.2 cm. This corresponds to a slight shift of the magnetic axis of our system. The precise centering of the plasma core in the "anode end" ring electrode appears to determine how symmetric the distribution is. It is so critical that, in fact, it is never in practice perfectly symmetric.

3. Visual Observations

One of the most striking features of the hollow-cathode arc discharge is the appearance of the plasma in the diffusion chamber. The characteristics of the plasma are independent of whether one uses two cathodes, a single cathode, or a single cathode with a limiting aperture. We shall now discuss the behavior of the diffusion chamber plasma with an additional anode A_I and a 0.64-cm limiting aperture in E_I, which are shown in Fig. 1. The conditions of the arc in the cathode region in this case are relatively unaffected by the conditions in the diffusion chamber, and a lower diffusion chamber pressure can be achieved. The pressure in the cathode region is of the order of 10 to

20 mTorr He. Almost all the 20-A discharge current runs to the anode A_I and to the electrode E_I, with a current only of the order of 200 mA traversing the diffusion chamber and being collected on anode A_{II}.

At low neutral pressures in the diffusion chamber, P_T = 0.8 mTorr He, the arc as observed through the front access window is very faint. The plasma density estimated from saturated ion-current measurements at r = 2 cm is low, on the order of 10^{10} to 10^{11} cm^3. A floating probe placed on the axis assumes a potential as much as -100 V, indicating the presence of hot streaming electrons on the axis.

As the neutral pressure is raised to 1 mTorr the plasma density in the diffusion chamber increases. This indicates that under these conditions most of the plasma in the diffusion chamber is produced by ionization of the neutral gas atoms by bombardment with the fast electrons from the source region, rather than plasma streaming from the source. The plasma shows a bright central column which falls off in brightness to a radius of 2 or 3 cm. The radial density profile is quite rounded, with large, 100% fluctuations in time. The electrons are reasonably hot, kT_e = 5 eV, throughout the volume of the plasma. This operating regime is quite similar to the low-pressure deuterium arc studied by Gibbons, Lazar, and Rayburn,[27] and is characterized by large radial plasma loss driven by fluctuations. The transport is so rapid that the electrons are not significantly cooled in being transported across the magnetic field.

As the neutral pressure is raised to about 1.4 mTorr He, the plasma changes modes abruptly. The plasma density continues to increase

with neutral pressure, but suddenly the plasma develops two distinct regions. The central arc column glows a bright pink, characteristic of helium, out to a radius of about 1 cm. Beyond the radius is the secondary plasma, whose glow is much fainter, and whose electron temperature is of the order of 0.5 eV. The central arc colum is still quite hot, $kT_e \approx 5$ to 10 eV, and there is a steep temperature gradient at about r = 1 cm at the boundary between the two regions. A distinct green glow appears throughout the entire volume of the diffusion chamber as the plasma changes modes, corresponding to the 5016-Å (3^1p - 2^1s) He I transition. Evidently the neutral helium 3^1p state is excited from the ground state by resonant absorption of the 537 Å (3^1p - 1^1s) photon, due to excitation and decay of helium neutrals in the central arc column. The 3^1p state subsequently decays some of the time into the 2^1s level, which is a metastable state 20.38 eV above the ground state.

As the neutral pressure is raised from 1.4 mTorr He, a bluish halo appears surrounding the central arc column in the region between about r = 4 and r = 8 cm. The halo tends to become brighter as the neutral pressure is increased. The appearance of the halo coincides with the excitation of helium neutral excited states and the subsequent appearance of decay transitions such as the 4471-Å (3^3d - 4^3d), 5875.6-Å (3^3p - 4^3d), and 6678-Å (2^1p - 3^1d) He I lines. It is quite evident that collisional excitation of the He I metastable levels by the electron distribution is taking place, because there are almost no electrons in the secondary plasma with sufficient energy to excite

these states from the ground state. There is some evidence that the rms potential fluctuations and electron temperature may be slightly higher in the halo, although there is certainly no profound difference.

Photographs of the central arc and the secondary plasma region are shown in Fig. 32. The arc was run with an axial magnetic field of 560 G, with the end electrodes electrically floating and with a diffusion chamber neutral pressure of P_T = 4.0 mTorr He. The central arc column is visible in the center of each photograph as the pinkish glow which is characteristic of helium discharges. The Langmuir probe extending from the top of the chamber is about 4 cm behind the central arc. The asymmetric appearance of the halo surrounding the central arc is quite evident. On the left the halo is mostly at the top, appearing as a bluish glow. The green glow just below the central arc on the left is due to the 5016-Å He I transition and at lower pressures is evident throughout the entire secondary region of the chamber. On the right the halo is predominantly below the central arc. The change in the plasma distribution between the photographs on the left and on the right occurs by decreasing the applied transverse bias magnetic field B_{vert} from 0.0 G to -1.4 G.

The asymmetric halo was one of the first indications that the azimuthal plasma distribution might be asymmetric. When the edge of the halo is sharp its edge is found to correspond with a sharp drop in the plasma density. When the halo falls off slowly, the plasma density is observed to fall off slowly. The intensity of the halo appears to be dependent on the plasma density. Halos were observed

SEE PHOTOGRAPH ON

FOLLOWING PAGE.

Fig. 32. Photographs of the plasma column, showing central arc, asymmetric halo, and green glow. B = 560 G, P_T = 4.0 mTorr He, ends floating, B_{horiz} = 0.9 G. On the left, B_{vert} = 0.0 G. On the right, B_{vert} = -1.4 G.

in argon and in helium, both of which have metastable levels. Observations in H_2 for similar conditions indicate that there is very little plasma or neutral gas glow beyond r = 3 cm.

The essential character of the halo remains unchanged as on increases the neutral pressure until one reaches a pressure of 15 to 20 mTorr He. As the neutral pressure is increased, eventually the cooling because of collisions with neutrals becomes sufficient to cool the secondary plasma. The halo begins to become reduced in size, and the outer plasma no longer radiates even though plasma is still present. The measurements of the spatial dependence of the plasma parameters which are reported in Data Sets 1 through 6 were made in the intermediate pressure range between 1.4 and 7 mTorr He where the plasma remains in the same operating regime.

4. Observations of Fluctuations in the Plasma

Measurement of the frequency spectrum of probe potential and saturated ion-current fluctuations have been made up to a maximum frequency of 26 MHz with electronic spectrum analyzers and by observing the signals on an oscilloscope. The plasma under study exhibits fluctuations in essentially three frequency ranges: low frequencies 1 to 20 kHz, intermediate frequencies 20 to 100 kHz, and high frequencies above 100 kHz. Experimental conditions were set up so that the flucutations of the plasma generally exhibited a simple character, with only a few discrete modes or types of oscillations present at any one time.

The high frequency above 100 kHz appears primarily on the probe floating potential measurements. The fluctuations in the secondary

plasma are of small amplitude and appear as general hashiness, as shown in Fig. 15. Frequency analysis of potential fluctuations under typical conditions was done with a Nelson Ross Model 205 spectrum analyzer, and is shown in Fig. 33, photograph (a). The amplitude of the potential fluctuations as a function of frequency is shown for a probe at r = 3.5 cm in the secondary plasma for a neutral pressure of 3.4 mTorr in a single cathode discharge with floating end electrodes.

There is a broad-band peak indicated at about 6 MHz, which has an amplitude of about 60 mV peak to peak. The high-frequency fluctuations in the secondary plasma are not strongly dependent on magnetic field strength, diffusion chamber pressure, or end electrode conditions; although when the neutral pressure is reduced to below 2 mTorr, at which the halo disappears, the high-frequency fluctuation level drops. From observations of the fluctuations on an oscilloscope, and from survey of the frequency spectrum with a Pentrix Model L-20 spectrum analyzer capable of detecting signals up to 4 GHz, we find no evidence for fluctuations above 26 MHz that would significantly affect the macroscopic transport of the plasma.

The intermediate-frequency fluctuations are at a discrete frequency, sometimes with phase-locked harmonics. This instability originates in the hot highly ionized central arc column and as a m = 1 rotation of the plasma in the electron diamagnetic drift direction. This is the drift direction in an inward radial electric field crossed with the axial magnetic field. This instability propagates into the

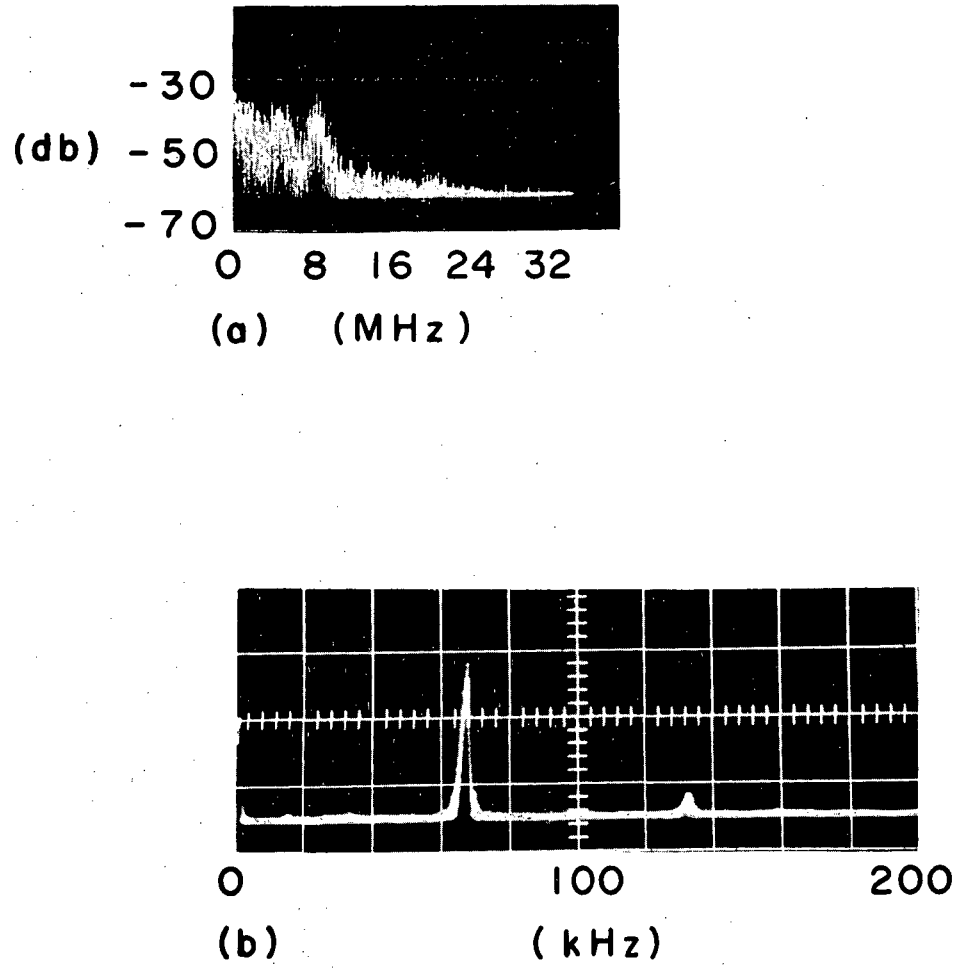

Fig. 33. Amplitude of typical potential fluctuations as a function of frequency. (a) P_T = 3.4 mTorr He, B = 560 G, and r = 3.5 cm, showing broad-band noise spectrum at about 6 mHz with amplitude of about 60 mV peak to peak. (b) P_T = 3.2 mTorr He, B = 560 G, and r = 2 cm, showing large-amplitude discrete frequency oscillations at 68 kHz and a small second harmonic at about 134 kHz. The vertical scale is linear, and the amplitude of the dominant peak is typically 2 volts peak to peak.

secondary plasma from the central arc column. In Fig. 33, photograph (b), we see the amplitude of the potential fluctuation as a function of frequency in the range 0 to 200 kHz. The measurement was made with a Panoramic Ultrasonic Analyzer Model SB-7a. The frequency indicated by the large peak is about 68 kHz with a small second harmonic at 136 kHz also visible. The fluctuations in this range are typically of moderate amplitudes $\delta\phi$ = 0.7 V rms in the secondary plasma, and are confined to discrete frequencies.

In Fig. 34 we see oscillographs of typical probe potential and saturated ion-current fluctuations as a function of neutral pressure for a single-cathode helium discharge with an axial magnetic field of 560 G. At fairly large pressure, 3.7 and 4.6 mTorr, the distribution is stable, demonstrating only that 24- to 26-μsec potential and density fluctuations are driven from the central arc column, as shown in pictures (c) and (d). As one goes to lower neutral pressures the oscillation goes to higher frequencies, and the density fluctuation starts to break up, with large-amplitude low-frequency 1- to 5-kHz motion of the plasma, as shown in photographs (a) and (b) of Fig. 34. The choice of experimental conditions for making measurements of the plasma profiles was determined by trying to suppress the low-frequency fluctuations by varying cathodegas flow rates, cathode alignment, pumping speeds, and magnetic alignment of the system. The low-frequency fluctuations appear to be due to macroscopic electric fields, which cause the plasma to move back and forth or to become asymmetric azimuthally and to rotate. Conditions are found in which the plasma appears to have two

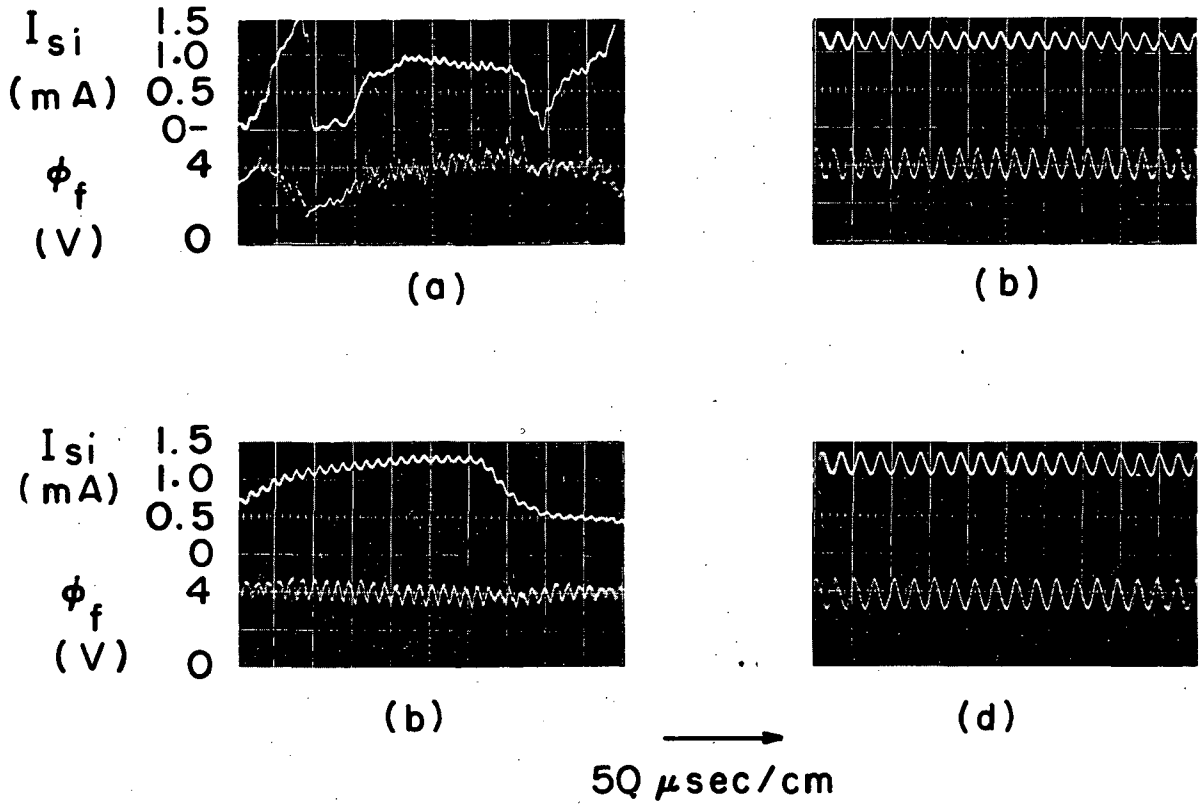

Fig. 34. Typical potential and density fluctuations on a probe at r = 5 cm as a function of neutral pressure. Single cathode, ends grounded. B = 560 G. (a) 1.9 mTorr He, τ = 11 μsec; (b) 2.4 mTorr He, τ = 15.5 μsec; (c) 3.7 mTorr He, τ = 24 μsec; and (d) 4.6 mTorr He, τ = 26 μsec.

semistable operating modes for the same operating conditions, one without and the other with low-frequency fluctuations. There is a discontinuous change from one mode of operation to the other. To a certain extent the asymmetry of the plasma can be minimized, and the low-frequency instability can be suppressed by adjusting the horizontal and vertical magnetic fields to change the magnetic and physical alignment of the system.

The period of the intermediate-frequency fluctuations is strongly dependent on the neutral gas pressure in the diffusion chamber. In Fig. 35 we see the oscillation period of the fluctuation as a function of neutral pressure in the range 1.6 to 6 mTorr He. The period tends to be a linear function of the neutral pressure of the system, with the period increasing with pressure up to about 6 mTorr. At about 6 mTorr in He the instability is damped out. This appears to be due to neutral collisional damping of the instability. Shown on Fig. 35 are measurements for three different magnetic field strengths. Although there is some scatter in the measurements, the oscillation period is insensitive to changes in the magnetic field, especially at the neutral pressures of 2 to 4 mTorr. As the magnetic field is lowered to about 330 G the plasma becomes completely stable to this mode of oscillation. Other measurements indicate that the oscillation period was insensitive to a change of the discharge current by a factor of 2 for constant neutral pressure in the diffusion chamber. Apparent change in the period as a function of discharge current was observed, but the dependent variable was found to be neutral pressure due to pumping by

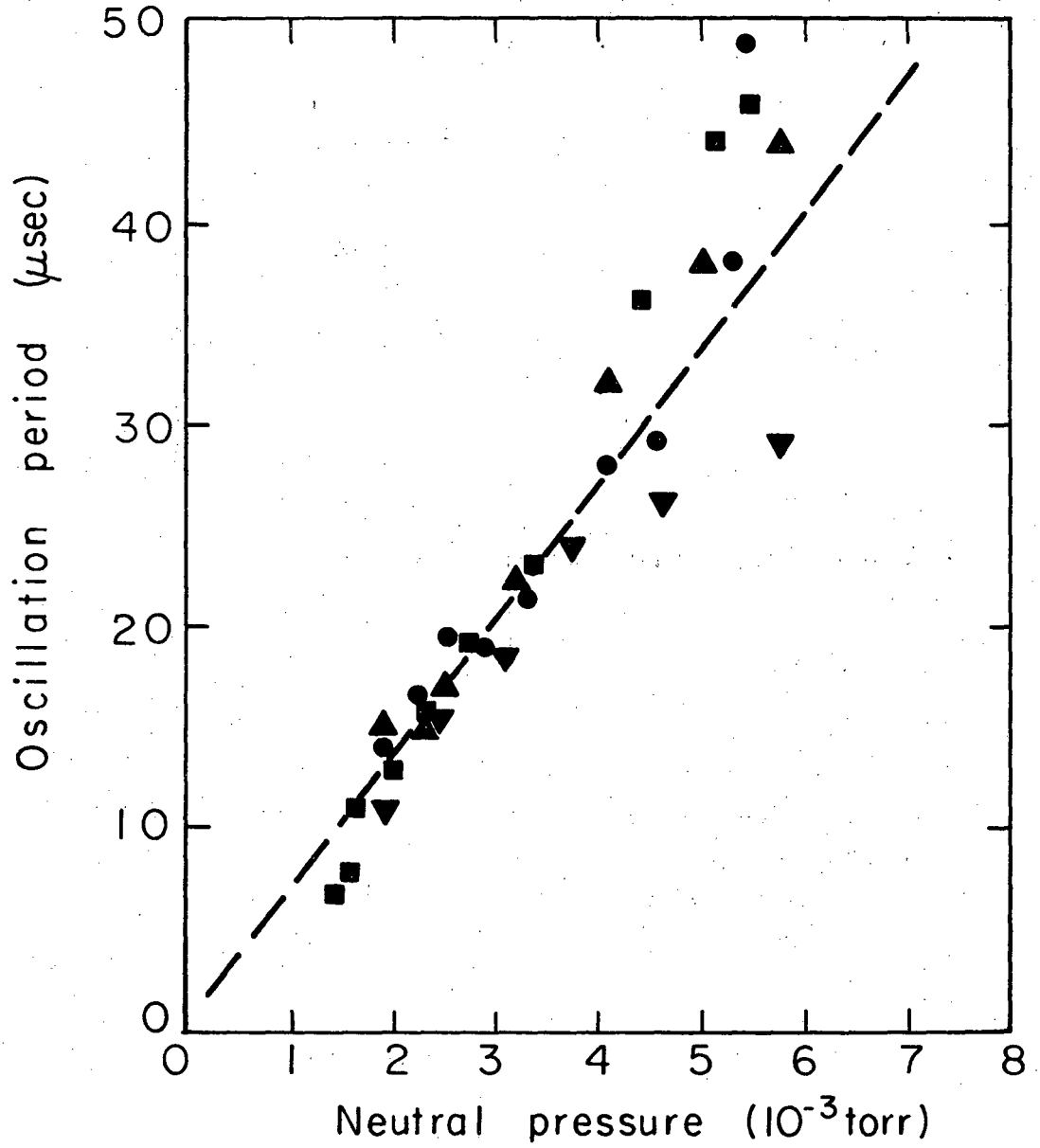

XBL 688-3636

Fig. 35. Period of the intermediate frequency fluctuations as a function of neutral pressure for a single cathode arc with 0.6 cm limiting aperture in A_I and E_I. ●, B = 420 G; ■, B = 500 G; and ▲, 560 G. For same data as Fig. 34, with no limiting aperture and a bare single cathode. ▼, B = 560 G.

the arc. This same instability is also observed in both hydrogen and argon plasmas. The oscillation period is longer for hydrogen and shorter for argon at the same neutral pressure.

V. DISCUSSION

We have presented measurements of the detailed spatial properties of our plasma for a variety of experimental conditions. We shall now relate these measurements to the overall transport of a bounded, partially ionized plasma along and across a magnetic field. From our measurements of the spatial variation of the saturated ion-current curves and probe floating potential, we can infer the plasma density and gradients, the electron temperature, the plasma potential, and electric fields. From our measurements of the fluctuations we can infer the contribution to transport of the plasma due to enhanced diffusion and convective transport.

A. Transport Rates and Coefficients

A theoretical description of the transport, as given by Eqs. (2.1), (2.2), (2.5), (2.8), and (2.9) in Sect. II, involves various diffusion coefficients. These depend on the ion and electron temperatures, the plasma and neutral density, and the magnetic field strength, as well as the momentum transfer cross sections for various processes. We now consider the measurements of Data Set 1 in detail, calculating the transport coefficients and the ion and electron particle balance. We then discuss the effects of the boundary conditions, the radial electric field, the azimuthal symmetry of the plasma, and the fluctuations. Finally we discuss the electron temperature, the halo, and the effects of excited states on the plasma. References to other data sets will be brought in where appropriate.

1. Collision Rates

From our theoretical discussion of the transport coefficients in Appendix C we find that the transport coefficients depend on the collision rates for momentum transport between species, which in turn depend on the collision cross sections. The elastic collision cross section for collisions between electrons and neutrals, and the elastic and charge-exchange cross sections for collisions between ions and neutrals, are discussed in Appendix A. As both the electron and ion cross sections for collisions with neutrals are quite independent of velocity at low energies, we can approximate the average of the cross sections over the velocity distribution, $\langle \sigma_{\alpha n} v \rangle^{\alpha}$, by the product of the averages $\sigma_{\alpha n} v_{\alpha}$. The collision rates and mean free paths for various processes are indicated in Table A.1 of Appendix A.

The collisions between species determine not only the diffusion rates, but also the rate of energy exchange between species. In order to evaluate the diffusion coefficients for the plasma, we must estimate the ion temperature. We calculate the ion temperature on the basis of local energy exchange between species.

2. The Ion Temperature

We consider the specific conditions of the radial ion temperature profile of Data Set 1. The ion temperature is established by heating the ions by collisions with the much hotter electrons and by cooling by collisions with the cold neutral background gas. The ions in the plasma experience many collisions before they reach the walls. We assume that the thermal convection is sufficiently slow that the ion

temperature at a given position is determined solely by the local energy exchange. The ion energy exchange rate per ion can be written as[28]

$$\frac{3}{2}\frac{1}{n}\frac{\partial nkT_i}{\partial t} = 2\nu_{ei}\frac{m_e}{m_i}\frac{3}{2}(kT_e - kT_i)$$

$$+ 2\left(\frac{\nu_{in}^{el}}{2} + \nu_{in}^{cx}\right)\frac{3}{2}(kT_N - kT_i) + H^i, \qquad (5.1)$$

where H^i is the ion heating due to other processes, such as randomization by collisions with neutrals of the E x B drift motion. The factor 3/2 indicates that even though there is a magnetic field the collision rate is sufficiently large that the kinetic temperatures are isotropic; ν^{ei} is the collision frequency for Coulomb collisions, ν_{in}^{cx} and ν_{in}^{el} are the charge exchange and elastic scattering, respectively. These are evaluated in Table A.2 of Appendix A. The factor of 1/2 for the elastic collisions indicates that half the average energy difference is lost in a collision. However, in charge exchange all the energy difference is lost.

The ion heating due to Coulomb collisions is given by

$$2\nu_{ei}\frac{m_e}{m_i}\left(\frac{3}{2}kT_e - \frac{3}{2}kT_i\right) = 6.9 \times 10^{-9}\, n_e \frac{kT_e - kT_i}{(kT_e)^{3/2}}$$

$$= 1.7 \times 10^4 \text{ eV/sec.} \qquad (5.2a)$$

The cooling of the ions by collisions with neutrals is given by

$$2\left(\frac{\nu_{in}^{el}}{2} + \nu_{in}^{cx}\right)\left(\frac{3}{2}kT_N - \frac{3}{2}kT_i\right) = 5.5 \times 10^{-9}\, n_0(kT_i)^{1/2}(kT_N - kT_i)$$

$$= 1.7 \times 10^{4}\ \text{eV/sec}. \qquad (5.2b)$$

The heating due to randomization of the E x B motion is negligible by comparison, $(m_i/2)(E_r/B)^2\nu_{in} = 2.7 \times 10^{-3}$ eV/sec. Evaluating the above expression for Data Set 1 at r = 4 cm, we find that for the calculated ion temperature the ions are transferring 1.7×10^{4} eV/sec per ion of energy between the electrons and neutrals.

The ion temperature is determined by evaluating Eq. (5.1) for steady state, $(3/2n)(\partial nkT_i/\partial t) = 0$. When this is done we find that

$$kT_i = (kT_e + FkT_n)/(1 + F), \qquad (5/3)$$

where $$F = 1.59 \times (n_0/n_i)(kT_e)^{3/2}(kT_i)^{1/2}.$$

F is also a function of the ion temperature. By iteration, however, one rapidly converges on the value for kT_i. The neutrals in the secondary plasma are in good thermal contact with the walls of the system and are approximately at room temperature, $kT_n = 0.03$ eV. At r = 4 cm the measured electron temperature is $kT_e = 0.28$ eV. By solving for the ion temperature at steady state we find $kT_i = 0.074 \pm 0.011$ eV. The radial dependence of the ion temperature together with the estimated fractional uncertainty is shown in Table 5.1.

For r < 2 cm in the central arc column cold neutrals are rapidly being lost in ionizing collisions with the hot streaming electrons in the core and by charge exchange with the ions, so that the neutral

Table 5.1. Data Set 1. Calculated ion temperature as a function of radial position. Uncertainty estimates are discussed in Appendix D.

r (cm)	n_i (10^{12} cm^{-3})	kT_e (eV)	kT_i (eV)	Fractional uncertainty in kT_i
1	4.3	7.0	0.061	0.16
2	4.2	0.46	0.103	0.17
3	2.6	0.36	0.085	0.16
4	1.8	0.28	0.074	0.15
5	1.11	0.28	0.062	0.14
6	0.60	0.30	0.050	0.13
7	0.44	0.26	0.046	0.12
8	0.30	0.22	0.042	0.11
9	0.19	0.19	0.039	0.098

Evaluated for B = 560 G, $n_0 = 1.3 \times 10^{14}$ cm^{-3} and $kT_n = 0.03$ eV.

density and ion cooling by neutral collisions in the core is appreciably smaller than in the secondary plasma. One can experimentally observe some pumping of neutrals from the diffusion chamber to the "anode end" by the arc. The ions are losing energy to the neutrals at a rate smaller than the estimate used in our calculation; therefore the calculated ion temperature near the central arc column is too low. The ion temperature should decrease monotonically outward from the center. In Appendix D, Sect. 6, we discuss the uncertainties in the calculated ion temperature in the secondary plasma based on local energy exchange between species. The calculated ion temperature is estimated to be reliable to within 10% to 20%, and this is reflected in the uncertainty in the plasma transport coefficients.

Spectroscopic measurements of the ion temperature in a strontium-seeded argon plasma produced in a hollow-cathode arc have been made by Berkner et al.[3] and Winocur and Pyle.[29] In the central arc column the ion temperature is typically 0.5 ± 0.2 eV as measured from the plasma emission spectra. From optical absorption measurements the ion temperature in the secondary plasma was found typically to be $kT_i = 0.1 \pm 0.1$ eV. Hudis, Chung, and Rose[18] have also measured Ar ion temperatures in the range 0.15 to 0.8 eV in a similar argon arc. To this author's knowledge the ion temperature in helium arc discharges has not been measured directly; however, we can expect it to be of the order of 0.5 eV in the central arc column.

The observed electron temperature is considerably above the temperature of the neutral background gas in the secondary plasma. There is a constant energy loss to the neutrals and ions. There must be

some mechanism by which the electron temperature is maintained significantly above the neutral temperature. This is discussed in Sect. V. G.

3. Molecular Ions and Recombination

The collisional diffusion coefficients can be estimated from a knowledge of the neutral density, the ion species, the ion density, the electron and ion temperatures, and the momentum transfer cross sections. It has long been known that the helium molecular ion He_2^+ can be formed in helium discharges.[30] It is formed primarily in the collision of a ground-state neutral with an excited neutral within 1.5 eV from the helium ionization energy of 24.51 eV. There must be at least 23.1 eV available before the molecular ions are formed. The helium metastable levels lie too low to produce this reaction.[31] The inverse process is dissociative recombination.

The balance between production and loss of molecular ions determines the density. In the positive column of a glow discharge in helium in the 1-Torr pressure range the molecular ion is known to contribute significantly.[32] At a constant electron temperature the molecular ion density is proportional to the neutral pressure squared. The electron temperature in the central column of our arc discharge is of the order of 5 eV, which is approximately the same as the electron temperature in a glow discharge. The molecular ion production in the central arc column should be negligible, as our neutral pressure is three orders of magnitude lower.

In the secondary plasma, in which the electron temperature is typically of the order of 0.5 eV or less, the production of excited

states in inelastic collisions is much smaller than in the central arc column. In addition, the coefficient for dissociative recombination of the molecular ions is $\alpha_D = 4 \times 10^{-9}$ cm^3/sec.[33] Expressions for three-body collisional and radiative recombination for helium are given by Hinnov and Hirshberg.[34] Evaluating these for the experimental conditions of Data Set 1 at r = 4 cm, we find that the three-body collisional recombination coefficient for helium ions is $\alpha_C = 3.10 \times 10^{-12}$ cm^3/sec. This gives us a total helium-ion recombination coefficient of 3.8×10^{-12} cm^3/sec. This gives us for Data Set 1 a volume recombination rate of 7 sec^{-1} per particle, as indicated in Table 5.3. This is much smaller than the particle accumulation rate due to various transport processes. The dissociative recombination coefficient for molecular ions is three orders of magnitude larger, so that recombination should effectively wipe out any molecular ions that are produced before they are lost by transport. We can then assume that the only important ion species in our plasma is the helium ion He^+.

4. Collisional Diffusion

One can calculate the transport coefficients for neutral collisional diffusion as given by Eqs. (C.4) and (C.5) and for fully ionized diffusion as given by Eq. (C.12) in Appendix C. The transport coefficients as a function of plasma and neutral density, ion and electron temperatures, and magnetic field strength are listed in Table A.2 of Appendix A. The coefficients evaluated for the conditions of Data Set 1 are indicated in Table 5.2. Also shown are the estimated uncertainties in various quantities as determined from the error analysis given in Appendix D.

Table 5.2. Data Set 1. Values of various quantities at r = 4 cm. The uncertainty estimates are discussed in Appendix D.

Quantity	Value	Fractional uncertainty
B	560 ± 28 G	(0.05)
P_T	4.0 ± 0.8 mTorr	(0.20)
n_0	$1.3 \pm 0.3 \times 10^{14}$ cm^{-3}	(0.22)
kT_n	0.03 ± 0.003 eV	(0.10)
$n_i = n_e$	$1.8 \pm 0.3 \times 10^{12}$ cm^{-3}	(0.31)
kT_e	0.28 ± 0.04 eV	(0.15)
kT_i	0.074 ± 0.011 eV	(0.15)
q	2.3 ± 0.17	(0.077)
E_r	0.2 ± 0.15	(0.75)
$D_{\parallel}^{in}$	$7.2 \pm 1.7 \times 10^{4}$ cm^2/sec	(0.23)
$D_{\perp}^{in}$	$9.8 \pm 3.2 \times 10^{2}$ cm^2/sec	(0.33)
$\mu_{\perp}^{in}$	$1.3 \pm 0.3 \times 10^{4}$ cm^2/V sec	(0.25)
D^{ei}, D^{ie}	$1.3 \pm 0.5 \times 10^{3}$ cm^2/sec	(0.34)
$D_{\parallel}^{en}$	1.6×10^{8} cm^2/sec	
$D_{\perp}^{en}$	7 cm^2/sec	
D_{enh}^{i}	$\leq$ 130 cm^2/sec	(0.50)
L_{eff}	64.5 cm	
λ_{in}	1.15 cm	
$\frac{\langle nv_r \rangle_{conv}^{\alpha}}{n}$	1050 ± 440 cm/sec	(0.42)

5. Weakly Ionized versus Fully Ionized

In our experiment the transport due to ion neutral collisions and due to ion electron collisions are both significant even though our plasma is only 1.4% ionized at r = 4 cm. To study the diffusion process we should like to work either in the weakly ionized regime, so that we can neglect Coulomb collisions entirely; or in the fully ionized regime, so that we can neglect collisions with neutrals. One can decrease the plasma density, reducing the effect of Coulomb collisions, by reducing the arc current or by using a thermionic cathode. However, if the plasma density is sufficiently low that Coulomb collisions are unimportant, it becomes almost impossible to obtain reliable Langmuir probe measurements of the spatial properties of the plasma. At low densities the Langmuir probe curve has a long slope on the ion current curve which does not saturate. One cannot determine the "saturated ion current" and ion density without careful analysis of the probe collection characteristics.[35] At low densities one usually must resort to measuring the particle collection at the end walls as the plasma decays, as Geissler has done.[36]

If one increases the neutral gas pressure in the diffusion region, the neutral collisional diffusion becomes larger; however, there is more cooling of the ions and electrons, lowering the electron temperature and increasing the cross section for Coulomb scattering. This increases the transport due to fully ionized diffusion. Finally, one can go to the fully ionized regime by lowering the neutral pressure; however, the fully ionized diffusion coefficient depends on the plasma

density, the transport equations are quadratic in the plasma density and nonlinear, and one can no longer study the parametric dependence of the transport with neutral pressure. Our discharge at low pressure goes into a mode characterized by large-amplitude fluctuations, and by rapid radial transport to which simple diffusion analysis does not apply. Therefore in studying transport in an active discharge of this type one is forced to consider the intermediate regime, the partially ionized plasma, where both Coulomb collisions and collisions with neutrals play important roles in determining the transport.

The relative importance of diffusion due to Coulomb collisions and ion-neutral collisions depends on the ion and electron temperatures. Simon, in analyzing Neidigh's experiments,[4] assumes that $kT_e = kT_i = 2$ eV. If this is true then $D^{ie} = 4.9 \times 10^2$ cm^2/sec, which is much less than $D_\perp^{in} = 1.4 \times 10^5$ cm^2/sec. From the expressions for the diffusion coefficients in Table A.2 of Appendix A we see that $D_\perp^{in} \approx (kT_i)^{3/2}$ while $D^{ie} \approx (kT_e + kT_i)/(kT_e)^{3/2}$. As kT_i becomes smaller $D_\perp^{in}$ becomes smaller. As kT_e becomes smaller, D^{ie} becomes larger. If we use as a criterion for neutral collisional diffusion to dominate the ion motion of our plasma that $D_\perp^{in} = 10 \times D^{ie}$, we have then the condition that

$$\frac{n_i}{n_0} \ll 0.12 \frac{(kT_i)^{3/2}(kT_e)^{3/2}}{kT_i + kT_e},$$

where the temperatures are in eV. This condition is not satisfied in our plasma, as it requires that $n_i/n_0 \approx 10^{-3}$ and our plasma is typically about 1% ionized. As both the ion and electron temperatures in

the secondary plasma are typically found to be much less than 2 eV, the agreement between theory and experiment in the work of Simon and Neidigh[4,17,11] may have been fortuitous.

6. Enhanced Transport

In the presence of transverse electric field and density fluctuations in the plasma there is the possibility of enhanced transport of the plasma across the magnetic field due to $\vec{E} \times \vec{B}$ drift effects. If the spectrum of the fluctuating electric fields is broadened by variations in phase, amplitude, or frequency, so that the plasma drift motion takes on a stochastic character, there may be enhanced diffusion. The enhanced diffusion depends on the self-correlation time of the electric field fluctuations as defined by Eq. (C.29) and gives a transport which is proportional to the plasma density gradient. If the fluctuating transverse electric fields are correlated with the density fluctuations, there may also be convective transport of the plasma across the magnetic field. The convective transport depends on the phase relationship between the electric field and density fluctuations, and is independent of the self-correlation time of the electric field fluctuations.

a. Enhanced Diffusion

The expression for the enhanced diffusion coefficient is Eq. (C.32),

$$D_{enh} = \frac{2c^2 \langle [E(t)]^2 \rangle}{B^2} \tau_s .$$

The "correlation time" τ_s of the oscillation is given in Appendix C by Eq. (C.33),

$$\tau_s = \frac{\nu}{\nu^2 + \omega_0^2} ,$$

where $2\nu/2\pi$ is the bandwidth of the oscillations in Hz and $\omega_0/2\pi$ is the frequency of the oscillation in Hz. $\langle [E(t)]^2 \rangle$ is the mean square electric field fluctuation.

For the experimental conditions of Data Set 1[37] there is an observed azimuthal fluctuating electric field at a frequency $\omega_0/2\pi = 48$ kHz, with an amplitude $E_\theta = 0.12 \pm 0.04$ V/cm rms at $r = 4$ cm in the secondary plasma. The bandwidth of the 48-kHz fluctuations was estimated crudely. From observations with a Panoramic Ultrasonic Analyzer such as are shown in Fig. 34, photograph (b), we find that the width of the spectrum is of the order of the instrument resolution, which is about 2 kHz. We assume that $2\nu/2\pi = 2$ kHz is an upper bound on the bandwidth of the 48-kHz oscillation spectrum.

Using Eq. (C.33), we can calculate an upper bound on the "correlation time" for the 48-kHz oscillation,

$$\tau_s \leq 2.8 \times 10^{-7} \text{ sec.}$$

From Eq. (C.32) we then get an upper bound on the contribution to enhanced diffusion due to the 48-kHz azimuthal electric field fluctuations of

$$D_{enh} \leq 130 \text{ cm}^2/\text{sec},$$

which is shown in Table 5.2.

The contribution due to the higher-frequency fluctuations is even smaller. From Fig. 33, photograph (a), we find typically a peak in the fluctuation spectra at about 6 MHz which is perhaps 2 MHz wide. This would give us a "correlation time" $\tau_s = 1.6 \times 10^{-8}$ sec. From the azimuthal and axial electric field fluctuations presented in Fig. 15 we find that the high-frequency component of the electric field fluctuations is of the order of 0.03 V/cm peak to peak, or about 0.01 V/cm rms. From Eq. (C.28) this then gives us a contribution to enhanced diffusion due to the high-frequency fluctuations of the order of

$$D_{enh} = 5 \times 10^{-2} \quad cm^2/sec.$$

b. Convection

The effective transport due to convection is given by Eq. (C.26). In our cylindrically symmetric system we assume that there is no zero-order azimuthal electric field E_0. The convective transport for both the ions and electrons is then given by

$$\langle nv_r \rangle^{\alpha}_{conv} = \frac{cn_1E_1}{B} \frac{\cos \delta}{2} ,$$

where n_1 and E_1 are the amplitudes of the density and electric field perturbations. For a sinusoidal perturbation the amplitudes n_1 and E_1 are a factor of $\sqrt{2}$ larger than the rms values. From Fig. 11 we find that the maximum of the density perturbation at $r = 4$ cm is approximately 45 deg earlier in time than the maximum of the potential perturbation. The maximum of the electric field is about 90 deg earlier

in time than the maximum of the potential fluctuation, as shown in Fig. 15. This gives an overall phase shift between the density and electric field fluctuations of the order of $\delta = 45$ deg.

The dynamics of the perturbation of the secondary plasma is considered in Sect. V.F.7 below, where it is found that a long axial wavelength perturbation of the plasma with finite electron resistivity along the magnetic field is sufficient to cause a phase shift between the density and potential perturbations. For the ions the effect of collisions with neutrals and ion inertia provides the necessary currents, so that the ion continuity equation is satisfied.

A positive E_θ electric field crossed with the magnetic field B_z gives a drift in the positive radial direction. The density perturbation from Fig. 5 is measured and found to be $n_1 = 0.13 \times 10^{12}$ cm^{-3} rms out of a mean density at $r = 4$ cm of 1.8×10^{12} cm^{-3}, giving a 7% rms density fluctuation. The fluctuating electric field is of the order of 0.12 ± 0.04 V/cm rms. The convection velocity per particle due to the fluctuating density and azimuthal electric field in a magnetic field of 560 G is then

$$\langle nv_r \rangle^{\alpha}_{conv}/n = 1050 \pm 440 \quad \text{cm/sec.}$$

Including a 30% uncertainty in E_θ and a 15 deg uncertainty in the phase angle δ, we get an overall uncertainty of 42%, as is shown in Table 5.2.

B. Ion-Paricle Balance

The contributions of various processes to the radial and axial ion transport are given by Eqs. (2.1) and (2.5),

$$nv_r^i = + (D_\perp^{in} + D^{ie}) \frac{n}{q} + \mu_\perp^{in} n E_r + D_{enh}^i \frac{n}{q} + \langle nv_r \rangle_{convection}^i, \qquad (5.5)$$

$$nv_z^i = + D_\parallel^{in} \left[1 + \frac{T_e}{T_i} \right] n \frac{\pi}{L_{eff}}, \qquad (5.6)$$

assuming that the plasma distribution can be adequately represented by $n(r,z) = e^{-r/q} \cos(\pi z/L_{eff})$ and that the distribution is azimuthally symmetric. We can evaluate the contribution of various processes to the radial and axial plasma transport at a specific point, say at $r = 4$ cm in the midplane of the diffusion chamber. Using the results of Data Set 1 and assuming that the ion temperature is given by our previous rate balancing calculation, we evaluate the contribution to transport due to various processes. These are listed in Table 5.3, where we have normalized the transport rates to a single particle.

The ions have significant radial transport due to both ion-neutral collisions and fully ionized diffusion. The contribution in this case due to enhanced diffusion is negligible. The mobility term may be large; however, there is considerable uncertainty as to what value of radial electric field to use. The mean electric field from Fig. 6 is of the order of 0.2 ± 0.15 V/cm. We note, however, that the plasma potential profile is pretty flat in the immediate vicinity of $r = 4$ cm, indicating that the radial electric field could locally be as small as 0.05 V/cm. From the Einstein relationship one can see that the transport due to ion mobility is determined by $\mu_\perp^{in} E_r = (eD_\perp^{in}/kT_i) E_r$. An electric field of only $kT_i/eq = 0.040$ V/cm would cause the mobility transport to be as large as the transport due to

Table 5.3. Ion Balance for Data Set 1 at r = 4 cm.

Process	Ion transport rate (cm/sec)	Ion accumulation rate (sec^{-1})
Neutral collisional diffusion	$\frac{D_\perp^{in}}{q} = 4.2 \pm 1.4 \times 10^2$	$-\left(\frac{1}{q} - \frac{1}{r}\right)\frac{1}{q} D_\perp^{in} = 1.3 \pm 0.5 \times 10^2$
Fully ionized diffusion	$\frac{D^{ie}}{q} = 5.8 \pm 2.0 \times 10^2$	$-\left(\frac{2}{q} - \frac{1}{r}\right)\frac{}{q} D^{ie} = 3.6 \pm 1.3 \times 10^2$
Enhanced diffusion	$\frac{D_{enh}^{i}}{q} = \leq 57$	$-\left(\frac{1}{q} - \frac{1}{r}\right)\frac{1}{q} D_{enh}^{i} = \leq 10$
Mobility in electric field	$\mu_\perp^{in} E_r = 2.6 \pm 1.8 \times 10^3$	$\left(\frac{1}{q} - \frac{1}{r}\right)\mu_\perp^{in} E_r = 4.9 \pm 3.9 \times 10^2$
Radial convection	$\frac{\langle nv_r \rangle_{conv}^{i}}{n} = 1.0 \pm 0.4 \times 10^3$	$\left(\frac{1}{q} - \frac{1}{r}\right)\frac{\langle nv_r \rangle_{conv}}{n} = 1.9 \pm 0.8 \times 10^2$
Total radial transport and accumulation	$4.8 \pm 2.6 \times 10^3$	$1.2 \pm 0.6 \times 10^3$
Axial diffusion current to walls	$\frac{\pi}{L_{eff}} D^{in}\left(1 + \frac{T_e}{T_i}\right) = 1.7 \pm 0.5 \times 10^4$	$\left(\frac{\pi}{L_{eff}}\right)^2 D^{in}\left(1 + \frac{T_e}{T_i}\right) = 8.1 \pm 2.2 \times 10^2$
Recombination		$-\alpha n_e = -7$

neutral collisional diffusion in this experiment.

The effect of convective transport due to fluctuations is significant. Because of the measured phase relationship between the azimuthal electric field E_θ and the density perturbation, the transport is directed radially outward. For the ions this effect adds to the radial transport due to mobility. The effect is large, being of the magnitude of the transport due to both neutral collisional and fully ionized diffusion. It convects ions as well as electrons at the same rate.

The axial ion current to the ends of the system is estimated on the assumption that the electrons are axially in Maxwell-Boltzmann equilibrium and that the axial distribution is approximately cosinusoidal, with the effective length $L_{eff} = 64.5$ cm. From Table 5.3 the axial diffusion velocity is $1.7 \pm 0.5 \times 10^4$ cm/sec per particle relative to the midplane plasma density of 1.8×10^{12} cm^{-3}. The third concentric end electrode has an inner radius of 3.5 cm and an outer radius of 5.4 cm for a total ring area of $A_3 = 53.1$ cm^2. The density is falling off exponentially with a scale length $q = 2.3$ cm, and by integrating between 3.5 and 5.4 cm we find that the estimated ion current is

$$I_3 = e\langle v_z \rangle^i_{wall} \int_{A_3} n(r)dA \approx 0.18 \text{ A}. \qquad (5.7)$$

Because of the electron-reflecting end sheath this is approximately the total current drawn by the electrode. This is in agreement with the measured values, for the third ring, of 0.13 to 0.34 A, as shown in Table 4.2.

One can also estimate the rate at which particles are accumulating in a unit volume per particle, using Eq. (2.8). On the assumption that $n(r,z)=n_0 e^{-r/q}\cos(\pi z/L_{eff})$, Eq. (2.8) becomes

$$\frac{\partial n_i}{\partial t} = +\left(\frac{1}{q}-\frac{1}{r}\right)\frac{n}{q}D_{\perp}^{in} + \left(\frac{2}{q}-\frac{1}{r}\right)\frac{n}{q}D^{ie} + \left(\frac{1}{q}-\frac{1}{r}\right)\frac{n}{q}D_{enh}^{i} + \left(\frac{1}{q}-\frac{1}{r}\right)\mu^{in}nE_r$$

$$+\left(\frac{1}{q}-\frac{1}{r}\right)\langle nv_r\rangle_{convection} - \left(\frac{\pi}{L}\right)^2 nD_{\perp}^{in}\left(1+\frac{T_e}{T_i}\right), \qquad (5.8)$$

where the 1/r terms are generated by taking the divergence of the particle flux in cylindrical geometry. The values for the various terms, normalized per particle, are listed in Table 5.3.

The largest contributions to the radial accumulation of ions come from the divergence of the mobility term, and from the fully ionized term, whose divergence has an extra term because the fully ionized diffusion coefficient also varies as the plasma density. The net particle accumulation rate due to the divergence of all radial currents as shown in Table 5.3, including the contribution due to convection, is $1.2 \pm 0.6 \times 10^3$ sec^{-1} particle. This agrees with the estimated axial loss of plasma due to diffusion along the magnetic field of $8.1 \pm 2.2 \times 10^2$ sec^{-1}. It is quite evident from Table 5.3 that the neutral collisional diffusion plays only a small part in the ion transport of the secondary plasma in this experiment. The transport due to convection, mobility, and fully ionized diffusion must be included to account for the ion transport across the magnetic field.

C. Electron Particle Balance

1. Radial Electron Transport

The contributions of various processes to the radial electron transport are given by Eq. (2.2). The axial electron flux, because of the reflecting end sheaths and axial electric field, should be zero to lowest order. Assuming, as in the case of ions,

$$n(r,z) = n_0 e^{-r/q} \cos(\pi z/L_{eff}), \tag{5.9}$$

and that the distribution is azimuthally symmetric, we can write

$$nv_r^e = (D_\perp^{en} + D^{ei}) \frac{n}{q} + D_{enh}^e \frac{n}{q} - \mu_\perp^{en} n E_r + \langle nv_r \rangle_{conv}^e. \tag{5.10}$$

The particle transport rate for various processes evaluated at $r = 4$ cm for the conditions of Data Set 1 are listed in Table 5.4. Because of the axial magnetic field and the small electron mass and gyroradius, the electron transport due to neutral collisional diffusion and mobility in the radial electric field is negligible. Fully ionized diffusion due to charged particle collisions, and convection due to fluctuating density and azimuthal electric fields, dominate the radial electron transport.

2. Electron Accumulation

From Eq. (2.9) we can estimate the rate at which electrons are being accumulated in a unit volume in the secondary plasma. Assuming that the accumulation is given by

Table 5.4. Electron balance for Data Set 1 at r = 4 cm.

Process	Electron transport rate (cm/sec)	Electron accumulation rate (sec^{-1})
Neutral collision diffusion	$\frac{D_{\perp}^{en}}{q} = 3$	$\left(\frac{1}{q} - \frac{1}{r}\right) \frac{1}{q} D_{\perp}^{en} = 0.6$
Fully ionized diffusion	$\frac{D^{ei}}{q} = 5.8 \pm 2.0 \times 10^{2}$	$\left(\frac{2}{q} - \frac{1}{r}\right) \frac{1}{q} D^{ei} = 3.6 \pm 1.3 \times 10^{2}$
Enhanced diffusion	$\frac{D_{enh}^{e}}{q} = \leq 57$	$\left(\frac{1}{q} - \frac{1}{r}\right) \frac{1}{q} D_{enh}^{e} = \leq 10$
Mobility in radial electric field	$+\mu_{\perp}^{en} n E_r = -5$	$+\left(\frac{1}{q} - \frac{1}{r}\right) \mu_{\perp}^{en} n E_r = -0.9$
Radial convection	$\frac{\langle nv_r \rangle_{conv}^{e}}{n} = 1.0 \pm 0.4 \times 10^{3}$	$+\left(\frac{1}{q} - \frac{1}{r}\right) \frac{\langle nv_r \rangle_{conv}^{e}}{n} = 1.9 \pm 0.8 \times 10^{2}$
Total radial transport and accumulation	$1.6 \pm 0.6 \times 10^{3}$	$5.7 \pm 2.1 \times 10^{2}$
Axial current to walls	$\frac{\langle nv_z \rangle_{wall}^{e}}{n} = 1.7 \pm 0.6 \times 10^{4}$*	$\frac{2\langle nv_z \rangle^{e}}{Ln} = 5.7 \pm 2.1 \times 10^{2}$*
Recombination		$-\alpha n = -7$

*Estimated by considering that the total electron accumulation rate is zero.

$$\frac{\partial n_e}{\partial t} = \left(\frac{1}{q} - \frac{1}{r}\right)\frac{n}{q} D_{\perp}^{en} + \left(\frac{2}{q} - \frac{1}{r}\right)\frac{n}{q} D^{ei} + \left(\frac{1}{q} - \frac{1}{r}\right)\frac{n}{q} D_{enh}^{e} - \left(\frac{1}{q} - \frac{1}{r}\right) \mu_{\perp}^{en} n E_r$$

$$+ \left(\frac{1}{q} - \frac{1}{r}\right) \langle nv_r \rangle_{conv}^{e} - \frac{2\langle nv_z \rangle_{wall}^{e}}{L} . \qquad (5.11)$$

The electron accumulation rate per unit volume per electron is evaluated for the conditions of Data Set 1 ar r = 4 cm and also listed in Table 5.4. Only fully ionized diffusion and convective transport contribute significantly to the accumulation of electrons by radial transport.

The net electron accumulation per unit volume due to radial electron transport is dominated by the radially outward, fully ionized diffusion term. The 48-kHz perturbation in the plasma density and azimuthal electric field is driven by an instability in the central arc column. The phase relationships between the density and electric field fluctuations are adjusted so that the ion and electron densities are equal, i.e., so that the condition of quasi neutrality is satisfied everywhere in the plasma except in the vicinity of the end sheaths. The plasma density in the total plasma volume reaches steady state on a time scale on the order of an ion-diffusion time. In this case the phase angle for the sinusoidal density and azimuthal electric field fluctuation is of the order of 45 deg, which produces a radially outward transport of electrons. For the ions the same effect operates, but the radial ion transport is dominated by neutral collisional diffusion and mobility current due to the radial electric field. Stix[38]

has pointed out in considering the transport across a magnetic field due to particles resonating with low-frequency fluctuations that it is possible to produce both "pump out" radially outward transport or "pump in" radially inward transport of the plasma.

3. Axial Electron Loss

Because of the long electron-neutral collision mean free path along the magnetic field lines, an axial electric field is established to limit the axial electron loss to the same order of magnitude as the ion loss rate. As this depends sensitively on the magnitude of the electric field and the end-sheath potential drop, we cannot calculate the axial electron transport directly, but must infer it from other measurements.

a. From Quasi Neutrality

Assuming that in steady state the net electron accumulation per unit volume is zero, $\partial n_e/\partial t = 0$, the accumulation due to radial transport must be balanced by axial loss. From Table. 5.4, then, we estimate that the axial electron loss per unit volume is $5.7 \pm 2.1 \times 10^2$ sec^{-1} per electron. If this loss is evenly distributed along the volume along the magnetic field lines, as is assumed in Eq. (2.9), we should have an electron flux to the end walls $\langle nv_z \rangle^e_{wall}/n = 1.7 \pm 0.6 \times 10^4$ cm/sec per electron, with an uncertainty of about 40%.

The axial ion flux to the end walls is given in Table 5.3 to be $\langle nv_z \rangle^i_{wall}/n = 1.7 \pm 0.5 \times 10^4$ cm/sec per ion. From this we calculate the ratio of electron collection to ion collection,

$$\beta = \frac{\langle nv_z \rangle^e_{wall}}{\langle nv_z \rangle^i_{wall}} . \qquad (5.12)$$

For these conditions and using these experimental data we estimate $\beta = 1 \pm 0.5$. Within our ability to deduce the electron axial loss rate from particle accumulation rates, the electron current to the end electrodes should be of the same order of magnitude as ion current.

b. From Concentric-End Ring-Electrode Current Collection

In Section IV[39] we discussed the current drawn by one of the end concentric ring electrodes C_4 as its voltage was changed, with all other discharge parameters held constant. When the electrode was electrically floated it assumed a potential of 3.3 V. When grounded the electrode collected a net current of 0.5 A. When the electrode was negatively biased it collected about 0.6 A. From the shape of the curve shown in Fig. 9 it was deduced that $\beta = 0.2$. The comment was made that one could not be sure what effect varying the voltage on the end electrode would have on the overall plasma transport. The ratio $\beta = 0.2$ can only be taken as an estimate; however, the grounded end electrode did collect more ions than electrons.

c. From Sheath Considerations

One can also estimate the axial electron loss rate from the presence of a potential drop and sheath at the ends of the system along magnetic field lines. Most of the axial potential drop occurs at the sheath. The measured probe floating potential just inside the sheath is, from Fig. 6, $\phi_f = 1.8$ V. The measured probe floating potential is related to the plasma potential by Eq. (B.4),

$$\phi_p = \phi_f + \frac{kT_e}{2e} \ln \frac{m_i}{kT_i} \frac{kT_e}{m_e} .$$

The plasma potential just inside an electron reflecting sheath is given by Eq. (2.14),

$$\phi_p = \phi_{wall} + \frac{kT_e}{2e} \ln \frac{m_i}{kT_i} \frac{kT_e}{m_e} + \frac{kT_e}{e} \ln \frac{\langle nv_z \rangle^e_{wall}}{\langle nv_z \rangle^i_{wall}} .$$

These two equations, when evaluated along the same field line where the electron temperature is constant, give

$$\phi_f = \phi_{wall} - \frac{kT_e}{e} \ln \frac{\langle nv_z \rangle^e_{wall}}{\langle nv_z \rangle^i_{wall}} , \qquad (5.13)$$

which can also be written as

$$\beta = \frac{\langle nv_z \rangle^e_{wall}}{\langle nv_z \rangle^i_{wall}} = \exp \frac{e[\phi_{wall} - \phi_f(t)]}{kT_e} , \qquad (5.14)$$

where β is defined as the ratio of electron current to ion current through the end sheath.

The probe floating potential changes in time, with the fluctuations well correlated along the magnetic field lines. The end sheath potential drop also changes with time, changing the rate at which electrons are lost out the ends. The fluctuations are at a frequency $f = 48$ kHz, which is slow compared with an electron transit time, which is of the order of 2×10^{-6} sec. The electrons are reflected at the

sheath many times as the potential changes. Let us estimate the average rate at which electrons are lost through the end sheath.

The potential fluctuations are large, $\delta\phi$ = 0.7 V rms, and predominantly at f = 48 kHz. Let us assume that the floating potential at a point just inside the sheath edge can be adequately represented as

$$\phi_f(t) = \phi_f + \phi_1 \cos(2\pi ft),$$

where ϕ_f = 1.8 V, ϕ_1 = 1.0 V, and ϕ_{wall} = 0.0 V. The mean value of the ratio of electron current to ion current through the sheath β is given by averaging over one cycle,

$$\beta_{ave} = \frac{1}{2\pi} \int_0^{2\pi} \exp\left[- \frac{e(\phi_f - \phi_{wall})}{kT_e} + \frac{e\phi_1}{kT_e} \cos 2\pi ft \right] d(2\pi ft), \qquad (5.15)$$

$$\beta_{ave} = \beta_0 I_0(e\phi_1/kT_e),$$

where β_0 is the value of β for $\phi_1 = 0$, $I_0(e\phi_1/kT_e)$ is the Bessel function of imaginary argument evaluated at $e\phi_1/kT_e$ for kT_e = 0.28 eV, $e\phi_1/kT_e = 3.6$, and $I_0(3.6) = 7.8$; $\beta_0 = \exp -e(\phi_f - \phi_{wall})/kT_e$, $\beta_0 = e^{-6.4} = 1.6 \times 10^{-3}$, and $\beta_{ave} = 1.2 \times 10^{-2}$. Both β_0 and $I_0(e\phi_1/kT_e)$ depend exponentially on the ratio of the potential or potential difference to the electron temperature, and any uncertainty is magnified considerably; for instance, a 20% uncertainty in the potential difference produces an uncertainty in β_{ave} of as much as a factor of 4, so that the estimate of the average ratio of electron to ion collection depends sensitively on accurate knowledge of the sheath conditions.

In summary, each of the three estimates of the ratio of the axial

electron-to-ion flux to the ends of the system contains considerable uncertainty. The axial electron flux depends sensitively on such factors as the time behavior of the axial electric field, the potential fluctuations, and end sheath conditions throughout the plasma. We have obtained estimates of the ratio of electron-to-ion flux to the ends by using only time-averaged quantities such as the mean sheath potential drop, the rms potential fluctuations, and particle transport based on other mean values. Our calculations of the ion and electron particle balance indicate that the axial electron loss is reduced to at least the same order of magnitude as the axial ion loss rate. From our consieration of the potential drop at the end sheath, the axial electron flux is probably much lower than the ion loss flux to the end wall. Our estimate of the ratio of electron-to-ion collection from the current voltage characteristics of the fourth cathode end ring C_4 lies between the other two estimates. All of this is consistent with the assumption that the majority of electrons in the secondary plasma are trapped in a potential well formed by the end sheaths.

D. The Radial Electric Field

1. Effect on Ion Transport

In Data Set 1 we find that although there is considerable uncertainty in the exact magnitude of the radial electric field, it is the mobility in the presence of the radial electric field of about 0.2 ± 0.15 V/cm which contributes most to the radial ion transport.

In Data Set 2 we find that for similar conditions, but with two cathodes and a larger overall arc current of 30 A, the radial density

scale length and radial electric field are larger. The radial ion transport is dominated by the radial mobility of the ions in the presence of the radial electric field. The contribution due to diffusion is decreased by a reduction in the density gradient, i.e., the density scale length increases from $q = 2.3$ cm in Data Set 1 to $q = 3.0$ cm.

In Data Set 3, which was also run with two cathodes but with a lower total arc current of 20 A, the data are generally similar to Data Set 1. Figure 22 shows that the radial electric field increases from about 0.25 V/cm to about 0.6 V/cm as the neutral pressure is reduced. In Fig. 21 the slope of the density profile does not change significantly with neutral pressure, as we would expect if neutral collisional diffusion were the dominant radial ion-transport process, and is of the order of 3×10^3 cm/sec per ion in the secondary plasma at both pressures, even though the radial ion mobility is much smaller at the lower pressure.

In Data Set 4 we find that as one increases the magnetic field the radial electric field also tends to increase. In Fig. 24 we find electric fields of 1.0 ± 0.2 V/cm and 1.5 ± 0.3 V/cm, where again the radial electric field is larger at lower pressures. In Table 5.5 various parameters, diffusion coefficients, and radial transport rates are evaluated at $r = 4$ cm. Unfortunately no measurements of the azimuthal electric field fluctuations were made for this case, so that we cannot estimate the effect of convective transport. The ion temperatures are again deduced by rate balancing between heating by the

Table 5.5. Values of various quantities for Data Set 4 evaluated at r = 4 cm. Fractional uncertainties are indicated in parenthesis and discussed in Appendix D.

Quantity		Case A	Case B
P_T	(0.20)	2.9 ± 0.6 mTorr He	3.9 ± 0.8 mTorr He
n_0	(0.22)	$9.6 \pm 2.1 \times 10^{13}$ cm^{-3}	$1.3 \pm 0.3 \times 10^{14}$ cm^{-3}
B	(0.05)	1680 ± 64 G	1680 ± 64 G
kT_n	(0.10)	0.03 ± 0.003 eV	0.03 ± 0.003 eV
$n_i = n_e$	(0.31)	$2.33 \pm 0.27 \times 10^{12}$ cm^{-3}	$3.9 \pm 1.2 \times 10^{12}$ cm^{-3}
kT_e	(0.15)	0.56 ± 0.08 eV	0.39 ± 0.06 eV
kT_i		0.088 ± 0.016 eV (0.18)	0.10 ± 0.017 eV (0.17)
q	(0.08)	1.25 ± 0.1 cm	1.5 ± 0.1 cm
E_r	(0.20)	1.5 ± 0.3 V/cm	1.0 ± 0.2 V/cm
L_{eff}		73.4 cm	65.7 cm
Transport coefficients			
$D_{\parallel}^{in}$		$1.1 \pm 0.3 \times 10^{5}$ cm^2/sec (0.24)	$8.4 \pm 0.2 \times 10^{4}$ cm^2/sec (0.24)
$D_{\perp}^{in}$		104 ± 37 cm^2/sec (0.36)	173 ± 60 cm^2/sec (0.35)
$\mu_{\perp}^{in}$		$1.2 \pm 0.3 \times 10^{3}$ cm^2/V-sec (0.26)	$1.7 \pm 0.4 \times 10^{3}$ cm^2/V-sec (0.26)
$D^{ei} = D^{ie}$		125 ± 43 cm^2/sec (0.34)	275 ± 93 cm^2/sec (0.34)
Radial ion transport			
$D_{\perp}^{in}/q$		83 ± 30 cm/sec (0.37)	115 ± 42 cm/sec (0.36)
D^{ie}/q		100 ± 35 cm/sec (0.35)	183 ± 93 cm/sec (0.35)
$\mu_{\perp}^{in} E_r$		$1.8 \pm 0.6 \times 10^{3}$ cm/sec (0.34)	$1.7 \pm 0.6 \times 10^{3}$ cm/sec (0.34)
Total radial collisional transport		$2.0 \pm 0.7 \times 10^{3}$ cm/sec	$2.0 \pm 0.7 \times 10^{3}$ cm/sec

electrons and cooling by the neutrals as given by Eq. (5.1). The radial transport is dominated by the ion mobility current. Even though we have increased the neutral pressure from Case A to Case B the radial electric field is reduced, and the total estimated radial ion transport is almost the same for the two cases.

2. Plasma Rotation

The presence of a radial electric field, in addition to dominating the radial ion transport, causes the plasma as a whole to rotate. Figure 36 shows this relation quite clearly. Time-resolved measurements of the saturated ion currents to two probes 90 deg apart were made at $r = 4$ cm for a neutral pressure of 3.5 mTorr by using a single cathode discharge, a 0.64-cm collimator in electrodes A_I and E_I, and a magnetic field of 560 G. In photograph A of Fig. 36, where the chamber ends are grounded, the maximum of the plasma density reaches the side probe about 50 μsec before it reaches the bottom probe. The period of rotation appears to be of the order of 2.5 msec. The large amplitude of the fluctuation and its irregular period indicate that one has a highly asymmetric distribution, which is rotating. As the probes are at $r = 4$ cm we have a rotation velocity of

$$v \approx \frac{2\pi r}{\tau} \approx 10^4 \text{ cm/sec},$$

which could be obtained with a radial electric field $E_r = 0.056$ V/cm, which is quite small indeed. In photograph B of Fig. 36 the diffusion chamber end electrodes are allowed to float electrically. The large-

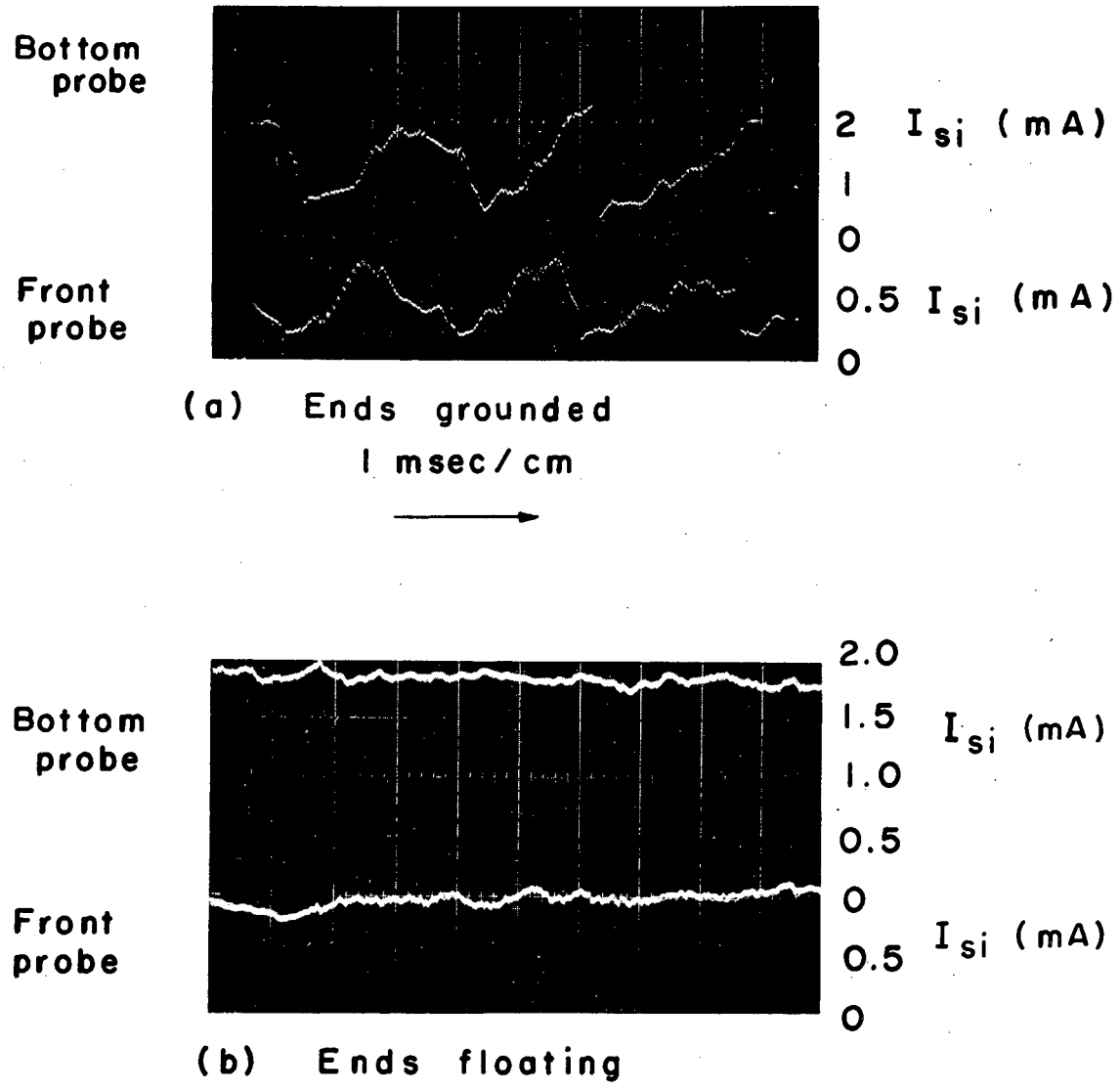

Fig. 35 Time-resolved saturated ion current for two probes at r = 4 cm on azimuths 90 deg apart. B = 560 G. (a) P_T = 3.5 mTorr He, ends grounded, showing plasma rotation; (b) P_T = 3.7 mTorr He, ends electrically floating, showing no rotation.

amplitude fluctuations are gone, indicating that the axial distribution no longer rotates and that the radial electric field is gone. The magnitudes of the saturated ion currents are quite different even though the probe areas are similar, indicating an azimuthally asymmetric density distribution.

3. Origin of the Radial Electric Field

The early arguments of Bohm et al.[1] suggested that for a plasma in a magnetic field there should be an ambipolar radial electric field of the order of $E_r \approx (kT_i/e)(\nabla_r n/n) \approx 0.03$ V/cm, which would retard the radial ion flux to be equal to the radial electron flux. Simon[17] later argued that the presence of conducting ends on the plasma system should "short circuit" the radial electric field so that $E_r \approx 0$ V/cm. However, in our experiments on the secondary plasma of a hollow-cathode arc discharge we observe an outward radial electric field, which increases the radial ion transport beyond that due to collisional diffusion alone. An outward radial electric field has also been observed in experiments on the plasma from a duo-plasmatron source in a magnetic field by Schwirzke.[40,14]

The potential within the plasma is determined by the potential drop, due to the axial electric field, along a magnetic field line from the point to the sheath edge, by the potential drop across the sheath to the end wall, and by the potential of the end wall. The sheath drop is related to the electron and ion temperature and the ion and electron currents through the sheath by Eq. (2.14). Schwirzke[40,14] and Schwirzke and Eggers[41] attempt to relate this electric field to

the radial temperature gradient in the plasma, and the radial variation of the enhanced transport of the electrons across the magnetic field. Schwirzke[42] also argues that the enhanced radial electron transport changes as a function of radius, changing the rate at which electrons are lost axially. The enhanced radial electron transport, he argues, explains the observed slow falloff of electron temperature with radius. His measurements extend only over the first centimeter of radius in the vicinity of the central arc column, where there is the possibility of electron heating by fluctuating fields and by inelastic collisions with the electrons streaming from the source region. In our experiments we are primarily concerned with transport in the secondary plasma, where the temperature gradients are quite small, and where the fluctuation amplitudes are also small.

In Data Set 5 we present measurements for a case similar to Data Sets 1 and 3 in which the end walls are allowed to float electrically. The radial density scale length as indicated in Fig. 26 is $q \approx 1.6$ cm, which is much less than for Data Set 3. In Fig. 27 we see that the electron temperature, probe floating potential, and plasma potential profiles are all flat beyond $r \approx 3$ cm, indicating that the radial electric field is zero within our ability to measure it. In Fig. 28 the axial plasma distribution is cosinusoidal.

It appears that the radial electric field is a consequence of the radial temperature gradient, the long mean free path of the electrons along the magnetic field, and a differential electron-to-ion current through the end sheath. If enhanced radial electron transport were

responsible for the establishment of the radial field, as Schwirzke[14,42] has suggested, we should expect to find a radial electric field even with the concentric ring end plates electrically floating.

In the secondary plasma every ion that reaches the sheath edge is collected, and the ion flux $\langle nv_z \rangle^i_{wall}$ is limited only by the rate at which the ions can diffuse along the magnetic field to the edge of the sheath. The axial electron flux $\langle nv_z \rangle^e_{wall}$, however, is determined by the potential drop across the end sheath, which may change with radius, thus producing a radial electric field in the plasma. Our diffusion system is constrained only by the potential of the end walls and by the necessity of conserving charge over the entire diffusion chamber volume.

The plasma density and electron temperature are falling off rapidly in the first 2 cm of radius. The potential of the plasma near the central arc column is largely determined by the sheath potential drop at the equipotential surface defined by the first end plate rings, C_1 and A_1. The sheath potential drop at a particular radius is determined by the ratio of ion to electron collection, and is given by Eq. (2.14),

$$\phi_p = \phi_{wall} + \frac{kT_e}{2} \ln \frac{kT_e}{m_e} \frac{m_i}{kT_e} + kT_e \ln \frac{\langle nv_z \rangle^e_{wall}}{\langle nv_z \rangle^i_{wall}} .$$

When the end electrode is electrically floated, ϕ_{wall} adjusts itself so that the total current collected over the entire surface of the electrode is zero. Neglecting the current collected across the magnetic field lines to the inner surface of the first electrode aperture,

we can write this condition for a floating electrode as

$$\int_{\text{Electrode}} \left[\langle nv_z \rangle^e_{wall} - \langle nv_z \rangle^i_{wall} \right] dA_z = 0. \tag{5.16}$$

As is discussed above in Sect. V.C.3, the average ratio of electron current to ion current through the end sheath β_{ave} in the presence of potential fluctuations of amplitude ϕ_1 is given by Eq. (5.15),

$$\beta_{ave} = \exp\left[- \frac{e(\phi_f - \phi_{wall})}{kT_e} \right] \left(I_0 \ \frac{e\phi_1}{kT_e} \right).$$

For Data Set 1 in Fig. 6 we see that for $r \approx 1$ cm at the edge of the central arc column, $\phi_f \ll \phi_{wall}$, and that the first end electrode draws a net electron current. This is also shown in Table 4.2, where the boundary currents on ring C_1 and A_1 are negative, indicating a net electron current $\langle nv_z \rangle^e_{wall} \gg \langle nv_z \rangle^i_{wall}$ and $\beta_{ave} \gg 1$. For larger radii, $\phi_f \gg \phi_{wall}$. Beyond $r = 3.5$ cm the end electrodes collect a net ion current, indicating $\langle nv_z \rangle^e_{wall} \ll \langle nv_z \rangle^i_{wall}$. The potential drop across the sheath is of the order of 2 V, whereas the electron temperature is typically $kT_e = 0.28$ eV. This provides an effective barrier to trap all but a small part of the electrons that hit the sheath. The plasma establishes a radial electric field by adjusting the ratio $\beta_{ave} = \langle nv_z \rangle^e_{wall} / \langle nv_z \rangle^i_{wall}$ as a function of radius. Between $r = 2$ cm and $r = 3.5$ cm, the region of ring 2, we find from Table 4.2 that the cathode ring C_2 collects a net electron current, while the anode ring A_2 collects a net ion current. This is an effect apparently

due to the fact that the single-cathode arc plasma distribution is slightly asymmetric toward the "cathode" end of the discharge.

E. Azimuthal Asymmetry

1. Asymmetry Experiments

In the presence of grounded end electrodes in our experiment we find a radial electric field which dominates the radial ion transport and causes the plasma as a whole to rotate. The secondary plasma is azimuthally symmetric when averaged over several fluctuation periods, as is shown by Data Set 2. When the end electrodes are allowed to electrically float, we find that both the radial electric field, as is shown in Data Set 5, and plasma rotation, as shown in Fig. 36, disappear. However, there is a strong tendency for the plasma to be azimuthally asymmetric, as shown in Data Set 6. The degree of asymmetry depends sensitively on the alignment of the physical axis of the system with the magnetic axis.

This author has found that since the early experiments of Bohm et al. there has been only one other attempt to check the symmetry of transport experiments on plasmas by using arc sources. Boeschoten, Geissler, and Siller,[43] in experiments with a duoplasmatron source plasma, found that for identical probes at opposite sides of the plasma at the same radius the saturated ion currents and thus the plasma density were different by an order of magnitude. The ion current was strongly dependent on the alignment of the metal cylinder which served as the radial and axial boundary of the plasma. It was possible to get reasonable agreement at one value of magnetic field, but agreement over a range of B required compromising. Better than a factor-of-two

agreement in saturated ion current was not to be expected. For insulating end plates the adjustment was even more difficult. Furthermore they experienced difficulty in reproducing the probe floating potential measurements, and the experiment was discontinued.

2. Origin of the Asymmetry

The mechanism for producing the azimuthally asymmetric plasma distribution with floating end electrodes is essentially the same mechanism as produces the radial electric field with grounded end electrodes. The ions produced on the axis of the discharge tend to be transported across the magnetic field in the most rapid manner possible. Diffusion is a very slow process compared with the E x B drift motion. The radial ion transport in the case of grounded end electrodes is dominated by the radial electric field established by the plasma's adjusting the electron currents through the end sheaths. For floating end electrodes the radial electric field is small and it appears that the plasma distribution is basically unstable. Any slight misalignment of the system can set up transverse components of electric field which cause the plasma to drift across the magnetic field lines in some preferred direction.

In considering the azimuthal asymmetry of the secondary plasma surrounding our hollow-cathode arc discharge, one is reminded of the early work of Bohm et al.[10] The detailed measurements of their rectangular arc showed that their plasma was never really symmetric. The equipotential lines were such that the arc plasma could easily E x B drift across magnetic field lines to the chamber wall. The degree of

asymmetry depended particularly on the cathode filament lifetime. The filament would wear in such a way as to reduce the asymmetry.[44] The asymmetry was larger at low pressures, and less at high pressures, where the effect of neutral collisions and diffusion is more important.

One of their comments is particularly pertinent,[45] "It has not yet been possible to account in detail for the asymmetrical ion distribution exhibited by the arc. However, there seems to be little doubt that the asymmetry is associated with the necessity that ions be removed from the arc column, where they are formed, to the walls of the chamber in order for the arc to run stably. If the ion distribution were completely symmetrical, the plasma equipotentials would be symmetric about the central arc column. Thus, under the action of the crossed magnetic and electric field, the ions and electrons would tend to drain around the equipotential surfaces without ever reaching the walls. This would tend to cause a piling up of ionization and a breakdown of the space charge neutralization condition. Such a state of affairs might cause the onset of violent plasma oscillations and enable the ions to reach the walls owing to the action of the strongly oscillating plasma fields. Alternatively, the arc could pass over into another state in which the steady plasma equipotentials are such as to cause the transfer of ions from the arc column to the vicinity of the sheath. It is believed that the latter behavior is that which occurs when the arc runs in an asymmetrical state."[45]

It seems remarkable in the light of this comment made in 1949 that few observers have checked the symmetry of the arc plasma and instead

have attempted to fit their experimental observations with "Bohm" diffusion caused by fluctuating fields. This observer's measurements confirm that there is a strong tendency for the secondary plasma of a hollow-cathode arc discharge with conducting ends to run in an asymmetric manner. The transport appears to be determined largely by the electric fields involved.

F. Fluctuations

The experimental evidence for various types of plasma instabilities has been reviewed by Lehnert.[46] There has been extensive theoretical work done on various instabilities that occur in plasmas, and there has been considerable success in observing them experimentally. However, many of the experiments present only plausible explanations for the observed phenomenon because of the many difficulties connected with laboratory plasmas. In the experiments several different types of instabilities may behave similarly over the available range of parameters. Also modes of different instabilities may occur concurrently, and effects due to collisions, finite geometry, particle diffusion, and drifts may further complicate the understanding of experiments.

In Sect. IV.C.4 we discussed the observed fluctuations in our experiment. There have been many observations of such fluctuations in similar experiments in arc and reflex arc discharges with both hot and cold cathodes; for a variety of geometries and gases in the neutral pressure range of 10^{-2} to 10^{-3} Torr; and for magnetic fields in the range of 100 to 1000 G. A variety of instability mechanisms have been proposed as plausible explanations for the observed phenomena.

Briffod, Gregoir, and Gruber[47] concluded that the 5-, 10-, and 20-MHz bursts of oscillation in their cold-cathode reflex arc were the result of a two-stream instability caused by fast electrons accelerated through the cathode sheath.

Oscillations in the intermediate frequency range of 20 to 100 kHz have been observed by Neidigh and Waver,[48] Chen and Cooper,[49] Thomassen,[50,51], Kerr,[52] and Chung and Rose[53] for a variety of experimental conditions. The observed fluctuations have been interpreted by Thomassen[50,51] and Kerr[52] as due to the neutral drag instability driven by the radial electric field, and by Chung and Rose[53] as possibly being an electrostatic ion cyclotron wave. The possibility of ion sound waves has been ruled out by Chen and Cooper[49] on the basis of axial wavelength.

Observations in the low-frequency range of 1 to 20 kHz have been made by Morse,[54] Kerr,[52] and Chung and Rose.[53] The neutral drag instability[54] and drift waves due to the radial density gradient[53] have been suggested as plausible explanations of their observations. We shall now discuss in more detail the various instabilities and their relationship to this experiment.

1. Ion Waves

Chen[55] speculates on the possibility of generating ion waves due to an instability in the end electrode or cathode sheaths, which may propagate along magnetic field lines into the plasma as a low-frequency acoustic wave. Measurements which show that the instabilities have a very long axial wavelength by Chen and Cooper[49] and theoretical arguments by Chen[56] rule out the possibility of ion sound waves. Chung

and Rose[53] have proposed electrostatic ion cyclotron waves as a possible mechanism on the basis of a simple model; however, Chen[57] rules them out because ion cyclotron waves would have to be much higher in frequency than observed.

2. Electron Streaming

Both in reflex arc discharges[47] and in our experiment there are high-energy electrons, 50 to 100 eV, streaming from the cathode through the primary plasma. Particularly in the case of the collimated discharge these electrons provide one of the primary mechanisms for generating the plasma in the central arc column. Assuming a cross section for ionization of a neutral helium by electron impact of 3.5×10^{-17} cm^2,[58] a neutral helium density of 10^{14} cm^{-3}, a primary discharge current of the order of 1 A over a cross sectional area of 1 cm^2, and an ion lifetime in the primary plasma of 10^{-4} sec, we would have a steady-state plasma density of 2×10^{12} cm^3 by this mechanism alone.

The relaxation of the electron velocity distribution to a Maxwellian can produce instabilities such as the two-stream instability, which would generate high-frequency fluctuations on the order of the plasma frequency,[59] i.e., 1.2×10^{10} Hz. In addition, wave-wave coupling of the plasma oscillations could produce lower-frequency fluctuations of the plasma.[60,61]

3. Neutral Drag Instability

In a partially ionized plasma there is an interaction of both the ions and the electrons with the neutral background gas. If there is motion of the plasma with respect to the neutrals, there is a drag,

primarily on the ions, which if sufficient causes a space-charge separation to develop. This gives rise to an instability of the plasma. The first neutral drag instability was found by Kadomtsev and Nedospasov.[62] Guest and Simon[63a] showed that a similar instability occurs if there is unequal streaming of electrons and ions to the ends of the system. Simon[63b] applied this theory to a partially ionized plasma in the presence of crossed electric and magnetic fields and found that if $\vec{E}\cdot\vec{\nabla}n > 0$ there was an instability. He considered a slab model and included the effect of finite resistivity. Hoh[64] studied the instability of a Penning discharge with cylindrical geometry and a radially inward electric field. He found that there was a critical magnetic field for the onset of this instability. The charge separation was due to a differential azimuthal particle drift in the radial electric field. Bingham[65] considered the possibility of a helical instability in a hot cathode reflex arc and found that the helical mode was unstable only for very long systems in which the axial wavelength $\lambda_z > 1200\ R$, where R is the system radius.

Morse[66] considered the effect of possible radial variation of the phase of the perturbation and found that the instability could be produced for both directions of the electric field, if the electric field of Hoh[64] were replaced by an effective electric field that depends on the electron and ion temperatures, the density gradient, the ion and electron neutral collision rates, and the magnetic field.

4. Resistive Drift Waves

For a plasma in a magnetic field with density gradients there are

electron and ion diamagnetic drifts perpendicular to the density gradient and magnetic field. If there is some mechanism by which charge separation can occur, then a perturbation of the plasma with these drifts grows. Chen[67a] has considered the fully ionized plasma and has found that viscosity, centrifugal force, and ion inertia can all give the necessary charge separation.

The phase velocity of the resistive drift wave is given by the electron diamagnetic drift velocity $v = \omega/k_\perp = kT_e/cB\nabla_\perp \ln n$.[67b,68] In the central arc column, which is about 1 cm in radius, there is plasma production by collisional excitation and we can expect the plasma distribution to be somewhat flatter than in the secondary plasma. Also the central arc column is rotating at 48 kHz and the instability has grown to a large-amplitude nonlinear limit. This may also contribute to the observed flattening of the time-averaged density measurement. The density near the center of the arc is changing rapidly as a function of time and there is also a steep electron-temperature gradient at the edge of the central arc column, so that it is difficult to estimate the local density gradient. Let us assume that the local radial density scale length at the edge of the central arc column is of the order of $q = 2.3$ cm or greater (as it is in the secondary plasma), that the electron temperature in the central arc column is typically 5 eV, and that the axial magnetic field is 560 G; this gives an azimuthal drift velocity of $v_\theta \leq 3.9 \times 10^5$ cm/sec. If the azimuthal wavelength corresponds to an $m = 1$ propagation of the perturbation at a radius of 1 cm, this gives us a frequency of 63 kHz

or less, which compares favorably with the observed oscillation of 48 kHz in Data Set 1.

Our measurements of the rotation of the 48-kHz potential fluctuations are indeed in the electron diamagnetic drift direction. However, our observations of the effect of mass rotation on probe current collection on a probe inserted perpendicular to a radius in Data Set 2 indicate that the mass rotation of the plasma is in the ion diamagnetic direction. Similar observations on fluctuations in the core of an arc discharge have been reported by Boeschoten, Demeter, and Kretschmer.[69]

5. Temperature Gradient Instabilities

Rudakov and Sagdeev[70] have discussed the possibility of drift waves being drive by the presence of large temperature gradients. They indicate that it is possible to have a low-frequency drift instability if the ion temperature falls off twice as fast as the plasma density, i.e.,

$$(d \ln kT_i)/(d \ln n_i) > 2.$$

The ion temperature in the secondary plasma is typically $kT_i = 0.1$ eV. Spectroscopic evidence indicates that the ion temperature in the central arc column is of the order of 0.5 eV.[71] At the edge of the central arc column the ion and electron temperatures fall off rapidly. We can estimate the gradient at the edge of the central arc column by assuming that kT_i falls off from 0.5 eV to 0.1 eV, in about 1 cm or less, and that in this region the typical ion temperature is 0.2 eV:

$$d(\ln kT_i)/dr = (1/kT_i)(dkT_i/dr) > 2.$$

From our previous discussion the radial density scale length in the central arc column is $q = 2.3$ cm or larger, giving a density gradient $d(\ln n_i)/dr = 1/q \leq 0.43$, so that $d(\ln kT_i)/d(\ln n_i) \geq 4.6 > 2$. We cannot rule out the possibility that the 48-kHz fluctuation of the central arc column may be driven by the radial ion-temperature gradient.

6. Plasma Rotation

Because of the presence of a radial electric field, a rotating asymmetric plasma distribution appears as a low-frequency (less than 20 kHz) fluctuation of the plasma. This is probably the dominant mechanism for producing low-frequency fluctuations observed in our experiment. This mechanism depends on the presence of end electrodes and sheaths, which allow the necessary electric fields to be established. This low-frequency instability can be suppressed or made worse by changing the magnetic field alignment.

In summary, although there have been many theoretical explanations for instabilities in the plasma of arc discharges, no complete theory has been put forward which explains in detail the time behavior of the arc plasma. The central arc column rotates in the electron diamagnetic drift direction as an azimuthal $m = 1$ perturbation in the frequency range of 20 to 100 kHz. There is a linear dependence of the period of the fluctuations on the neutral pressure of the diffusion region. There is only weak dependence on the magnetic field strength at low magnetic field values, and the instability disappears entirely below about 330 G in helium. The instability has been observed in hydrogen and argon as well. As our main concern is the study of

transport mechanisms of the plasma, we leave the detailed explanation of the plasma instability mechanism still in doubt.

7. Fluctuations and Convection

The radial convection of the plasma in the presence of potential and density fluctuations depends on the phase shift between the density and radial velocity perturbations. We have observed a phase shift between the density and azimuthal electric field fluctuations of the order of 45 deg. It is interesting to consider the origin of this phase shift to ascertain what dynamic process is contributing to the increased radial plasma transport.

In the absence of volume production or recombination, the dynamics of each species must satisfy the continuity equation

$$\frac{\partial n^{\alpha}}{\partial t} + \vec{\nabla}\cdot\vec{n v}^{\alpha} = 0.$$

If we expand the density and velocity of each species as a function of time, $n^{\alpha}(t) = n_0^{\alpha} + \delta n^{\alpha}$ and $\vec{v}(t) = \vec{v}_0^{\alpha} + \delta\vec{v}^{\alpha}$, and subtract the time-dependent contribution, $\vec{\nabla}\cdot(n_0\vec{v}_0^{\alpha}) = 0$, we find that the continuity for the perturbed quantities is given by

$$\frac{\partial \delta n^{\alpha}}{\partial t} + \nabla\cdot\delta(n\vec{v}^{\alpha}) = 0,$$

which can also be written as

$$\frac{\partial \delta n^{\alpha}}{\partial t} + \delta\vec{v}^{\alpha}\cdot\vec{\nabla}(n_0^{\alpha} + \delta n^{\alpha}) + (n_0^{\alpha} + \delta n^{\alpha})\vec{\nabla}\cdot\delta\vec{v}^{\alpha} + n_0^{\alpha}\overleftrightarrow{v}_0^{\alpha}\cdot\vec{\nabla}\frac{\delta n^{\alpha}}{n_0^{\alpha}} = 0. \qquad (5.17)$$

Neglecting δn compared with n_0, assuming quasineutrality $\delta n^i = \delta n^e = \delta n$, and assuming that

$$\delta n = n_1 \exp(-i\omega t + ik_r + im\theta + ik_z z),$$

we find that this equation becomes

$$(-i\omega + ik_r v_{r0} + \frac{im}{r} v_{\theta 0} + ik_z v_{z0})\delta n + \delta v_r \frac{\partial n_0}{\partial z} + n_0(\vec{\nabla}\cdot\delta\vec{v}) = 0. \qquad (5.18)$$

For the conditions of Data Set 1 we find that $\omega = 2\pi f \approx 3 \times 10^5$ sec^{-1}, and that $n_1/n_0 \approx 0.1$. The axial and radial variations of the density and plasma potential perturbations are observed to be of long wavelengths, $k_r \ll 1/R$ and $k_z \ll i/L$, where $R = 10$ cm is the radius and $L = 58.2$ cm is the length of the diffusion chamber. The contribution due to azimuthal drift $v_{\theta 0}$ due to the static radial electric field $E_r \approx 0.2$ V/cm is of the order of 3.6×10^4 cm/sec, so that the term $mv_{\theta 0}/r \approx 9 \times 10^3$ sec^{-1} is negligible compared with the ω term. The observed azimuthal fluctuating electric field is $\delta E_\theta \approx 0.12$ V/cm rms, so that the perturbed radial velocity $\delta v_r \approx c\delta E_\theta / B_z$ is of the order of 3×10^4 cm/sec.

On the assumption of a zero-order density distribution of the form $n_0(r,\theta,z) = n_0 e^{-r/q} \cos \pi z/L$, Eq. (5.18) can be approximated by

$$i\omega\delta n = -\frac{n_0 \delta v_r}{q} + n_0(\vec{\nabla}\cdot\delta\vec{v}). \qquad (5.19)$$

If for the moment we neglect the contribution due to $n_0(\vec{\nabla}\cdot\delta\vec{v})$, we find

that δn and δv_r by Eq. (5.19) are 90 deg out of phase, and

$$\delta v_r = - iq\omega \frac{n_1}{n_0} \exp (-i\omega t + ik_r r + im\theta + ik_z z)$$

$$= v_{r1} \exp(-i\pi/2) \exp (-i\omega t + ik_k r + im\theta + ik_z z).$$

In magnitude $v_{r1} \approx 7 \times 10^4$ cm/sec, which is the same order of magnitude as δv_r estimated from the measured azimuthal electric field. From this simple analysis δv_r reaches a maximum of 90 deg earlier in time than δn. Our experimental results, however, indicate that the azimuthal electric field perturbation reaches a maximum not 90 deg but rather 45 deg earlier than the maximum of the density perturbation. There is significant experimental evidence which confirms the 45 deg phase shift between the density and electric field fluctuations.

Measurements of drift wave fluctuations in a thermal cesium plasma by Chu, Hendel, and Politzer[72] indicate that the maximum of the density perturbation is approximately 45 deg earlier in time than the maximum of the potential fluctuation, and 45 deg later than the maximum of the electric field perturbation, in agreement with our observations. This phase relationship provides significant convective transport of the plasma across the magnetic field. They have observed a reduction in the plasma density indicative of enhanced plasma loss at the onset of this instability.

Other experiments conducted on a helium plasma in the Etude stellarator by Bol and Ellis[73] also indicate convective transport due to density and electric field fluctuations. They have shown that

this gradient is zero, indicating negligible convective transport. However, when a limiting aperture is inserted into the plasma so that the magnetic field lines in the vicinity of the probe terminate on a conducting surface, the gradient becomes nonzero, indicating convective transport. Correlation measurements in the case of low shear also indicate that convective transport is taking place.

In a paper on the identification and stabilization of collisional drift waves and the enhanced transport which is produced, Hendel, Chu, and Politzer[72b] calculate the relationship between the density perturbation and the potential fluctuations, using the electron equation of motion including ion-electron collisions and the electron continuity equation. Their analysis can be applied to the description of the dynamics of the secondary plasma in our experiment.

Neglecting the zero-order drifts due to the static radial electric field and diffusive transport, which are small, but explicitly including the electron diamagnetic drift current $v_{de} = -(ckT_e/eB)\vec{\nabla}n_0 \times \vec{B}$, we can write the perturbation of the electron continuity equation as

$$\frac{\partial \delta n}{\partial t} + n_0(\vec{\nabla}_\perp \cdot \delta\vec{v}_\perp^{\,e}) + n_0(\vec{\nabla}_\parallel \cdot \delta\vec{v}_\parallel^{\,e}) + (\delta\vec{v}_\perp^{\,e} \cdot \vec{\nabla}_\perp)n_0 + n_0\vec{v}_d^{\,e} \cdot \vec{\nabla}\frac{\delta n}{n_0} = 0. \quad (5.20)$$

The perturbation expansion of the parallel and transverse electron equation of motion, neglecting electron inertia and collisions with neutrals, but including the zero-order diamagnetic drift, can be written as

$$0 = -kT_e n_0 \left[\frac{\vec{\nabla}_\perp \delta n}{n_0} - \frac{\vec{\nabla}_\perp e\delta\phi}{kT_e} \right] - (n_0 e\delta\vec{v}_e + \delta n e\vec{v}_{de}) \times \frac{\vec{B}}{c} \qquad (5.21)$$

$$0 = -kT_e n_0 \left[\frac{\nabla_\parallel \delta n}{n_0} - \frac{\nabla_\parallel e\delta\phi}{kT_e} \right] - n_0 m_e \nu_{ei} \delta v_\parallel^e . \qquad (5.22)$$

On the assumption that

$$\delta n = n_1 \exp(-i\omega t + ik_r r + im\theta + ik_z z),$$

$$\delta\phi = \phi_1 \exp(-i\omega t + ik_r r + im\theta + ik_z z + i\delta),$$

and that $n(r,\theta,z) \approx n_0 e^{-r/q} \cos(\pi z/L)$,

the electron continuity equation can be written as

$$-i\omega\delta n + \frac{ckT_e}{eB} \frac{\partial n_0}{\partial r} \left(\frac{im}{r} \right) \left[\frac{\delta n}{n_0} - \frac{e\delta\phi}{kT_e} \right] + \frac{k_z^2 kT_e n_0}{m_e \nu_{ei}} \left[\frac{\delta n}{n_0} - \frac{e\delta\phi}{kT_e} \right] = 0. \qquad (5.23)$$

The second term in Eq. (5.23) arises from the $\vec{E}_\theta \times \vec{B}$ drift and Hall drift due to the spatial variation of δn. The last term in Eq. (5.23) results from the divergence of the parallel electron current. If we write the magnitude of the electron diamagnetic drift $v_{de} = -(ckT_e/eB)(1/n_0)(\partial n_0/\partial r)$ and define $1/t_z = k_z^2 kT_e/m_e\nu_{ei}$, Eq. (5.23) becomes

$$-i\omega \frac{\delta n}{n_0} + \left[\frac{imv_{de}}{r} + \frac{1}{t_z} \right] \left[\frac{\delta n}{n_0} - \frac{e\delta\phi}{kT_e} \right] = 0. \qquad (5.24)$$

In the limit of low frequency $\omega = 0$, or infinite conductivity along the magnetic field $\nu_{ei} = 0$, $1/t_z = \infty$, Eq. (5.24) has the solution $\delta n/n_0 = e\delta\phi/kT_e$. The potential and density fluctuations would

be in phase, and there would be no convective transport. However, in our experiment, because of the finite conductivity of electrons along the magnetic field lines, $\nu_{ei} \neq 0$ and there will be a phase shift between the density and potential fluctuations. When Eq. (5.24) is solved for $\delta n/n_0$, we find

$$\frac{\delta n}{n_0} = \frac{(1/t_z - imv_{de}/r)}{(1/t_z - imv_{de}/r - i\omega)} \left[\frac{e\delta\phi}{kT_e}\right]. \tag{5.25}$$

The electron diamagnetic drift velocity $v_{de} \approx 8 \times 10^3$ cm/sec. The observed fluctuation is an azimuthal m = 1 mode and our calculations are for a radius r = 4 cm, so that $mv_{de}/r \approx 2 \times 10^3$ sec^{-1}, which is small compared with the oscillation frequency $\omega \approx 3 \times 10^5$ sec^{-1}. From our experiment we have observed that the density perturbation δn is 45 deg out of phase with $\delta\phi$. This would imply that $mv_{de}/r \approx 1/t_z = k_z^2 kT_e/m_e\nu_{ei}$ and that $1/k_z \approx 50$ cm. The axial wavelength of the perturbation is of the order of $\lambda_z = 2\pi/k_z \approx 314$ cm, which is much larger than the length of our system.

In their analysis, Hendel, Chu, and Politzer[72b] consider the dynamics of a system which is unstable to the growth of drift waves. In our experiment we are dealing with a system which is driven by a large-amplitude instability in the central arc region. The dynamics of our system is given by the continuity equations and the equations of motion for the ions and electrons, including collisions between ions and neutrals, and between ions and electrons. One adjustable parameter in the dynamics of our system is the axial wavelength λ_z of

the perturbation. This parameter also adjusts the phase relationship between the density and potential fluctuations through Eq. (5.25). Although the indicated wavelength for the axial perturbation is much longer than the length of our system, Chen[74] has pointed out that the presence of end sheaths allows the axial wavelength to be longer than the system length. In our experiment we observe that the falloff with axial position of the potential fluctuations is negligible, and the density fluctuation is slight. This is consistent with a very-long-wavelength perturbation.

Thus far we have only looked at the electron equations. It is interesting to look at the ion equations. The ion continuity equation is similar to Eq. (5.20), where we explicitly include the ion diamagnetic drift current $v_{di} = + (ckT_i/eB)\vec{\nabla}n \times \vec{B}$. It is given by

$$\frac{\partial \delta n}{\partial t} + \delta\vec{v}^i \cdot \vec{\nabla} n_0 + n_0 \vec{\nabla}_{\parallel} \cdot \delta\vec{v}_{\parallel}^{\,i} + \vec{v}_{di} \cdot \vec{\nabla}\delta n + n_0(\vec{\nabla}_{\perp} \cdot \delta\vec{v}_{\perp}^{\,i}) = 0. \tag{5.26}$$

The parallel and transverse ion equations for the perturbed motion, including collisions with neutrals but for simplicity neglecting the drag due to the electrons, is given by

$$n_0 m_i \frac{\partial \delta\vec{v}_{\perp}^{\,i}}{\partial t} = -kT_i n_0 \left(\frac{\vec{\nabla}_{\perp}\delta n}{n_0} + \frac{\vec{\nabla}_{\perp} e\delta\phi}{kT_i} \right) + (n_0 e\delta\vec{v}_{\perp}^{\,i} + \delta n e\vec{v}_{di}) \times \frac{\vec{B}}{c} - \nu_{in} n_0 m_i \delta\vec{v}_{\perp}^{\,i}, \tag{5.27}$$

$$n_0 m_i \frac{\partial \delta\vec{v}_{\parallel}^{\,i}}{\partial t} = -kT_i n_0 \left(\frac{\vec{\nabla}_{\parallel}\delta n}{n_0} + \frac{\vec{\nabla}_{\parallel} e\delta\phi}{kT_i} \right) - \nu_{in} n_0 m_i \delta\vec{v}_{\parallel}^{\,i}. \tag{5.28}$$

Assuming that $\delta\vec{v}^{i} = \vec{v}_{1}^{\,i} \exp(-i\omega t + ik_r r + im\theta + ik_z z)$, we find that the transverse perturbation of the ion velocity is given by

$$(-\omega + \nu_{in})\delta\vec{v}^{\,i} = -\frac{kT_i}{m_i}\left(\frac{\vec{\nabla}_\perp \delta n}{n_0} + \frac{\vec{\nabla}_\perp e\delta\phi}{kT_i}\right) + \Omega(\delta\vec{v}_\perp^{\,i} + \frac{\delta n}{n_0}\vec{v}_{di}) \times \frac{\vec{B}}{B} . \qquad (5.29)$$

This equation can also be written as

$$(-i\omega + \nu_{in})\delta\vec{v}_\perp^{\,i} - \Omega_i \delta\vec{v}_\perp^{\,i} \times \frac{\vec{B}}{B} = \vec{A} , \qquad (5.30)$$

where

$$\vec{A} = -\frac{kT_i}{m_i}\left(\frac{\vec{\nabla}_\perp \delta n}{n_0} + \frac{\vec{\nabla}_\perp e\delta\phi}{kT_i}\right) + \Omega_i \frac{\delta n}{n_0}\left(\vec{v}_{di} \times \frac{\vec{B}}{B}\right),$$

$$\vec{A} = -\frac{kT_i}{m_i}\left(\frac{\vec{\nabla}_\perp \delta n}{n_0} + \frac{\delta n}{n_0}\vec{\nabla} n_0 + \frac{\vec{\nabla}_\perp e\delta\phi}{kT_i}\right). \qquad (5.31)$$

We are now in a position to evaluate the ion continuity equation Eq. (5.26). The time derivative term is just $-i\omega\delta n$. The term $\delta\vec{v}^{\,i}\cdot\vec{\nabla}n_0$ has two components, $\delta v_r^{\,i}(\partial n_0/\partial r)$ and $\delta v_z^{\,i}(\partial n_0/\partial z)$. Using Eqs. (5.30) and (5.31), we can evaluate $\delta\vec{v}_\perp^{\,i}$,

$$\delta\vec{v}_\perp^{\,i} = \frac{\Omega_i}{\Omega_i^{\,2} + (-i\omega + \nu_{in})^2}\left[\vec{A} \times \frac{\vec{B}}{B} - \left(\frac{-i\omega + \nu_{in}}{\Omega_i}\right)\vec{A}\right] . \qquad (5.32)$$

In the limit that $\omega, \nu_{in} \ll \Omega_i$ this reduces to

$$\delta\vec{v}_\perp^{\,i} = \frac{ckT_i}{eB}\left(\frac{\vec{\nabla}_\perp \delta n}{n_0} + \frac{\delta n}{n_0}\vec{\nabla}_\perp n_0 + \frac{\vec{\nabla}_\perp e\delta\phi}{kT_i} \times \frac{\vec{B}}{B}\right) . \qquad (5.33)$$

The transverse perturbed ion velocity is given by the diamagnetic and $\vec{E} \times \vec{B}$ drifts due to the perturbed potential and plasma density,

$$\delta v_r{}^i = \frac{c\delta E_\theta}{B} + \frac{ckT_i}{EB}\left(\frac{im}{r}\right)\frac{\delta n}{n_0} . \tag{5.34}$$

Because of the low ion temperature, $kT_i \approx 0.1$ eV, and because of the small density perturbation, $n_1/n_0 \approx 0.1$, only the δE_θ x B drift term contributes, and the radial velocity perturbation term is just

$$\delta v_r{}^i \frac{\partial n_0}{\partial r} = - \frac{c\delta E_\theta}{B}\frac{1}{q} n_0 . \tag{5.35}$$

The parallel ion transport is given by the solution to Eq. (5.28) and the contribution to the perturbed continuity equation is just

$$n_0 \frac{\partial \delta v_z{}^i}{\partial z} + \delta v_z{}^i \frac{\partial n_0}{\partial z} \approx - \frac{kT_i n_0}{m_i(i\omega - \nu_{in})}\left[\left(\frac{\nabla_\parallel \delta n}{n_0} + \frac{\nabla_\parallel \delta\phi}{kT_i}\right)\frac{\sin(\pi z/L)}{\cos(\pi z/L)}\right.$$

$$\left. + \vec{\nabla}_\parallel \cdot \left(\frac{\vec{\nabla}\delta n}{n_0}\right) + \frac{\nabla_\parallel{}^2 \delta\phi}{kT_i}\right] .$$

The axial perturbed ion motion is diffusion-limited due to the large collision frequency for collisions with neutrals, and the axial wavelength $k_z \ll 1/L$, so that the contribution due to axial ion motion is small compared with other terms. The contribution due to the density perturbation in the presence of the zero-order diamagnetic drift is

$$\vec{v}_{di}\cdot\vec{\nabla}\delta n = -\frac{ckT_i}{eB}\frac{1}{n_0}\frac{\partial n_0}{\partial r}\left(\frac{im}{r}\right)\delta n \approx \frac{ckT_i}{eB}\frac{1}{q}\left(\frac{im}{r}\right)\delta n, \qquad (5.36)$$

and this term is also negligible compared with the time-derivative term $-i\omega\delta n$.

The last term in Eq. (5.26), $n_0(\vec{\nabla}_\perp\cdot\delta\vec{v}_\perp^{\,i})$, can be evaluated by using the ion equations of motion as given in Eqs. (5.30) and (5.31). When this is done one finds

$$\vec{\nabla}\cdot\delta\vec{v}_\perp^{\,i} = \frac{\Omega_i}{\Omega_i^2 + (-i\omega + \nu_{in})^2}\left[\vec{i}_z\cdot(\vec{\nabla}\times\vec{A}) + \left(\frac{-i\omega + \nu_{in}}{\Omega_i}\right)\vec{\nabla}\cdot\vec{A}\right], \qquad (5.37)$$

which becomes

$$\vec{\nabla}\cdot\delta\vec{v}_\perp^{\,i} = \frac{\Omega_i}{\Omega_i^2 + (-i\omega + \nu_{in})^2}\left[\frac{kT_i}{m}\left(\frac{2im}{qr}\right)\frac{\delta n}{n} + \left(\frac{-i\omega + \nu_{in}}{\Omega_i}\right)\frac{kT_i}{m}\right.$$
$$\left.\times\left\{\left[k_r^2 + \left(\frac{m}{r}\right)^2 + \left(\frac{1}{q}\right)^2\right]\frac{\delta n}{n_0} + \left[k_r^2 + \left(\frac{m}{r}\right)^2\right]\frac{e\delta\phi}{kT_i}\right\}\right],$$

where the term in $\delta\phi/kT_i$ dominates. For $-\omega,\ \nu_{in} < \Omega_i$

$$\vec{\nabla}\cdot\delta\vec{v}_\perp^{\,i} \approx \frac{ckT_i}{eB}\left(\frac{-i\omega + \nu_{in}}{\Omega_i}\right)\left[k_r^2 + \left(\frac{m}{r}\right)^2\right]\frac{e\delta\phi}{kT_i}. \qquad (5.38)$$

Substituting from Eq. (5.25), we find

$$n_0(\nabla\cdot\delta v_\perp^{\,i}) \approx \frac{ckT_i}{eB}\left(\frac{-i\omega + \nu_{in}}{\Omega_i}\right)\left[k_r^2 + \left(\frac{m}{r}\right)^2\right]\left[\frac{1/t_z - i\omega}{1/t_z - imv_{de}/r}\right]\delta n.$$

Although $\left|\frac{i\omega - \nu_{in}}{\Omega}\right| \approx 0.2$

$$\left|\frac{1/t_z - i\omega}{1/t_z - im v_{de}/r}\right| \approx \frac{\omega r}{v_{de}} \approx 10^2.$$

Writing the dominant terms, we find that the continuity equation, Eq. (5.26), becomes

$$-i\omega\delta n + \frac{im}{r} v_{di}\delta n + \frac{c\delta E_\theta}{B}\frac{n_0}{q} + \frac{ckT_e}{eB}\left(\frac{-i\omega + \nu_{in}}{\Omega}\right)$$

$$\times \left(k_r^2 + \frac{m^2}{r^2}\right)\left(\frac{1/t_z - i\omega}{1/t_z - im v_{de}/r}\right)\delta n = 0. \qquad (5.39)$$

In the limit of negligible ion neutral collisions and infinite axial wavelength $k_z = 0$, the last term in Eq. (5.39) becomes purely imaginary, and there will again be a 90-deg phase shift between δn and δE_θ. However, both k_z and ν_{in} are significant in our experiment, so that there can be a 45-deg phase shift between the density and azimuthal electric field perturbations and convective transport.

In summary we find that the relationship between the amplitudes and phases of the plasma density and potential perturbations is established by conservation of electrons in the presence of a large, but not infinite, axial wavelength perturbation, and finite resistivity along magnetic field lines. The presence of conducting end electrodes and end sheaths allows axial perturbations whose wavelengths are much longer than the length of the system. Coupling of the axial ion and electron currents to the end electrodes through the end sheaths provides

a nasty boundary condition on the currents and potentials. In this calculation we have assumed a long axial wavelength perturbation which demonstrates the dynamics of the plasma, the possibility of a 45-deg phase shift, and the possibility of radial plasma convection consistent with the continuity equations for both the ions and electrons. Treatment of the complexities of sheath boundaries is beyond the scope of this work.

When one examines the ion conservation one finds that both the effects of ion inertia and collisions with neutrals introduce the necessary currents so that $\vec{\nabla}_\perp \cdot \delta\vec{v}_\perp^{\,i} \neq 0$, even through the radial perturbation velocity is dominated by the $\delta\vec{E}_\theta \times \vec{B}$ drift motion. Because the radial velocity perturbation is in phase with the $\delta\vec{E} \times \vec{B}$ drift motion in the fluctuating azimuthal electric field and is 45 deg out of phase with the density perturbation, there will be, on the average, a convective transport of the plasma across the magnetic field. This mechanism is significant in our experiment,and in some experiments such as those of Hendel, Chu, and Politzer[72b] can dominate the radial transport.

G. Electrons, Excited States, and the Halo

The transport of the ions in the secondary plasma is governed by diffusion due to the density gradients, and by mobility and convection due to electric fields set up by the electrons. The electrons are axially trapped in a potential well formed by the sheaths at the end plates at each end of the system. The electron density in steady state is established by balancing the radial electron transport and accumulation with the axial loss out the ends through the sheath.

Small adjustments in the end sheath potential drop will spill sufficient electrons to maintain charge neutrality.

The electron temperature in the secondary plasma is considerably above the temperature of the neutral background gas. The electron temperature in steady state is established by a balance between cooling by collisions with the neutrals and ions, and heating by a variety of mechanisms. In the secondary plasma the electron temperature is uniform along magnetic field lines within out ability to measure it, and it changes very slowly as a function of radius, so that thermal convection plays little role in determining the electron temperature. Heating of the electrons by electric fields, recombination superelastic collisions of the electrons with metastables or excited neutrals, and loss and production of electrons at the end walls are possible mechanisms that are discussed.

1. Collisional Cooling of the Electrons

The electron energy-exchange rate equation is given by[75,76]

$$\frac{1}{n}\frac{\partial}{\partial t}\left(\frac{3}{2}nkT_e\right) = 2\nu_{ei}\frac{m_e}{m_i}\left(\frac{3}{2}kT_i - \frac{3}{2}kT_e\right) + 2\nu_{en}\frac{m_e}{m_n}\left(\frac{3}{2}kT_n - \frac{3}{2}kT_e\right) + H^e, \qquad (5.40)$$

where H^e represents electron heating due to other mechanisms. The collision frequencies are sufficiently large that we can assume that the pressure tensor and energy exchange are isotropic. Evaluating the first two terms of the above equation for the conditions of Data Set 1

at r = 4 cm, we find that the rate of cooling of the electrons by collisions with the ions is 1.7×10^4 eV/sec per electron, as is also shown in Eq. (5.2), and that the cooling rate by collisions with neutrals is 8.8×10^2 eV/sec per electron. These are indicated in Table 5.6. Because there is a constant drain of energy away from the electrons at the rate of 1.8×10^4 eV/sec we must consider possible heating mechanisms for the electrons.

2. Electron Heating Due to Electric Fields

The contribution to Joule heating of the secondary plasma is given by $H_{Joule} = \vec{j} \cdot \vec{E}$. In the secondary plasma the electron temperature is low, so that the cross section for Coulomb scattering is large (see Table A.1 of Appendix A) and we can neglect the dissipation due to collisions with the neutral background gas. Assuming that E is parallel to the magnetic field, the current is given by $j = \sigma_{\parallel} E_{\parallel}$, where $\sigma_{\parallel} = 1.98/\eta_{\perp}$ in the absence of thermal gradients.[77] Joule heating is then given by

$$H_{Joule} = \sigma_{\parallel} E_{\parallel}^2 = 10^{19} \left(\frac{kT_e}{n_e} \right)^{3/2} \langle (E_{\parallel} V/cm)^2 \rangle \quad \text{eV/sec per electron.} \quad (5.41)$$

To produce a heating of 1.8×10^4 eV/sec for the conditions of Data Set 1 at r = 4 cm would require an electric field of 1.5×10^{-2} V/cm, which is quite modest. However, the potential drop along a magneutic field line is of the order of 7×10^{-3} V/cm, and the fluctuations appear to be well correlated along magnetic field lines. The parallel electric field is established to slow the axial loss rate of

Table 5.6. Electron energy exchange rate for Data Set 1 evaluated at r = 4 cm.

Electron ion cooling	$2\nu_{ei}\frac{m_e}{m_i}\left[\frac{3}{2}kT_i - \frac{3}{2}kT_e\right]$	$= 6.9 \times 10^{-9} n_e (kT_e)^{-3/2}(kT_e - kT_i)$ eV/sec $= 1.7 \times 10^{4}$ eV/sec
Electron neutral cooling	$2\nu_{en}\frac{m_e}{m_n}\left[\frac{3}{2}kT_n - \frac{3}{2}kT_e\right]$	$= 5.0 \times 10^{-11} n_0 (kT_e)^{1/2}(kT_e - kT_n)$ eV/sec $= 8.8 \times 10^{2}$ eV/sec
Joule heating	$H_{Joule} = \sigma_{\parallel} E_{\parallel}^{2}$	$= 10^{19}\frac{(kT_e)^{3/2}}{n_e}\langle(E_{\parallel}\ \mathrm{V/cm})^2\rangle$ eV/sec
Randomization heating	$H^{\alpha}_{ExB} = \frac{1}{2} m_\alpha (cE_\perp/B)^2 \nu_{\alpha n}$	$= 1.7 \times 10^{2}$ eV/sec (ions) $= 0.7$ eV/sec (electrons)
Stochastic heating	$H^{\alpha}_{stoc} = \frac{1}{2} m_\alpha (cE_\perp/B)^2 \nu$ (for $\nu, \omega_0 \ll \Omega_\alpha$)	$= 10$ eV/sec (ions) $= 1.6 \times 10^{-3}$ eV/sec (electrons)
Recombination heating	$H_R = \alpha_C n_e E_R$	$= 10^{2}$ eV/sec
Super elastic heating	$H_{se} = \frac{1}{t_{eq}}\frac{2kT_e}{\pi^{1/2}}\left(\frac{E_m}{kT_e}\right)^{3/2}\frac{n_m}{n_e}$	$= 1.3 \times 10^{8}\frac{n_m}{n_e}$ eV/sec
Heating by photoelectron emission from ends	$H_{pe} = \frac{E_{pe}2F_{pe}}{Ln_e}$	$= 22$ to 110 eV/sec

electrons and it is difficult to see in our experiment how this could couple to any significant energy source to give electron heating.

Randomization heating can occur whenever there is drift motion of a plasma through a stationary background gas. In the presence of a radial electric field, such as that observed in our experiments, the plasma distribution rotates. The background gas is in collisional contact with the chamber walls and remains stationary. When the particles of the rotating plasma experience collisions with the background gas, some of the drift motion is converted into random motion and the ions and electrons may be heated. The rate of heating is given by

$$H_{ExB} = \frac{1}{2} m_\alpha (cE_\perp/B)^2 \nu_{\alpha n}, \qquad (5.42)$$

where α = i or e for the ions or electrons respectively. For a radial electric field of 0.2 V/cm and a magnetic field of 560 G, typical of this experiment, this gives us a drift velocity of $v_{ExB} = 3.4 \times 10^4$ cm/sec, which is much less than the electron mean thermal speed, and somewhat less than the ion mean thermal speed. The heating rates for ions and electrons evaluated for the conditions of Data Set 1 at r = 4 cm are indicated in Table 5.6. This mechanism may have a small effect on ion heating but it does not affect electron heating.

Stochastic heating occurs if the fluctuating electric fields in the plasma have statistical variation. In the presence of electric field fluctuations of amplitude E_1 at a frequency ω_0, with a bandwidth 2ν in a magnetic field B with a gyrofrequency Ω_α, Puri[78] has calculated the stochastic heating of the plasma. He finds

$$H^{\alpha}_{stoc} = \frac{e^2}{m_\alpha}\frac{E_1^2}{2}\frac{\nu(\omega_0^2 + \Omega_\alpha^2 + \nu^2)}{\left[\nu^2 + (\Omega_\alpha - \omega_0)^2\right]\left[\nu^2 + (\Omega_\alpha + \omega_0)^2\right]} . \qquad (5.43)$$

In the limit that ν, $\omega_0 \ll \Omega_\alpha$ we find that this reduces to

$$H^{\alpha}_{stoc} = \frac{1}{2} m_\alpha (cE_1/B)^2 \nu .$$

For the experimental conditions of Data Set 1 there is an azimuthal fluctuating electric field at a frequency $\omega_0/2\pi$ = 48 kHz with an amplitude of E_θ = 0.12 V/cm rms. Previously we have estimated the bandwidth to be of the order of $2\nu/2\pi$ = 2 kHz. Electron and ion heating due to stochastic heating are calculated and shown in Table 5.6; they are quite small.

3. Recombination Heating

When the electrons and ions of a plasma recombine there is a volume loss of particles and energy is either liberated as radiation, in the case of radiative recombination, or the excess energy is carried off by a third particle, usually the electron. The energy released in the recombination of a helium ion and an electron, E_R, is of the order of 20 eV. For an electron density of $n_e = 1.8 \times 10^{12}$ cm^{-3} and a collisional recombination coefficient $\alpha_C = 3.1 \times 10^{-12}$ cm^3/sec, as is discussed in Appendix A, we find that the energy added to the electron distribution by collisional recombination is of the order of $\alpha_C n_e E_R = 10^2$ eV/sec per electron, as is indicated in Table 5.6. This is small compared with the rate at which the electrons are losing energy to the ions and neutrals, so that recombination heating of the electrons is not a significant mechanism.

4. Production of Excited and Metastable Atoms

Because the primary arc plasma is an intense source of ultraviolet radiation, there may be production of excited states and metastable neutral helium atoms in the secondary plasma region of our experiment. Observations made with a vacuum ultraviolet spectrograph in helium indicate the presence of resonance He I and He II transitions into the ground state from n = 2 level up to the continuum cutoff. The He II Lyman α transition (2p-1s) requires 40.6 eV to excite, and it is thought that the excitation is due to 50- to 100-eV electrons which are produced by acceleration through the cathode sheath region and stream along the central arc plasma.

The He I resonance radiation from the central arc plasma is Doppler-broadened because the ion temperature is of the order of 1 eV. The neutral helium gas in the secondary plasma region is much colder, $kT_n = 0.03$ eV, so the Dopper width for absorption of the resonance radiation is much narrower. The center of the emission line, however, is absorbed by the cold neutrals to produce excited atoms in the secondary plasma region. Some of the excited atoms decay into one of the metastable states, some are destroyed in super-elastic collisions with the plasma electrons, and some spontaneously radiate a resonance line that is quickly reabsorbed by the other cold neutrals imprisoning the energy of the resonance radiation in the secondary plasma region.

Holstein[79] calculates the absorption coefficient for resonance radiation at the center of the line. For a neutral temperature $kT_n = 0.03$ eV, for the $(3^1p, 1^1s)$, $\lambda_0 = 537.1$ Å, resonant He I transition, we find that the absorption coefficient is

$$k_0 = \frac{\lambda_0^3 n_0}{8\pi^{1/2}} \frac{g_2}{g_1} \frac{1}{v_{th}^n \tau} = 17.6 \text{ cm}^{-1}. \qquad (5.44)$$

Here $g_2 = 3$ and $g_1 = 1$ are the statistical weights of the upper and lower states, the mean thermal velocity of the neutrals is $v_{th}^n = 7.8 \times 10^4$ cm/sec, and τ is the excited state lifetime, where $1/\tau = 5.66 \times 10^8$ sec^{-1}. The neutral background gas is opaque to this typical He I resonance line, and the energy at this wavelength is emitted and reabsorbed many times before the radiation escapes to the walls of the system.

Not all excited atoms in the secondary region decay back into the ground state. Some of them decay into the 2^1s metastable level, giving rise, for instance, to the green spectrum line, 5016 Å (3^1p - 2^1s), which has been observed in the secondary region of our system. Other excited atoms may experience collisions with the plasma electrons. The He I triplet states cannot be directly excited from the ground state and require collisions with electrons to be produced. Super-elastic collisions with an electron may cause an atom in the 2^1s metastable state to go into the 2^3s metastable state, transferring about 0.6 eV to the incident electron. Super-elastic collisions of electrons with the metastable atoms can also cause decay back into the ground state, giving most of the extra energy to the incident electron.

Metastable atoms may also be produced by collisional excitation in the central arc column, and may move unimpeded by the magnetic field into the secondary plasma region. Metastables can also be produced by

recombination of the electrons and ions, both in the central arc column and in the secondary plasma; however, because of the small recombination rates, this is probably not a significant mechanism.

5. Electron Heating by Super-Elastic Collisions

The actual density of excited states of the neutral background gas can only be calculated from detailed balancing between all states, including all known excitation and deexcitation mechanisms. There is a lack of knowledge of the photon flux and spectra from the primary plasma, and the calculation is beyond the scope of the present work on particle transport. We can, however, get some estimate of what excited-state population would be needed to contribute significantly to electron heating.

All the excited states of He I lie between 19 and 24 eV above the ground state. These states can give up their energy to an electron in a super-elastic collision. We assume that the process for all excited states is similar to that for the metastables. We then estimate the metastable population necessary to give the observed electron heating, and use this as an estimate of the total neutral excited state population in the secondary plasma.

Ingrahan and Brown[80] calculate the electron heating which can be expected from super-elastic collisions of cold electrons $kT_e \ll E_m$ on metastable atoms of density n_m. The metastable energy level $E_m \approx 20$ eV for both the singlet and triple helium metastable level. They find that the heating is given by

$$H_{se} = \frac{1}{t_{eq}} \left[\frac{2kT_e}{\pi^{1/2}} \left(\frac{E_m}{kT_e} \right)^{3/2} \right] \frac{n_m}{n_e} , \qquad (5.45)$$

where $t_{eq} = 1.4 \times 10^{-6}$ sec is the energy equipartition time for a group of electrons with energy E_m on the background electrons as given by Spitzer.[81]

When these expressions are evaluated, we find that the electron heating due to collisions with metastables is given by $H_{se} = 1.3 \times 10^{8}$ eV/sec n_m/n_e. To produce the heating of the electrons, because of the large amount of energy available from a single neutral in a metastable state, only a very small metastable population is needed to produce the 1.8×10^{4} eV/sec per electron which is lost in collisions with the ions and neutrals. The conditions of Data Set 1 at r = 4 cm would require only a metastable population of $n_m = 2.5 \times 10^{8}$ cm^{-3} to produce this heating.

If the presence of metastables alone were responsible for maintaining the high electron temperature, it would be quite easy to quench them with the addition of some other gas such as H_2. However, such quenching takes place by ionizing the admitted gas. Because of the difference in energy levels between the metastable and the ionization energy, this process gives up 3 to 4 eV to the electrons produced. In addition, metastables are constantly being produced by photoexcitation of neutral helium. It is not trivial to determine what the effect on quenching the metastables will have on the electron temperature.

Because the electrons that undergo super-elastic collision have such a large energy, $E_m = 20$ eV, one can ask whether these electrons

might not be immediately lost from the system. Because of the large energy difference it takes many collisions before the electron is thermalized. The mean free path for large-angle scattering of 20 eV electrons off the ions of the plasma can be calculated by following Spitzer,[82] and is typically 7 cm. The electrons from superelastic collisions are emitted isotropically. Those with large velocity perpendicular to the static magnetic field are confined to their gyro orbits, and there is a good chance that a fast electron experiences energy-losing collisions before it is lost from the system.

6. Electron Energy Gain and Loss from End Walls

At the end walls of the system along magnetic field lines there is the possibility of both energy gain and loss. The end sheath potential drop is typically 2 V, while the electron temperature in the secondary plasma is typically 0.3 eV. The Maxwell tail of the electron distribution and hot electrons from superelastic collisions with metastable atoms have sufficient energy to penetrate the sheath potential barrier and be collected at the end wall. This is the most energetic part of the distribution. However, the potential barrier does work on the electrons, reflecting almost all of them. Collection through the sheath provides only a small energy-loss mechanism for the electron distribution.

Because of the high intensity of ultraviolet radiation from the primary plasma there is the possibility of photoemission of electrons from the copper end electrodes. The work function of copper is 4.7 V, and this provides a potential barrier against the emission of photoelectrons. If the photoelectron is formed with sufficient energy,

however, it penetrates this barrier and is accelerated into the plasma by the sheath potential drop. Resonance radiation from He I and He II excited states gives rise to photoelectrons with an energy of 20 to 50 eV, which is sufficient to penetrate the potential barrier. If the photoemission is sufficient, it can provide heating of the electrons in the secondary plasma. The hot photoelectrons from the end walls are randomized by Coulomb collisions in the secondary plasma.

A simple measurement was made to estimate the photoelectron flux from the walls in our experiment. Light from the central arc column was allowed to shine on a 0.32-cm^2 copper target placed at a radius of 21 cm from the center of the arc. A maximum photoelectron current of 0.2 μA was collected on a second electrode, which was shielded from the light. The measured current was independent of neutral pressure in the diffusion chamber, indicating the absence of volume ionization of the neutral gas. Other experiments using a pulsed arc showed that the collected current is directly proportional to the amplitude of the light from the central arc column as measured by a photomultiplier tube. Angular measurments along different chords indicate that most of the radiated light that causes the photoemission is from the central arc column.

From our measurements of the photoelectron flux above, we can make a crude estimate of the photoemission and contribution to electron heating which one might expect from the copper end electrodes of our system. A current of 0.2 μA on 0.32 cm^2 gives a photoemission current of 10^{13} electrons/sec cm^2 at a radius of 21 cm. Assuming that most of the

radiation comes from the central arc column, the intensity of the light should fall off something like $1/r$, as for an infinite source, or $1/r^2$, as for a point source. At a radius of 4 cm we should expect the photoemission current from the end walls, F_{pe}, to be of the order of 5 to 25 x 10^{13} electrons cm^{-2} sec^{-1}. From Table 5.4 we find that the estimated electron velocity from the plasma to the end wall is $\langle nv_z \rangle^e_{wall}/n_e = 1.7 \times 10^4$ cm/sec, so that the electron loss is $\langle nv_z \rangle^e_{wall} = 3 \times 10^{16}$ cm^{-2} sec^{-1}. This is much larger than the estimated photoelectron current, F_{pe}, so that photoemission from the end walls of the system does not contribute significantly to the electron particle balance of the plasma. If the photoelectron energy were typically E_{pe} = 25 eV, and the photoemission occurred at two ends of the system and contributed to heating the electrons in a flux tube of about L = 60 cm length, there would be a net energy input per unit volume of 4 to 20 x 10^{13} eV/sec cm^{-3}. With a typical electron density of 1.8 x 10^{12} at r = 4 cm this then gives a heating rate of 22 to 110 eV/sec per electron. This is much smaller than the estimated electron heating required to maintain the electrons above the temperature of the neutral background gas, so that the effect of this mechanism is not large.

7. The Halo

As was discussed in Section IV, there is a bluish halo present in helium discharges which surrounds the central plasma at a radius of from about 4 to 8 cm. It is probable that the halo is generated by hot electrons in the secondary plasma which are produced by superelastic colli-

sions with metastable atoms, photoemission from the end electrodes, or some other mechanism; and which experience inelastic collisions with other metastable neutrals, exciting them to higher levels. These excited states in turn decay spontaneously, giving the line radiation and volume glow that is observed as a halo surrounding the central plasma. The inner edge of the halo generally stops at some radius, typically r = 4 cm. It may be that the plasma density becomes sufficiently large at this point to efficiently depopulate the neutral metastable states. The distinct halo is observed both in He and Ar discharges where there is a metastable level considerably above the ground state. In a hydrogen discharge there is no observed halo and there is no atomic metastable level.

It is difficult to assess all the processes involved in excitation, neutral excited states, and metastables. Our estimates of the electron heating by superelastic collisions of electrons with metastable neutrals indicate that only a small metastable population would be necessary to heat the electrons. Although it is not possible at this point to rule out other mechanisms on the basis of quantitative argument, it seems likely on the basis of spectroscopic and other evidence that excitation of metastable neutrals by hot electrons is responsible for the production of the halo surrounding the central plasma.

In summary, the electrons in the secondary plasma are losing energy by collisions with both the neutral background gas and the ions, and in addition may lose some energy to the end walls of the system.

The electron heating by electric fields, through Joule heating, randomization of the E x B drift motion, and stochastic heating are all too small to maintain the electron temperature significantly above that of the neutral background gas. Both collisional and radiative recombination are small, and the amount of energy liberated in recombination is also small.

In the central arc itself there is excitation of neutral atoms and ions, and production of metastable atoms. Also there is intense resonance radiation from the central arc plasma where both the He I and He II resonance lines are observed. The absorption length for resonance radiation by the neutral background gas is typically small, so that there is appreciable trapping of the resonance radiation energy in the secondary plasma region and production of excited neutrals. Some of these excited neutrals decay into a metastable level, producing a metastable population.

The electrons in the secondary plasma can gain energy from the excited atoms and metastables by superelastic collisions. In addition there may be a small energy gain from the photoelectrons produced at the end walls of the system. This added electron energy is in part thermalized, heating the electron distribution; in part it may excite some of the other metastable atoms to higher excited states, thereby producing the halo observed in He and Ar discharges; and in part it may be lost out the ends of the system.

VI. CONCLUSIONS

The transport of a partially ionized secondary plasma of a hollow-cathode arc discharge in the range of axial magnetic fields, neutral pressure, and discharge parameters of our experiments is determined by diffusion, mobility, and convection. The radial ion transport by diffusion due to collisions between charged particles and due to collisions with the neutral background gas are shown to be comparable. The relative importance of charged-particle diffusion on the ion transport depends sensitively on the ion and electron temperatures in the plasma. Even though the secondary plasma is only a few percent ionized, the electron temperature is low and the Coulomb scattering between the electrons and ions is quite large. For the electrons the radial diffusion by charged-particle collisions is much larger than that due to collisions with neutrals.

The radial ion transport is also affected by the mobility current in the presence of an outward radial electric field produced by the radially changing axial end sheath conditions when the end electrodes are electrically grounded. This radial electric field tends to be largest at lower pressures and higher magnetic field strengths, at which the mobility current tends to dominate the radial ion transport. At higher pressures and lower magnetic field strengths the electric field is smaller and the uncertainties in the electric field measurements are large; however, even in these cases the electric field contributes significantly to the radial ion transport.

In the case of grounded end electrodes the radial electric field

is shown to give rise to a rotation of the plasma as a whole. If the distribution is azimuthally asymmetric, it is observed as a low-frequency fluctuation of the plasma. This fluctuation can be controlled somewhat by adjusting the magnetic field alignment with the small externally applied transverse magnetic field.

It is possible to eliminate the radial electric field by allowing the various rings of the end electrodes to electrically float. The plasma distribution was then found to be nonrotating, but it was azimuthally asymmetric. The results are qualitatively similar to those of Bohm et al.[83] in their rectangular arc. The radial density gradients are different on different azimuths. It appears that small macroscopic transverse electric fields are established by the sheaths at the ends of the system, which causes the plasma to E x B drift in a preferred direction. The degree and direction of the asymmetry depend critically on the alignment of the electrodes and the magnetic field. The alignment is so critical that the distribution is almost never symmetric. This results casts doubt on previous transport measurements for which the azimuthal variation of the density distribution was not checked experimentally.

Radial convection of the plasma due to fluctuations in the plasma density and azimuthal electric field is also shown to be a significant radial transport mechanism. Estimates of the transport from measurements of the azimuthal electric field fluctuations, the relative density fluctuation, and the phase difference between the electric field and density fluctuations give a transport which is of the same

order of magnitude as the radial ion and electron transport due to other processes. The fluctuations are found to be driven from the central arc column, and are probably density or temperature gradient-driven drift instabilities, although there is still insufficient experimental evidence to determine the excitation mechanism in detail. Because the observed electric field fluctuations are coherent over many periods, the effect of enhanced diffusion is negligible in this experiment.

The axial ion transport is determined by diffusion and mobility in the presence of the small axial electric field established by the electrons. The estimated ion flux to the end electrodes is in agreement with the observed ion current collected by the electrodes. The electrons, on the other hand, because their mean free path for collisions with the neutrals is of the order of the system length, are trapped in a potential well formed by the end sheaths. Estimates of the electron collection from electron penetration of the end sheath and from total particle balance, and measurements of the end electrode current as a function of potential show general agreement.

The measured electron temperature of the secondary plasma is considerably above the temperature of the neutral background gas. From consideration of the possible heating mechanisms, it is thought that superelastic collisions of the electrons with the excited and metastable neutral atoms in the secondary plasma region produce both the heating of the electrons and excitation of other metastable atoms to produce the halo observed surrounding the discharge. The metastable

and excited neutral atoms are produced by collisional excitation in the central arc column, and by absorption of resonance radiation from the central arc by neutrals in the secondary plasma region.

One of the major difficulties encountered in the experimental work was making accurate measurements of the plasma potential. The plasma potential is not measured directly, but is deduced from measurements of the Langmuir probe floating potential, and a large correction term proportional to the electron temperature. The electron temperature measurements are good only to within about 15%. This introduces uncertainty in the value of the plasma potential. Also, the time required to make a complete set of spatial measurements of the potential density and electron temperature is typically on the order of 30 min. Although the arc runs quite stably over this slow time scale, slight variations in the pumping speed, gas flow rates, and system pressures can introduce minor changes in the sheath conditions, and at times cause the probe floating potential to wander as much as 0.1 V. This is particularly a problem in the case of floating end electrodes, where the reference potential for the entire system is established at the sheath over the small surface areas of the anode apertures.

Our experiments indicate conclusively that diffusion, mobility, and convection all play an important role in determining the plasma transport in our experiments. The analysis of the ion and electron transport and particle balance is consistent within the experimental uncertainties without requiring additional "anomalous" transport mechanisms. However, the experimental uncertainties in some of the

quantitative measurements are large and further experiments would be of value. Refined experiments of this sort should be carefully designed so that magnetic field and electrode alignment can be easily made, so that the system pressure can be carefully controlled without overloading the vacuum system, and so that there is a variety of probe access and both radial and axial measurements can be made over more than one azimuth. In addition, rapid data-acquisition equipment would allow the experimenter to make repeated measurements while the experiment is in progress.

Although our results indicate that at the intermediate frequency, 20 to 100 kHz, fluctuations of the central arc column are probably due to a density or temperature gradient-driven drift instability; and although the halo observed in the secondary plasma region appears to be the result of excitation of metastable atoms by hot electrons in the secondary plasma, further study of the details of the phenomena is necessary for a quantitative understanding of the effects.

ACKNOWLEDGMENTS

The author wishes to give special thanks to Dr. Robert V. Pyle for his encouragement and sustaining interest both in the research and in the writing, to Prof. Wulf B. Kunkel for many fruitful discussions, to Margaret R. Thomas for her careful and prompt typing of the manuscript, and to my wife Idena for her patience, understanding, and love through the long period of this work.

This work was performed under auspices of the U. S. Atomic Energy Commission.

APPENDIX

A. Plasma Parameters

1. Cross Sections

In helium the electron neutral momentum thransfer cross section is almost constant at low energies, being 0.50×10^{-16} cm^2 at zero energy.[84] The total momentum transfer cross section for ion-neutral collisions at low energy has a contribution both from elastic and from resonant charge-exchange collisions. The measurements by Cramer and Simons[85] at 4 eV give the elastic scattering cross section as $\sigma_{in}^{ei} = 0.16 \times 10^{-14}$ cm^2 (42%), and the charge-exchange cross section is $\sigma_{in}^{cx} = 0.22 \times 10^{-14}$ cm^2 (58%), giving a total cross section $\sigma_{in} = 0.38 \times 10^{-14}$ cm^2. Extrapolation of these measurements below 4 eV gives consistent agreement with the total cross section, 0.67×10^{-14} cm^2, estimated from the zero electric field mobility measurements at 300°K of Chanin and Biondi.[86] As our ion temperature is considerably below 4 eV we use this latter measurement for the total ion neutral momentum transfer cross section and assume that there is a 42% contribution due to elastic scattering and 58% due to resonant charge exchange, giving us at zero energy a cross section for elastic scattering of $\sigma_{in}^{el} = 0.28 \times 10^{-14}$ cm^2 and a cross section for charge exchange of $\sigma_{in}^{cx} = 0.39 \times 10^{-14}$ cm^2.

2. Recombination

Expressions for the three-body collisional and radiative recombination coefficients for helium are given by Hinnov and Hirschberg.[34] Evaluating these expressions for the conditions of Data Set 1 at

$r = 4$ cm, we find that the radiative coefficient is $\alpha_R = 7 \times 10^{-13}$ cm^3/sec and the collisional coefficient is $\alpha_C = 3.1 \times 10^{-12}$ cm^3/sec. This gives us a total loss of ions and electrons of $(1/n)(\partial n/\partial t) = (\alpha_R + \alpha_C)n_e \approx 7$ sec^{-1} per particle, as shown in Tables 5.3 and 5.4. This is much less than the particle loss rate due to transport processes, and we can ignore the effect of recombination on transport.

Table A.1. Basic parameters for a helium plasma, where the densities n_i, n_e, and n_0 are in cm^{-3}, B is in gauss, M is the ion mass in amu (m = 4 for He), Z is the ion charge, and the temperatures kT_e and kT_i are in eV. The quantities are evaluated for the conditions of Data Set 1 at r = 4 cm, P_T = 4.0 mTorr He, B = 560 G, $n_0 = 1.3 \times 10^{14}$ cm^{-3}, $n_i = n_e = 1.8 \times 10^{12}$ cm^{-3}, and kT_e = 0.28 eV and kT_i = 0.074 eV.

Mean free path and cross sections

Ion-neutral		
(elastic)	$\lambda_{in}^{el} = 1/n_0\sigma_{in}^{el} = 2.7$ cm	where $\sigma_{in}^{el} = 0.28 \times 10^{-14}$ cm^2
(charge exchange)	$\lambda_{in}^{cx} = 1/n_0\sigma_{in}^{cx} = 2.0$ cm	where $\sigma_{in}^{cx} = 0.39 \times 10^{-14}$ cm^2
(total)	$\lambda_{in} = 1/n_0\sigma_{in} = 1.15$ cm	where $\sigma_{in} = 0.67 \times 10^{-14}$ cm^2
Electron-neutral	$\lambda_{en} = 1/n_0\sigma_{en} = 15.4$ cm	where $\sigma_{en} = 5.0 \times 10^{-16}$ cm^2
Neutral-neutral	$\lambda_{nn} = 1/n_0\sigma_{nn} = 5.1$ cm	where $\sigma_{nn} = 15 \times 10^{-16}$ cm^2

Gyrofrequency $\Omega_\alpha = e_\alpha B/m_\alpha c$

Electron	$\Omega_e = 1.76 \times 10^7 B$ $sec^{-1} = 10^{10}$ sec^{-1}
Ion	$\Omega_i = 10^4 ZB/M$ $sec^{-1} = 1.4 \times 10^6$ sec^{-1}

Mean thermal velocity

Ion	$v_{th}^i = 1.38 \times 10^6 (kT_i/M)^{1/2}$ cm/sec $= 1.87 \times 10^5$ cm/sec
Electron	$v_{th}^e = 6.0 \times 10^7 (kT_e)^{1/2}$ cm/sec $= 3.2 \times 10^7$ cm/sec

Gyroradius

Ion	$r_{gi} = v_{th}^i/\Omega_i = 1.38 \times 10^2 M^{1/2} (kT_i)^{1/2} B$ cm $= 0.13$ cm
Electron	$r_{ge} = v_{th}^e/\Omega_e = 3.4 (kT_e)^{1/2}/B$ cm $= 3.2 \times 10^{-3}$ cm

Table A.1. continued

Collisions frequencies

ν_{in}^{cx} (charge exchange) $= v_{th}^{i}/\lambda_{in}^{cx} = 0.94 \times 10^{5}$ sec^{-1}

ν_{in}^{el} (elastic) $= v_{th}^{i}/\lambda_{in}^{el} = 0.69 \times 10^{5}$ sec^{-1}

$\nu_{in} = v_{th}^{i}/\lambda_{in} = 1.6 \times 10^{5}$ sec^{-1}

$\nu_{en} = v_{th}^{e}/\nu_{en} = 2.1 \times 10^{6}$ sec^{-1}

Plasma frequency

Electron $\omega_{pe} = \left(\frac{4\pi n_e e^2}{m_e}\right)^{1/2} = 5.7 \times 10^{4}(n_e)^{1/2}$ sec^{-1} $= 7.6 \times 10^{10}$ sec^{-1}

Ion $\omega_{pi} = \left(\frac{4\pi n_i e^2}{m_i}\right)^{1/2} = 1.32 \times 10^{3}\left(\frac{n_e}{M}\right)^{1/2}$ sec^{-1} $= 8.9 \times 10^{8}$ sec^{-1}

Debye length $\lambda_D = 740(kT_e/n_e)^{1/2}$ cm $= 2.9 \times 10^{-4}$ cm

Plasma resistivity $\eta_\perp = (8/3)(\pi/2)^{1/2}(e^2 m_e^{1/2})(kT_e)^{-3/2} \ln \Lambda$

$= (6.8 \times 10^{-14})/(kT_e)^{3/2}$ sec $= 4.7 \times 10^{-13}$ sec

Electron-ion collision frequency $\nu_{ei} = \frac{n_e e^2}{m_e}\eta_\perp = 1.7 \times 10^{-5} n_e (kT_e)^{3/2} = 2.1 \times 10^{8}$ sec^{-1}

Electron-ion collisions cross section $\sigma_{ei} = \frac{\nu_{ei}}{n_e v_{th}^{e}} = \frac{2.8 \times 10^{-13}}{(kT_e)^2}$ cm^2 $= 3.6 \times 10^{-12}$ cm^2

Debye Shielding parameter $\Lambda = \lambda_0/r_0 \sim 460$, $\ln \Lambda \sim 6$

Distance of closest approach $r_0 = e^2/kT_e = (1.44 \times 10^{-8})/kT_e$ cm

Table A.2. Diffusion coefficients in a helium discharge, where the neutral density n_0 and the ion density n_i are in cm^3, the magnetic field strength B is in gauss, and the ion temperature kT_i and electron temperature kT_e are in eV, assuming $\sigma_{in} = 0.67 \times 10^{-14}$ cm^2 and $\sigma_{en} = 5.0 \times 10^{-16}$ cm^2.

Ion-Neutral Collisional Diffusion

Parallel $$D_{\parallel}^{in} = \frac{\lambda_{in} v_{th}^{i}}{3} = 3.43 \times 10^{19} \left(\frac{kT_i}{n_0}\right)^{1/2} \text{ cm}^2/\text{sec}$$

Perpendicular $$D_{\perp}^{in} = \frac{D_{\parallel}^{in}}{1 + (\lambda_{in}/r_{gi})^2} = 1.17 \times 10^{-4} \frac{n_0 (kT_i)^{3/2}}{B^2} \text{ cm}^2/\text{sec},$$

where $$\lambda_{in}/r_{gi} = \Omega_i/\nu_{in} = 0.54 \times 10^{12} \frac{B}{n_0 (kT_i)^{1/2}}$$

Electron-Neutral Collisional Diffusion

Parallel $$D_{\parallel}^{en} = \frac{\lambda_{en} v_{th}^{e}}{3} = 4.0 \times 10^{22} \left(\frac{kT_e}{n_0}\right)^{1/2} \text{ cm/sec}$$

Perpendicular $$D_{\perp} = \frac{D_{\parallel}^{en}}{1 + (\lambda_{en}/r_{gi})^2} = 1.15 \times 10^{-7} \frac{n_0 (kT_e)^{3/2}}{B^2} \text{ cm}^2/\text{sec},$$

where $$\lambda_{en}/r_{gi} = \Omega_e/\nu_{en} = 5.9 \times 10^{14} \frac{B}{n_0 (kT_e)^{1/2}}$$

Fully Ionized Diffusion

$$D^{ei} = D^{ie} = \eta_{\perp} c^2 \frac{(kT_e + kT_i) n_e}{B^2} = 0.98 \times 10^{-4} \frac{n_e (kT_e + kT_i)}{B^2 (kT_e)^{3/2}} \text{ cm}^2/\text{sec}$$

Bohm Diffusion

$$D_{Bohm} = \frac{ckT_e}{16eB} = 6.25 \times 10^{6} \frac{kT_e}{B} \text{ cm}^2/\text{sec}$$

B. Use of Langmuir Probes

A Langmuir probe is a small metal electrode that is inserted into a plasma and connected to external circuitry by an insulating support. It gets its name from Irving Langmuir, who developed the technique in his early fundamental plasma studies in the 1920's. When a negative voltage relative to the plasma is applied to a probe the probe collects ions and repels electrons in the absence of positive ions. When a positive voltage is applied it repels ions and attracts electrons. From the magnitude and shape of the probe characteristic--i.e., the probe current as a function of probe voltage--one can obtain a measurement of local plasma parameters such as plasma density, potential, and electron temperature in the immediate vicinity of the probe tip. By use of Langmuir probes one can obtain spatially resolved information about the state of the plasma system.

The theory of Langmuir probes and their use in plasma diagnostics has been discussed by many authors.[87-92] The plasma has a strong tendency to maintain charge neutrality; however, in the vicinity of a current-collecting probe, this condition breaks down, giving rise to space-charge electric fields and a sheath. The sheath thickness is of the order of the Debye length λ_D of the reflected species. If the plasma density is sufficiently large the Debye length and sheath thickness are small compared with the plasma radius $a/\lambda_D \gg 1$, and the collection area of the probe is approximately equal to the geometrical area of the probe tip. If the collision mean free path for the species being collected, α, is large compared with the probe radius $\lambda_{\alpha n} \gg a$,

then any particle that is collected is immediately replaced by randomly moving particles from further away in the plasma.

For typical conditions of our plasma, Data Set 1 at r = 4 cm as listed in Table A.1 in Appendix A, we find that $n_e = 1.8 \times 10^{12}$ cm^{-3}, $kT_e = 0.28$ eV, $kT_i = 0.074$ eV, $\lambda_D = 2.9 \times 10^{-4}$ cm. A 0.020-in. tungsten wire probe has a radius of 2.5×10^{-2} cm, so that in the range of interest $a/\lambda_D = 86 \gg 1$. The mean free path for ion-neutral collisions is 1.15 cm, so that both of these conditions are satisfied in our experiment. At lower plasma densities the Debye length becomes larger and the electric field penetrates further into the plasma, and more elaborate analysis of the measurements, such as those of Chen et al.[87] or Laframboise,[88] are required. But for the conditions of this experiment the simple theory suffices.

1. Use of Probes in the Absence of a Magnetic Field

In the absence of a magnetic field a probe with a positive voltage with respect to the plasma collects electrons and reflects ions. The plasma has a remarkable ability to shield out electric fields, so that most of the potential drop occurs within the plasma sheath. Although there is a continuous transition from the plasma to the probe, one can consider roughly that the sheath edge begins where the condition of charge neutrality breaks down and large space-charge fields occur. Making the probe voltage more positive increases the thickness of the sheath somewhat; however, in the thin-sheath case, $s \ll a$ and the electron collection does not increase significantly. The current collected is known as the saturated electron current.

The flux of electrons that strike a surface per unit area per unit time is given by $F = 1/4\ n_e v_{th}^e$. The saturated electron current to a positive probe is given by Bohm, Burhop, and Massey[93] as

$$I_{se} = \frac{n_e v_{th}^e e A_{probe}}{4} . \qquad (B.1)$$

For a negatively biased probe the probe collects ions and reflects electrons. There is, however, in the case that $kT_i \ll kT_e$, an electric field that penetrates beyond the sheath edge into the plasma. The ions, when they reach the sheath edge, have a directed velocity equal to the most probably velocity of an ion at the electron temperature $v_i = (2kT_e/M)^{1/2}$. This condition is known as the Bohm sheath criterion, and is a necessary condition for the sheath conditions to have a stable solution. The ion collection for the case of $kT_i \ll kT_e$ then depends not on the ion temperature, as predicted by Langmuir's early theory, but on the electron temperature.

Bohm, Burhop, and Massey consider the effect of these space-charge electric fields on the ion collection and give the result that the saturated ion current is given by[94]

$$I_{si} = Cn_i e(2kT_e/M)^{1/2} A_{probe}, \qquad (B.2)$$

for the case of a plane probe $C = 0.25$. For a spherical probe they obtained $C = 0.40$. It is assumed that 0.40 should also give a fairly reliable estimate for ion collection by a cylindrical probe under the conditions that the effective probe radius is much smaller than the

collisional mean free path of the collected species.[94]

Solving Eq. (B.2) for the ion density and evaluating the expression, we find that the ion density is given by

$$n_i = 1.13 \times 10^{12}\ \text{cm}^{-3}\ \frac{I_{si}}{A_{probe}} \left(\frac{M}{kT_e} \right)^{1/2}, \qquad \text{(B.3)}$$

where I_{si} is the saturated ion current in mA, where A_{probe} is the area of the probe in mm^2, kT_e is the electron temperature in eV, and M is the ion mass in amu.

As one increases the probe potential from the saturated ion current region one gets to the point at which one begins to collect the tail of the electron distribution. If the electron distribution is reasonably Maxwellian, when one plots the natural log of the electron contribution to the observed current as a function of probe voltage one can obtain a measure of the electron temperature,

$$\frac{e}{kT_e} = \frac{d}{dV} \left\{ \ln \left[I(V) - I_{si} \right] \right\}. \qquad \text{(B.4)}$$

The floating potential is defined as the potential at which the ion currents and electron currents are equal. The probe floats and draws no net current. The plasma potential is defined as the probe potential at which no electric fields are present. The probe then draws a current given by the sum of the electron and ion fluxes to it. For similar temperatures the electron thermal velocity is much larger than the ion thermal velocity by the ratio $\sqrt{(kT_e/m_e)(m_i/kT_i)}$, so that the plasma potential is near the point at which the electron current

begins to saturate. Hall[91] gives the relationship between the plasma potential and the probe floating potential as

$$\phi_p = \phi_f + \frac{kT_e}{2} \ln\left(\frac{kT_e}{m_e}\frac{m_i}{kT_i}\right). \tag{B.5}$$

2. Use of Probes in the Presence of a Magnetic Field

The presence of a magnetic field may profoundly affect the probe curves. The electron mean free path across the magnetic field is reduced to the electron gyroradius, which even for moderate magnetic fields is small compared with the probe dimensions. For our typical case $r_{ge} = 3.2 \times 10^{-3}$ cm $\ll a \approx 2.5 \times 10^{-2}$ cm. Chen has worked out the current to a probe near the plasma potential, and considers both transverse and longitudinal electron collection. He finds that

$$I \approx \frac{en_0 v_{th}^e}{4} A_p \frac{4}{3}\frac{\lambda}{a}\left(\frac{D_\perp^{en}}{D_\parallel^{en}}\right)^{1/2}, \tag{B.6}$$

where $D_\perp^{en}$ and $D_\parallel^{en}$ are the transverse and logitudinal electron diffusion coefficients, respectively.

For diffusion due to collisions with neutral background gas, $D_{\perp e} \approx D_{\parallel e}/\left[1 + (\lambda_{en} r_{ge})^2\right]$. For $r_{ge} \ll \lambda_{en}$ this gives

$$I_e = \frac{en_0 v_{th}^e}{4} A_{probe} \frac{4}{3}\left(\frac{r_{ge}}{a}\right),$$

thus the electron collection current is greatly reduced. This analysis

was done assuming the probe is at the plasma potential and does not give the saturated value for the electron current. In fact the electron current in a magnetic field does not saturate, but increases slowly as the effective collecting area increases with the probe voltage. This expression, then, must be regarded as an estimate of the electron current and not be taken too seriously in regard to absolute magnitudes.

Because for the conditions typical of our experiment the ion gyroradius $r_{gi} = 1.3 \times 10^{-1}$ cm is much larger than the probe radius, the effect of the magnetic field on ion collection should be small. The saturated ion current should be roughly equal to the zero magnetic field value as given by Eqs. (B.2) and (B.3). In the secondary plasma the ion temperature is more or less constant as a function of radius. From the discussion in Bohm et al.[94] we shall estimate the uncertainty in the constant C to be 20%. Other uncertainties in the deduction of plasma parameters from Langmuir probe measurements are discussed in Appendix D.

Because the electron collection to a probe in a magnetic field as given by Eq. (B.6) depends on the transverse electron diffusion coefficient, and the ion collection is largely unaffected, some authors[95,96] have studied ratio of saturated ion current to saturated electron current of a Langmuir probe in a plasma to investigate enhanced diffusion. This is, however, a crude technique, for in a magnetic field the electron current does not completely saturate, because the sheath becomes larger and the electron collection increases with probe voltage.

Figure 37 shows the time-resolved Langmuir probe measurements for a plasma in the presence of fluctuations in potential and density. The measurements were made with an axial magnetic field of 560 G with a neutral pressure P_T = 5.6 mTorr He at a radius of r = 4 cm. The measurements were made with the sweep circuit shown in Fig. 4. The oscilloscope trace is enhanced for 1 to 2 μsec out of the 25-μsec period of the plasma fluctuations. The different photographs correspond to the probe characteristics at four different delay times relative to the maximum of the saturated ion-current fluctuation to a probe at approximately the same position in the plasma.

The probe consists of a 0.051-cm-diam tungsten wire which extends 0.2 cm beyond a 0.3-cm-diam quartz sleeve which serves to limit the collection area of the probe. The probe is introduced into the diffusion chamber through numerous sliding seals. Our measurements are made with a single probe with the reference electrode for current return being the system gound, i.e., the anodes, the outer wall of the diffusion chamber and the end electrodes when they are electrically grounded.

As the probe potential is changed from the floating potential at which no net current is drawn to a more negative voltage some of the electrons are reflected. Eventually one reaches a voltage at which only ions are collected. For a relatively high-density plasma in the absence of a magnetic field, the ion current collected does not increase as the probe is made more negative, so the collected current is referred to as the saturated ion current. As is evident from Fig. 37,

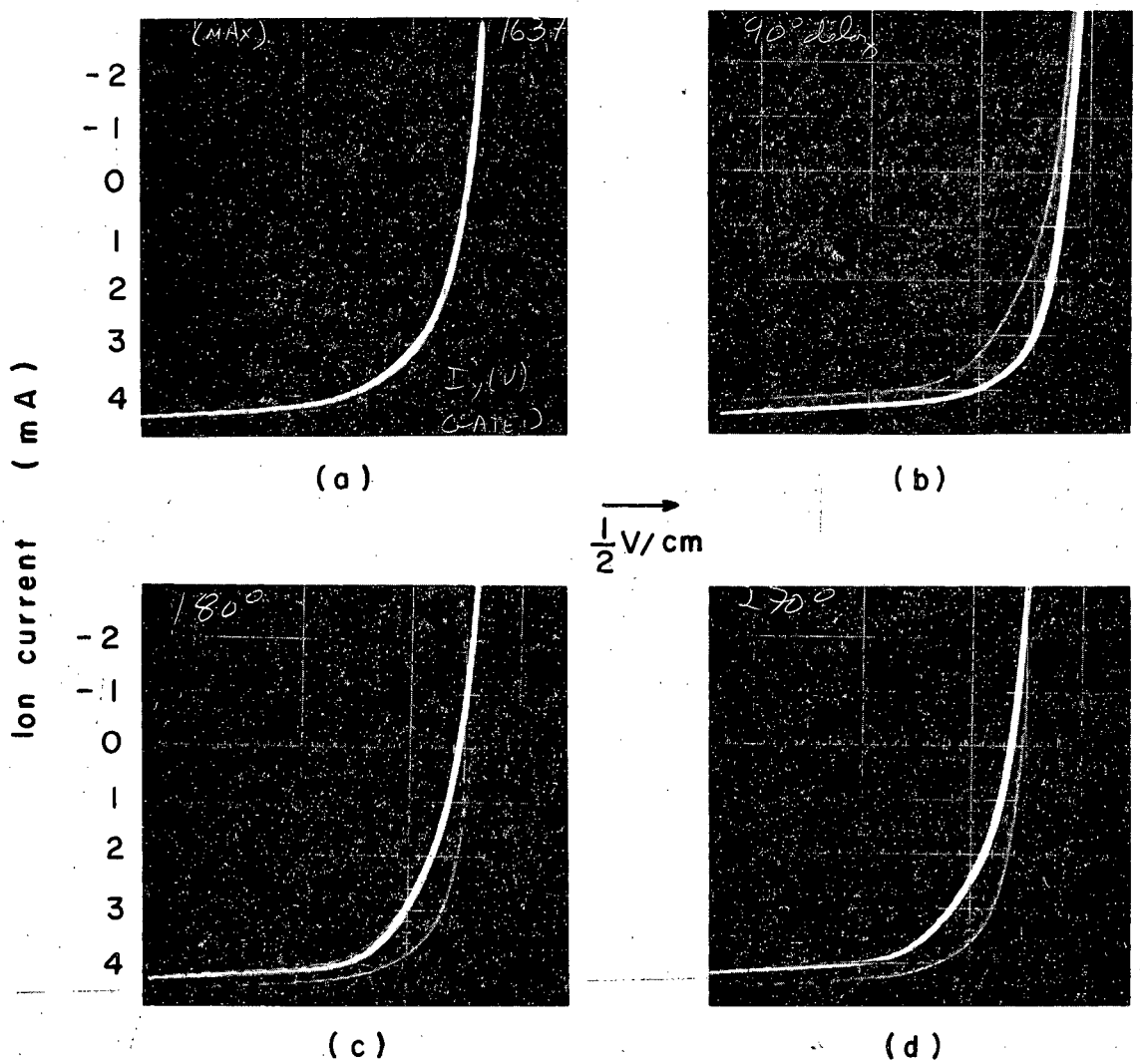

Fig. 37. Gated Langmuir probe curves showing effect of potential and density fluctuations on electron temperature measurements. Radial probe r = 4 cm, P_T = 5.6 mTorr He, and B = 560 G. Ends grounded. Double cathode. The oscilloscope trace is enhanced for 1 to 2 psec out of the 25 μsec period of the fluctuation by use of a phase delay, θ_{gate}, relative to the maximum of the saturated ion current fluctuation on another probe at about the same position. (a) θ_{gate} = 0 deg. (b) θ_{gate} = 90 deg. (c) θ_{gate} = 180 deg. (d) θ_{gate} = 270 deg.

however, the ion current does not completely saturate. The current collection increases slowly as the probe is made more negative due to the increasing sheath size and due to penetration of the electric field into the plasma. This effect becomes quite pronounced at low densities, $n_i \ll 10^{11}$ cm^{-3}, and can complicate the interpretation of Langmuir probe measurements at low densities.

The electron temperature calculation depends on the electron collection of the probe as a function of probe voltage as one goes from ion saturation and begins to pick up the Maxwell tail of the electron distribution. Because of the lack of saturation of the ion current, there is some uncertainty as to the ion current contribution to the net current in the electron-collection region. Careful analysis of the measurements would require fitting to some theory such as that of Lam.[90] However, for our work we assume that a first-order linear correction is sufficient to give a reliable result. The ion current contribution to the net current is estimated from a straight-line extrapolation of the saturated ion current curve in the region of electron collection.

Ecker, Masterson, and McClure[96] have commented that the presence of probes in a plasma such as that found in the positive column of a glow discharge may introduce errors by changing the conditions of the plasma in the vicinity of the probe. In our experiment the plasma potential is established by current flow through the end sheaths to the conducting end rings. The electron mean free path along the magnetic field lines is long, so that potential changes in the center of

the plasma are dominated by the conditions at the end walls. The probe is a small perturbation compared with the end walls. In our experimental configuration probes are usually inserted along a radius. Introduction of other probes while measurements are being made has little effect on the probe measurements unless the probe is inserted near the central arc column or unless the probe is drawing electron current and is on or near the same field line. When the probe is oriented perpendicular to a radius, as is discussed in Data Set 2 in Sec. IV, there is some shielding of the probe tip by the quartz sleeve on the probe and a reduction of ion current collection. Because of the large plasma volume compared with the size of the probes, and because the plasma conditions are dominated by the presence of conducting end electrodes, the effect of introducing a probe into the plasma should have negligible effect on the plasma behavior.

The electron temperature is determined by the collection of the tail of the Maxwellian distribution of electrons as a function of probe voltage. The electrons in the plasma have a very long mean free path for neutral collisions, $\lambda_{en} = 15.4$ cm, along the magnetic field lines. The potential drop at the end sheath reflects most of the electrons; however, the tail of the electron distribution is depleted. Coulomb collisions, however, are sufficient to keep the plasma distribution in the plasma Maxwellian and isotropic. Spitzer[97] gives the self-collision time for a distribution of electrons to relax to a Maxwellian distribution due to collisions with other electrons. This is also approximately the time required to relax anisotropy in the electron velocity distribution. For the conditions of our experiment, Data

Set 1 at r = 4 cm, $t_c = 4.6 \times 10^{-9}$ sec, the mean electron thermal speed $v_{th}^e = 2.6 \times 10^7$ cm/sec, so that the mean free path for self-collisions is $\lambda_{ee} = 0.1$ cm, which is much shorter than our system. Loss of high energy electrons through the end sheath may contribute to some energy loss from the system; however, self-collisions between electrons keep the electron distribution approximately isotropic and Maxwellian, and the electron temperature measurement should not be affected. Measurements by Schwirzke and Eggers[98] have confirmed the validity of electron-temperature measurements in plasma similar to ours with magnetic field strengths of up to 2 kG.

3. Use of Probes in the Presence of Fluctuations

Langmuir probe measurements in the presence of fluctuations have been discussed by many authors: Garscadden and Emeleus,[99] Crawford,[100] Sugawara and Hatta,[101] Garscadden and Bletzinger,[102] and Demetriades and Doughman.[103] We must consider the effect that fluctuations in the plasma potential, local ion density, and electron temperature may have on the signals that are actually measured. The fluctuations affect the current voltage characteristics of the probe, but they also change the currents in the measurement circuitry. A schematic of the output stage of the Langmuir probe sweeper chassis appears in Fig. 4. The sweep driver, upon being triggered, sweeps the probe voltage between the voltage limits. This circuit has been specially designed to keep the stray capacitance C_s between the probe and ground to a minimum. Also shown in Fig. 4 is the equivalent circuit. The probe current is measured from the voltage drop across resistor R_I, which is 100 or

1000 ohms. The probe sweeper can be approximated by an electromotive force $\phi_{emf}(t)$ and an internal impedance R_{emf} = 50 ohms. The probe potential ϕ_{probe} is measured through a 100-megohm resistor to the oscilloscope, which gives a 100-to-1 voltage reduction and a very large measuring impedance.

For plasma conditions with constant plasma density, electron temperature, and plasma potential one obtains a specific curve of probe current as a function of probe voltage, as is shown by the enhanced portion of the gated Langmuir probe curves in Fig. 37. An increase in the plasma density at a constant plasma potential and electron temperature causes the magnitude of the probe current to increase, but the shape of the curve and its location on the voltage axis is shifted by an amount $\Delta\phi = \Delta I(R_I + R_{emf})$. A change in the plasma potential leaves the magnitude and shape of the curve unchanged; however, the curve moves along the voltage axis. A change in the electron temperature causes both the magnitude and shape of the curve to change somewhat. The presence of potential, density, and possibly electron temperature fluctuations of the plasma cause the Langmuir probe curves to be broadened considerably, as is shown by the fainter curves in Fig. 37.

A fluctuation of the plasma potential changes the potential drop across the probe sheath and also changes the current drawn by the probe, depending on what part of the probe curve we are on. We can define a dynamic resistance of the sheath as $R_d = \Delta\phi/\Delta I$, which changes with probe and plasma potential, the electron temperature, and the plasma density. Looking at probe curve (a) in Fig. 37, where the ion

current has saturated, we see that there is a slight slope and we find that the dynamic sheath resistance is of the order of $R_d = 10^4$ ohms. Near the probe floating potential the dynamic resistance is much smaller, $R_d = 75$ ohms. In addition to the dynamic impedance of the probe sheath in the presence of fluctuations, there is also a capacitive effect. However, Kunkel and Guillory[104] comment that the capacitive contribution is negligible for frequencies well below the ion plasma frequency, which in our case is 10^9 sec^{-1}.

A change in the plasma potential therefore changes the current in our measurement circuit by an amount $\Delta I = \Delta\phi/(R_I + R_{emf} + R_d)$. For the conditions of Fig. 37 with $R_I = 1000$ ohms, a change of plasma potential of 1 V causes a small change in the current of 0.1 mA out of a saturated ion current of 4.2 mA. However, near the probe floating potential a change of 1 V causes a 0.8-mA change in the probe current. This effect is even larger at small values of R_I, and explains the observed variation in noise amplitude as a function of resistance R_I. For the conditions of the potential and saturated ion-current fluctuation measurements of this experiment, the sensing resistor R_I was kept large and the probes were biased well onto the saturated part of the probe curve, so that effects of potential and density fluctuatons are separated.

The time-resolved measurements of our plasma show that both the potential and density fluctuations are important. To determine the effect of these fluctuations on the electron temperature measurements we undertook experiments similar to those done by Garscadden and

Bletzinger.[102] The potential and density fluctuations were quite regular, so that a density signal on another probe was used as a time reference. The electron beam of the 502-A oscilloscope was then gated on for 1 μsec at different times relative to the maximum of the saturated ion current fluctuation. Results are shown in Fig. 37 for four different delays.

In photograph (a) the electron beam is gated on in phase with the maximum of the saturated ion current at the same position. We see that even though this corresponds to maximum plasma density the gated curve lies between the minimum and maximum values of the probe curve, which is shown much fainter. In photograph (c) we see the curve gated 180 deg later than the maximum of the saturated ion current. Note that this does not quite correspond to the minimum of the probe curve. Photographs (b) and (d) correspond to gating the probe curve 90 and 270 deg later than the maximum of the saturated ion current. These correspond quite well with the maximum and minimum of the probe curves respectively.

When one measures the electron temperatures from the maximum of the probe curve T_{max}, from the minimum of the probe curve T_{min}, and from the gated curve T_{gate}, one finds that T_{min} and T_{max} differ by as much as 30% with the value of T_{gate} lying between them, as shown in Table B.1. The electron temperature is pretty constant as a function of radius at these radii and so the electron temperature itself is probably not changing; also T_{gate} at 0 and 180 deg is almost the same. The presence of fluctuations introduce uncertainty into the electron

temperature measurements. For the purposes of estimating transport we usually use the average of T_{max} and T_{min} as an estimate of the average electron temperature.

Table B.1. Temperature measurements from gated Langmuir probe curves of Fig. 37. The oscilloscope trace is enhanced for 1 to 2 μsec out of the 25-μsec period of the fluctuations by using a phase delay θ_{gate} after the maximum of the saturated ion-current fluctuation to another probe at approximately the same position in the plasma.

Curve	θ_{gate} (deg)	T_{gate} (eV)	T_{min} (eV)	T_{max} (eV)
a	0	0.36	0.44	0.34
b	90	0.30	0.37	0.30
c	180	0.34	0.38	0.34
d	270	0.39	0.39	0.26

C. Theory of Transport of a Partially Ionized Plasma in a Magnetic Field

The calculation of the transport of plasma particles across a magnetic field is an extension of the fundamental work of Chapman and Cowling on The Mathematical Theory of Nonuniform Gases.[105] The plasma is produced in a state that is not in thermal equilibrium. By dissipation processes the plasma tends toward equilibrium by transporting itself across the magnetic field. In general the motions of the ions and electrons of the plasma must be treated statistically. The individual particle motions and interactions between the ions, electrons, and neutrals can be averaged over to obtain the fluid equations.[106,107] In principle this requires a knowledge of the distribution functions for the different species, which can be gained only by solving the velocity-space kinetic equations. In practice, however, any plasma in which collisional effects are important has relaxed to approximately a local Maxwell-Boltzmann distribution. Alternatively, one may consider the transport as a stochastic process due to displacements of the particles in collisions. One calculates the displacements due to specific collisions as an initial-value problem and then averages over the distribution of initial values to obtain the net displacement and net transport. Chandrasekhar considers this method in detail.[108] Both types of calculations should ultimately yield the same result.

1. Weakly Ionized Transport

The transport of a weakly ionized plasma, in which Coulomb collisions are unimportant, is given by Allis.[109] In the absence of tem-

perature gradients the transport flux in a direction j for species α, nv_j^α is given by

$$nv_j^\alpha = - D_{jk}^{\alpha n}(\partial n/\partial x_k) + \mu_{jk}^{\alpha n} n E_k, \tag{C.1}$$

where E_k is the kth component of the electric field and $\partial n/\partial x_k$ is the kth component of the density gradient, and the summation over k is implied. The diffusion tensor $D_{jk}^{\alpha n}$ is given by

$$D_{jk}^{\alpha n} = \frac{v_{\alpha th}^2}{3\nu_{\alpha n}} \begin{pmatrix} \frac{1}{1+\Omega_\alpha^2\tau_{\alpha n}^2} & \frac{\Omega_\alpha\tau_{\alpha n}}{1+\Omega_\alpha^2\tau_{\alpha n}^2} & 0 \\ \frac{-\Omega_\alpha\tau_{\alpha n}}{1+\Omega_\alpha^2\tau_{\alpha n}^2} & \frac{1}{1+\Omega_\alpha^2\tau_{\alpha n}^2} & 0 \\ 0 & 0 & 1 \end{pmatrix}, \tag{C.2}$$

where Ω_α is the gyrofrequency, $\tau_{\alpha n} = 1/\nu_{\alpha n}$ is the mean time between collisions with the neutrals, and $v_{\alpha th}^2$ is the mean square thermal velocity for species α. The mobility tensor $\mu_{jk}^{\alpha n}$ is related to the diffusion tensor $D_{jk}^{\alpha n}$ by the Einstein relationship

$$\mu_{jk}^{\alpha n} = \frac{q_\alpha D_{jk}^{\alpha n}}{kT_\alpha}, \tag{C.3}$$

where q_α is the charge and kT_α is the mean therm energy of species α.

A particle goes, on the average, a transport mean free path $\lambda_{\alpha n}$ before experiencing a collision with a neutral. In a collision we assume that the particle loses the sense of its original direction and

velocity, and proceeds randomly. We then can treat the problem as a Markov process, in which the next step in the random walk of the particle is statistically independent of the previous step. In the presence of a density gradient there is a net flux of particles given by $\vec{nv} = - D\vec{\nabla}n$, where the diffusion coefficient D is just the mean square displacement per unit time. D is isotropic in the absence of a magnetic field.

In the presence of a magnetic field the transverse motion of the particles can be described as a rotation at the gyrofrequency in a circle $r_{g\alpha} = v_{th}^{\alpha}/\Omega_{\alpha}$ about the guiding center. The guiding center is the center of momentum of the gyrating particle, and undergoes drift motion and accelerations in the presence of electric fields and magnetic field gradients.[110] In the absence of drifts a particle gyrates about a magnetic field line until its position is displaced in a collision by the order of the gyroradius. The diffusivity across the magnetic field is reduced by a factor $1/[1 + (\Omega_{\alpha}\tau_{\alpha n})^2]$, where $\Omega_{\alpha}\tau_{\alpha n}$ is the mean number of orbits the particle makes between collisions. The diffusion coefficients transverse to the magnetic field are related to the coefficient for diffusion parallel to the magnetic field by

$$D_{xx}^{\alpha n} = D_{yy}^{\alpha n} = D_{\perp}^{\alpha n} = \frac{D_{\parallel}^{\alpha n}}{1 + (\Omega_{\alpha}\tau_{\alpha n})^2} . \qquad (C.4)$$

The diffusion coefficient along the magnetic field direction z is the same as the field-free value

$$D_{zz}^{\alpha n} = D_{\parallel}^{\alpha n} = \frac{v_{th}^{\alpha\,2}}{3\nu_{\alpha n}} = \frac{\lambda_{\alpha n}\nu_{\alpha n}}{3} . \qquad (C.5)$$

The off-diagonal terms of the diffusion and mobility tensors give the diamagnetic drift current due to density gradients,

$$n\vec{v}_{\alpha} = \frac{q_{\alpha}c}{e^2}\frac{kT_{\alpha}}{B^2}\vec{\nabla}n \times \vec{B}, \qquad (C.6)$$

and the drift motion due to electric field components transverse to the magnetic field, the well-known $\vec{E} \times \vec{B}$ drift motion

$$n\vec{v}_{\alpha} = nc\frac{\vec{E} \times \vec{B}}{B^2} . \qquad (C.7)$$

Both these terms are reduced by a factor of $\Omega_{\alpha}^2\tau_{\alpha n}^2/(1 + \Omega_{\alpha}^2\tau_{\alpha n}^2)$ because of collisions with neutral particles. In the limit of large magnetic fields, where $\Omega_{\alpha}\tau_{\alpha n} \gg 1$, this factor becomes unity and the presence of collisions does not significantly affect these drifts.

2. Fully Ionized Transport

The presence of Coulomb collisions also gives rise to diffusion of particles. The early calculations by Landshoff[111] showed that because of the long range of the Coulomb interaction, attempts to evaluate the Coulomb interaction term of the Boltzmann collision integral would give divergent results. Cohen, Spitzer, and Routley[112] successfully calculated the electrical conductivity of a plasma in the absence of a magnetic field by assuming that the Coulomb interaction was cut

off at the Debye shielding distance. Spitzer and Härm[113] extended this theory, also in the case of no magnetic field. Spitzer[114] has shown that in the fluid approximation the diffusion flux is related to the plasma pressure gradient and the plasma resistivity. The detailed calculation of the transport of particles because of collisions with like and unlike particles, considering the detailed trajectories in the presence of a magnetic field, was done by Longmire and Rosenbluth[115] for the case of equal ion and electron temperatures. They found, in agreement with Simon,[116] that the diffusive flux due to like-particle collisions was proportional to the third derivative of the density and did not obey Fick's law. Rosenbluth and Kaufman[117] extended the calculation to resistivity, thermal conductivity, and the thermoelectric effect in the presence of temperature gradients, considering that collisions were sufficiently frequent that the distribution functions were locally Maxwellian and that the ion and electron temperatures were equal. They found that the transport flux was given by[117]

$$n\vec{v}_D = -\eta_\perp \frac{c^2}{B^2} \vec{\nabla}_\perp P + \frac{3}{4} \eta_\perp \frac{c^2 n}{B^2} \vec{\nabla}_\perp kT + nc \frac{\vec{E} \times \vec{B}}{B^2}, \qquad (C.8)$$

where the transverse resistivity is

$$\eta_\perp = \frac{8}{3} \left(\frac{\pi}{2}\right)^{1/2} \frac{e^2 M_e^{1/2}}{(kT)^{3/2}} \ln \Lambda, \qquad (C.9)$$

where Λ is the usual shielding parameter $\Lambda \approx (\lambda_D / r_0)$.[118] The transverse resistivity $\eta_\perp = 1.98\eta_{SH}$ is the resistivity calculated by Spitzer and Härm[113] in the absence of a magnetic field.

Kaufman[119] calculates the transport to be expected in the case of unequal ion and electron temperatures. Neglecting thermal gradients, the particle flux is given by

$$n\vec{v}_D = - \eta_\perp \frac{c^2 n}{B^2} \left[(kT_i + kT_e) \vec{\nabla}_\perp n \right], \qquad (C.10)$$

which is identical to the Rosenbluth and Kaufman result in the limit of equal temperatures. Taylor[120] also considers the problem and includes the effects of ion-electron energy exchange and temperature relaxation on the transport. He finds

$$n\vec{v}_D = - \eta_\perp \frac{c^2 n}{B^2} \left[(kT_i + kT_e) \nabla_\perp n - 2(kT_i - kT_e) \nabla_\perp n \right], \qquad (C.11)$$

where the additional term represents the effect of temperature relaxation. He concludes that his result is "appropriate to a situation in which the temperature difference is allowed to relax at its natural rate as the diffusion proceeds, and that (Kaufman's result) is applicable when the diffusion is forced to proceed at a constant temperature difference."[121] This latter condition is appropriate to our experiment, so we use Kaufman's result to estimate the transport due to fully ionized diffusion. Both the ions and the electrons are transported at the same rate. The diffusion coefficient is given by

$$D^{ie} = D^{ei} = \eta_\perp \frac{c^2 n}{B^2} (kT_i + kT_e). \qquad (C.12)$$

The presence of transverse components of electric field in a fully ionized plasma induces only E x B drift motion, and does not cause transport in the direction of the electric field components.

3. The Effect of Temperature Gradients

From Eq. (C.8) we find that the particle transport across the magnetic field depends upon the gradient both of the plasma pressure and of the plasma temperature. The transport due to the thermal gradients contributes a transport flux of the order of

$$n_i D^{ie} \frac{\nabla_\perp kT_i + \nabla_\perp kT_e}{kT_i + kT_e}$$

compared with the transport due to the density gradient of the order of $D^{ie}\nabla_\perp n$. At the edge of the central arc column the electron temperature falls from $kT_e = 7$ eV at $r = 1$ cm to $kT_e = 0.46$ eV at $r = 2$ cm, giving a steep electron-temperature gradient of the order of $\nabla_\perp kT_e/kT_e \approx 1.6$ cm^{-1}. As was discussed in Sect. V.F.5, $\nabla_\perp kT_i/kT_i \approx 2$ cm^{-1} at the edge of the central arc column, and the density gradient is of the order of $\nabla_\perp n/n \approx 0.43$ cm^{-1} or less. The presence of a large temperature gradient near the central arc column can contribute both to the transport of the primary plasma and to the generation of possible drift instabilities.

In the secondary plasma beyond $r = 2$ cm, where the transport measurements are made, the ion and electron temperatures fall off very slowly. From $r = 3$ cm to $r = 7$ cm, as indicated in Table 5.1, the electron temperature falls off from $kT_e = 0.36$ to 0.26 eV and the ion

temperature falls off from 0.074 to 0.046 eV

$$(\nabla_\perp kT_e + \nabla_\perp kT_i)/(kT_e + kT_i) \approx 0.06 \ll \nabla_\perp n/n \approx 0.43 \text{ cm}^{-1}.$$

The change in electron and ion temperatures with radius may change the transport coefficients somewhat; however, there is negligible transport due to temperature-gradient effects in the secondary plasma region.

4. The Partially Ionized Plasma

The partially ionized plasma is a three-component system in which the interactions between the ions, electrons, and neutrals are all important. Shkarofsky[122] has shown for the electrons, and Golant[107] has shown more generally for a system whose particle distributions are in locally Maxwellian-Boltzmann equilibrium, that the transport fluxes due to ion-electron collisions and due to collisions with neutrals are additive. In the limit where $\Omega_{\alpha n}\tau_{\alpha n} \gg 1$ for both the ions and electrons, the diffusion and mobility tensors for a partially ionized plasma become

$$D^{\alpha}_{jk} = \begin{pmatrix} D_\perp^{\alpha n} + D^{ie} & \dfrac{+q_\alpha ckT_\alpha}{e^2 B} & 0 \\ \dfrac{-q_\alpha ckT_\alpha}{e^2 B} & D_\perp^{\alpha n} + D^{ie} & 0 \\ 0 & 0 & D_\parallel^{\alpha n} \end{pmatrix} \qquad \text{(C.13)}$$

and

$$\mu_{jk}^{\alpha} = \begin{pmatrix} \mu_{\perp}^{\alpha n} & c/B & 0 \\ -c/B & \mu^{\alpha n} & 0 \\ 0 & 0 & \mu_{\parallel}^{\alpha n} \end{pmatrix} \tag{C.14}$$

where

$$D_{\perp}^{\alpha n} = \frac{D_{\parallel}^{\alpha n}}{1 + \Omega_{\alpha}^{2}\tau_{\alpha n}^{2}} ,$$

$$D_{\parallel}^{\alpha n} = \frac{\lambda_{\alpha n}^{2}\nu_{\alpha n}}{3} ,$$

$$D^{ei} = D^{ie} = \eta_{\perp} c^{2} n \frac{kT_e + kT_i}{B^2} ,$$

$$\mu_{\perp}^{\alpha n} = \frac{q_{\alpha} D_{\perp}^{\alpha n}}{kT_{\alpha}} ,$$

and

$$\mu_{\parallel}^{\alpha n} = \frac{q_{\alpha} D_{\parallel}^{\alpha n}}{kT_{\alpha}} .$$

The transport flux is given by

$$nv_{j}^{\alpha} = - D_{jk}^{\alpha} \frac{\partial n}{\partial x_k} + \mu_{jk}^{\alpha} n E_k . \tag{C.15}$$

5. Ambipolar Diffusion

Quite generally, in a weakly ionized plasma the transport due to diffusion is different for the electrons and ions. As a result one species tends to diffuse away faster than the other and charge neutrality is quickly violated. An electric field is set up,

$\vec{\nabla}\cdot\vec{E} = 4\pi e(n_i - n_e)$, which tends to reduce the transport of the faster species and speed the transport of the slower. If there is congruence between the electron and ion currents in one or more directions j, $nv_j^e = nv_j^i$, then the transport is described as ambipolar diffusion. The concept of ambipolar diffusion was first used by Schottky[123] in his early discussion of the positive column.

In the absence of a magnetic field, the electrons, which generally have a much larger than mean thermal velocity, will diffuse much faster than the ions. The ambipolar electric field in this case is given by Golant[107]

$$\vec{E} = \frac{D_{\parallel}^{in} - D_{\parallel}^{en}}{\mu_{\parallel}^{in} - \mu_{\parallel}^{en}} \frac{\nabla n}{n} \approx \frac{kT_e}{e} \frac{\vec{\nabla} n}{n} . \tag{C.16}$$

This is also the ambipolar field expected from equal ion and electron currents along the magnetic field direction. Substituting the ambipolar electric field into the diffusion equation, we find

$$nv_{\parallel}^i = nv_{\parallel}^e = - D_{a\parallel} \nabla n , \tag{C.17}$$

where

$$D_a = \frac{\mu_{\parallel}^{en} D_{\parallel}^{in} - \mu_{\parallel}^{in} D_{\parallel}^{en}}{\mu_{\parallel}^{en} - \mu_{\parallel}^{in}} \approx \frac{kT_i + kT_e}{m_i \nu_{in}} \tag{C.18}$$

is the ambipolar diffusion coefficient.

In the presence of a strong magnetic field, because of the much smaller electron mass, transverse diffusion of the electrons is much less than that of the ions. Under the condition of congruence of the perpendicular ion and electron fluxes, there is an ambipolar electric

field given by

$$E_\perp = \left(\frac{D_\perp^{in} - D_\perp^{en}}{\mu_\perp^{in} - \mu_\perp^{en}} \right) \frac{\vec{\nabla}_\perp n}{n} , \tag{C.19}$$

where perpendicular, $\perp$, refers to the direction orthogonal to the magnetic field and antiparallel to the density gradient. There is an ambipolar diffusion coefficient given by Golant[107]

$$D_{a\perp} = \frac{\mu_\perp^{en} D_\perp^{en} - \mu_\perp^{in} D_\perp^{en}}{\mu_\perp^{en} - \mu_\perp^{in}} \approx \frac{kT_i + kT_e}{m_i \nu_{in} \left(1 + \frac{\Omega_e \Omega_i}{\nu_{en} \nu_{in}} \right)} , \tag{C.20}$$

assuming $\Omega_i \tau_{in} \ll \Omega_e \tau_{en}$.

In a fully ionized plasma the perpendicular transport of the ions and electrons by diffusion are equal. There is no space-charge separation due to diffusion, and the diffusion can be considered to be ambipolar to start with.

In a partially ionized plasma there is transport due to both ion-electron collisions and collisions with neutral gas atoms. One must investigate the detailed conditions of the plasma to see if condition of congruence applies along any direction. If so, there will be ambipolar diffusion in this case; however, it is a complicated expression and does little to facilitate understanding of transport.

In a steady-state plasma the constraint on the system is that $\partial n_\alpha / \partial t = 0$. From the continuity equation, in the absence of volume production or recombination, we have

$$\frac{\partial n_\alpha}{\partial t} + \sum_j \frac{\partial n v_j^\alpha}{\partial x_j} = 0 \qquad \text{(C.21)}$$

for each species α. We also have the condition of quasi-neutrality which must be satisfied for any plasma for which the dimensions L are much greater than the Debye length. These conditions do not necessarily imply congruence, i.e., that $nv_j^i = nv_j^e$ for any or all components. This condition is fulfilled only in certain special circumstances such as in the positive column of a glow discharge which is enclosed in a dielectric cylinder and which is sufficiently long that end effects are negligible. One must carefully investigate each case to determine if the condition of congruence of the ion and electron currents is a reasonable assumption.

6. Enhanced Transport

The off-diagonal elements of the diffusion tensor, Eq. (C.13), in the transport Eq. (C.15) describe the diamagnetic electron and ion currents for our three-component plasma. The off-diagonal elements of the mobility tensor, Eq. (C.14), describe the $\vec{E} \times \vec{B}$ drift motion of the plasma. It is this latter drift motion which gives rise to enhanced transport of the plasma in the fluid approximation.

a. Convection

In the presence of static or fluctuating electric fields one can get convective transport of the plasma. Suppose there is a fluctuating electric field $E_\theta(t)$, where θ is the direction perpendicular to both the density gradient $(\partial n/\partial r)\vec{i}_r$ and the magnetic field $\vec{B} = B\vec{i}_z$.

If the fluctuation frequency of the electric field ω is much less than the ion gyrofrequency Ω_i, then the drift motion in the radial direction is given by $v_r(t) = cE_\theta(t)/B$. The net transport due to convection is given by Thomassen,[124]

$$\langle nv_r \rangle_{conv} = \langle n(t)[cE_\theta(t)/B] \rangle, \qquad (C.22)$$

where the brackets indicate time averaged over many fluctuation periods.

Because of the large plasma dielectric constant, low-frequency electromagnetic waves in the plasma travel at the Alfvén speed, which is much slower than the speed of light. Fluctuations in the magnetic field in the plasma may be produced. If these are significant they could affect the average transport in Eq. (C.22) and we would have to expand the magnetic field in terms of the zero-order magnetic field plus a perturbation $\vec{B}_1(t)$. Fluctuations in the magnetic field are coupled to the electric field fluctuation by Maxwell equations. For a transverse wave of the form $\vec{E}_1(t) = \vec{E}_1 e^{i\omega t - i\vec{k}\cdot\vec{r}}$ there is a magnetic field fluctuation $\vec{B}_1(t) = (c/\omega)\vec{k} \times \vec{E}_1(t)$, where $\vec{E}_1(t)$ is in stat volts/cm and $\vec{B}_1(t)$ is in gauss. The phase velocity of the transverse wave is $\omega/k = v_A = c/\sqrt{K}$ for Alfvén waves. The plasma dielectric constant K is given by

$$K = 1 + 4\pi\rho c^2/B^2 = 1 + 0.017\, n_i A/B^2,$$

where A is the ion mass in amu, n_i is the ion density in cm^3, and B is in gauss. In the secondary plasma n_i is typically 1.8×10^{12} cm^{-3}, which gives us a dielectric constant $K = 3.8 \times 10^5$. The amplitude of the axial magnetic field fluctuation B_{z1} due to a transverse electric

fluctuation E_θ is

$$B_{z1} = \frac{\sqrt{K}}{300} E_\theta \text{ (V/cm)} = 2.1\, E_\theta \text{ gauss}, \tag{C.23}$$

where E_θ is in V/cm and the factor of 1/300 is due to the change in units.

Measurements indicate that the dominant fluctuation in the plasma is an m = 1 azimuthally fluctuating electric field at 48 kHz. The amplitude of the corresponding potential fluctuations are of more or less constant amplitude ϕ_1 beyond r = 2, and are in phase axially and radially, so that the azimuthal electric field fluctuations are of the form

$$E_\theta = \frac{\phi_1}{r} e^{i\omega t - im\theta}. \tag{C.24}$$

The measured amplitude of E_θ at r = 4 cm is E_θ = 0.12 V/cm rms.

Let us consider what effect this has on radial transport. From Eq. (C.22) we can expand the magnetic field B in terms of the static axial magnetic field B_z and a small perturbation $B_{1z}(t)$. Equation (C.22) then becomes

$$\langle nv_r \rangle_{conv} = \left\langle \frac{n(t) c E_\theta(t)}{B_z + B_{z1}(t)} \right\rangle = \left\langle \frac{n(t) c E_\theta(t)}{B_z} \times \left(1 - \frac{B_{z1}(t)}{B_z} + \cdots \right) \right\rangle. \tag{C.25}$$

If the fluctuation in E_θ is in a purely transverse mode, then from Eq. (C.23) we would expect to find a corresponding magnetic field fluctuation of amplitude B_{z1} = 0.25 G rms. The correction term in Eq. (C.25) is of the order $B_{z1}/B_z = 5 \times 10^{-4} \ll 1$, and it is completely negligible

compared with the zero-order term.

When one takes the curl of the electric field fluctuations as given by Eq. (C.24), we find that curl $E_\theta = 0$. The dominant electric field fluctuations in our plasma are purely longitundinal and produce no fluctuations in the magnetic field. Other fluctuations in the plasma at higher frequencies are of smaller amplitude, so that the time variation of the magnetic fields due to transverse waves and the effect on transport should be negligible in this experiment.

Let us now consider the effect that density and electric field fluctuations at a single frequency have on the convective transport of the plasma as given by Eq. (C.22). The density at a point in space can be written $n(t) = n_0 + n_1 \cos(\omega t)$. The electric field is $E_\theta(t) = E_0 + E_1 \cos(\omega t + \delta)$, where δ is the phase angle between the electric field and density fluctuation. The net convection is then given by

$$\langle nv_r \rangle^{\alpha}_{conv} = \frac{cn_0E_0}{B} + \frac{cn_1E_0}{B} \langle \cos \omega t \rangle + \frac{cn_0E_1}{B} \langle \cos (\omega t) + \delta) \rangle + \frac{cn_1E_1}{B} \langle \cos(\omega t) \cos(\omega t + \delta) \rangle .$$

Taking the time average, the $\langle \cos (\omega t) \rangle$ and $\langle \cos (\omega t + \delta) \rangle$ terms go to zero. The product term $\langle \cos (\omega t) \cos (\omega t + \delta) \rangle$ averages to $1/2 \cos \delta$. This then gives

$$\langle nv_r \rangle^{\alpha}_{conv} = \frac{cn_0E_0}{B} + \frac{cn_1E_1}{B} \frac{\cos \delta}{2} . \qquad (C.26)$$

The first term on the right-hand side is the net transport because of a static transverse electric field E_0. The second term is the net transport due to mutual fluctuation of the electric field and density perturbations. If they are 90 deg out of phase there will be no net transport. This mechanism transports ions and electrons at the same rate.

b. Enhanced Diffusion

Because of the presence of fluctuating electric fields there is also the possibility of enhanced diffusion of the plasma. Bohm, Burhop, and Massey[125] in an attempt to explain the observations in a rectangular arc consider the possibility of a "drain diffusion" mechanism. The arc under study tended to run asymmetrically with equipotential lines skewed in such a way that the electrons and ions under the influence of $\vec{E} \times \vec{B}$ drift would drain away from the arc region to the chamber walls with a velocity given by $\vec{v} = c[(\vec{E} \times \vec{B})/B^2]$. In a cylindrically symmetric arc, they argue, there cannot be a static drain, since the equipotentials are circles concentric about the source. They state, "It has been found, however, that a static distribution of this type is unstable and it tends to break up into an oscillating distribution, with waves traveling around the center. These waves create electric fields transverse to the radius which causes the electrons to drain inward and outward."[126] Because of the density gradient, the net drain is outward. They go on to state that these unstable waves will grow until damping by diffusion stops the growth. "With the aid of the theory, the value of $D_\perp$ (the diffusion coefficient), at which this balance occurs, can be calculated. It is

$$D_{\perp} = \frac{1}{16}\frac{ckT_e}{eB} ." \qquad (C.27)$$

Thus they postulate into existence an enhanced diffusion process, which has come to be known as Bohm Diffusion. A detailed calculation was never published, but this estimate has served to spark considerable interest in the nature of enhanced transport of a plasma across a magnetic field.

Spitzer[127] was able to derive a Bohm-type diffusion coefficient by considering fluctuations in an electric field transverse to the magnetic field. He assumes that the electric potential fluctuates more or less independently on different field lines with an amplitude $\delta\phi$. This gives rise to a transverse electric field E_θ. By calculating the random walk of particles due to the $\vec{E} \times \vec{B}$ drift motion he obtains

$$D = 2\langle E_\theta^2\rangle/B^2\tau_s, \qquad (C.28)$$

where the brackets indicate averaging over a time long compared with a fluctuation; τ_s is the self-correlation time of the electric field fluctuations

$$\tau_s = \int_0^\infty \frac{d\tau\langle E_\theta(t)E_\theta(t+\tau)\rangle}{\langle [E_\theta(t)]^2\rangle} . \qquad (C.29)$$

By assuming that the potential fluctuations are of the order of the electron temperature $\delta\phi = kT_e/e$ and that the electric field is of the order of $E_\theta = \delta\phi/r_{ge}$ and that $\tau_s = 1/\Omega_e$, Spitzer gets $D \approx ckT_e/eB$,

which except for the undetermined numerical factor is the same as Bohm's result.

Tchen[128] considers the stochastic transport due to both collisions and fluctuating electric fields. He finds that "the diffusion by collective oscillations is determined by the wave energy, while the collisional diffusion is determined by the thermal energy." For the enhanced diffusion he is in agreement with Spitzer's general result quoted above. The enhanced diffusion is proportional to the energy in the electric field fluctuation $\langle E^2 \rangle / 8\pi$ and to the self-correlation time of the field fluctuations, τ_s.

One must consider the self-correlation time τ_s carefully. In a sinusoidal transverse electric field a particle oscillates back and forth indefinitely. Its average position is not displaced until the coherence of the oscillation is broken up by amplitude, frequency, or phase modulation. Sometimes it is assumed that $\tau_s = 1/\Delta f$, where Δf is the bandwidth of the oscillation spectrum, but this is not correct. This choice can give a diffusion coefficient which may be too large by orders of magnitude. For a pure sine wave, $\Delta f = 0$ and τ_s is zero, not infinite.

Puri[129] considers the diffusion due to stochastic fields in detail. Suppose there is an electric field $E(t) = E_1 \cos(\omega t)$ which is dephased randomly with a probability given by

$$P(t)dt = \nu e^{-\nu t} dt.$$

He finds that the diffusion coefficient is given by

$$D = \frac{\pi}{B_0^2}\left[\phi(\Omega) + 2\phi(0)\right]. \qquad (C.30)$$

B_0 is the magnetic field strength. The power spectrum on the electric field fluctuations is

$$\phi(\omega) = \frac{E(\omega)^2}{8\pi} = \frac{E_1^2}{2\pi}\,\frac{\nu(\omega_0^2 + \omega^2 + \nu^2)}{[\nu^2 + (\omega - \omega_0)^2][\nu^2 + (\omega + \omega_0)^2]}\ ; \qquad (C.31)$$

ω_0 is the oscillation frequency and 2ν is the bandwidth of the fluctuations. If the oscillation frequency is close to the gyrofrequency Ω there is significant diffusive transport due to the $\phi(\Omega)$ terms above. However, we are considering the transport due to fluctuations, where $\omega \ll \Omega_i$. In this case

$$D^{\alpha}_{enh} = \frac{c^2 E_1^2}{B^2}\,\frac{\nu}{(\nu^2 + \omega_0^2)} = \frac{2c^2\langle [E(t)]^2\rangle}{B^2}\,\tau_s. \qquad (C.32)$$

The correlation time is

$$\tau_s = \nu/(\nu^2 + \omega_0^2). \qquad (C.33)$$

If the amplitude of the electric field fluctuations and the correlation time are independent of the magnetic strength, then the enhanced diffusion coefficient is proportional to $1/B^2$, just as is collisional diffusion. Only if the amplitude and correlation time of the fluctuations change in the proper manner with the magnetic field, as in Spitzer's argument, do we arrive at a Bohm-type coefficient which varies as $1/B$.

There has been a tendency to label any experimental observation that seems to indicate that the radial plasma transport scales as 1/B as due to Bohm diffusion.

D. Error Analysis

Various parameters of the experiment have been measured to various degrees of certainty. In order to get an estimate of the reliability of our estimates for the different processes, we must discuss sources of error and uncertainty.

1. The Magnetic Field

The axial magnetic field measurements at the midplane of the diffusion chamber was made by using a Rawson rotating-coil gaussmeter as a function of the current through the magnetic field coils. The measured value for the flat-field coil configuration is 5.60 G/A with the magnetic field pointing toward the cathode for positive field current. This measurements is probably good to about 1%. The calculated magnetic field for the observed current distribution in the various coils shows that the magnetic field on the axis is uniform to within 5% over the 60 cm of the diffusion chamber length. We therefore estimate the uncertainty in the axial magnetic field to be $\delta B/B = 0.05$.

In addition, measurements on the transverse magnetic field components B_{vert} and B_{horiz} were made by using a 5800-cm^2 search coil with an integrating amplifier. Transverse fields of as much as 2 G were observed in the vicinity of the ends of the diffusion chamber. Two pairs of the field coils were used to produce an external transverse magnetic field to control the magnetic alignment of the system. The external field produced by these coils was measured and found to be 0.115 G/A, and because of the noise level and drift in the amplifier the measurement is probably good to about 10%.

2. Neutral Pressure and Density

The neutral pressure of the system is measured by using a VG-1/A ionization gauge with an emission current of 56 mA located at the rear access port of the diffusion chamber. The magnetic field effect on the gauge is neutralized by magnetic shielding. Calibration of a typical VG-1/A against a capacitance manometer in the 10^{-3} Torr range gives $P_{mano}/P_{VG-1/A} = 7$ to 8 in helium, in agreement with the estimate of gauge sensitivity of 14 μA/mTorr in helium compared with 100 μA/mTorr in nitrogen. The manometer measures the absolute pressure, the same for all gases. The uncertainty in the calibration factor is about 14%. Similar measurements using a Bayard-Alpert type gauge versus a capacitance manometer shows that at 3 mTorr in helium there is about a 10% scatter in the readings with a single gauge.[130] We estimate that our uncertainty in measurement of the neutral pressure is $\delta P_T/P_T = 0.20$.

To deduce the neutral density one must know the neutral temperature. The neutral gas in the diffusion chamber is in good thermal contact with the walls of the system, which are at room temperature, 20 to 30°C. This gives us a neutral temperature of about 300°K or 0.03 eV, which is good to about 10%. $\delta kT_n/kT_n = 0.10$. This gives us an overall uncertainty in the neutral density of $\delta n_0/n_0 = 0.22$.

3. Probe Position

The absolute positioning of the radial probes with respect to the central arc column is of the order of 0.2 cm. The relative position of the same probe at different radii is good to 0.05 cm. The positioning of the axial probe is of the order of 0.2 cm. This is not so

critical, since the axial density profile changes slowly with position. The absolute radial position of the axial probe is good to about 0.5 cm. The relative position of the axial probe as it moves along a field line is of the order of 0.2 cm. Positioning of the probes introduces a minimal amount of error.

4. Langmuir Probe Measurements

(a) Saturated Ion Current

The measurements of the saturated ion current to a particular Langmuir probe has uncertainty from several sources. The current is determined by measuring the voltage drop across a 1%, 10^2- or 10^3-ohm resistor with a digital voltmeter which is accurate to about 1 mV. Except for relatively low densities this should contribute negligible error. A more serious source of error comes from choosing the point at which the saturated ion current is to be evaluated. As the probe becomes more negative the effective probe collection area increases and the total ion current also increases. There is no definitive judgment as to where the saturated ion current curve is to be evaluated. Generally it is measured at the point at which the tail of the electron distribution just ceases to affect the curve; however, often it is evaluated at some fairly large negative voltage such as $\phi_{probe} = -22.5$ V on the "flat" part of the curve. This choice can introduce 15 to 20% uncertainty in the absolute value of the saturated ion current. For relative measurements the probe curves are more or less similar and, except at low densities, where the change in the flat part of the saturated ion curve with increasing negative voltage becomes more pro-

nounced, this error should be of the order of 10 to 15%. In addition there can be some variations from measurement to measurement because of slight drift in the arc conditions. We estimate the overall uncertainty in the saturated ion current measurement is of the order of $\delta I_{si}/I_{si} = 0.20$.

(b) Electron Temperature

Based on repeated measurements at the same point we estimate the measurement of the local electron temperature kT_e to be reliable within $\delta kT_e/kT_e = 0.15$. The error is introduced in estimating the slope of the $\ln [I_{si}-I(V)]$ plot. Due to frequent collisions the electron temperature is in this system most likely isotropic, so that as long as the electron temperature is evaluated in the vicinity of the floating potential or lower, the effect of the magnetic field should not introduce any additional uncertainty.[131]

5. Ion Density

The ion density of the plasma is derived from a knowledge of the saturated ion current, electron temperature, and probe collection area, and is given by

$$n_i = \frac{0.453 \times 10^{12}}{C} \frac{I_{si}}{A_{probe}} \sqrt{\frac{M}{kT_e}} \ \text{cm}^{-3},$$

where M is the ion mass in amu, A_{probe} is the probe area in mm^2, I_{si} is the saturated ion current in mA, the numerical factor is to take care of the units, and C is given by Bohm, Burhop, and Massey[132] as $C = 0.40$. The uncertainty in the ion density is found by application

of the theory of error (see, for instance, Beers[133]),

$$(\delta n_i/n_i)^2_{abs} = (\delta I_{si}/I_{si})^2 + (0.5\delta kT_e/kT_e)^2 + (\delta A_{probe}/A_{probe})^2 + (\delta C/C)^2.$$

The probe area is found by measuring the diameter and length of the cylindrical tungsten probe tip. Because of some uncertainty as to how much of the probe really sees the plasma, we estimate the uncertainty in the probe to be 10%: $\delta A_{probe}/A_{probe} = 0.10$. Finally, there is the uncertainty in the constant C. Bohm, Burhop, and Massey[132] estimate that in the case of $kT_i \ll kT_e$ the "ion collection is independent of the positive ion temperature, within a factor of 20%." For the case of a plane probe $C = 0.25$. For a spherical probe they obtained $C = 0.40$, due to the effect of space-charge electric field on ion collection. It is assumed that this should also give a fairly reliable estimate for a cylindrical probe. Because the probe radius, $a = 2.5 \times 10^{-2}$ cm, is much less that the ion gyroradius, $r_{gi} = 1.3 \times 10^{-1}$, $a < r_{gi}$, the effect of the magnetic field on ion collection should be small. We estimate the uncertainty in the constant to be $\delta C/C = 0.20$. Later and more sophisticated discussions of the theory of Langmuir probes in plasmas, which include the dependence of saturated ion current on probe voltage, are discussed by Chen,[89] but for the analysis of our experimental measurements we use the simple analysis of Bohm, Burhop, and Massey.

Considering the uncertainty due to the above sources we find that the absolute uncertainty in the ion density measurements is

$\delta n_i/n_{i(abs)} = 0.31$. For relative density measurements with the same probe we need to consider only the error in saturated ion current and electron temperature. In this case one gets $\delta n_i/n_{i(rel)} = 0.21$.

6. Ion Temperature

The ion temperature is determined by rate balancing between heating of the ions by the electrons and cooling by the neutrals. It depends on the plasma and neutral density, the electron and neutral temperatures, as well as the momentum-transfer cross sections for ion-neutral and ion- electron collisions. The ion-neutral cross sections at low energy in helium are accurately known from the zero-field mobility measurements.[134] From Eq. (5.1) we find that the ion temperature is given by the solution of

$$kT_i = \frac{kT_e + C(kT_e)^{3/2}(kT_i)^{1/2}kT_n}{1 + C(kT_e)^{3/2}(kT_i)^{1/2}} = \frac{kT_e + FkT_n}{1 + F},$$

where $C = n_0/n_i$ (n_0 and n_i are in units of cm^{-3}), where $F = C(kT_e)^{3/2} \times (kT_i)^{1/2}$, and the temperatures kT_e, kT_i, and kT_n are in eV. From the propagation of error in the temperatures and densities we find that the uncertainty in the ion temperature is given by

$$(1 - 0.5G)^2\left(\frac{\delta kT_i}{kT_i}\right)^2 = (-G)^2\left(\frac{\delta n_i}{n_i}\right)^2 + (G)^2\left(\frac{\delta n_0}{n_0}\right)^2$$

$$+\left(\frac{kT_e}{kT_e + FkT_n} + \frac{3}{2}G\right)^2\left(\frac{\delta kT_e}{kT_e}\right)^2 + \left(\frac{FkT_n}{kT_e + FkT_n}\right)^2\left(\frac{\delta kT_n}{kT_n}\right)^2,$$

where $G = [F(kT_n + kT_e)]/[(1 + F)(kT_e + FkT_n)]$. The results for Data Set 1 are shown in Table 5.1 and indicate that at $r = 2$ cm, $kT_i = 0.10$ eV with $\delta kT_i/kT_i = 0.17$; at $r = 4$ cm, $kT_i = 0.074$ eV with $\delta kT_i/kT_i = 0.15$; and at $r = 6$ cm, $kT_i = 0.050$ eV with $\delta kT_i/kT_i = 0.13$. The ion temperature calculation is good to 10 to 20% depending on the experimental conditions.

7. The Density Gradient

The radial plasma density profile is observed to fall off exponentially over an order of magnitude in density. We would like to measure the density scale length $q = -[(\partial \ln n)/(\partial r)]^{-1}$. We make a least-squares fit to the function $a + br$, where $b = -1/q$. This is equivalent to fitting $n(r) \approx A \exp(-r/q)$.

Given a set of k pairs of points (x_i, y_i), where $y_i = \ln n_i$ and $x_i = r_i$, the best fit to the line $a + bx$ is given by minimizing S, where

$$S = \sum_{i=1}^{k} (\delta y_i)^2 = \sum_{i=1}^{k} (y_i - a - bx_i)^2.$$

See, for instance, the discussion in Beers.[133] The least-squares fit is found by setting $\partial S/\partial a = 0$ and $\partial S/\partial b = 0$ and solving

$$a = \frac{\sum x_i^2 \sum y_i^2 - \sum x_i \sum x_i y_i}{k\sum x_i^2 - (\sum x_i)^2}$$

and

$$b = \frac{k\sum x_i y_i - \sum x_i \sum y_i}{k\sum x_i^2 - (\sum x_i)^2},$$

where the sums run from i = 1 to k. The uncertainty in the slope b, s_b, is given by

$$s_b = s_y \left(\frac{k}{k\sum x_i^2 - (\sum x_i)^2} \right)^{1/2} .$$

The uncertainty in y, s_y, has two parts. First there is the uncertainty due to scattering in the fitted data points $s_{y1} = \sum(\delta y_i)^2/2k$. In addition there is uncertainty in the measurements of y_i, $s_{y2} = \delta \ln n_i = \delta n_i / n_{i(rel)} = 0.21$. This last is the dominant source of error. When this analysis is applied to the eight data points from r = 2 cm to r = 9 cm of Fig. 5 one gets $q = 2.26 \pm 0.17$ cm, where $\delta q/q = \delta b/b = 0.077$.

8. Potential Measurements and Electric Fields

The measurements of the floating potential of the plasma ϕ_f has uncertainty because of some drift in the plasma potential over the measurement period, as well as due to the typically large potential fluctuations which obscure the exact value of the mean floating potential. This measurement is good to $\delta\phi_f = 0.05$ V.

In order to determine the radial electric fields in the plasma, we must know the plasma potential, which is related to the probe floating potential by Eq. (B.4),

$$\phi_p = \phi_f + \frac{kT_e}{2e} \ln \frac{m_i kT_e}{kT_i m_e} .$$

Propagation of errors gives us the uncertainty in the plasma potential

$$(\delta\phi_p)^2 = (\delta\phi_f)^2 + \left(\frac{\delta kT_e}{kT_e}\right)^2\left(\frac{kT_e}{2e}\right)^2\left(\ln\frac{m_i}{m_e} - \ln kT_i + \ln kT_e + 1\right)^2 + \left(\frac{\delta kT_i}{kT_i}\right)^2\left(\frac{kT_e}{2e}\right)^2 .$$

The dominant term comes from the uncertainty in the electron temperature. In Data Set 1, Fig. 6, at r = 4 cm, we have $\delta\phi_p$ = 0.30 V, which is rather large. The uncertainty in the radial electric field E_r determined from two points 4 cm apart would be of the order of $\delta E_r = 2\delta\phi_p/\Delta r$ = 0.15 V/cm. The fit to the data over 7 cm in radius gives an average electric field of $E_r = 0.2 \pm 0.15$ V/cm. However, from r = 4 cm to r = 6 cm the data are relatively flat, indicating $E_r \approx 0.5$ V. Because of the uncertainty in the electron temperature measurement, one can get only a rough estimate of the radial electric fields in the plasma.

For a larger magnetic field the radial electric field becomes more pronounced (see Fig. 24). As the electron temperature is much larger there is a larger uncertainty in the potential $\delta\phi_p$ = 0.54 V. However, the estimated radial electric field E_r = 1.5 V/cm is indicated over at least 4 cm in radius with a good fit. We can estimate the uncertainty in E_r to be $\delta E_r = 2\delta\phi_p/\Delta r$ = 0.3 V/cm. Even with this large an uncertainty the radial field is still in evidence.

Along a magnetic field line the electron temperature is constant due to the long electron mean free path. In addition, the electron temperature falls off only slowly with radius in the secondary plasma.

The electron temperature should be constant along the path of measurement of the axial probe, and the probe floating potential should be a pretty good indication of the relative axial plasma potential, $\delta\phi_p = \delta\phi_f = 0.05$ V. There is considerable scatter in the plot of the plasma density as a function of probe floating potential in Fig. 10. However, different measurements under different conditions show this same tendency for the axial density profile to be related to the relative probe potential axially.

9. Transport Coefficients

We are now in a position to evaluate the uncertainties in the transport coefficients, $D_{\parallel}^{in}$, $D_{\perp}^{in}$, D^{ie}, and $\mu_{\perp}^{in}$. By propagation of error we find

$$\left(\frac{\delta D_{\parallel}^{in}}{D_{\parallel}^{in}}\right)^2 = \left(\frac{1}{2}\frac{\delta kT_i}{kT_i}\right)^2 + \left(\frac{\delta n_0}{n_0}\right)^2,$$

$$\left(\frac{\delta D_{\perp}^{in}}{D_{\perp}^{in}}\right)^2 = \left(\frac{3}{2}\frac{\delta kT_i}{kT_i}\right)^2 + \left(\frac{\delta n_0}{n_0}\right)^2 + \left(\frac{2\delta B}{B}\right)^2,$$

$$\left(\frac{\delta D^{ie}}{D^{ie}}\right)^2 = \left(\frac{kT_i}{kT_i + kT_e}\right)^2\left(\frac{\delta kT_i}{kT_i}\right)^2 + \left(\frac{kT_e}{kT_e + kT_i} - \frac{3}{2}\right)^2\left(\frac{\delta kT_e}{kT_e}\right)^2 + \left(\frac{2\delta B}{B}\right)^2 + \left(\frac{\delta n_e}{n_e}\right)^2,$$

$$\left(\frac{\delta \mu_{\perp}^{in}}{\mu_{\perp}^{in}}\right)^2 = \left(\frac{1}{2}\frac{\delta kT_i}{kT_i}\right)^2 + \left(\frac{\delta n_0}{n_0}\right)^2 + \left(\frac{2\delta B}{B}\right)^2.$$

The estimated uncertainties in the various coefficients are listed in Tables 5.2 and 5.5.

E. Partial List of Symbols

a	radius of Langmuir probe
A_I, A_{II}	anode I, and II
A_n	anode end ring, n = 1 to 5
A_{probe}	area of probe tip
$\vec{B}$, B	magnetic field, magnetic field strength in gauss
B_{horiz}	horizontal component of bias magnetic field
B_{vert}	vertical component of bias magnetic field
B_z	axial magnetic field component
B_1	magnetic field perturbation
c	speed of light
C	constant in Langmuir probe, Eq. (B.2)
C_n	cathode end ring, n = 1 to 5
C_s	stray capacitance in Langmuir probe sweep chassis
C_I, C_{II}	cathode I, and II
d	spacing between tips of double probe
D_{Bohm}	Bohm diffusion coefficient
$D_{jk}^{\alpha n}$	diffusion tensor for neutral diffusion of species α
D_{enh}^{α}	enhanced diffusion coefficient for species α
$D_{\parallel}^{\alpha n}$	longitudinal diffusion coefficient for neutral collisional diffusion of species α
$D_{\perp}^{\alpha n}$	transverse diffusion coefficient for neutral collisional diffusion of species α
$D_{\perp eff}^{\alpha}$	effective transverse diffusion coefficient for species α

D^{ei}, D^{ie}	transverse diffusion coefficient for collisions between ions and electrons
e	electron charge, electron species
E	electric field
E_m	metastable energy level
E_r, E_θ, E_z	radial, azimuthal, and axial components of electric field
E_R	energy released in recombination
E_0	magnitude of static electric field
E_1	magnitude of electric field perturbation
E_I, E_{II}	end electrodes I, and II
$E_\perp$, $E_\parallel$	perpendicular and parallel components of electric field
f(r)	function of r
Δf	bandwidth of oscillation spectrum Hz
F	coefficient relating neutral, electron, and ion energy exchange as defined in Eq. (5.3)
F_{pe}	photoelectron flux
g_1, g_2	statistical weights
i	ion species
I	current
ΔI	change in current
I_{se}	saturated electron current
I_{si}	saturated ion current
I_B	current in axial magnetic field coils

I_T	current to diffusion chamber wall
I_{A_I}, $I_{A_{II}}$	current to electrode A_I, A_{II}
I_{Cn}, I_{An}	current to electrode C_n, A_n
I_{E_I}, $I_{E_{II}}$	current to electrode E_I, E_{II}
j, k	spatial indices
K	plasma dielectric constant
k_0	optical absorption coefficient
kT_α	mean kinetic temperature of species, e, i, and n
L	length of the system
L_{eff}	effective length of the system as seen by the plasma
m	azimuthal mode number, metastable species
m_e	electron mass
m_i	ion mass
m_n	neutral atom mass
M	ion mass in amu
n	plasma density, neutral atom species
n_α	density of species α = i, e
n_0	neutral density, or zero-order density
n_1	amplitude of density function
n(r,z)	radial and axial density function
$\langle nv_z \rangle^\alpha_{wall}$	particle current to end wall of species α = i, e
$\langle nv_r \rangle^\alpha_{conv}$	radial particle current due to convection of species α = i, e
nv_r, nv_θ, nv_z	species components of particle flux

nv_D	diffusion flux
P	plasma pressure
P_T	neutral pressure in diffusion chamber
q	radial density scale length
q_α	charge on species α
r_0	distance of closest approach of electron to ion
r_{gi}	ion gyroradius
r_{ge}	electron gyroradius
R	radial position
R_d	dynamic resistance of probe sheath
R_{emf}	effective resistance of Langmuir probe sweep circuit
R_I	current-sensing resistance
s	sheath thickness
t	time
t_c	self-collision time for the electron distribution
t_D	mean 90-deg deflection time for an electron
t_{eq}	mean energy equipartition time
T_{gate}	electron temperature from gated probe curves
T_{min}, T_{max}	electron temperature from minimum (or maximum) of probe curve envelope
v_α	mean velocity of species
v_{th}^α	mean thermal velocity of species
V	voltage difference between probe and plasma
α	species type α = i, e, n, m (for ion, electron, neutral, and metastable)

α_C	collisional three-body recombination coefficient
α_D	molecular ion dissociative recombination coefficient
α_R	radiative recombination coefficient
β	ratio of electron to ion flux to the end walls
β_{ave}	averaged ratio of electron flux to ion flux to end walls
β_I	ionization rate
δ	phase angle between density and electric field fluctuations
$\eta_\perp$, η_{SH}	plasma resistivity
θ_{gate}	phase delay for gated Langmuir probe curves
λ_0	wavelength of light
λ_{in}	ion transport mean free path for ion-neutral collisions (total)
λ_{in}^{cx}	mean free path for charge exchange in ion-neutral collisions
λ_{in}^{el}	mean free path for elastic scattering in ion-neutral collisions
λ_{ee}	mean free path for electron self-collisions
λ_{en}	mean free path for electron-neutral collisions
λ_{nn}	mean free path for neutral-neutral collisions
λ_{eff}^{in}	effective ion-neutral mean free path for axial transport
λ_D	Debye length
Λ	Debye shielding parameter

$\mu_{jk}^{\alpha n}$ mobility tensor for neutral collisional mobility of species α = i, e

$\mu_{\perp}^{\alpha n}$ transverse mobility coefficient for neutral collisional mobility of species α = i, e

$\mu_{\parallel}^{\alpha n}$ longitudinal mobility coefficient for neutral collisional mobility of species α = i, e

ν_{in}^{cx} collision frequency for charge-exchange collisions between ions and neutrals

ν_{in}^{el} collision frequency for elastic collisions between ions and neutrals

ν_{in} total collision frequency for collisions between ions and neutrals

ν_{en} collision frequency for collisions between electrons and neutrals

ν_{ei} collision frequency for collisions between electrons and ions

ν half bandwidth of oscillations sec^{-1}

ρ mass density of plasma

σ_{in}^{cx} cross section for charge-exchange collisions between ions and neutrals

σ_{in}^{el} cross section for elastic collisions between ions and neutrals

σ_{in} total cross section for collisions between ions and neutrals

σ_{en}	cross section for collisions between electrons and neutrals
σ_{ei}	cross section for collisions between electrons and ions
σ_C	plasma conductivity
τ	excited-state lifetime
τ_s	"correlation time" of electric field fluctuations
ϕ_A, ϕ_B	floating potential on probe A, and B
ϕ_l	potential fluctuation
ϕ_p	plasma potential
ϕ_f	Langmuir probe floating potential
$\Delta\phi$	change in potential
ϕ_{probe}	potential applied to probe
ϕ_{emf}	electromotive force of probe sweep chassis
ϕ_{ref}	potential on reference probe
ϕ_{wall}	potential of wall of diffusion chamber
ω	frequency sec^{-1}
ω_{pe}	electron plasma frequency sec^{-1}
ω_{pi}	ion plasma frequency sec^{-1}
Ω_α	gyrofrequency of species α sec^{-1}

REFERENCES

1. David Bohm, E. H. S. Burhop, and H. S. W. Massey, in The Characteristics of Electrical Discharges in Magnetic Fields, A. Guthrie and R. K. Wakerling, Eds. (McGraw-Hill Book Company, New York, 1949), Ch. 2.

2. W. P. Allis, Motions of Ions and Electrons, in Handbuch der Physik, Vol. XXI (Springer-Verlag, Berlin, 1956), pp. 383-444.

3. Klaus H. Berkner, Robert V. Pyle, Henry F. Rugge, J. Warren Stearns, and Joseph Winocur, Diffusion from a Line Source in a Magnetic Field, in VI Conference Internationale sur les Phenomenes d'Ionisation dans les Gas, 8-13 July 1963 (SERMA, Paris, 1965), Vol. 1, p. 389.

4. A. Simon and R. V. Neidigh, Diffusion of Ions in a Plasma across a Magnetic Field, Oak Ridge National Laboratory report ORNL-1890, July 11, 1955.

5. Fred Schwirzke, Diffusion eines Plasmas in Abhangigkeit von Magnetfeld und Druch und von der Längs Ausdehnung in Magnetfeldrichtung, Z. Naturforsch. 18a, 889-895 (1963).

6. A. V. Zharinov, The Diffusion of Electrons in a Magnetic Field, J. Nucl. Energy: Pt. C 1, 271 (1960).

7. Lewi Tonks, Diffusion through a Finite Plasma in a Uniform Magnetic Field, Phys. Fluids 3, 758 (1960).

8. A. Simon, Diffusion of Arc Plasmas across a Magnetic Field, in Proceedings of the Second International Conference on the Peaceful Uses of Atomic Energy (United Nations, Geneva, 1958), 32, 343.

9. Albert Simon, Introduction to Thermonuclear Research (Pergamon Press, New York, 1959).

10. D. Bohm, E. H. S. Burhop, H. S. W. Massey, and R. M. Williams, in The Characteristics of Electrical Discharges in Magnetic Fields, A. Guthrie and R. K. Wakerling, Eds. (McGraw-Hill Book Company, New York, 1949), Ch. 9.

11. R. V. Neidigh, Some Experiments Relating Ion Diffusion in a Plasma to the Neutral Gas Density in the Presence of a Magnetic Field, Oak Ridge National Laboratory report ORNL-2024, June 15, 1956.

12. F. Boeschoten and F. Schwirzke, Investigation of a Stationary Plasma in a Magnetic Field, Nucl. Fusion 2, 54 (1962).

13. Fred Schwirzke, Diffusion of Charged Particles across a Magnetic Field in "Short Circuiting Geometry," Phys. Fluids 7, 311 (1964).

14. Fred Schwirzke, Electric Fields Caused by the Diffusion of Charged Particles across a Magnetic Field, Phys. Fluids 9, 2244 (1966).

15. R. V. Meghreblain and D. K. Holmes, Reactor Analysis (McGraw-Hill Book Company, New York, 1960), p. 179.

16. D. Bohm, E. H. S. Burhop, H. S. W. Massey, and R. M. Williams, in The Characteristics of Electrical Discharges in Magnetic Fields A. Guthrie and R. K. Wakerling, Eds. (McGraw-Hill Book Company, New York, 1949), p. 199.

17. Albert Simon, Ambipolar Diffusion in a Magnetic Field, Phys. Rev. 98, 317 (1955).

18. Martin Hudis, K. Chung, and D. J. Rose, Ion Temperature in a Hollow Cathode Arc Plasma, Bull. Am. Phys. Soc. 12, 694 (1967).

19. F. C. Hoh, Low Temperature Plasma Diffusion in a Magnetic Field, Revs. Mod. Phys. 34, 267 (1962).

20. F. Boeschoten, Review of Experiments on the Diffusion of Plasma across a Magnetic Field. J. Nucl. Energy: Pt. C 6, 339 (1964).

21. S. Yoshikawa and D. J. Rose, Anomalous Diffusion of a Plasma across a Magnetic Field, Phys. Fluids 5, 334 (1962).

22. Stephen D. Rothleder, Charged Particle Diffusion and Energy Transport in a Highly Ionized Magnetically Confined Plasma (Ph.D. Thesis), Nuclear Engineering Department, Massachusetts Institute of Technology, Aug. 1962 (unpublished).

23. F. Boeschoten, Review of Experiments on the Diffusion of Plasma across a Magnetic Field, J. Nucl. Energy: Pt. C 6, 339 (1964), p. 365.

24. L. M. Lidsky, S. D. Rothleder, D. J. Rose, S. Yoshikawa, C. Michelson, and R. J. Mackin, Jr., Highly Ionized Hollow Cathode Discharge, J. Appl. Phys. 33, 2490 (1962).

25. Klaus H. Berkner et al., in Controlled Thermonuclear Research Semiannual Report, January through June 1965, UCRL-14285, p. 82-84.

26. Klaus H. Berkner et al., in Controlled Thermonuclear Research Semiannual Report, January through June 1964, UCRL-12028, p. 80.

27. R. A. Gibbons, N. J. Lazar, and T. F. Rayburn, in Thermonuclear Division Semiannual Progress Report for Period Ending October 31, 1963, ORNL-3564, Feb. 12, 1964, Section 5.1.

28. See, for instance, L. M. Lidsky et al., Ref. 24.

29. Joseph Winocur and Robert V. Pyle, A Spectroscopic Technique for probing an Ionized Gas, J. Appl. Phys. 36, 2740 (1965).

30. Roland Meyerott, Exchange Forces Between Li^+ and He, and the Mobility of Li^+ in He, Phys. Rev. 66, 242 (1944).

31. John A. Hornbeck and J. P. Molnar, Mass Spectrometric Studies of Molecular Ions in the Noble Gases, Phys. Rev. 84, 621 (1951).

32. Von M. Pahl, Zur Bildung von Molekülionen in stationären Edelgasentladungen, Z. Naturforsch. 14a, 239 (1959).

33. A. von Engel, Ionized Gases (Oxford University Press, Oxford, 1965), 2nd Ed., p. 166.

34. Einar Hinnov and Joseph G. Hirschberg, Electron-Ion Recombination in Dense Plasmas, Phys. Rev. 125, 795 (1962).

35. Francis F. Chen, Claude Etievant, and David Mosher, Measurement of Low Plasma Densities in a Magnetic Field, Phys. Fluids 11, 811 (1968).

36. K. H. Geissler, Investigation of the diffusive Decay of a Plasma Contained in a Conducting Cylinder in the Presence of a Magnetic Field, Institut für Plasmaphysik, Garching, report IPP-2/51, Sept. 1966.

37. See pages 62-63 above.

38. T. H. Stix, Resonant Diffusion of Plasma Across a Magnetic Field, Phys. Fluids 10, 1601 (1967).

39. See page 43 above.

40. Fred Schwirzke, Potential Distribution Correlated with the Diffusion of Charged Particles Across a Magnetic Field, General

Atomic report GA-6106, Feb. 3, 1956, unpublished.

42. Fred Schwirzke, Electron and Ion Transport Across a Magnetic Field in an Arc Diffusion Experiment, Phys. Fluids 9, 2250 (1966).

43. F. Boeschoten, K. Geissler, and G. Siller, Comparison of a Few Methods for Measuring the Diffusion Rate of a Plasma Across a Magnetic Field, Institut für Plasmaphysik, Garching, report IPP-2/35, Feb. 1964.

44. D. Bohm, E. H. S. Burhop, H. S. W. Massey, and R. M. Williams, in The Characteristics of Electrical Discharges in Magnetic Fields, A. Guthrie and R. K. Wakerling, Eds. (McGraw-Hill Book Company, New York, 1949), Ch. 9, pp. 184-185.

45. D. Bohm et al., op. cit. pp. 186-188.

46. B. Lehnert, Experimental Evidence of Plasma Instabilities, Plasma Phys. 9, 301 (1967).

47. G. Briffod, M. Gregoire, and S. Gruber, Instability in a Cold Cathode Reflex Discharge, J. Nucl. Energy: Pt. C 6, 329 (1964).

48. R. V. Neidigh and C. H. Weaver, Effect of an Applied Pressure Gradient on a Magnetically Collimated Arc, in Proceedings of the 2nd United Nations International Conference on the Peaceful Uses of Atomic Energy (United Nations, Geneva, 1958), 31, 315.

49. Francis F. Chen and Alfred W. Cooper, Electrostatic Turbulence in a Reflex Discharge, Phys. Rev. Letters 9, 333 (1962).

50. K. I. Thomassen, Rotational Instability in a Penning Type Discharge, Phys. Rev. Letters 14, 587 (1965).

51. K. I. Thomassen, Turbulent Diffusion in a Penning Type Discharge, Phys. Fluids 9, 1836 (1966).

52. Donald M. Kerr, Jr., Helical Instability in a Penning Discharge, Phys. Fluids 9, 2531 (1966).

53. K. Chung and D. J. Rose, Interpretation of Fluctuations in the Discharge Arc Column, Bull. Am. Phys. Soc. 12, 694 (1967).

54. David L. Morse, Plasma Rotation in a Hollow-Cathode Discharge, Phys. Fluids 8, 516 (1965).

55. Francis F. Chen, Low-Frequency Oscillations in Gas Discharges, Phys. Fluids 4, 1448 (1961).

56. F. F. Chen, Electrostatic Stability of a Collisionless Plane Discharge, Nuovo Cimento 26, 4530 (1962).

57. Francis F. Chen, Preliminary Results on the Interpretation of Low-Frequency Fluctuations Observed in the Reflex Arc, Princeton Plasma Physics Laboratory report MATT-249, Jan. 1964.

58. Earl W. McDaniel, Collision Phenomena in Ionized Gases (John Wiley and Sons, Inc., New York, 1964), p. 182.

59a. I. F. Kharchenko, Ya. B. Fainberg, E. A. Kornilov, and N. S. Pedenko, Excitation of Oscillations in a Plasma by an Electronic Beam, Zh. Tek. Fix. 34, 1031 (1964); [English translation: Soviet Phys.-Tech. Phys. 9, 798 (1964)].

59b. V. N. Tsytovich and V. D. Shapiro, The Passage of a Charged Particle Through a Plasma, Zh. Tek. Fiz. 35, 1925 (1965); [English translation: Soviet Phys.-Tech. Phys. 10, 1485 (1966)].

60. E. A. Kornilov, O. F. Kovpik, Ya. B. Fainberg, and I. F. Khrachenko, Investigation of Particle Energy and Conditions of Excitation of Low Frequency Oscillations in a Plasma Formed by

the Growth of Instabilities in a Beam-Plasma System, in Interactions of Beams of Charged Particles with a Plasma, K. D. Sinel'nikov et al., Eds. (Naukova Dumka, Kiev, 1965), pp. 24-35 (in Russian).

61. R. E. Aamodt and W. E. Drummond, Wave-Wave Scattering of Beams and Plasma Oscillations, Phys. Fluids 8, 171 (1965).

62. B. B. Kadomtsev and A. V. Nedospasov, Instability of the Positive Column in a Magnetic Field and the "Anomalous" Diffusion Effect, J. Nucl. Energy: Pt. C 1, 230 (1960).

63a. Gareth Guest and Albert Simon, Instability in Low-Pressure Plasma Diffusion Experiments, Phys. Fluids 5, 503 (1962).

63b. Albert Simon, Instability of a Partially Ionized Plasma in Crossed Electric and Magnetic Fields, Phys. Fluids 6, 382 (1963).

64. F. C. Hoh, Instability of Penning-Type Discharges, Phys. Fluids 6, 1184 (1963).

65. Robert Bingham, Long Wavelength Instability in a Reflex Discharge, Phys. Fluids 7, 1001 (1964).

66. David L. Morse, Low-Frequency Instability of Partially Ionized Plasma, Phys. Fluids 8, 1339 (1965).

67a. Francis F. Chen, Low-Frequency Instabilities of a Fully Ionized Gas, Princeton Plasma Physics Laboratory report Matt-214, Sept. 1963.

67b. Francis F. Chen, Resistive Overstabilities and Anomalous "Diffusion," Phys. Fluids 8, 912 (1965).

68. B. B. Kadomtsev, Plasma Turbulence (Academic Press, New York, 1965), pp. 79-84.

69a. F. Boeschoten, L. J. Demeter, and C. B. Kretschmer, Discrete Frequency Oscillations in Vacuum Arc Generated Plasmas, in Proceedings of the 8th International Conference on Phenomena in Ionized Gases, Vienna, 1967 (IAEA, Vienna, 1967), p. 144.

69b. F. Boeschoten and L. J. Demeter, Measurements of Plasma Rotation in a Hollow-Cathode Discharge, Plasma Phys. 10, 391 (1968).

69c. C. B. Kretschmer, F. Boeschoten, and L. J. Demeter, Plasma Waves and Rotation in a Gas-Fed Hollow-Cathode Arc, Phys. Fluids 11, 1050 (1968).

70. L. I. Rudakov and R. Z. Sagdeev, Microscopic Instabilities of Spatially Inhomogeneous Plasma in a Magnetic Field, Nucl. Fusion 1962 Suppl., Part 2, p. 481 (in Russian); [English translation: AEC-tr-5589, Book 1, p. 268].

71. See page 107.

72a. T. K. Chu, H. W. Hendel, and P. A. Politzer, Measurements of Enhanced Plasma Losses Caused by Collisional Drift Waves, Phys. Rev. Letters 19, 1110 (1967).

72b. H. W. Hendel, T. K. Chu, and P. A. Politzer, Collisional Drift Waves--Identification, Stabilization, and Enhanced Plasma Transport, Princeton Plasma Physics Laboratory report MATT-586, May 1968.

73. K. Bol and R. Ellis, Fluctuation and Transport Measurements on Helium Plasmas with Varying Shear, Princton Plasma Physics Laboratory report MATT-Q-24, May 1967, p. 31.

74. Francis F. Chen, Effect of Sheaths on Drift Instabilities in

Thermionic Plasmas, Phys. Fluids 8, 752 (1965).

75. Allan N. Kaufman, in Plasma Physics in Theory and Application, Wulf B. Kunkel, Ed. (McGraw-Hill Book Company, New York, 1966), p. 108.

76. E. H. Holt and R. E. Haskell, Foundations of Plasma Dynamics (The Macmillan Co., New York, 1965), p. 166.

77. Allan N. Kaufman, op. cit., p. 113.

78. S. Puri, Plasma Heating and Diffusion in Stochastic Fields, Phys. Fluids 9, 2043 (1966).

79. T. Holstein, Imprisonment of Resonance Radiation in Gases, Phys. Rev. 72, 1212 (1947).

80. J. C. Ingraham and Sanborn C. Brown, Helium Afterglow and the Decay of the Electron Energy, Phys. Rev. 138A, 1015 (1965).

81. Lyman Spitzer, Jr., Physics of Fully Ionized Gases (Interscience Publishers, New York, 1962), 2nd Ed., p. 135.

82. Lyman Spitzer, Jr., op. cit., p. 131.

83. D. Bohm, E. H. S. Burhop, H. S. W. Massey, and R. M. Williams, in The Characteristics of Electrical Discharges in Magnetic Fields, A. Guthrie and R. K. Wakerling, Eds. (McGraw-Hill Book Company, New York, 1949), Ch. 9.

84. L. S. Frost and A. V. Phelps, Momentum-Transfer Cross Sections for Slow Electrons in He, Ar, Kr, and Xe from Transport Coefficients, Phys. Rev. 136, A1538 (1964).

85. W. H. Cramer and J. H. Simons, Elastic and Inelastic Scattering of Low-Velocity He^+ Ions in Helium, J. Chem. Phys. 26, 1272 (1957).

86. Lorne M. Chanin and Manfred Biondi, Temperature Dependence of Ion Mobilities in Helium, Neon, and Argon, Phys. Rev. 106, 473 (1957).

87. Francis F. Chen, Calude Etievant, and David Mosher, Measurement of Low Plasma Densities in a Magnetic Field, Phys. Fluids 11, 811 (1968).

88. J. G. Laframboise, Theory of Spherical and Cylindrical Langmuir Probes in a Collisionless, Maxwellian Plasma at Rest, University of Toronto Institute for Aerospace Studies report UTIAS-100, June 1966.

89. Francis F. Chen, Electric Probes, in Plasma Diagnostics Techniques, Richard H. Huddlestone and Stanley L. Leonard, Eds. (Academic Press, New York, 1965).

90. S. H. Lam, Unified Theory for the Langmuir Probe in a Collisionless Plasma, Phys. Fluids 8, 73 (1965).

91. Laurence S. Hall, Probes and Magnetic Pumping in Plasma, Lawrence Radiation Laboratory report UCRL-6535, July 19, 1961.

92. David Bohm, E. H. S. Burhop, and H. S. W. Massey, in The Characteristics of Electrical Discharges in Magnetic Fields, A. Guthrie and R. K. Wakerling, Eds. (McGraw-Hill Book Company, New York, 1949), Ch. 2.

93. David Bohm et al., op. cit., p. 33.

94. David Bohm et al., op. cit., p. 48.

95a. David Bohm et al., op. cit., pp. 57-75,

95b. A. V. Zharinov, A. Stepwise Increase in the Electron Current to a Probe Places in a Discharge in a Magnetic Field, J. Nucl. Energy: Pt. C 1, 267 (1960).

96. G. Ecker, K. S. Masterson, and J. J. McClure, Probe Theory in Dense Plasma, Lawrence Radiation Laboratory report UCRL-10128, March 21, 1962.

97. Lyman Spitzer, Jr., Physics of Fully Ionized Gases (Interscience Publishers, New York, 1962), 2nd Ed., p. 133.

98. Fred Schwirzke and G. H. Eggers, Measurement of the Electron Diffusion Coefficient Across a Magnetic Field, General Atomic report GA-6106, Feb. 3, 1965.

99. A. Garscadden and K. G. Emeleus, Notes on the Effect of Noise on Langmuir Probe Characteristics, Proc. Phys. Soc. (London) 79, 535 (1962).

100. F. W. Crawford, Modulated Langmuir Probe Characteristics, J. Appl. Phys. 34, 1897 (1963).

101. Minoru Sugawara and Yoshisuke Hatta, Langmuir Probe Method for a Plasma Having Small Amplitude Oscillations, Nagoya University Institute of Plasma Physics report IPPJ-4, Feb. 1963.

102. A Garscadden and P. Bletzinger, Langmuir Probe Measurements in the Presence of Oscillations, Rev. Sci. Instr. 35, 912 (1964).

103. Anthony Demetriades and Ernest L. Doughman, Langmuir Probe Diagnostics of Turbulent Plasmas, AIAA J. 4, 451 (1966).

104. W. B. Kunkel and J. J. Guillory, Interchange Stabilization by Incomplete Line-Tying, in Proceedings of the Seventh International Conference on Phenomena in Ionized Gases, Beograd, 1966. Vol. II.

105. Sidney Chapman and T. G. Cowling, The Mathematical Theory of Non-uniform Gases (Cambridge University Press, 1958).

106. Lyman Spitzer, Jr., Equations of Motion for an Ideal Plasma, Astrophys. J. 116, 299 (1952).

107. V. E. Golant, Diffusion of Charged Particles in a Plasma in a Magnetic Field, Sov. Phys. Uspekhi 6, 161 (1963); Usp. Fiz. Nauk. 79, 377 (1963).

108. S. Chandrasekhar, Transport Phenomena in Ionized Gases, in Plasma Physics Notes, compiled by S. K. Trehan (University of Chicago Press, Chicago, 1960), Ch. 7.

109. W. P. Allis, Motions of Ions and Electrons, in Handbuch der Physik, Vol. XXI (Springer-Verlag, Berlin, 1956), pp. 383-444.

110. Lyman Spitzer, Jr., Physics of Fully Ionized Gases (Interscience Publishers, New York, 1962), 2nd Ed., Sec. 12.

111. Rolf Landshoff, Transport Phenomena in a Completely Ionized Gas in the Presence of a Magnetic Field, Phys. Rev. 76, 904 (1949).

112. Robert S. Cohen, Lyman Spitzer, Jr., and Paul McR. Routly, The Electrical Conductivity of an Ionized Gas, Phys. Rev. 80, 230 (1950).

113. Lyman Spitzer, Jr. and Richard Härm, Transport Phenomena in a Completely Ionized Gas, Phys. Rev. 89, 977 (1953).

114. Lyman Spitzer, Jr., Physics of Fully Ionized Gases (Interscience Publishers, Inc., New York, 1956), p. 38.

115. C. L. Longmire and M. N. Rosenbluth, Diffusion of Charged Particles Across a Magnetic Field, Phys. Rev. 103, 507 (1956).

116. Albert Simon, Diffusion of Like Particles Across a Magnetic Field, Phys. Rev. 100, 1557 (1955).

117. M. N. Rosenbluth and A. N. Kaufman, Plasma Diffusion in a Magnetic Field, Phys. Rev. 109, 1 (1958).

118. Lyman Spitzer, Jr., Physics of Fully Ionized Gases (Interscience Publishers, Inc., New York, 1962), 2nd Ed., p. 127.

119. Allan Kaufman, Plasma Transport Theory, in La Theorie des Gaz Neutres et Ionises, C. DeWitt and J. F. Detoeuf, Eds. (John Wiley and Sons, Inc., New York, 1960), p. 331.

120. J. B. Taylor, Diffusion of Plasma Ions Across a Magnetic Field, Phys. Fluids 4, 1142 (1961).

121. J. B. Taylor, op. cit., p. 1144.

122. I. P. Shkarofsky, Values of the Transport Coefficients in a Plasma for Any Degree of Ionization Based on a Maxwellian Distribution, Can. J. Phys. 39, 1619 (1961).

123. W. Schottky, Diffusiontheorie der positiven Säule, Physik. Z. 25, 635 (1924).

124. K. I. Thomassen, Measurement of an Anomalous Diffusion Coefficient, Phys. Fluids 9, 626 (1966).

125. David Bohm, E. H. S. Burhop, and H. S. W. Massey, in The Characteristics of Electrical Discharges in Magnetic Fields, A. Guthrie and R. K. Wakerling, Eds. (McGraw-Hill Book Company, New York, 1949), Ch. 2.

126. David Bohm et al., op. cit., p. 63-64.

127. Lyman Spitzer, Jr., Particle Diffusion Across a Magnetic Field, Phys. Fluids 3, 659 (1960).

128. C. M. Tchen, Stochastic Theory of Diffusion in a Plasma Across

a Magnetic Field, in Proceedings of the International Symposium on Diffusion of Plasma Across a Magnetic Field, Feldafing/Starnberger See, Germany, June 29-July 3, 1964, IPP (Garching) 2/36, Dec. 1964.

129. S. Puri, Plasma Heating and Diffusion in Stochastic Fields, Phys. Fluids 9, 2043 (1966).

130. Nyle G. Utterback and Thomas Griffith, Jr., Reliable Submicron Pressure Readings with Capacitance Manometer, Rev. Sci. Instr. 37, 866 (1966).

131. F. Schwirzke and G. H. Eggers, Determination of the Electron Temperature of a Plasma in a Strong Magnetic Field by Electrostatic Probes, General Atomic report GA-6046, Jan. 26, 1965.

132. David Bohm et al., op. cit., p. 48.

133. Yardley Beers, Introduction to the Theory of Error (Addison Wesley Publishing Co., Inc., Reading, Mass., 1957).

134. Earl W. McDaniel, Collision Phenomena in Ionized Gases (John Wiley and Sons, Inc., New York, 1964), p. 466.

LEGAL NOTICE